

Dissertation zur Erlangung des Doktorgrades
der Fakultät für Chemie und Pharmazie
der Ludwig-Maximilians-Universität München

Click chemistry as powerful bioconjugation tool applied to DNA
nanotechnology and cytogenetic analysis

Valentina Cassinelli

aus

Pavia, Italy

2016

Erklärung

Diese Dissertation wurde im Sinne von § 7 der Promotionsordnung vom 28. November 2011 von Herrn Prof.Dr. Thomas Carell betreut.

Eidesstattliche Versicherung

Diese Dissertation wurde eigenständig und ohne unerlaubte Hilfe erarbeitet.

München, 09.09.2016

Valentina Cassinelli

Dissertation eingereicht am 29.09.2016

1. Gutachterin / 1. Gutachter: Prof. Dr. Thomas Carell

2. Gutachterin / 2. Gutachter: Prof. Dr. Tim Liedl

Mündliche Prüfung am 02.05.2017

To my father

Acknowledgment

This work was supported by the European Commission under the Seventh Framework Programme (FP7), as part of the Marie Curie Initial Training Network, EScoDNA (GA no. 317110).

I would like to thank the company baseclick GmbH and my industrial supervisors - Dr. Thomas Frischmuth and Dr. Antonio Manetto - for involving me in the European School of DNA nanotechnology (EScoDNA) program. The opportunity I got had an inestimable value for the development of my scientific knowledge and industrial formation as well.

I would like to express my sincere gratitudes to Dr. Thomas Frischmuth for his support during my permanence at baseclick and the useful discussions during the writing process.

Special thanks go to Dr. Antonio Manetto. Since the beginning of my PhD he welcomed me with a volcano of ideas and transmitted to me his great passion for research. He supported me every day giving me new inputs, being always available and giving me motivation in the unsuccessful moments.

I am extremely grateful to Prof. Dr. Thomas Carell who accepted me as his external student providing me open access to all his laboratories and instruments.

I am truly thankful to Prof. Dr. Tim Liedl for the helpful collaboration during the entire course of my PhD, especially for hosting me in his facilities during my secondment period, for the help during the writing of the manuscript and for refereeing this thesis.

Dr. Birgit Oberleitner and Jessica Sobotta deserved a great mention. Besides her help in the research, Birgit involved me in many company's related activities helping me to understand what I want to do after the PhD. Jessica shared with me not only the office but also the difficulties of starting a new project with a lot of engagement and creativity. Since the beginning I shared with them work and free time building a sincere friendship which I hope can last during the years.

A special thank goes also to the other PhD student of baseclick: Stefano Croce. During the last year I really enjoyed with him good times in the lab and our brainstorming coffee breaks. I will miss those moments.

I would like to express my sincere acknowledgement to all supervisors of the EScoDNA network. Even though they were very busy, they always showed a great availability towards fellows during meetings and secondments.

I am really grateful to Dr. Lise Refstrup Linnebjerg Pedersen, administrator of the EScoDNA network, for the outstanding work of coordination she did during the entire period of the grant.

I want to thank all EScoDNA fellows. The different nationalities and backgrounds characterizing everyone of us contributed to create an awesome group! The opportunity of secondments allowed to increase scientific collaborations as well as friendships. I would like to thank in particular the Aarhus people - Ana Carolina Suarez, Ilenia Manuguerra, Guido Grossi and Mattia De Stefano. I never felt alone in Denmark. Regarding Munich, I thank especially Samet Kocabey and Anna Kostina for being always helpful for scientific issues and up for a beer at the Biergarten.

At baseclick I knew valuable people who I want to thank for their working help and friendship during all these three years. I appreciated Antje's "mum" attitude and her engagement in organizing events. With Michael Kollaschinski I enjoyed the time spent together in the lab and our German-Italian tandem. I thank Laura Schröder for her technical help and for remembering me always to water plants. The new baseclick member Dr. Sascha Serdjukov gave me many tips on the preparation of the thesis. Finally, I want to thank all the present and previous co-worker/student worker - Alexandra, Vanessa, Daria, Matthias, Vanessa and Rajesh – for the great time we had together.

I want also to say thank you to all the members of the AK Carell for their precious help in each circumstance and the interesting meetings.

A special thanks goes to my beloved mother who supported me in all my decisions. I thank also all my friends in Italy for their lasting and true friendship.

A last big thank is for Alessandro. I am truly grateful to him for being always at my side and support me every day. This experience would have not be possible without him.

Table of contents

TABLE OF CONTENTS	6
1. GENERAL INTRODUCTION.....	9
1.1. SUMMARY	9
1.2. DNA STRUCTURE	13
1.3. CHEMICAL AND PHYSICAL PROPERTIES OF DNA	13
1.5. INCORPORATION OF MODIFICATIONS INTO NUCLEIC ACIDS	17
1.6. CLICK CHEMISTRY	19
1.7. CLICK CHEMISTRY ON DNA.....	20
1.7.1. <i>In vitro application: DNA synthesis detection using EdU</i>	21
1.8. NANOTECHNOLOGY	22
1.9. STRUCTURAL DNA NANOTECHNOLOGY	23
1.9.1. <i>Tile-based method</i>	24
1.9.2. <i>DNA origami method</i>	25
1.9.3. <i>Scaffold-free Single Strand Tile assembly (SST)</i>	26
1.9.4. <i>Polyhedral mesh</i>	28
1.10. DESIGN	28
1.11. ANNEALING PROCEDURE	29
1.12. CHARACTERIZATION TECHNIQUES FOR DNA NANOSTRUCTURES	29
1.13. DNA NANOSTRUCTURES APPLICATIONS	30
1.14. STABILITY OF DNA NANOSTRUCTURES	32
2. CELLULAR UPTAKE OF TILE-ASSEMBLED DNA NANOTUBES.....	35
2.1. INTRODUCTION	35
2.2. RNA INTERFERENCE (RNAi)	35
2.3. FOLATE TARGETED DELIVERY	37
2.4. ABSTRACT OF THE PUBLICATION "CELLULAR UPTAKE OF TILE-ASSEMBLED DNA NANOTUBES"	39
2.5. AUTHOR'S CONTRIBUTION	39
2.6. ASSOCIATED PUBLICATION	40
CELLULAR UPTAKE OF TILE-ASSEMBLED DNA NANOTUBES	40
2.6.1. <i>Introduction</i>	41
2.6.2. <i>Results and Discussion</i>	41
2.6.2.1. <i>Design and self-assembly of six-helix DNA nanotubes</i>	41
2.6.2.2. <i>Tubule-like tile-assembled DNA nanostructures are delivered to the endosome of HeLa cells independently of folic acid and are not capable of releasing siRNA into the cytosol</i>	43
2.6.2.3. <i>Stability of DNA nanotubes differs in various conditions in vitro</i>	44
2.6.2.4. <i>Strong extra-endosomal uptake can be feigned by dye cleavage</i>	46
2.6.2.5. <i>Single-stranded DNA molecules, but not desoxynucleotide triphosphates, are internalized at similar levels as the tile-assembled nanotube structures</i>	47
2.6.3. <i>Experimental Section</i>	48
2.6.3.1. <i>DNA Nanotube Design</i>	48
2.6.3.3. <i>Dye Labeling of DNA Nanotubes</i>	48
2.6.3.4. <i>DNA Nanotube Assembly and Purification</i>	49
2.6.3.5. <i>Gel electrophoresis and Transmission Electron Microscopy</i>	49
2.6.3.6. <i>Stability of DNA Nanotubes</i>	49
2.6.3.7. <i>Cell culture experiments</i>	49
2.6.4. <i>Conclusions</i>	50

2.6.5.	References and Notes of the publication "Cellular Uptake of Tile-Assembled DNA Nanotubes"	51
2.7.	SUPPORTING INFORMATION OF THE PUBLICATION "CELLULAR UPTAKE OF TILE-ASSEMBLED DNA NANOTUBES"	54
3.	ONE-STEP FORMATION OF "CHAIN-ARMOR"-STABILIZED DNA NANOSTRUCTURES	59
3.1.	INTRODUCTION.....	59
3.2.	DNA CATENANE.....	59
3.3.	ABSTRACT OF THE PUBLICATION "ONE-STEP FORMATION OF CHAIN ARMOR STABILIZED DNA NANOSTRUCTURES"	63
3.4.	AUTHOR CONTRIBUTION.....	63
3.5.	ASSOCIATED PUBLICATION:	64
	ONE-STEP FORMATION OF CHAIN ARMOR STABILIZED DNA NANOSTRUCTURES.....	64
3.5.1.	Introduction.....	65
3.5.2.	Results.....	66
3.5.3.	Conclusion and outlook	69
3.5.4.	Experimental Section.....	70
3.5.5.	References and Notes of the publication "One-Step Formation of Chain Armor Stabilized DNA Nanostructures"	70
3.5.6.	Supporting Information of the publication "One-Step Formation of Chain Armor Stabilized DNA Nanostructures"	72
3.5.6.1.	General methods.....	72
3.5.6.2.	Oligonucleotides	74
3.5.6.3.	Tubes folding.....	79
3.5.6.4.	Folding mixture	79
3.5.6.5.	Click reaction.....	80
3.5.6.6.	Click reaction optimization.....	83
3.5.6.7.	Stability of catenane.....	85
3.5.6.8.	Resistance to heating (95 °C) of DNA catenanes after click reaction.....	86
3.5.6.9.	Resistance of DNA catenanes to ethanol precipitation.....	87
3.5.6.10.	Competitive click reaction.....	88
3.5.6.11.	RP-HPLC and MS.....	89
3.5.6.12.	Desalting experiments	96
3.5.6.13.	Melting profiles ^[5]	97
3.5.6.14.	Thermal denaturing and subsequent Exo I digestion	98
3.5.6.15.	Incubation in Dulbecco's modified Eagle Medium (DMEM).....	98
3.5.6.16.	Rate of strand incorporation in the structure and DNA-catenane formation yields	98
3.5.6.17.	Catenation between terminal 28mers.....	110
3.5.6.18.	References for the supporting information of the publication "One-Step Formation of Chain-Armor-Stabilized DNA Nanostructures"	112
4.	ULTRA-STABLE DNA NANOSTRUCTURES AND THEIR APPLICATIONS IN LIFE SCIENCE.....	113
4.1.	INTRODUCTION.....	113
4.2.	TARGETED DELIVERY	113
4.3.	DESIGN	114
4.4.	RESULTS	116
4.4.1.	Gel detection limit.....	116
4.4.2.	Local alkyne/azide concentration	117
4.4.3.	Body-labeling.....	120
4.4.4.	Head-labeling	124
4.4.5.	One-pot reaction	128
4.4.6.	Cell delivery applications.....	131
4.5.	CONCLUSION AND OUTLOOK	134
4.6.	MATERIALS AND METHODS.....	136

4.6.1.	Buffer used in this work.....	136
4.6.2.	Gel electrophoresis	136
4.6.3.	TEM imaging	137
4.6.4.	RP-HPLC analysis.....	137
4.6.5.	Folding procedure.....	138
4.6.6.	Gel detection limit.....	139
4.6.7.	Click Reaction	139
4.6.8.	Local alkyne/azide concentration.....	140
4.6.9.	Head labeling (incorporation of labeled rc-azido-ODN within the nanostructure).....	141
4.6.10.	One-pot click reaction.....	141
4.6.11.	Cell culture.....	141
4.6.12.	Nanostructure incubation	141
4.6.13.	Cell proliferation assay.....	142
4.7.	APPENDIX	143
5.1.	INTRODUCTION.....	146
5.2.	FLUORESCENCE <i>IN SITU</i> HYBRIDIZATION (FISH).....	146
5.3.	ABSTRACT OF THE PUBLICATION "FLUORESCENT LABELLING OF IN SITU HYBRIDISATION PROBES THROUGH THE COPPER-CATALYSED AZIDE-ALKYNE CYCLOADDITION REACTION"	149
5.4.	AUTHOR'S CONTRIBUTION	149
	FLUORESCENT LABELLING OF IN SITU HYBRIDISATION PROBES THROUGH THE COPPER-CATALYSED AZIDE-ALKYNE CYCLOADDITION REACTION	150
5.5.1.	Introduction.....	151
5.5.2.	Material and methods.....	153
5.5.2.1.	Plants materials	153
5.5.2.2.	Preparation of mitotic chromosomes for FISH.....	153
5.5.2.3.	Preparation and sorting of isolated nuclei.....	153
5.5.2.4.	FISH probe preparation	154
5.5.2.5.	Fluorescence in situ hybridisation using pre- or post-hybridisation click probes	155
5.5.2.6.	Combined EdU-based DNA replication analysis and FISH using pre-clicked probes	155
5.5.2.7.	Combined immunohistochemistry and hybridisation of pre-hybridisation CuAAC labelled FISH probes	156
5.5.2.8.	Quantification of telomeric FISH signals.....	156
5.5.3.	Results and discussion	156
5.5.4.	References for the publication "Fluorescent labelling of in situ hybridisation probes through the copper-catalysed azide-alkyne cycloaddition reaction"	161
6.	LIST OF ABBREVIATIONS	164
7.	BIBLIOGRAPHY	167

1. General introduction

1.1. Summary

This PhD thesis reports the results carried out within the Marie Curie network EScoDNA (European School of DNA Nanotechnology) in the laboratories of baseclick GmbH. The ultimate purpose of this EU-granted project is focused on the development of new DNA-based functional tools for significant applications in life science. DNA nanotechnology is an innovative and rapidly growing field originated in the USA at the beginning of the 1980's. The pioneering work of Seeman envisioned the use of DNA as building material to generate nanometer-controlled structures. In 2006, the work of Rothemund established a breakthrough in the field and since then other research groups all over the world approached this topic developing different assembly-strategies and generating a vast number of structures. All projects developed during this doctoral work are unified by the use of click chemistry, especially the copper(I)-catalyzed Alkyne-Azide Cycloaddition (CuAAC) variant, as bioconjugation tool.

A sought-after application of DNA nanostructures is targeted cell delivery of therapeutics molecules. Indeed the biocompatibility, biodegradability and programmability of DNA architectures are key features for the application of these structures for biomedical purposes. Nevertheless, the stability in extra- and intra-cellular environment of DNA-based structures constitutes a limiting factor to their *in vitro* and *in vivo* applications. Therefore, the focus of the first part of the work (Chapter 2, 3 and 4) is oriented on the study of a SST nanotubular structure used as delivery cargo into cells. Here click chemistry is applied for conjugation of functional moieties and for stabilization purposes.

In chapter 2 a SST six helix nanotube equipped with folate moieties was used as delivery cargo for siRNA. The folate moieties were quantitatively conjugated via CuAAC onto six terminal oligonucleotides, while GFP siRNA were hybridized to six elongated oligonucleotides already composing the structure. Some oligonucleotides were functionalized with a fluorescent dye for cell tracking purposes *via* either terminal transferase reaction or NHS chemistry (Fig. 1. 1). In the work was demonstrated that the functionalized nanotubes was taken up from cells *via* an endosomal pathway, but no significant down regulation of the GFP gene was detectable. Stability studies revealed that the siRNA modified nanotube was unstable at low Mg^{2+} concentration (2mM) and in DMEM supplemented with FCS. These factors may have been responsible for the unsuccessful siRNA delivery. A larger structure composed by oligonucleotides 84mer long showed higher stability at low Mg^{2+} concentrations and in all cell media, due to the longer complementary regions.

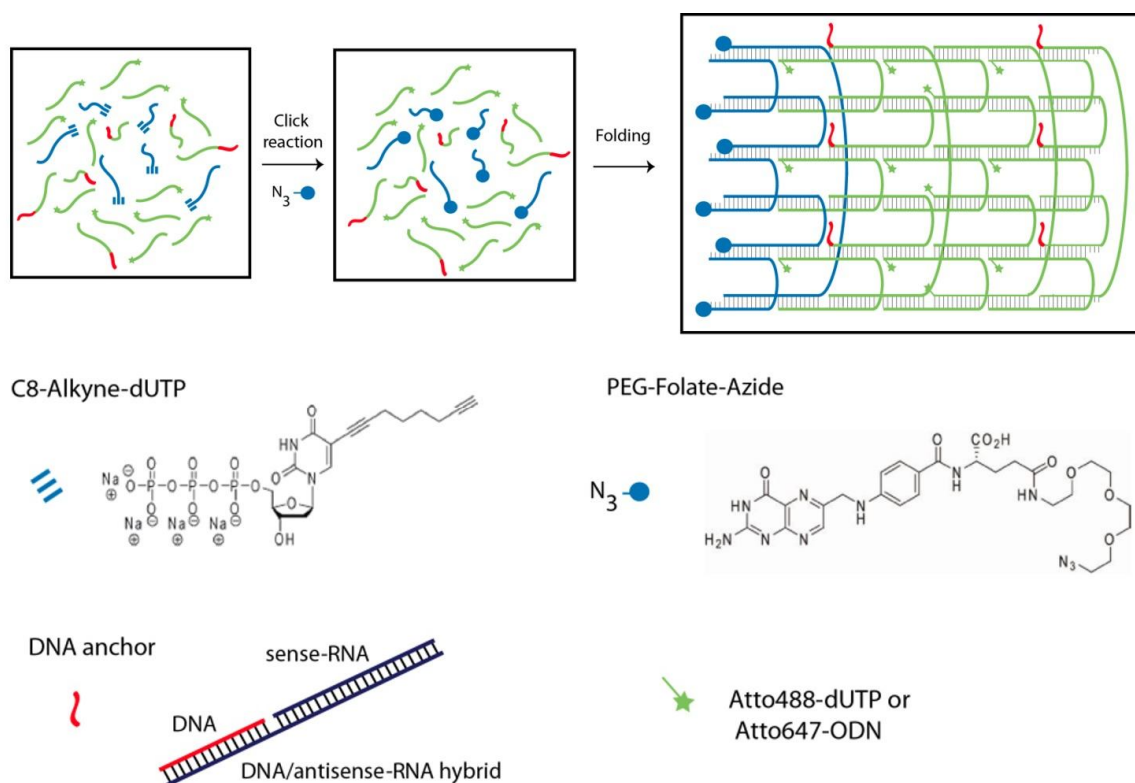


Figure 1. 1. DNA nanotube assembly. Left: Click reaction of alkyne modified oligonucleotides with azide modified PEGylated folate. Right: Self-assembly of 24 oligonucleotides into 6-helix tube after 17 hrs annealing process.

In chapter 3 the unmodified six-helix SST DNA nanotube, already used in the previous work, was efficiently modified by the use of click-tiles, namely oligonucleotides carrying at the 3'- and 5'-end alkyne and azide residues, respectively. Thanks to the spatial preorganization achieved within the architecture alkyne and azide on the same strand reacted with high efficiency resulting in the covalent intramolecular cyclization of the oligonucleotide. The strands intertwining achieved through the assembly of the nanotube and the subsequent click reaction allowed stoichiometric and high yield synthesis of DNA catenane with different geometries and size. The replacing of all 24 unmodified strands composing the structure with the respective click-tiles resulted, after click reaction, in the synthesis of a 24-membered DNA catenane, herein called DNA chainmail. The completely topologically interlocked structure remained intact even under strictly denaturing conditions for DNA nanostructures, such as ethanol precipitation, temperatures (up to 95°C) and Exonucleases digestion (Fig. 1. 2).

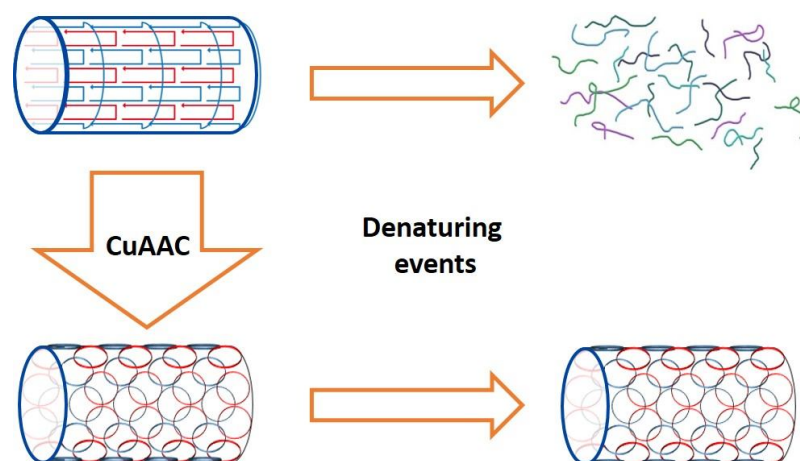


Figure 1. 2. Stabilization of six helix DNA nanotube via CuAAC. The click reaction on the structure containing 24 click-tiles results in a DNA chainmail resistant to denaturing events.

In chapter 4 the DNA chainmail architecture was further developed by the addition of “click-reactive” functionalization sites in two regions of the structure, the “head” and the “body”. This highly modified nanostructure was design to produce ultra-stable multi-functionalized DNA nanotubes with a single one-pot click reaction. The functionalization on the body region was carried out on alkyne groups incorporated within the sequences of five oligonucleotides. The preorganization of the strands within the structure enabled in a one-pot click reaction the intramolecular ring closure and the selective conjugation of an external azide on the alkyne residues on the body of the tube. The functionality in the head region was inserted through a “reporter” oligonucleotide, which is independently prepared with a two steps procedure and afterwards selectively incorporated in the nanotube by means of a splint. Once the functionalization of the two region was independently demonstrated, a one-pot click reaction resulted into a simultaneous stabilization and selective multi-functionalization of the DNA nanotube (Fig. 1. 3). A first attempt to apply this ultra-stable multi-functional DNA nanostructure for targeted cell delivery was carried out labeling the structure with different targeting ligand and a dye for cellular tracking. The stabilized nanotube was internalized in cells despite of the transfection moieties, revealing that the uptake in Hela cells is principally attributable to the tube compact structure and to a minor extent to the targeting agent used.

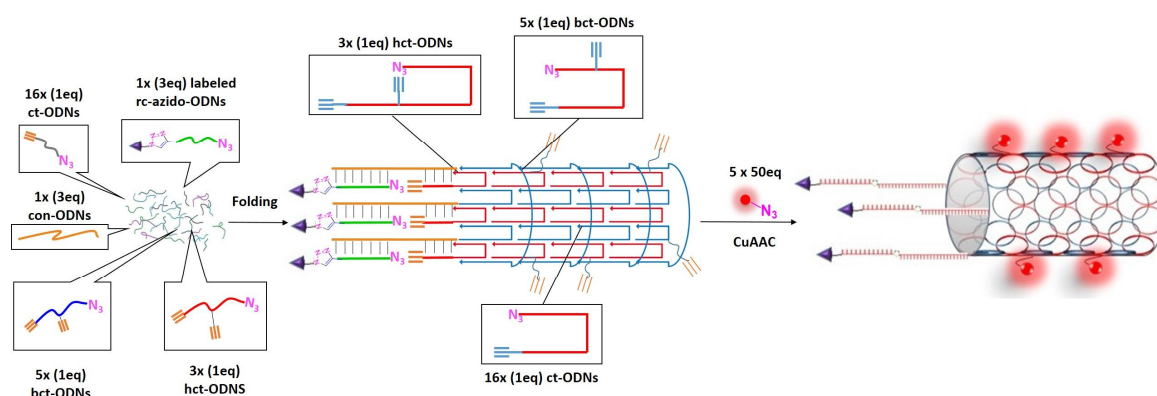


Figure 1. 3. Graphical representation of the components of the nanotube participating to the folding procedure and the subsequent one-pot click reaction on the structure.

In the last section (chapter 5) copper(I)-catalyzed alkyne azide cycloaddition was selected as strategy for fluorescent probes preparation for Fluorescent *in situ* Hybridization (FISH) analysis. In this study the click chemistry method was used as strategy to insert a higher number of fluorophore within the probe. Telomeric probes bearing from two to four fluorophores positions were compared in cell assays with probes normally labeled with other routinely used methods, such as Nick Translation. Two approaches were tested: *pre-hybridization* and *post-hybridization*. In the *pre-hybridization* setup, alkyne-modified telomers probes were labeled via CuAAC and afterwards hybridized to chromosomes, while in the *post-hybridization* approach the click reaction is performed on the hybridized probe. Both methods showed good detection of fluorescent signals on telomers, electing CuAAC as a valuable alternative labeling method for FISH probes preparation. Furthermore, *pre-hybridization* click demonstrated compatibility with other cytological analysis techniques, such as immunohistochemistry and labeling of DNA replication via 5-Ethynyl-deoxyuridine (EdU) uptake (Fig. 1. 4).

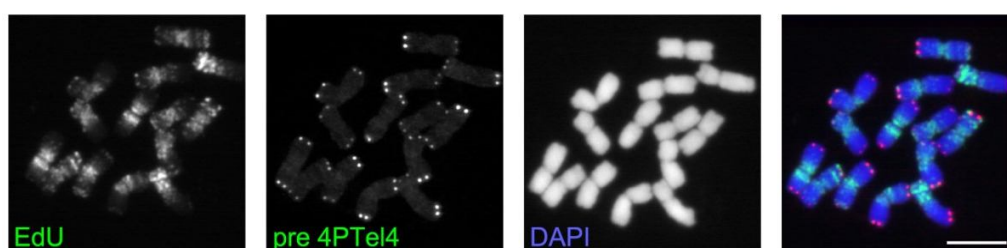


Figure 1. 4. Combination of CuAAC-labelled microsatellite probes with labelling of replication via 5-Ethynyl-deoxyuridine (EdU). (A) FISH of barley using pre-hybridisation click-labelled microsatellite (CTT)10 and telomeric probes combined with labelling of early and late replication via EdU.

1.2. DNA structure

DNA (Deoxyribonucleic acid) is the storage form of genetic information in most living organisms. This biopolymer is formed from repetitive elements, namely nucleosides. Each unit consists of a phosphate residue, a pentose sugar - 2-deoxyribose – and a planar aromatic heterocyclic base. DNA contains four bases classified as monocyclic pyrimidines - cytosine (C) and thymine (T) - and bicyclic purines - adenine (A) and guanine (G). The phosphate groups join the sugar residues forming phosphodiester bonds. In a single strand DNA filament (ssDNA) the hydroxyl group on the C3', is called 3'-end, and the phosphate group at the C5' is defined as 5'-end. The asymmetry of the phosphodiester bond confers directionality to the strand ($5' \rightarrow 3'$). A double strand DNA molecule (dsDNA) is generated when two single ssDNA are antiparallel aligned. This complex results in a helix where the sugar and the phosphate represent the external backbone and the bases are situated in the inner-helix cavity. The structure of the double helix was solved for the first time by Watson and Crick in 1953 using X-ray diffraction data collected in the years before by Maurice Wilkins and Rosalind Franklin.¹ The presented model showed how the bases form hydrogen bonds between each other, giving a stabilizing effect on the double helix. In details, thymine forms two H-bonds with adenine and guanine forms three H-bonds with cytosine (Fig 1.1).

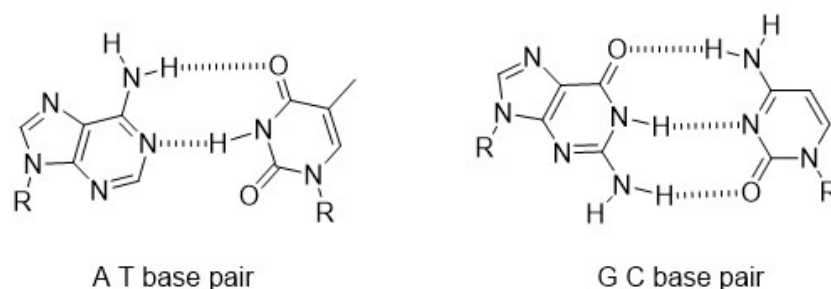


Figure 1. 5. Watson and Crick base pairing.

Besides inter-strand hydrogen bonding another double helix stabilizing factor is base stacking (also called π - π stacking). It is an attractive and noncovalent interaction depending on the aromaticity of the bases and their dipole moments. The degree of stabilization afforded by base stacking depends on the DNA sequence, hence some combinations of base pairs form more stable interactions than others.

Nowadays three main double-stranded conformations are known: A, B and Z DNA. The most common DNA double helix form and the one used in this thesis is the B conformation. In the B DNA the helix is right handed and it has 10.5 bases per turn. The distance between adjacent bases is 0.34 nm and the helical diameter is 2 nm. The knowledge of these defined structural characteristics of DNA strands is a fundamental aspect for the use of nucleic acids as building material in DNA nanotechnology.

1.3. Chemical and physical properties of DNA

In the double helix, the phosphate groups have a pKa around 1, meaning that protons are dissociated under physiological conditions, resulting in a highly negatively charged backbone. Cations in the

surrounding solution counterbalance the negative charge of the backbone, lowering the repulsion between two strands and preventing the double helix from denaturation. Consequently, at high salt concentration the duplex is more stable and the melting temperature is increased. In this context “melting” of the double helix means the transition phase from a duplex to its single-stranded components. The so-called “melting temperature” (T_m) of a DNA duplex is the temperature at which 50% of the double strands are separated into single strands. The dissociation of the duplex is depending mainly on the sequence of the strands. The presence of a higher G-C content (GC base pairs) can be translated in a higher melting temperature, as the G-C couple has a stronger pairing than A-T. Temperature is one of the easiest way to obtain denaturation of a double helix, because heat destabilizes the hydrogen bonding between the bases resulting into their final dissociation. Another factor influencing the stability of a double helix is the presence of denaturing chemicals like dimethyl sulfoxide, formamide or urea which can form hydrogen bonds with the nucleobases, competing with the Watson-Crick pairing. The stability of a dsDNA is also reduced if the sequences of the two ssDNA composing the duplex are not fully complementary. The presence of mismatches leads to decrease of the melting temperature as there is no interaction between the bases.²

Knowing the melting temperature of a duplex can be useful for many biotechnological application, for example Polymerase Chain Reaction, Southern and Northern blots, and *in situ* hybridization. To calculate the T_m there are many methods, which can be used depending on the length of the strand. The Wallace rules gives reliable results when used for strands below 20 nucleotides and allow T_m calculation by means of this simple equation:

$$T_m = 2^\circ C(A + T) + 4^\circ C(G + C)$$

Where A, T, G, and C are the number of occurrences of each nucleotide.³ A more accurate equation to calculate the T_m of DNA duplex using the nearest neighbor thermodynamic* for Watson and Crick base pair is:

$$T_m = \frac{\Delta H^\circ * 1000}{\Delta S^\circ + R * \ln(Ct/4)} - 273,15$$

Where ΔH° is the enthalpy change in kcal/mol, ΔS° is the entropy change, R is the gas constant (1.987 cal deg-1 mol-1) and Ct is the total molar concentration of strands.⁴

Double strand dissociation is usually observed using UV absorbance measurements. In this assay when a dsDNA in solution is heated, its absorbance at 260 nm increases by 37% because of single strands formation. This effect is called hyperchromicity and is due to the alteration of the electronic interaction between the stacked and hydrogen-bound bases, which are now free and can absorb more light. The opposite effect, namely hypochromicity, consists in the decrease of the ultraviolet light absorption upon hybridization of complementary strands into a double helix.⁵ Figure 1.2 represents the typical melting curve of a double helix recorded at 260 nm. The midpoint in the sigmoid is defined as the melting point (T_m) of a DNA strand.

* The nearest-neighbor model for nucleic acids assumes that the stability of a given base pair depends on the identity and orientation of neighboring base pairs.

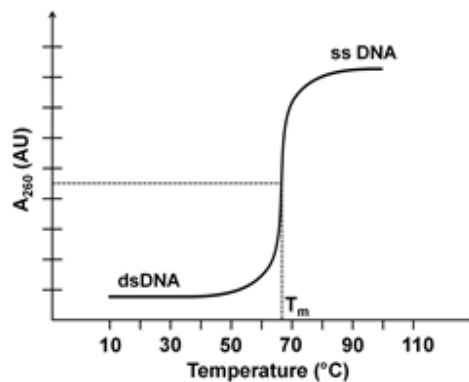


Figure 1. 6. Typical DNA melting curve. Source: <http://nptel.ac.in/courses/102103047/module2/lec7/1.html>

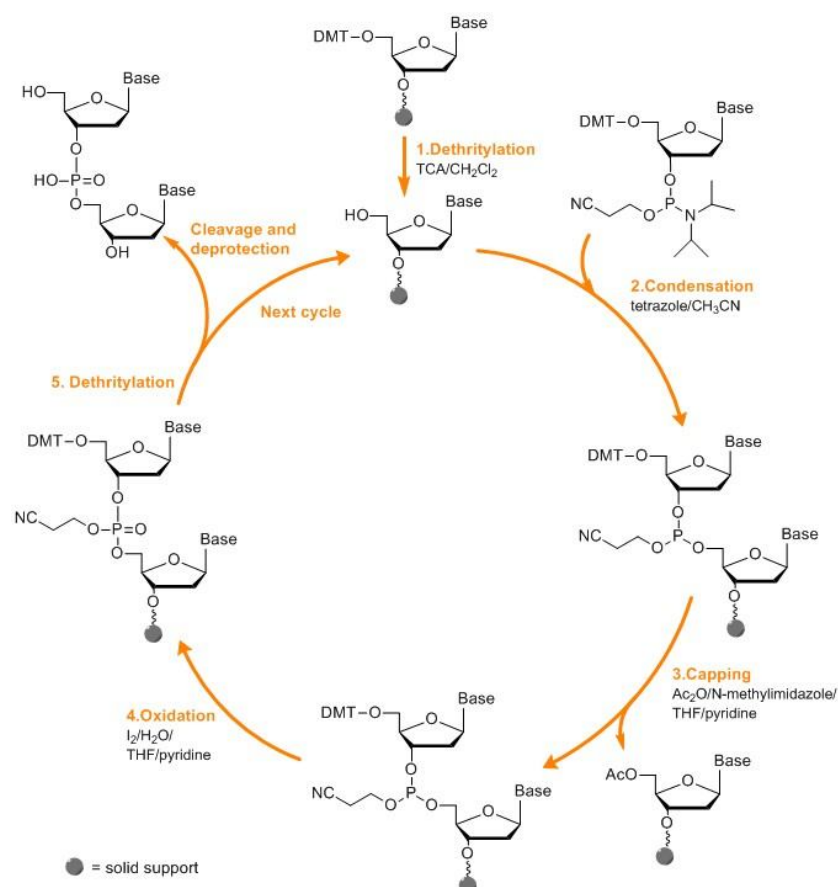
1.4. Artificial DNA synthesis

Since the origin of life, the production of DNA was confined only in living organisms and limited to their evolutionary established sequences. Within the last 70 years, many advances were made in the understanding of the nucleic acid structure¹ and its replication mechanism⁶ paving the way to the development of artificial methods for DNA manufacturing.

Among those strategies, polymerase chain reaction (PCR) is an enzymatic reaction in which a fragment of DNA having known or unknown sequence is exponentially amplified generating a high amount of copies of the original DNA template. PCR is based on the activity of the enzyme DNA polymerase, which is able to synthesize a new DNA strand complementary to the template by adding single nucleotide triphosphates onto a preexisting 3'-OH of a so called primer.

A further approach is represented by the chemical synthesis of short single-stranded DNA, namely oligonucleotides (from greek *oligos*, few). Since the 1950s many synthetic routes, like the phosphodiester⁷, phosphotriester⁸ or H-phosphonate⁹ methods were disclosed. Nevertheless, these laborious procedures are replaced nowadays by the phosphoramidite method¹⁰, which results in higher yields and can be enhanced by the application of solid-phase technology and automation. This synthetic strategy is based on the use of nucleoside 3'-(2-cyanoethyl-N,N-diisopropylphosphoramidite), shortened as phosphoramidite, added one by one in a sequence specific manner, from 3' to 5' direction. The 3' nucleosides is already loaded on the solid support, which is usually constituted by controlled pore glass (CPG) or polystyrene. The synthesis cycle depicted in scheme 1. 1 starts with a detritylation step in which the 5'-DMT protecting group (DMT = 4,4'-dimethoxytrityl) of the first nucleoside is removed by a weak acid. The next step is the *in situ* activation of the following phosphoramidites by means of tetrazole or one of its derivatives. The activated phosphoramidites reacts with the free 5'-hydroxyl group of the support-bound nucleoside generating a phosphite triester bond. The following capping step provides capping of unreacted phosphoramidites, preventing this molecules to participate to further oligonucleotides elongation steps. Finally the trivalent phosphite triester is oxidated to the

correspondent pentavalent phosphotriester. At this point the cycle can be repeated as many times as necessary until the full-length oligonucleotide is obtained.



Scheme 1. 1. Solid phase oligonucleotides synthesis cycle.

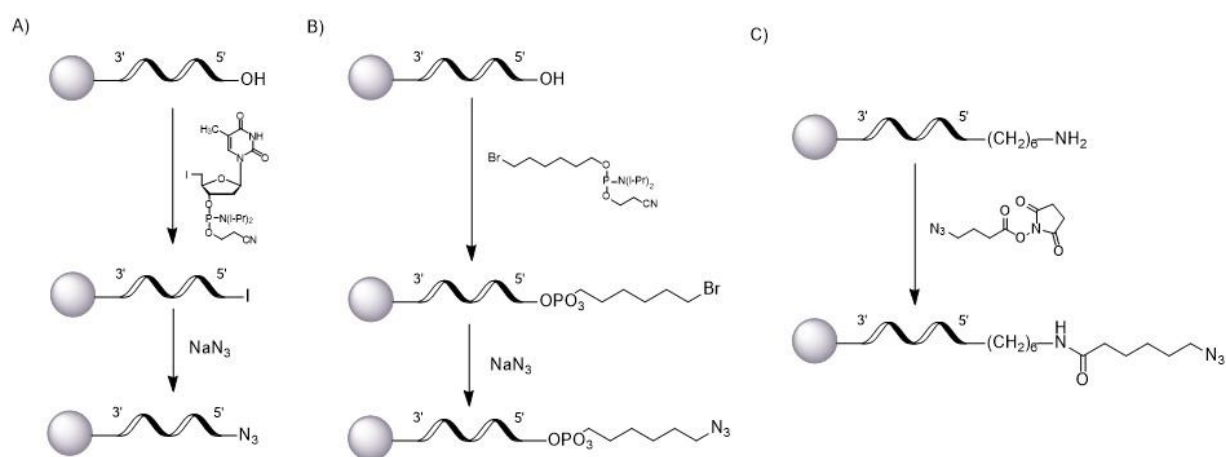
The continuous improving of the synthesis procedure and automation lead to the decrease of manufacturing time and costs, encouraging further the use of oligonucleotides in diverse scientific fields.

1.5. Incorporation of modifications into nucleic acids

The introduction of functional groups within nucleic acids is a key aspect for new DNA diagnostic strategy, such as prenatal, disease and cancer screening, and it can be achieved through different procedures.

For instance, modified nucleotide triphosphates can be incorporated in DNA during PCR. Several research groups demonstrated that dNTPs bearing a broad variety of chemical modifications (amino groups,¹¹ fluorescent groups,¹² click reactive groups¹³) can be easily incorporated in DNA strand by using a suitable DNA polymerase and optimized reaction conditions.

Moreover, solid phase synthesis is another reliable method to introduce modification within oligonucleotide sequences through the use of phosphoramidites already carrying the modifications. In this way, among others, fluorescent labels, biotin, alkyne and amino groups, can be easily introduced. Conversely, the phosphoramidite-mediated incorporation of an azide group is problematic because of the reaction of the N_3 group with the phosphorus(III) of the phosphoramidites *via* Staudinger reaction during the synthesis.¹⁴ To avoid this undesired reaction, N_3 groups are inserted post-synthetically with different strategies (Scheme 1. 2). The insertion of an azide group at the 5' terminus of the oligonucleotide can be effectively achieved by the incorporation of either 5'-iodo or 5'-bromohexyl phosphoramidites and subsequent displacement of the halogen atom with NaN_3 (Scheme 1. 2 A and B).¹⁵ Another efficient strategy for azide functionalization conceives the use of an amino modified oligonucleotide which is reacted with an azide N-hydroxysuccinimide (NHS) ester.¹⁶ This versatile method is employed for modification either at the 3'-end or at the 5'-end of the oligo, or even for internal modification on amino residues within the sequence (Scheme 1. 2 C).

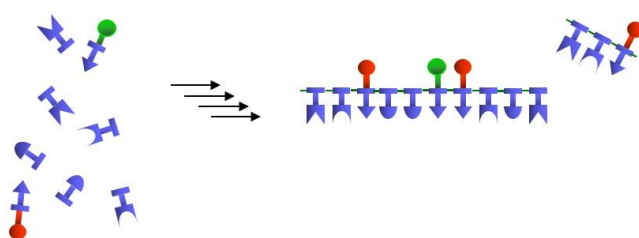


Scheme 1. 2. Azide group insertion strategies. A) Incorporation of an iodine at the 5'-end during the solid phase oligonucleotide synthesis and consequent conversion to an azide group by means of NaN_3 ; B) Incorporation of a bromine at the 5'-end during the solid phase oligonucleotide synthesis and consequent conversion to an azide group by NaN_3 ; C) An amino-modified oligonucleotide is reacted with a NHS-azido-linker.

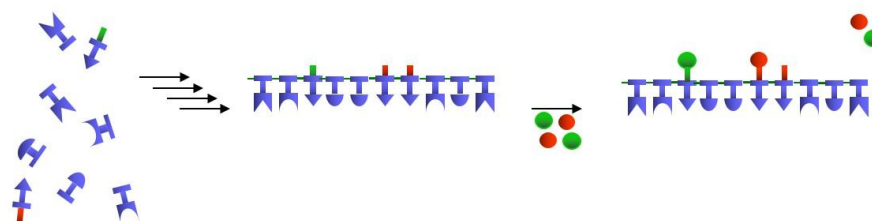
The detection of labeled nucleic acids is a key aspect in many research fields like diagnostic, medicine and nanotechnology. There are two approaches to perform labeling on oligonucleotides: pre- and post-synthetic (Fig 1. 3). In the pre-synthetic labeling approach the nucleotide carries the label before its incorporation into the DNA. In the pre-synthetic strategy the modified nucleotides need to be resistant to the harsh synthesis and deprotection conditions during solid phase oligo synthesis. Differently, in the post-synthetic method nucleotides bearing reactive moieties are incorporated in the strand during the DNA synthesis and are labeled only afterwards.

The post-synthetic strategy implies an additional coupling step, but on the other hand, it has the advantage to enable conjugation of nearly any kind of label.

A) Pre-synthetic:



B) Post-synthetic:



■ **handle / linker**
● **label / dye**

Figure 1. 7. Oligonucleotides labeling strategies. A) Pre-synthetic labeling. The nucleotides bearing the label are inserted during the oligonucleotide synthesis cycle. B) Post-synthetic labeling. Nucleotides bearing reactive moieties are incorporated in the strand during the DNA synthesis and afterwards they undergo labeling.

The easy modification of oligonucleotides - in particular with alkyne and azide groups - and the wide choice of azide/alkyne tags, elects click chemistry as a powerful method for labeling of nucleic acids.

1.6. Click chemistry

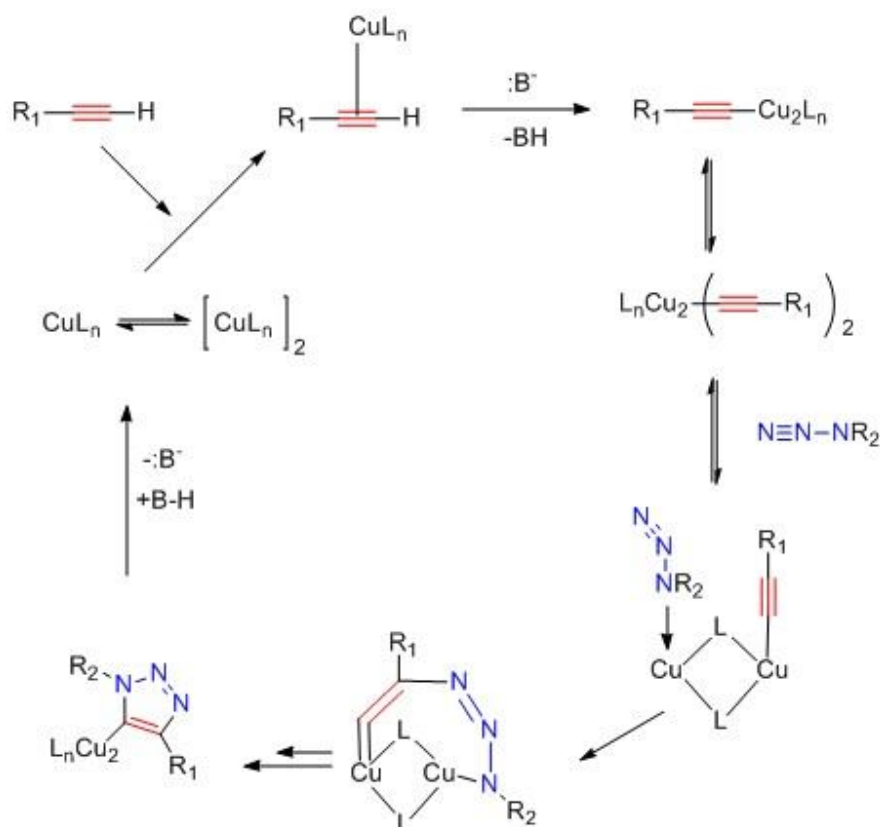
The term click chemistry denotes a category of chemical processes which show some common criteria elucidated by B. Sharpless in 2001.¹⁷ The reactions belonging to this group should e.g. be modular, wide in scope, give very high yields, stereospecific and generate only inoffensive byproducts that can be removed by non-chromatographic methods. Furthermore the process should be insensitive to oxygen and water, use benign solvents or even no solvent and the starting reagents have to be readily available. The products of click chemistry reactions must require simple isolation, such as distillation or crystallization, and they have to be stable under physiological conditions.

The Huisgen 1,3-dipolar cycloaddition, originally studied by Prof. Rolf Huisgen in the 1960's at the university of Munich (LMU), fulfills several of the click chemistry criteria. The reaction between an azide and an alkyne yields a mixture of two regioisomers, the 1,4 and 1,5 triazoles (Scheme 1.3).¹⁸ Nevertheless, this reaction needs high temperature and long reaction times.



Scheme 1. 3. Huisgen reaction. The reaction between a terminal alkyne and an azide gives a mixture of the two regioisomers 1,4 and 1,5 triazoles.

The regioselectivity and the kinetic of the Huisgen 1,3-dipolar cycloaddition were dramatically improved by the use of metallic catalysts as independently reported in 2002 by Sharpless¹⁹ and Meldal.²⁰ The reaction between a terminal alkyne and an azide carried out in presence of monovalent copper ions – Cu(I) – leads to only one regioisomer, the 1,4 triazole. Moreover the reaction rate is increased up to 10^7 times avoiding the use of high temperature. This copper(I)-catalyzed azide-alkyne cycloaddition (CuAAC) most fulfills the requirements listed from Sharpless in the click chemistry concept and is the most used click chemistry variant nowadays. The sources of Cu(I) include Cu(I) salts, such as copper bromide (CuBr) or copper iodide (CuI),²⁰ *in situ* reduction of divalent copper ions – Cu(II) – such as copper sulfate (CuSO₄)¹⁹ and comproportionation of Cu(I) and Cu(II).²¹ A plausible mechanism (Scheme 1. 4) of the reaction^{21b} starts with the formation of a pi complex, called Cu acetylide, between a terminal alkyne and Cu(I). Subsequently, the azide displaces one ligand to generate a copper-azide-acetylide complex and the cyclization occurs. This step is followed by protonation, leading dissociation of catalyst-ligand complex and to product formation. The use of nitrogen-based ligands in CuAAC accelerates further the reaction by protecting the copper(I) from oxidation in presence of oxygen. The widest used ligands are Tris[(1-benzyl-1H-1,2,3-triazol-4-yl)methyl]amine (TBTA) and its water soluble variant Tris(3-hydroxypropyltriazolylmethyl)amine (THPTA).



Scheme 1. 4. Copper(I)-catalyzed azide-alkyne cycloaddition (CuAAC) mechanism.

More recently, other mechanisms involving a kinetically favored bis-copper acetylide complex were proposed.²²

The “click-reactive” groups, namely azide and alkyne, have weak acid-base properties that make them almost inert towards biological molecules and living cells environment. This property - called bio-orthogonality – together with the formation of stable and non-toxic triazole and all the above listed characteristics make click chemistry one of the favorite methods for the functionalization of many classes of biomolecules, such as nucleic acids and proteins.

1.7. Click chemistry on DNA

During the years, click chemistry demonstrated its wide applicability in many sectors such as drug discovery, surfaces modification or supramolecular structure synthesis among others. The adoption of CuAAC as bioconjugation method for nucleic acids was extensively investigated by Prof. Thomas Carell from the LMU Munich resulting in the founding of the spin-off company baseclick GmbH.

The broad application spectrum of oligonucleotides and their derivatives for diagnostic and therapeutic purposes, delivered the need to add functionalities on DNA. Besides other labeling methods, such as amino-NHS ester chemistry, click chemistry is routinely used thanks to a clean, high yielding and mild conditions accomplishment. Preferably, the attachment of alkyne chains on DNA occurs on the 5-position of pyrimidines or at the 7-position of purines. Thus additional functional molecules attached to these alkynes protrude in the major groove of the double helix resulting in a minor interference in the hybridization with a counterstrand. Seela and coworkers, indeed demonstrated using melting point analyses the stabilizing effect of the oct-1,7- diynyl side chains when situated in the 5-position of the 2-deoxycytidine or in the 7-position of 7-deaza-2'-deoxyguanosine.²³

Carell's group studied intensively the click reaction on nucleic acids, successfully demonstrating incorporation of diverse alkyne modified nucleotides in oligonucleotides²⁴ and triphosphates in DNA during PCR.¹³ The alkyne-modified strands that underwent a click reaction show quantitative labeling rates, when different classes of azides, such as coumarin, fluorescein and sugar azide were tested. The group has shown that in the latter case, the sugar molecules can act as hindered aldehyde source, necessary for Ag cluster formation in metallization processes.²⁵ Another attempt of metallization was achieved by labeling alkyne modified DNA strand with gold nanoparticles.²⁶ Furthermore, selective labeling with different azides on the same oligonucleotide proved the extreme versatility of the click reaction.²⁷

1.7.1. *In vitro* application: DNA synthesis detection using EdU

A further application of click chemistry is the detection of DNA synthesis *in vitro* and *in vivo*, which is an important parameter to monitor during the test of e.g. pharmacological agents. To this end, the nucleotide 5-ethynyl-2'-deoxyuridine (EdU) is added to cells and thanks to the structural similarity between the alkynyluridine and the thymidine, the modified nucleotide is incorporated by the polymerase into DNA during the S-phase of the cell cycle.²⁸ After fixation and permeabilization of the cells the genomic DNA is stained *via* click reaction with an azide-fluorescent dye to quantify the rate of DNA synthesis and thus cell proliferation. The method was adopted for DNA detection in tissue of living mice, as well, exhibiting high efficiency and low toxicity against the test animals. This new technique has many advantages respect to the already established methodology of the field, which required the use of either a radioactive compound ([³H]thymidine) or the nucleotide bromodeoxyuridine (BrdU) which implies a time-consuming immunological staining.

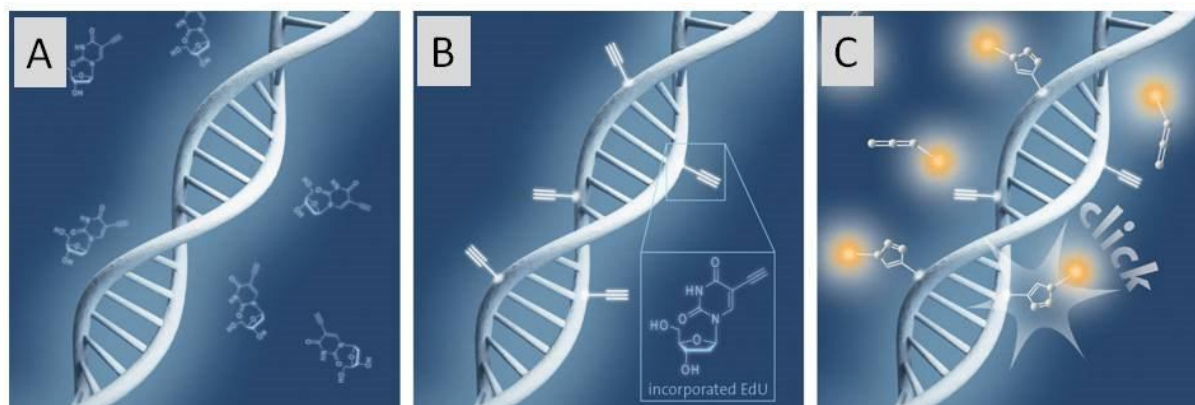


Figure 1. 8. EdU proliferation assay. A) Cells are incubated with EdU (5-ethynyl-2'-deoxyuridine); B) EdU is incorporated into DNA during active DNA synthesis in proliferating cells. C) Detection of newly synthesized DNA with a click chemistry procedure using fluorescent dye azides. Source: <https://www.baseclick.eu/>

1.8. Nanotechnology

The term nanotechnology refers to all objects with size between 1 and 100 nanometers, namely one billionth of a meter. The concept behind nanotechnology arose in 1959 from the talk of the physicist Richard Feynman "There is plenty of room at the bottom", in which he visionary described how to control and manipulate "things on a small scale".²⁹ In 1974, Professor Norio Taniguchi coined the term nanotechnology, describing the creation of semiconductor structures with nanometric precision.³⁰ The development of the Scanning Tunnelling Microscope (STM), which worth the Nobel Prize in physics in 1986 to G. Binnig and H. Rohrer, and derivatives microscopy techniques lastly empowered the growth of the modern nanotechnology. The manufacturing of objects at the nanoscale, namely nanomaterials, can be achieved with a top down approach, for example lithography, starting from a bulk material down to the nanoscale level. On the other hand, with the bottom up approach the manufacturing of nanomaterials of desired size and shape begins by complexing together single atoms or molecules by self-assembly or molecular recognition processes. At the nanoscale the materials present different physical, chemical and mechanical properties, extremely dissimilar from the one exhibited at the macroscale. For example, at the macroscale, carbon in form of graphite is soft, but at the nanoscale, carbon organized in nanotube shape present high strength and stiffness. Allotropes of carbon, such as carbon nanotubes, fullerenes and diamondoids, are well-known nanomaterials and are envisioned for applications in mechanical, energetic and medical field.³¹ Nanoparticles are one of the most appealing nanomaterials at our time, thanks to their easy preparation, functionalization and dimensional control.³² Nanostructures made of DNA constitute another class of nanomaterials which is gaining importance during the last 30 years. Nanotechnology is widely applied in the medical field for drug delivery, diagnostic, cancer treatment and gene therapy.³³ In this area DNA-based materials, in comparison to some inorganic nano-objects, have the great advantage to be biocompatible and degraded in biological

system preventing accumulation and toxicity issues. The structures of DNA objects are based on the self-assembly feature of nucleic acids and can be precisely predicted and modified for a specific purpose.

1.9. Structural DNA nanotechnology

Structural DNA nanotechnology implies the use of DNA molecules to create new objects at the nanometer scale. In this definition the term structural gains great relevance because it means that the DNA is considered a building material and not only a genetic carrier. Since the beginnings, this field was highly promising thanks to the extended knowledge of scientists on DNA thermo-dynamics^{34,4} and the rapidly falling costs and increasing quality of DNA synthesis.³⁵ The most appealing feature of DNA nanostructures is the highly predictable geometry and therefore the nanometer-precise positioning of nanoscale objects within their structure.³⁶ The crucial work, dated back to 1982, which initiated the field of DNA nanotechnology has to be attributed to Nadrian Seeman.³⁷ Pursuing his vision of using 3D DNA lattices as template to organize proteins to facilitate their crystallographic characterization, he designed DNA strands which assembled into immobile Holliday junctions. In 1991 Seeman and coworkers experimentally demonstrated the first DNA nanostructure.³⁸ This three dimensional cube was manufactured starting from branched DNA junctions, which are hold together with “sticky ends”, namely ssDNA extensions able to connect one unit to another exploiting the Watson and Crick base pairing.

In the following years lots of advancements in structural DNA nanotechnology were made leading to the development of new assembly strategies: DNA origami, scaffold free single-stranded tile assembled (SST) and polyhedral meshes. All these methods are based on the same fundament, namely DNA self-assembly, but each of them retains specific features addressable to diverse applications. Nowadays, the easy production of complex and dynamic structures broadens the DNA nanotechnology application range, with the consequent effect of an increasing number of new companies interested in this emerging field.

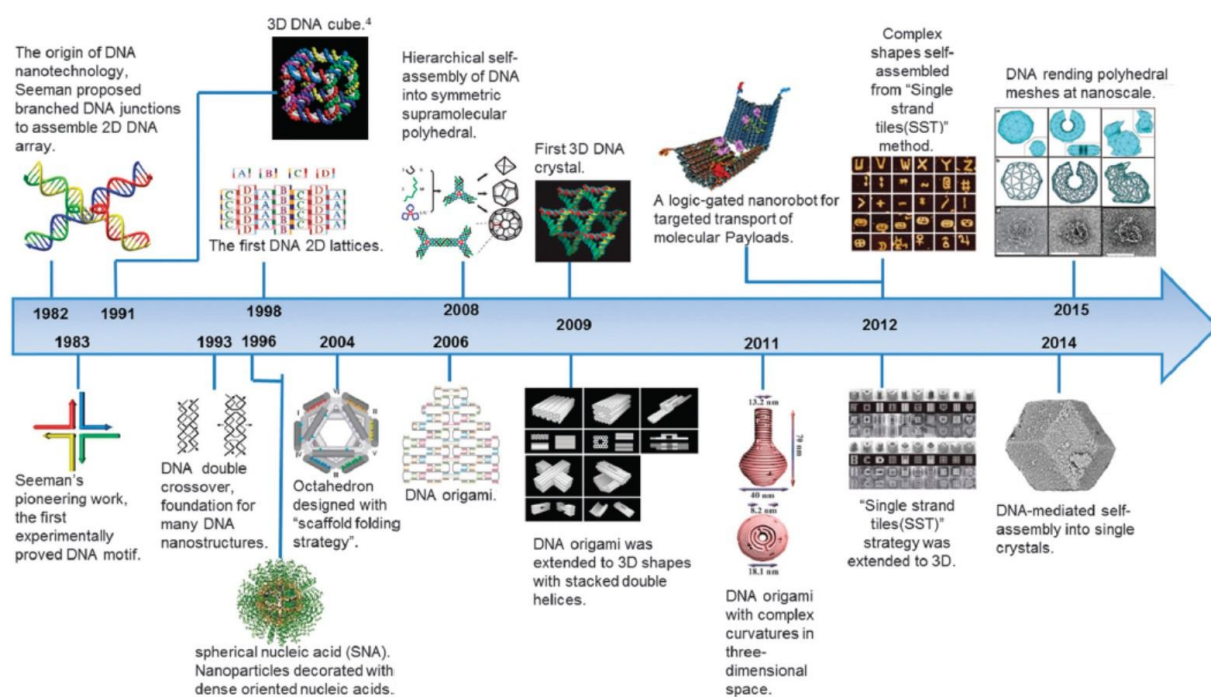


Figure 1. 9. Development of DNA nanotechnology over the years. Adapted from "Cellular processing and destinies of artificial DNA nanostructures" by D. S. Lee, H. Qian, C.Y. Tay, D.T. Leong, *Chem. Soc. Rev.* **2016**, 45(15), 4199-225.

1.9.1. Tile-based method

The tile-based approach was typical of the first examples of DNA nanostructures, in which only few DNA strands were used. Single-stranded DNAs were designed to form building blocks, so-called tiles, that can be combined together to form more complex structures. These fundamental elements contain crossovers and are used principally to confer rigidity to the structure.³⁹ Crossovers occur when double helices contain two or more positions where a single strand switches to the neighboring helix. Double crossovers (DX) are structure consisting of two helical domains and two crossovers,⁴⁰ while triple crossovers (TX) are tiles composed by three helical domains and two crossovers junctions between each domain (Fig 1. 10).⁴¹

In 1998, Winfree and coworkers, applying the knowledge on DNA tiles and sticky ends, demonstrated the assembly of micrometre-sized periodic DNA lattices.⁴²

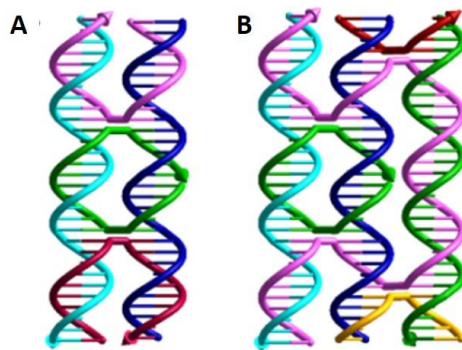


Figure 1. 10. DNA crossover models. A) Double DNA crossover (DX). B) Triple DNA crossover (TX). Adapted from "Structural DNA nanotechnology: from design to application" R. M. Zadegan, M. L. Norton, *Int. J. Mol. Sci.*, **2012**, 13(6), 7149-7162

1.9.2. DNA origami method

A decisive moment in the history of DNA nanotechnology was the year 2006 when Paul Rothemund reported the development of a new technique called DNA origami, naming it after the Japanese art of folding paper. Similarly, this method includes the folding of a long single strand DNA, named scaffold, into predetermined two-dimensional shapes using a set of complementary short oligonucleotides here called "staples". In his pioneering work⁴³ he used the genomic ssDNA from the M13 phage as scaffold strand (7249 nucleotides) and designed a set of 200 short "staple" strands which selectively bind to distinguished regions of the scaffold and fold it into shapes that are roughly 100 nm in diameter and have a spatial resolution of 6 nm (Fig 1. 11). The single strand genome of the M13 phage (M13mp18) is only one of the scaffolds used to assemble DNA origami. For instance, double stranded scaffold were used to fold simultaneously two different shapes of origami⁴⁴ or larger structures were folded using a PCR-amplified scaffold 26kb long.⁴⁵

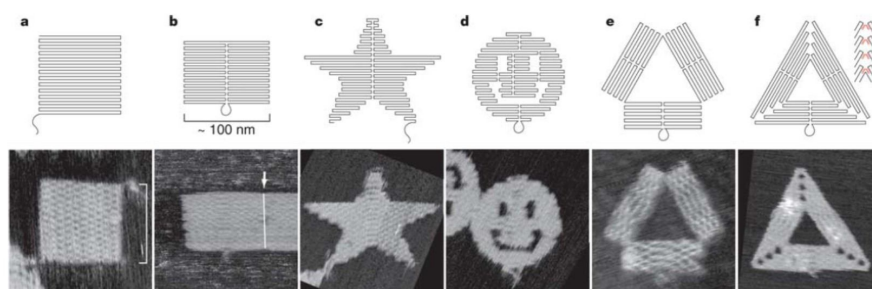


Figure 1. 11. DNA origami shapes. Top row, folding paths. A) square; B) rectangle; C) star; D) smiling face; E) triangle with rectangular domains; F) sharp triangle with trapezoidal domains. Bottom row, AFM images from the actually synthesized structures. Adapted from "Folding DNA to create nanoscale shapes and patterns", *Nature*, **2006**, 440 (7082), 297-302.

In the following years, Shih and his group developed further the DNA origami concept extending the design to the third dimension. He described two geometries of assembly: one based on honeycomb lattice⁴⁶ and the second relying on square lattice.⁴⁷

Another method to create 3D DNA origami structures is to combine 2D elements and connect them with sticky ends to obtain three dimensional objects. A well know example obtained with this strategy was a box with opening lid described by Andersen et al⁴⁸ (Fig 1. 12). Furthermore, exploiting the possibility to adjust the number of bp per helical turn, Han showed how to introduce curvature within the structure. The modulation of crossovers spacing between adjacent helices causes bending of the structures. Using this knowledge, different shapes, such as spheres, ellipsoids and a nanoflask, were created.⁴⁹

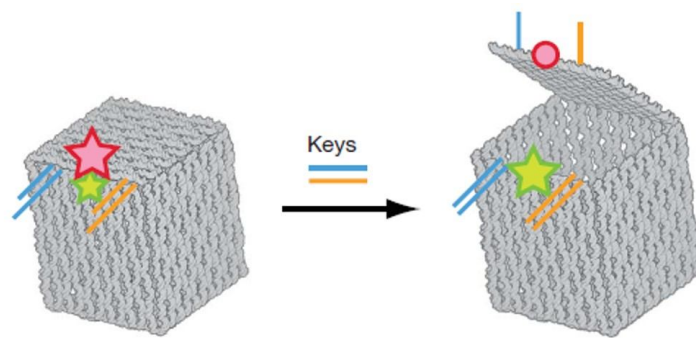


Figure 1. 12. DNA origami box with programmable opening lid. Adapted from “Self-assembly of a nanoscale DNA box with a controllable lid”, E. S. Andersen, M. Dong, M. M. Nielsen, K. Jahn, R. Subramani, W. Mamdouh, M. M. Golas, B. Sander, H. Stark, C. L. P. Oliveira, J. S. Pedersen, V. Birkedal, F. Besenbacher, K. V. Gothelf, J. Kjems, *Nature*, **2009**, 459 (7243), 73-76.

1.9.3. Scaffold-free Single Strand Tile assembly (SST)

Another assembly approach is the “Single Strand Tile” (SST) assembly method firstly investigated by Peng Yin.⁵⁰ In this strategy 42mer single stranded DNA strands consists of four domains each of them hybridize with four local neighboring sequences during the self-assembly procedure (Fig 1. 13). Each of those units, called also tiles or bricks, can be combined to assemble complex 2D shapes and tubes of various lengths.

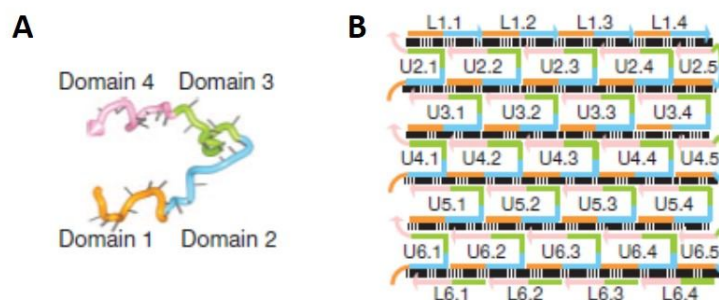


Figure 1. 13. A) Single-Stranded Tile (SST) motif; B) Design of an SST rectangle structure diagram. Adapted from “Complex shapes self-assembled from single-stranded DNA tiles”, B. Wei, M. Dai, P. Yin, *Nature*, **2012**, 485 (7400), 623-626.

The same research group extended the SST method to create 3D structures.⁵¹ In this approach, the tiles are 32 nucleotides long containing four 8-bases domains (Fig 1. 14A). Yin depicted this assembly as a LEGO-like model, in which each tile is considered a brick with 2 plugs (tail domains) and two holes (head domains). A tail domain hybridizes with the head domain of another brick forming a 90° angle, representing in the LEGO model the insertion of a plug in a hole (Fig 1. 14B). This insertion is only allowed between plugs and holes which have complementary sequences and matching polarity. Using this assembly approach Yin demonstrated the construction of 102 distinct 3D objects with sophisticated shapes, interior cavities and tunnels (Fig 1. 14C).

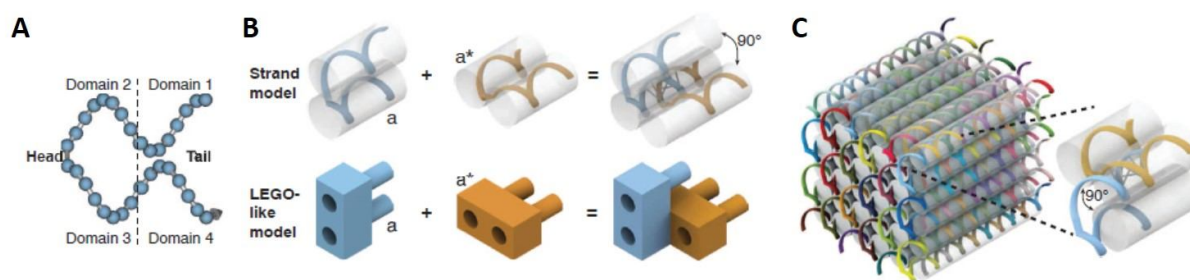


Figure 1. 14. DNA brick structures resembling LEGO constructions. A) Four-domain structured single-stranded DNA brick; B) Two-bricks assembly. Each brick hybridizes with a second one due to two complementary domains forming a 90° dihedral angle; C) Molecular model of a cuboid 3D DNA structure. Adapted from “Three-Dimensional Structures Self-Assembled from DNA Bricks” by Y. Ke, L. L. Ong, W. M. Shih, Y. Peng, *Science*, **2012**, 338 (6111), 1177-1183.

1.9.4. Polyhedral mesh

Recently, Björn Högberg's group developed a new method to create arbitrary polygonal meshes of DNA, very difficult to realize with previous strategies.⁵² Differently from DNA origami, which have a closed packed arrangement, these new structures have a double helix as a structural element and a more open conformation (Fig 1. 15). Thanks to these features polyhedral mesh objects have a reduced need of salt concentration for their stability, bringing them closer to applications in a real biological environment.

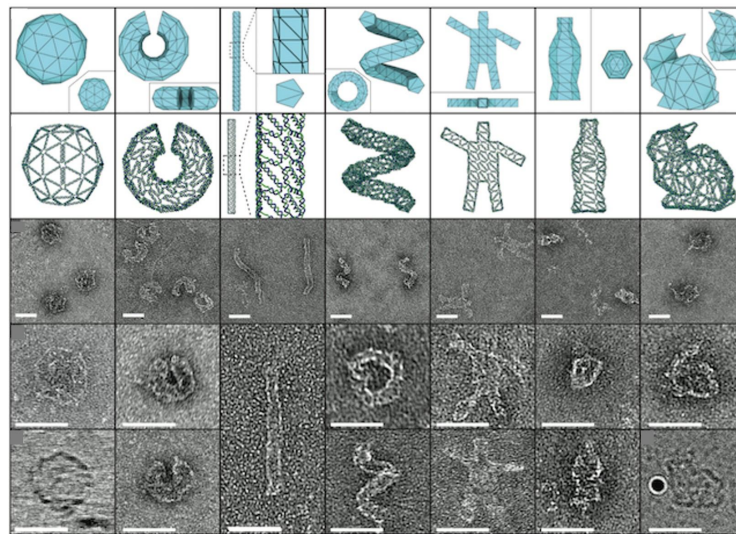


Figure 1. 15. Examples of Polyhedral mesh design (upper lanes) and TEM images (lower lanes). Adapted from "DNA rendering of polyhedral meshes at the nanoscale", E. Benson, A. Mohammed, J. Gardell, S. Masich, E. Czeizler, P. Orponen, B. Högberg, *Nature*, **2015**, 523 (7561), 441-444.

1.10. Design

At the beginning of its study, DNA origami designs were prepared by hand and/or by various "home-made" softwares. This was a long and error-prone procedure, which turned out to be impracticable when the structures started to become more complex. The first origami design software published was the sequence editing program SARSE that allowed to import a bitmap image and convert it to a 2D origami design.⁵³ A year later, a more user friendly program, caDNAno, was presented.⁵⁴ In this software the user routes the scaffold through the desired shape and then the program suggest automatically the positioning of the staples. Once the scaffold sequence is known, caDNAno calculates also the staple sequences. Releasing new versions and 3D viewer plugins, made caDNAno one of the preferred design softwares present.

1.11. Annealing procedure

The folding of DNA nanostructures is the step in which strands find their own complementary sequence on other strands or on the scaffold. A crucial aspect in this procedure is the salt concentration. As already explained above, DNA backbone is negatively charged and cations are required to lower electrostatic repulsion between strands. For this reason, folding buffers contain magnesium chloride as source of divalent cations (Mg^{2+}).^{43, 50} It was also showed that monovalent sodium ions (Na^+) are able to coordinate the negatively charged phosphate residues of the DNA and therefore decrease the repulsion between strands.⁵⁵ In SSTs folding the strands are mixed in 1:1 ratio in buffer, usually Tris-EDTA (TE) enriched with cations, while DNA origami assembly is achieved by mixing a scaffold with an excess of staples, normally from 5 to 10 fold. The folding mixture is heated up to temperatures typically in the range 80°C - 95°C to ensure denaturation of randomly formed secondary structures of single-stranded DNA. Afterwards the mixture is cooled down to room temperature over few hours till days. The concentration of salts in the folding buffer and the heating/cooling ramp are different for each structure and they need to be tuned whenever a new object is designed. Dietz's group also demonstrated that a correct folding of DNA origami can be achieved at constant temperature and in a short time-span (less than 1 hour).⁵⁶ Moreover, Jungmann et al. accomplished precise folding of 2D and 3D DNA origami structures at constant temperature but lowering the concentration (from 85% to 1%) of a denaturing agent, such as formamide.⁵⁷ After the folding process DNA origami objects coexist in a mixture with an excess of staples and only partially folded structures, hence they need a purification step to obtain a pure product. A routinely used purification method is agarose gel extraction. After agarose gel electrophoretic analysis well-folded objects are identified as a distinct band separated from aggregates and unincorporated strands which migrate differently. The band of interest is physically excised from the gel and DNA is extracted from the agarose matrix using different procedures.^{46, 58} Rate-zonal centrifugation provides higher yield of purified structures by separation of the folding mixture on a glycerol gradient.⁵⁹ An alternative method to obtain pure DNA nanostructure is the use of poly(ethylene glycol) (PEG) as a precipitation agent.⁶⁰ This approach allows additionally to concentrate the sample and exchange the buffer in which the structure is dissolved.

1.12. Characterization techniques for DNA nanostructures

Assembly of DNA nanostructures can be investigated by different techniques. One of the most accessible method is agarose gel electrophoresis, which allows the identification of the correctly folded structure since it migrates differently from unincorporated strands and aggregates. Visualization of the structure is obtained by recently developed microscopy techniques, such as Atomic Force Microscopy (AFM) and Transmission Electron Microscopy (TEM). The latter technique has been further improved resulting in the developing of cryo-electron microscopy (Cryo-EM). This methodology provides imaging of structures in their native state without the use of any staining.

1.13. DNA nanostructures applications

Since the early progresses of the field, the power and versatility of DNA origami was immediately recognized creating a variety of structures addressed to different applications. Shih and coworkers designed a six-helix bundle able to help the structure determination of membrane proteins by nuclear magnetic resonance (NMR).⁶¹ They showed that these nanotubes act like a detergent-resistant liquid crystal to induce weak alignment of proteins, allowing an accurate measurement of backbone residual dipolar couplings. DNA origami can be seen as a platform for the precise placement of various molecules such as proteins, fluorophores or nanoparticles and the study of their behavior at the nanoscale. Fu and coworkers positioned in close proximity enzymes on a rectangular DNA origami and demonstrated an enhanced catalytic activity in the origami-organized protein cascade.⁶² Fluorescent molecules were also placed on DNA origami at defined position and distance allowing study on Försters Resonance Energy Transfer (FRET)⁶³ and creation of brightness standard⁶⁴ and nanoscopic rulers.⁶⁵ Moreover, DNA nanotechnology can be applied also to super-resolution microscopy techniques such as PAINT (points accumulation for imaging in nanoscale topography). Jungmann et al, recently applied this methods on DNA nanostructures generating the DNA PAINT technique.⁶⁶ In this application the stochastic switching between fluorescent on- and off-state is carried out by transient binding of fluorescently labeled oligonucleotides (imager strands) to complementary (docking) strands on the origami. This technique was further implemented enabling important application such as FISH (Fluorescent in situ Hybridization) assays,⁶⁷ single-molecule detection of miRNA and precise discrimination between single nucleotide polymorphisms.⁶⁸ Furthermore, DNA structures were used to organize inorganic nanoparticles to study their plasmonic properties. Liedl's group arranged gold nanoparticles in a helical shape on a 24-helix bundle demonstrating a strong plasmonic circular dichroism and tunable plasmonic properties.⁶⁹ An origami-mediated precise organization of gold nanoparticles can also lead to the creation of a plasmonic hotspot in which the fluorescence of a dye can be increased hundred-fold (Fig. 1.16).⁷⁰ Metallic clusters can be deposited on a DNA origami by gold enhancement⁷¹ or reaction of silver ions on aldehyde groups⁷² leading to a continuous metallization of the structure. The programmability feature of DNA nanotechnology is very advantageous in this sense, offering an alternative to the conventional top-down lithography for nanoelectronics applications.

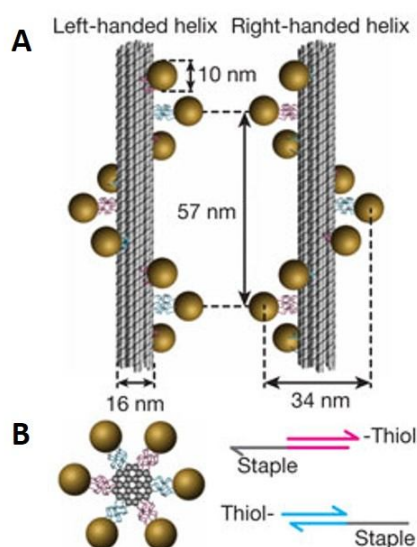


Figure 1. 16. A) 24-helix bundle DNA origami as a platform for the spatial organization of nine gold nanoparticles with either left- or right-handed orientation. B) 10 nm gold nanoparticles are attached to the helices using sticky-ends. Adapted from “DNA-based self-assembly of chiral plasmonic nanostructures with tailored optical response” A. Kuzyk, R. Schreiber, Z. Fan, G. Pardatscher, E. Roller, A. Hoge, F. C. Simmel, A. O. Govorov, T. Liedl, *Nature*, **2012**, 483 (7389), 311 – 314.

Furthermore, chemical reactions, like formation and cleavage of chemical bonds, were investigated at the single-molecule level by organizing reactive groups on a rectangular origami sheet.⁷³ Besides many other areas of interest, the biomedical field is an intriguing application domain for DNA nanotechnology thanks to its intrinsic biocompatibility, biodegradability and programmability. In the biomedical field the main target of nanotechnology is the cell with the primary aim to provide an efficient intracellular transport of drugs or therapeutics. The cellular membrane is the first obstacle to overcome in a cell delivery application, hence studies regarding interaction of membrane with DNA nanostructures were performed. Kocabey et al. created two different shapes of DNA origami which were anchored to a supported lipid bilayers exploiting the hydrophobic properties of cholesterol moieties attached to the origami.⁷⁴ With this system the researchers saw hierarchical formation of DNA origami arrays which could be used to help organization of protein complexes on the cytoplasmic membrane. Moreover, when this system is applied to a unilamellar lipid support bending of the membrane occurs encouraging the creation of DNA nanostructure mimicking the clathrin endocytotic pathway. Concerning interaction with cellular membrane, the creation of artificial nanopores has great relevance because it opens the way for the invention of new transport methods across the lipid bilayer. Simmel’s group created the first DNA origami transmembrane nanopore.⁷⁵ The structure was retained within the membrane thanks to 26 cholesterol molecules and showed an ions conduction similar to the natural pores. DNA nanopores were also used with a cytotoxic effect; in this case they served to span the membrane inducing cell death.⁷⁶ In respect to the shape, some DNA nanostructures are able to enter different types of cells with high efficiency without the help of transfection agents.⁷⁷ DNA origami were demonstrated as effective carriers for the anticancer drug Doxorubicin from many studies.⁷⁸ This drug on its own is characterized by

low solubility in aqueous media and causes undesirable side effects, hence a carrier that minimizes those features is desired for its administration in living systems. Doxorubicin's intercalation in DNA occurs especially in GC-rich regions of the DNA. Once it is loaded in DNA nanostructures anyhow, it shows the capability to circumvent drug-resistance in some cell lines.^{78a} The great versatility of functionalization on DNA nanostructure is an important feature to be exploited for targeted cell delivery purposes. The addressing to specific cellular types is of fundamental relevance in medical applications, for example when the treatment of cancer cells is desired or the release of the drug has to be triggered only in presence of particular conditions. The DNA box created by Andersen et al, is the first example of cargo origami structure with a lid controlled by a lock and key system that can be open only in presence of a specific oligonucleotide sequence by strand displacement.⁴⁸ Another example of dynamic opening structure is offered from a barrel-shape nanorobot bearing an aptamer-encoded logic-gate.⁷⁹ In this work, Douglas et al. demonstrated its opening in presence of the "right key" only and its capability to expose the payload for the binding on cell surface. Functionalization of DNA nanostructures with transfection agents was also demonstrated as a strategy to achieve targeted delivery. Lee organized targeting agents like folate and peptides on a tetrahedral structure, and tested the structure for targeted delivery of siRNA in cells and in mice.⁸⁰ He showed that a minimum of three folate groups in a specific spatial orientation is required to obtain a successful delivery of the structure and subsequent silencing of the associated luciferase gene. Besides DNA origami, also SSTs structures were used as delivery system into cells. Kocabey, in collaboration with the author, used a six-helix SSTs nanotube equipped with folate-modified strands for targeting and siRNA as therapeutic. In this case the specificity of the folate-uptake was not clear (further details on the work are discussed in chapter 2). Another therapeutic agent, which takes advantage of delivery *via* DNA nanostructures is the CpG motif. This unmethylated sequence is typical for bacterial genomes and stimulates an inflammatory response in mammalian immune cells. It has been discovered that CpG motifs are recognized by Toll-like receptors (TLR9) localized in endosome of the immune system cells and activate both the innate and the adaptive immune system producing cytokines, chemokines or antibodies. CpG motifs were attached to the edges of a tetrahedron structure and were efficiently delivered into macrophage-like cell triggering the secretion of the cytokines TNF- α , IL-6 and IL-12.⁸¹ Schüller et al. confirmed the induction of a strong immunitary response by using a hollow 30-helix bundle DNA origami tubes decorated with 62 CpG motifs.⁸² Recently, a SST tube was used to deliver CpG sequences into mice.⁸³ The "naked tube" did not show immune response in the living organism, but contrarily the CpG decorated structure was uptaken from macrophages and cause a strong immune response in consequence. The effective delivery of these synthetics oligonucleotides is envisioned as immunotherapy of infectious diseases, cancers, and allergies. An effective DNA origami transfection was also achieved by coating a rectangular shape structure with cowpea chlorotic mottle virus capsid proteins.⁸⁴ The viral protein had a positive charge at the N-terminus, which helped to contrast the negative charge of the DNA origami and led to high yield cell transfection.

1.14. Stability of DNA nanostructures

The use of DNA nanostructure for *in vitro* and *in vivo* assays is a fundamental practice for the establishment of future biomedical application. Thus, the structure stability in *extra*- and *intracellular* environment is an important aspect to take care about during those assays. DNA nanostructures are already more stable than simple oligonucleotides.⁸⁵ The lifetime of the latter in biological environment is

quite short because ssDNA are easily digested from nucleases. Complex DNA architectures on the other hand are more protected from specific and un-specific enzymes digestion. The difference in susceptibility against nucleases is due to the tight spatial organization of oligonucleotides composing the DNA nanostructures which may reduce the effective binding of the enzymes.⁸⁶ In biological assays nucleases attack is not the only destabilizing factor; indeed low cations concentration can negatively affect the folding of DNA nanostructures as well.

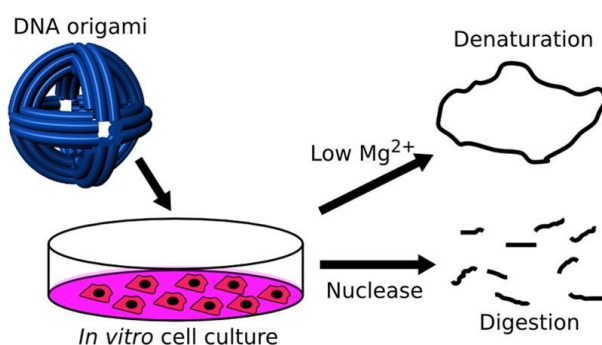


Figure 1. 17. Graphical representation of the stability issues that are encountered for DNA nanostructures when in contact with biological environment. Depletion of cations and nuclease digestion are destabilizing factors for DNA-based nanoarchitectures. Adapted from “Addressing the Instability of DNA Nanostructures in Tissue Culture” J. Hahn, S. F. J. Wickham, W. M. Shih, S. D. Perrault, *ACS Nano*, **2014**, 8 (9), 8765-8775.

Perrault and coworkers, studied thoroughly DNA origami behavior in cell culture medium recording a shape and time dependency regarding the sensitivity against low cation concentration.⁸⁷ Enzymatic digestion instead was proven to be not design dependent and became significant after 24 hours of incubation of DNA origami in cell culture medium supplemented with Fetal Bovine Serum (FBS). To increase its stability for *in vitro* applications, the researchers proposed to supplement cell culture medium with magnesium ions to maintain a correct structure and with actin to inactivate nucleases activity. These solutions were successful on the tested cell lines, but they may be not optimal for other assay set-ups. The stability issue of DNA nanostructures is mostly addressed by working on the structure itself than on the outer environment. Encapsulation of DNA octahedron into a virus-inspired lipid membrane demonstrated to confer protection against nuclease degradation. The PEGylated lipid bilayers anchored to the DNA nanostructure by means of 48 protruding “handle” helped to low the immune response as well.

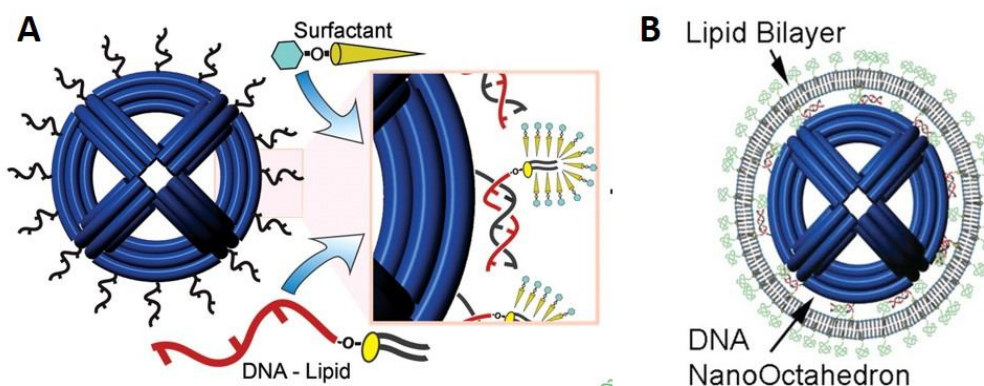


Figure 1. 18. Graphical representation of encapsulation strategy for DNA octahedron. A) Lipid–DNA conjugates are hybridized to protruding sticky ends in a surfactant solution that forms micelles around the conjugates. B) A lipid bilayer envelops the DNA octahedron. Adapted from “Virus-Inspired Membrane Encapsulation of DNA Nanostructures To Achieve In Vivo Stability” S. D. Perrault, W. M. Shih, *ACS Nano*, **2014**, 8 (5), 5132-5140

Björn Högberg recently developed a new design paradigm which allows the creation of structures more resistant to physiological conditions (see chapter 1.9.4).⁵² They showed successful folding of different designs in low magnesium concentration buffers, routinely used for several biological assay (Phosphate Buffered Saline – PBS - and Dulbecco’s Modified Eagle Medium – DMEM), and good stability in cell culture medium. Chemical modification of the strands composing the structure is also a strategy used to increase stability. Sleiman and coworkers produced oligonucleotides bearing hexaethylene glycol, hexane diol and phosphate modifications.⁸⁸ The modified strands were then used to fold triangular prism structure, which showed an increased resistance against nuclease with a lifetime of 62 hours in serum. The stability issues described above were the starting motivation for the author to develop a new stabilization strategy suitable for DNA nanostructures.⁸⁹ The selected model was a SST nanotube where each oligonucleotide composing the structure was modified by insertion at both ends click chemistry reactive groups. The entire structure underwent to catenation *via* click chemistry resulting in a covalently topologically interlocked “chain-armor” highly resistant to high temperature, low cation concentration and exonucleases attacks. This study is described in detail in chapter 3.

2. Cellular Uptake of Tile-Assembled DNA Nanotubes

2.1. Introduction

Targeted cell delivery is a key aspect for biological applications of DNA nano-objects, for example drug delivery. Advantageous features of DNA nanostructures are their structural programmability, which enables spatial organization of different elements with nanometric precision, and biocompatibility of DNA in living systems. Nanostructures have already shown high potentiality as delivery vehicle for biomolecules^{79, 82} or anticancer drugs.^{78c} Uptake of these carrier-cargo complexes can be enhanced by the help of transfection agents, such as small molecules or cell penetrating peptides⁹⁰. On the other hand, typical biological environmental factors such as depletion of cations or low pH values hamper the use of DNA-based structure as carrier system. Considering these challenges, a DNA-based nano-carrier for siRNA delivery was prepared. The structure, a Single-Stranded Tile (SST) assembled nanotube, was efficiently functionalized with a targeting ligand *via* copper catalyzed azide-alkyne cycloaddition (CuAAC) and further decorated with six siRNAs for GFP gene silencing. However, disassembly of the structure during cell incubation hindered significant siRNA delivery and therefore protein down-regulation. Further investigations on these models allowed a better understanding of the stability of these DNA nanostructures in biological environment.

2.2. RNA interference (RNAi)

RNA interference is a biological process that involves gene suppression at the transcriptional level by cleavage of target mRNA molecules. The mechanism starts when an exogenous dsRNA enters the cell. In the cytoplasm this RNA is processed by the Dicer enzyme, which cleaves the ds filament in a fragment of 20-25 base pairs with 2 nucleotides overhang at each 3' end, the so-called siRNA (small interfering RNA). These fragments, composed by a guide and a passenger strands, are loaded into the RNA-induced silencing complex (RISC). Here the two strands are separated, the passenger strand is degraded while the guide strand activates the complex. The active complex binds target messenger RNA (complementary to the guide strand) causing its cleavage and therefore protein expression inhibition. Since the discovery of this mechanism, RNAi raised immediately great interest in the medical field as a powerful therapeutic tool that can virtually provide silencing of any gene. Efforts to apply synthetic siRNA as therapeutic molecules have been so far not conclusive mainly due to off-target issues and unspecific or ineffective target delivery.

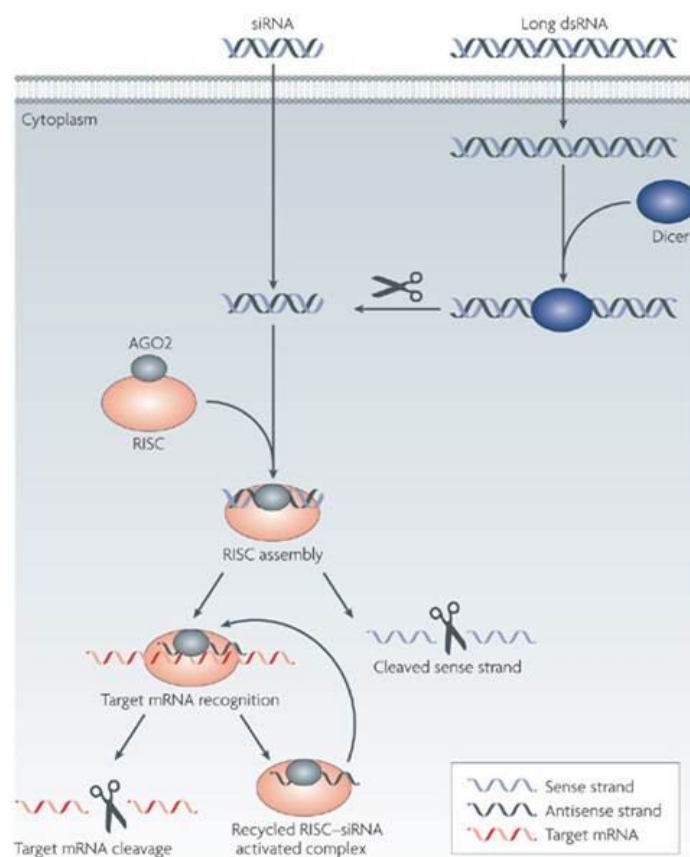


Figure 2. 1. RNA interference (RNAi) pathway. Adapted from “Knocking down barriers: advances in siRNA delivery” K. A. Whitehead, R. Langer, D. G. Anderson, *Nat. Rev. Drug Discov.* **2009**, 8, 129-138.

In physiological environment siRNA faces some issues like serum nucleases digestion or immune response stimulation. Thus, chemical modifications on the backbone, such as 2'-O-Methyl, 2' fluoro, locked or unlocked nucleic acids, or phosphorothioate linkages, can be used to avoid degradation or unwanted side effects.⁹¹ siRNA delivery into cells is the necessary requisite to obtain gene silencing and it can be achieved mainly with the help of delivery systems, since these nucleic acids are too large and hydrophilic to overcome the cell membrane alone. Cyclodextrin polymer (CDP) nanoparticles were used for this purpose.⁹¹ CDP are polycationics oligomers which, thanks to the strong basicity of the amidine functional groups, bind strongly nucleic acids enhancing their cellular uptake. Lipid nanoparticles are a further delivery strategy recently entered in the clinical trial for the administration of iRNA drugs.⁹² Positively charged lipids encapsulate the negatively charged siRNAs in liposomes able to carry efficiently the payload inside cells. Direct conjugation of siRNA to a delivery material is another effective method to obtain nucleic acids cell internalization. Dynamic PolyConjugates, for example, are constructs composed by siRNA connected to membrane-disruptive polymers *via* hydrolysable disulphide linker. The activity of the polymer is shielded by PEG chains that are cleaved once the construct is in the endosome. Hence, the membrane-disrupting polymer enables the escape of the siRNA complex from the endosome. In the

cytoplasm the disulphide linker is hydrolyzed and the siRNA is free to trigger RNA interference. Triantennary GalNac-siRNAs are other conjugates composed by siRNA connected with three ligand moieties by mean of a trivalent spacer. The targeting agent N-Acetylgalactosamine (GalNac) is an amino-sugar derivative of galactose and a selective ligand for asialoglycoprotein receptors on hepatocytes surface. Therefore this strategy is widely used for RNAi therapy for many liver diseases. Another noteworthy siRNA delivery method is the one proposed by Chad A. Mirkin.⁹³ Gold nanoparticles functionalized with dsRNA create a system with unique properties of cellular uptake, serum stability and gene regulation. siRNA loaded nanoparticles enter HeLa cells without the help of any transfection agent and down-regulate firefly luciferase in dose and time dependent manner. A recent development in siRNA delivery is obtained with the application of DNA nanostructure as carrier. DNA based structures are an inherently safe and effective delivery system as DNA objects are non-toxic, exhibit little immunogenicity, and can protect the siRNA from enzymatic degradation compared with other conventional carriers. Architectures like DNA-tetrahedron already showed efficient cellular uptake even without the help of any targeting agent.⁷⁷ More recently, Lee and coworkers incorporated single-stranded overhangs on each edge of the tetrahedral structure enabling hybridization of a maximum of six siRNAs.⁸⁰ The loaded structure is further modified with folate moieties as targeting agent and effective gene silencing both *in vitro* and *in vivo* is demonstrated. The presence and the position of the transfection agent in this approach were of fundamental relevance since without the help of the folate gene silencing did not occur. The important role of folate as targeting molecule is described in the next paragraph.

2.3. Folate targeted delivery

Targeted delivery is a promising method for safe and effective administration of therapeutics. The targeting agent folic acid and its derivatives are uptaken in cells through folate receptors, which are notably overexpressed in many tumoral forms. These receptors are N-glycosylated proteins and exist in two isoforms (α and β), which are identical for the 70% of the amino acids sequence. In a normal state, folate receptor (FR) is not necessary for the survival of the cell and has a low or absent expression in the majority of the healthy tissues. For this reason, FR overexpression in malignant cell lines is considered a potent targeting strategy for selective drug-delivery toward diseased cells. Folate receptor α (FR α) is highly expressed in several carcinomas forms, while folate receptor β (FR β) is consistently present in myeloid leukemia cells and in macrophages associated with chronic inflammatory diseases like reumatoids arthritis. Folate conjugates bind the receptors on the cell membrane with high affinity and are internalized by receptor-mediated endocytosis.⁹⁴

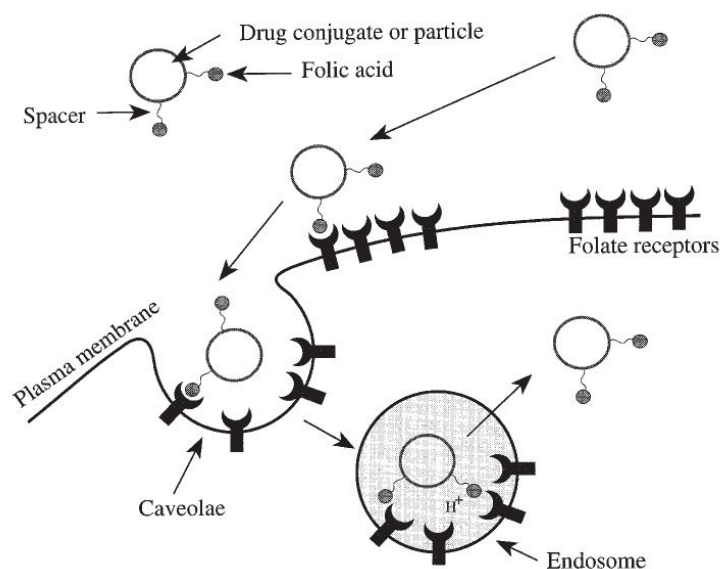


Figure 2. 2. Cell internalization of folate-conjugates. Adapted from “Folate as a Targeting Device for Proteins Utilizing Folate Receptor-Mediated Endocytosis”, R. J. Lee, P. S. Low, *Meth. Mol. Med.* **2000**, 25, 69-76.

A wide range of molecules have been conjugated to folate to obtain cell internalization. Imaging agents, haptens for immunotherapy and chemotherapeutics are only some examples of the molecules delivered to cells using folate-mediated uptake. Furthermore drug carriers, such as liposomes, lipid nanoparticles, polymeric nanoparticles and micelles, are themselves effective system to enable cell internalization of drugs⁹⁵. Conjugation of these delivery vehicles with folate enables a more selective uptake from specific cell-targets. However, the composition of these carriers can cause toxicity, immunitary response and not yet clear long-term effects in living systems. Since the development of the DNA nanotechnology field, intrinsically biocompatible and not immunogenic nucleic acids have been used to create carrier nanostructures for cell delivery purpose. Also in this case specificity of the target is greatly important to achieve a maximized effect of the carried therapeutic and reduced off-target effects. Mao's research group assembled a delivery vehicle using a single 52mer oligonucleotide.⁹⁰ This strand has four palindromic regions which allow it to fold in micrometer-long nanotube. Some strands composing the structure are conjugated alternatively with folate or Cyanine 3 (Cy3) dye through NHS ester chemistry and then used for the folding. Folate-modified nanostructures showed higher fluorescence in KB cells compared to structures without the transfection agent, claiming the positive effect of folate on the delivery efficacy. Another successful example of enhanced cell uptake mediated by folate is provided by the work of Lee already introduced above.⁸⁰ The tetrahedral structure is tested as carrier of siRNA both in *in vitro* and *in vivo* assays. The researchers screened a large number of targeting agents but with the use of folic acid they obtained the highest silencing rate. The position of the folate moieties within the tetrahedral architecture influenced also the final effect, in fact, higher local density of transfection agent gives higher gene silencing. The promising results obtained by functionalization of DNA nanostructure

with folate encourage deeper investigation for the developing of accurate delivery systems using DNA nanomaterials.

2.4. Abstract of the publication “Cellular Uptake of Tile-Assembled DNA Nanotubes”

DNA-based nanostructures have received great attention as molecular vehicles for cellular delivery of biomolecules and cancer drugs. Here we report on the cellular uptake of tubule-like DNA tile-assembled nanostructures 27 nm in length and 8 nm in diameter that carry siRNA molecules, folic acid and fluorescent dyes. In our observations, the DNA structures are delivered to the endosome and do not reach the cytosol of GFP-expressing HeLa cells that were used in the experiments. Consistent with this observation, no elevated silencing of the GFP gene could be detected. Also the presence of up to six molecules of folic acid on the carrier surface did not alter the uptake behavior and gene silencing. We further observed several challenges that have to be considered when performing *in vitro* and *in vivo* experiments with DNA structures: i) DNA tile tubes consisting of 42 nt-long oligonucleotides and carrying single- or double-stranded extensions degrade within 1 hour in cell medium at 37 °C while the same tubes without extensions are stable for up to 8 hours. The degradation is caused mainly by low concentration of divalent ions in the media. The lifetime in cell medium can be increased drastically by employing DNA tiles that are 84 nt long. ii) Dyes may get cleaved from the oligonucleotides and then accumulate inside the cell close to the mitochondria, which can lead to misinterpretation of data generated by flow cytometry and fluorescence microscopy. iii) Single-stranded DNA carrying fluorescent dyes are internalized at similar levels as the DNA tile-assembled tubes used here.

2.5. Author’s contribution

The author carried out the characterization of the folate-conjugated oligonucleotides via HPLC and MALDI-TOF.

2.6. Associated publication

Cellular Uptake of Tile-Assembled DNA Nanotubes

Published in: Kocabey, S.; Meinel, H.; MacPherson, I.S.; Cassinelli, V.; Manetto, A.; Rothenfusser, S.; Liedl, T.; Lichtenegger, F.S. Cellular Uptake of Tile-Assembled DNA Nanotubes. *Nanomaterials* **2015**, 5, 47-60.

2.6.1. Introduction

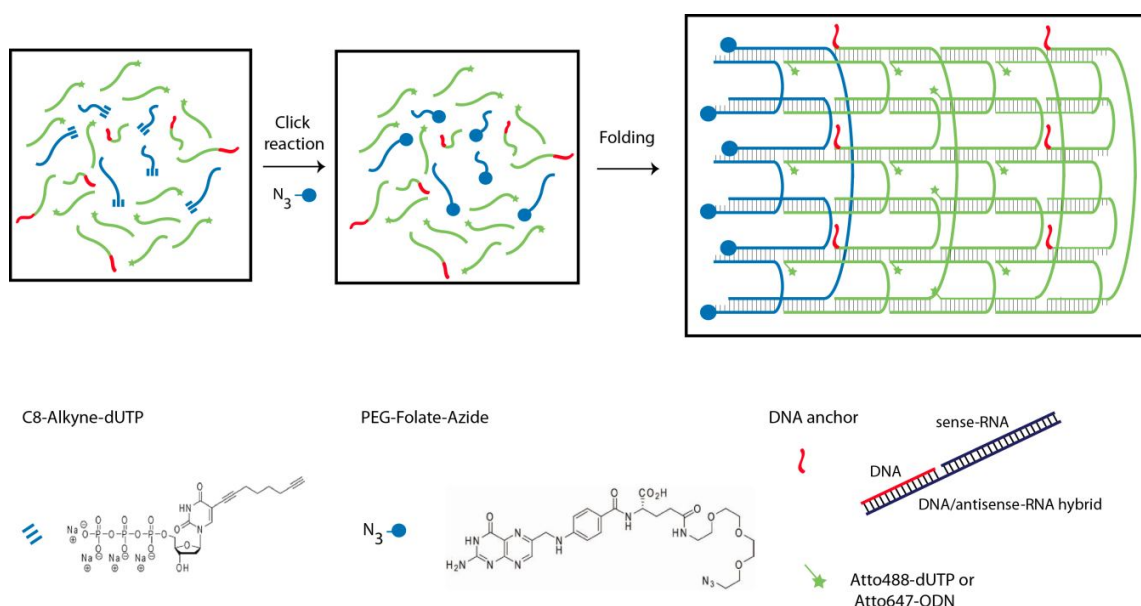
Therapeutic agents must overcome multiple barriers to reach their target. [1-2] For example, siRNAs have to reach the target tissue, enter the cells, be released from the endosomal compartment and finally silence the target gene via the RISC complex [3]. Up to now, researchers have developed a variety of nanoparticlecarrier systems to overcome these barriers such as polymers [4], liposomes⁹⁶ or conjugates [6] with various levels of efficiency and toxicity. Most recently, with improvements in the DNA Nanotechnology field, DNA-based nanostructures were developed as carrier systems for a variety of active components including siRNAs [7], antibodies [8], immunostimulants [9-10] and cancer drugs [11-12]. DNA nanostructures are promising for delivery applications because they can be easily modified with a variety of (bio)chemical moieties for targeting purposes at nanoscale precision, they are monodisperse with well-defined sizes and are non-cytotoxic [10,13-18]. To date, several groups have investigated the targeted delivery of DNA based nanostructures using different targeting agents such as cell penetrating peptides or small molecules. Among them folate is a commonly used molecule due to the high expression of its receptors on certain cancer cells. Efficient folate-mediated uptake has been demonstrated using various DNA-based structures such as DNA nanotubes built from a single palindromic DNA strand [19] or Y-shaped DNA nanostructures prepared by rolling circle amplification [20]. Although the DNA-based nanostructures are promising for targeted delivery applications as exemplified above, the stability of these structures at 37°C in blood or tissue is one of the main issues to be considered. In a recent study, the stability of a variety of DNA origami structures with different designs such as octahedron, six-helix bundle tube or 24-helix bundle rod were investigated using *in vitro* conditions and time and shape dependent denaturation and digestion were observed due to the Mg²⁺ depletion in the media and DNase activity of the serum [21]. As an alternative to the DNA origami method [14-15] and shape-specific designs such as DNA cubes [22], tetrahedrons [23] or octahedrons [24], single-stranded tile assembly has recently proved to be a versatile and modular design strategy to build a wide variety of two- and three-dimensional shapes [25,26]. In this study, we intended to show efficient folate-mediated uptake and subsequent gene silencing by tile-assembled DNA nanotubes carrying GFP siRNAs *in vitro*. However, we were not able to demonstrate the sought-after effects but instead observed untimely disassembly of our constructs under certain *in vitro* conditions and therefore investigated strategies to maintain the structural integrity in relevant environments. We examined the stability of tile-assembled structures under limited divalent cations and in the presence of nucleases in buffer and in cell media. We then describe a number of artifacts that should be taken into consideration during experiments with DNA based nanostructures *in vitro*.

2.6.2. Results and Discussion

2.6.2.1. Design and self-assembly of six-helix DNA nanotubes

We designed tubule-like DNA nanostructures consisting of 24 oligonucleotides that self-assemble into six parallel helices using the single-stranded DNA tile assembly method introduced by Yin et al. (Scheme 2. 1 and Tab. 2. 1-3) [25,27]. Six of the oligonucleotides were alkyne-modified during synthesis and conjugated in-house with PEG-folate-azide (baseclick GmbH, Germany) by a click reaction. Liquid chromatogram analysis and matrix-assisted laser desorption/ionization (MALDI) mass spectrometry

revealed the almost quantitatively conjugation of folate molecules to the alkyne-oligonucleotides. (Fig. 2. 8 and 2. 9, Tab. 2. 4). Another set of six oligonucleotides was extended by an 18 nt-long sequence at the 3' end to allow the attachment via hybridization of six siRNA molecules that potentially silence the expression of GFP upon delivery. To visualize the DNA nanotubes in vitro, two different labeling strategies were employed. In the first approach, Atto488-dUTP was enzymatically labeled to the 3' end of a set of 12 tile oligonucleotides using terminal transferase. In the second approach, the same set of oligonucleotides was extended with another 18 nt-long sequence allowing attachment via hybridization of 12 Atto647-modified (via NHS chemistry) oligonucleotides. The nanotubes have a designed length of ~ 27 nm and an expected diameter of ~ 6 nm for the dried sample. Note that the tube diameter of a six-helix bundle increases in buffer to 8 nm and that tubes decorated with additional molecules will have a larger effective diameter.[28]



Scheme 2. 1. DNA nanotube assembly. Left: Click reaction of alkyne modified oligonucleotides with azide modified PEGylated folate. Right: Self-assembly of 24 oligonucleotides into 6-helix tube after 17 hrs annealing process.

The nanotube structures containing the desired subsets of oligonucleotides and modifications were folded in TE-buffer containing 20 mM Mg^{2+} during a thermal annealing process starting at 80 °C and cooling down to room temperature over the course of 17 hrs. Analysis by gel electrophoresis analysis showed for all designs prominent bands representing the folded structures (Lane 2+3+4 in Fig. 2. 3). Conjugation of folate and folate-siRNA (Lane 3 and 4, respectively) to the DNA nanotubes leads to a decrease of their mobility in comparison to nanotubes without folate and siRNA (Lane 2). Transmission electron microscopy (TEM) demonstrates the correct assembly of the nanotubes and the monodispersity

of the samples. The measured length of 27 ± 1 nm and the measured diameter of 6 ± 1 nm perfectly match the expected dimensions (Fig. 2. 3B, C and D).

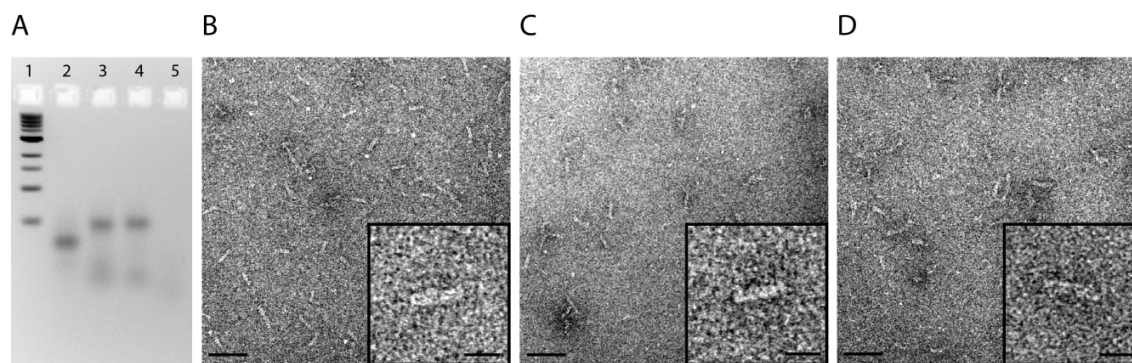


Figure 2. 3. Characterization of nanotubes. (a) Gel electrophoresis analysis of assembled nanotubes. 1) 1 kb ladder, 2) nanotube 3) nanotube+folate 4) nanotube+folate+siRNA 5) individual oligonucleotide. Electron micrographs of (b) nanotubes (c) nanotubes with folate and (d) nanotubes with folate and siRNA. (Scale bars: 50 nm, insets: 20 nm)

2.6.2.2. Tubule-like tile-assembled DNA nanostructures are delivered to the endosome of HeLa cells independently of folic acid and are not capable of releasing siRNA into the cytosol

DNA nanotubes labeled with Atto488 via enzymatic labeling were added to HeLa cell cultures at 10 nM, together with Dextran-AF647 as a marker for endosomal uptake. At various time points thereafter, confocal microscopy was performed to evaluate the localization of the construct. After 24 hours, we found clear co-localization of the nanotubes with Dextran (Fig. 2. 4A–C). Observations for up to 72 hours did not show any change in localization (Fig. 2. 10).

To determine a potential effect of uptake via the folate receptor, which is highly expressed on the surface of HeLa cells, nanotubes with and without folic acid were compared side by side. No influence on the endosomal staining pattern was noticed in the fluorescence microscopy images, neither after 24 hours nor after 72 hours (Fig. 2. 10). For a quantitative analysis of the uptake, we conducted flow cytometry-based measurements of the HeLa cells at different time points after addition of fluorophore-labeled nanotubes (Fig. 2. 4D). A minor signal was already detected after 4 hours, which further increased in the course of 24 hours. No significant difference was found between the uptake of nanotubes with or without folate.

On a functional level, we tested if the nanostructures released their siRNA cargo successfully to the cytoplasm by analyzing the knockdown capacity of siRNA molecules bound to the DNA nanotube. Stably GFP-transfected HeLa cell lines were used together with siRNA directed against GFP (siGFP). The siGFP was either bound to the nanostructure via hybridization or transfected into the cytoplasm by lipofection as a positive control. The GFP signal of the cells was measured by flow cytometry after 96 hours (Fig. 2. 4E). In the condition with lipofection of GFP-targeting siRNAs, the fluorochrome signal was markedly

decreased compared to lipofection of a control siRNA (siCTRL). However, addition of siGFP to the nanotubes did not result in GFP-knockdown, independent of folate labeling, consistent with endosomal trapping of the whole structure including their siRNA cargo.

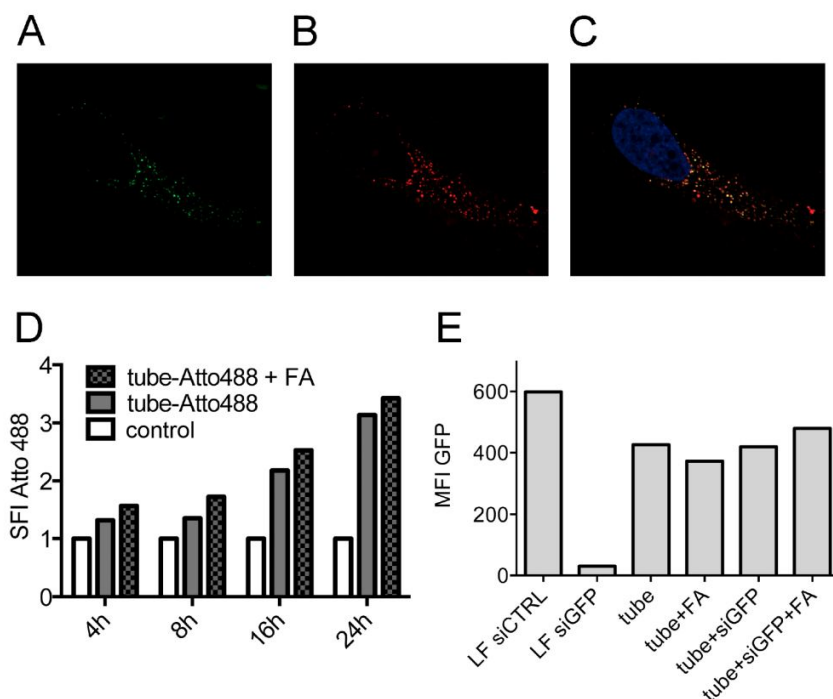


Figure 2. 4. Endosomal uptake of nanotubes in HeLa cells. Endosomal staining of nanotubes with dextran. (a) nanotubes (b) dextran (c) merged image. (d) Folate dependent uptake of nanotubes over 24 hrs. (e) Fluorescence intensity of stably GFP-expressing HeLa cells upon addition of nanotubes carrying GFP-targeting siRNAs or upon transfection of a GFP-targeting siRNA and a non-targeting siRNA respectively as controls using lipofection (LF).

2.6.2.3. Stability of DNA nanotubes differs in various conditions *in vitro*.

To address the stability of tile-assembled DNA nanostructures *in vitro* we incubated them in different buffers and cell media. First, we incubated the nanotubes in PBS with different Mg^{2+} concentrations at 37° C for 2 hrs. We used PBS as a buffer to simulate the cell media conditions as both cell media and PBS possess several monovalent and divalent cations at isotonic concentrations. Importantly, for the assembly and stabilization of the DNA nanostructures usually Mg^{2+} concentrations much higher than those found in PBS and cell media are used. While folding of DNA nanostructures can also be achieved at high Na^+ concentrations [29], the 135 mM NaCl present in PBS are not sufficient to stabilize DNA nanotubes at 37°C, if the individual DNA tiles are 42 nt long. Gel analysis revealed that the nanotubes without extensions were stable down to 1 mM Mg^{2+} , whereas the nanotubes carrying siRNA started to

degrade already below 4 mM Mg^{2+} (Figure 2. 5A and B). This indicates that the addition of extension sequences protruding from the DNA nanotubes destabilizes the structure, which may be explained by distorted stacking of the last base before the extension and with an increase of electrostatic repulsion between the elongated tail and the DNA duplexes in the nanotube [30]. Next, we compared the stability of nanotubes against DNases and incubated the structures in cell medium containing 10 % FCS. Gel analysis showed that under these conditions the plain nanotubes are stable up to 8 hrs (Figure 2. 5C). However, nanotubes carrying siRNA were degraded in 1 h when the structures were incubated in media containing 10% FCS. These nanotubes were also degraded slightly during 8 hrs in DMEM medium without FCS, likely due to Mg^{2+} depletion (in all cell media experiments the concentration of Mg^{2+} was 1.8 mM).

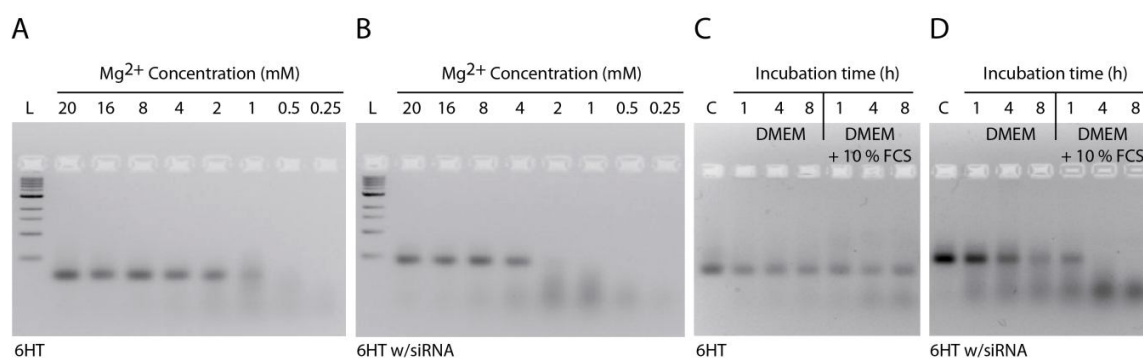


Figure 2. 5. Stability of nanotubes. (a) Stability of nanotubes in PBS with different Mg^{2+} concentrations. (b) Stability of nanotubes carrying siRNA in PBS with different Mg^{2+} concentrations. (c) Stability of nanotubes in DMEM medium in the absence or presence of FCS. (d) Stability of nanotubes carrying siRNA in DMEM medium in the absence or presence of FCS. (L: 1 kb ladder, C: control)

To overcome the problem of premature degradation, DNA tile tubes were assembled from 84 nt-long oligonucleotides. This design allows longer complementary regions (21 bp for the 84mers instead of 10 bp and 11 bp for the 42mers) within the tile assembly, which in turn yields much higher thermal stability but also higher resistance to Mg^{2+} depletion (Figure 2. 6). Our results show that the stability of tile-assembled nanotubes is dependent on sequence design, temperature, salt concentration and structural modifications such as the addition of single- or double-stranded extensions to the DNA tiles.

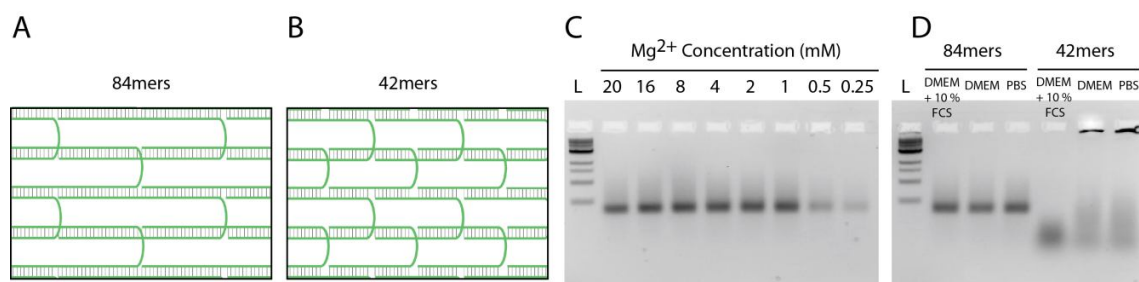


Figure 2. 6. Stability of nanotubes assembled from 84 nt-long oligonucleotides. (a) Schematic depiction of a section of the 6HT demonstrating the hybridization of 84mers. (b) Schematic depiction of a section of the 6HT demonstrating the hybridization of 42mers (c) Stability of nanotubes (84mers) in PBS with different Mg²⁺ concentrations. (d) Stability of nanotubes (84mers and 42mers) in DMEM + 10% FCS, DMEM and PBS. Nanotubes were incubated at 45°C for 2 hrs. (L: 1 kb ladder, C: control)

2.6.2.4. Strong extra-endosomal uptake can be feigned by dye cleavage

When nanostructures labeled with Atto647 *via* hybridization were incubated with HeLa cells, we repeatedly observed a very high fluorescence level in the cells during microscopy- or flow cytometry-based analysis. Furthermore, the fluorochrome did not co-localize with dextran as an endosomal marker (Fig. 2. 7A), but instead, mitochondrial localization was detected (Fig. 2. 7B). The level of uptake and the mitochondrial staining pattern were associated with the addition of serum to the culture medium (Fig. 2. 11). Similarly, when only the oligonucleotide labeled with Atto647 (*via* NHS chemistry) was added to the HeLa cells, we observed a rapid and strong staining of the cells only in the case when serum was added (Fig. 2. 7C). This effect was not observed when the fluorophores were attached *via* enzymatic binding. We therefore conclude that Atto647 is cleaved off the DNA by some component in the serum and is taken up independently of the nanostructure.

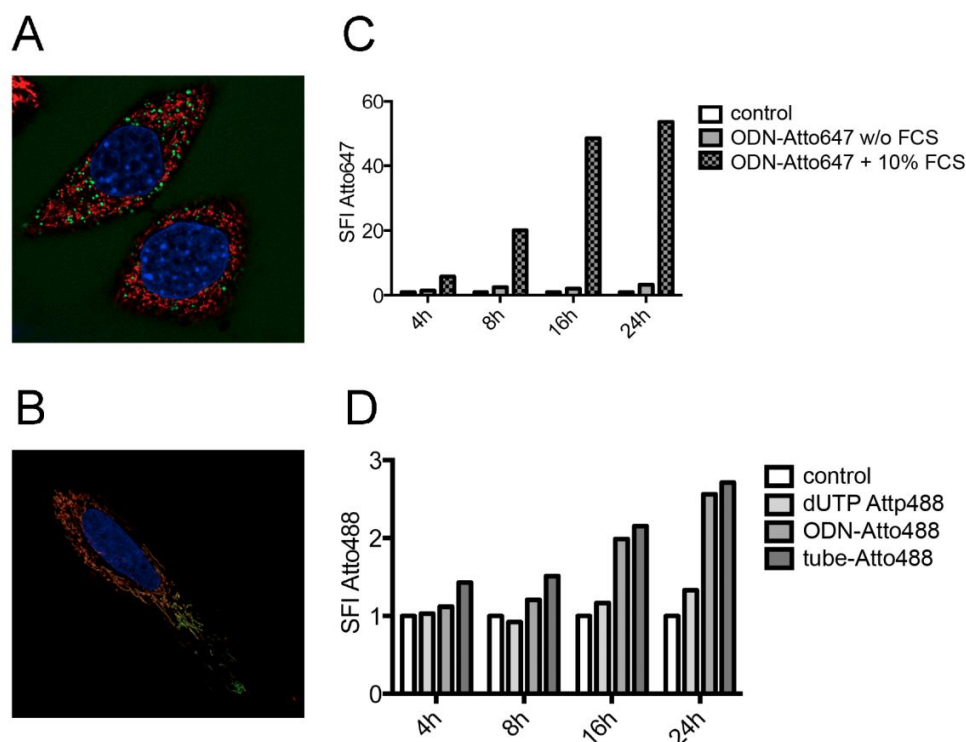


Figure 2. 7. Effect of dye cleavage on cellular uptake. (a) Endosomal staining using Alexa Fluor 488-coupled dextran (shown in green) of HeLa cells treated with ODN-Atto647 (shown in red). (b) Mitochondrial colocalization of Atto647 (shown in red) in HeLa cells stained with the mitochondrial dye MitoTracker Green (shown in green). Nuclei are stained with H ochst 33342. (c) Fluorescence intensity of cells treated with ODN-Atto647 in the absence or presence of FCS. (d) Fluorescence intensity of cells treated with Atto488-dUTP, ODN-Atto488 and nanotube labeled with Atto488.

2.6.2.5. Single-stranded DNA molecules, but not desoxynucleotide triphosphates, are internalized at similar levels as the tile-assembled nanotube structures

Specific uptake of the tubule-like tile-assembled DNA nanostructures was analyzed by direct comparison with oligonucleotides and desoxynucleotide triphosphates. All three molecules were labeled with Atto488 and incubated at identical molar concentrations with HeLa cells. Fluorochrome uptake was measured by flow cytometry at various time points (Fig. 2. 7D). No intracellular staining was found in the desoxynucleotide triphosphate condition. However, we observed similar uptake of the fluorochrome with the oligonucleotide as with the nanostructure.

2.6.3. Experimental Section

2.6.3.1. DNA Nanotube Design

DNA nanotubes were designed using the Yin's single strand tile (SST) method [27]. Each tile oligonucleotide is 42 bases long and consists of four domains with ten or eleven bases. 24 individual oligonucleotides were used to form 6 helix nanotube. The domains at the ends of the nanotube contain non-pairing poly-A sequences to prevent polymerization. siRNA hybridization to the nanotubes was done by extending 3' ends of six tiles with an 18-nt long overhang sequence (5'-AGGATGTAGGTGGTAGAG-3'). The used siRNA sequences for GFP silencing were sense: 5'-GCCACAACGUCUAUAUCAU-3', and antisense: 5'-AUGAUUAAGACGUUGUGGC CTCTACCACCTACATCCT-3'). Six oligonucleotides were modified with PEG-folate azide (baseclick GmbH, Germany) using click reactions. The underlined sequence shows the complementary overhang. All oligonucleotides were purchased from Eurofins Operon MWG (Ebersberg, Germany) with HPSF or HPLC purification.

2.6.3.2. Folate Conjugation and Characterization of Oligonucleotides

Each of the six alkyne-modified oligonucleotides (Baseclick GmbH) were submitted to click reaction, using CuBr as the Cu(I) source. Ten microliters of a freshly prepared CuBr (0.1 M)/THPTA (0.1 M) solution in a 1:2 v/v ratio were added to a 50 µL (0.1 mM, 5 nmol) solution of each alkyne-oligonucleotide. The addition of folate-PEG3-azide (2.5 µL, 10 mM in DMSO) completed the click reaction cocktail. The mixture was mixed for 1.5 h at 45 °C. Finally, the solution was purified *via* ethanol precipitation. Folate-conjugated oligonucleotides were analyzed by analytical RP-HPLC (e2695 system, Waters, Milford, MA, USA) coupled with a photodiode array detector (PDA 2998, Waters) using a reversed phase XBridge OST C18 column (4.6 mm × 50 mm, Waters). Before injection in RP-HPLC, samples were diluted to 10 µM concentration in HPLC-grade H₂O. Samples (2 µL) were desalted against ddH₂O using a nitrocellulose membrane (MerckMillipore, Frankfurt, Germany), and 0.4 µL were spotted onto a MALDI plate (Bruker Corporation, Billerica, MA, USA) along with 0.4 µL of 3-hydroxypicolinic acid (HPA, Sigma Aldrich, St. Luis, MO, USA). Measurements were carried out on the Autoflex MALDI-TOF (Bruker Corporation).

2.6.3.3. Dye Labeling of DNA Nanotubes

Fluorescent dyes were conjugated to the nanotubes using two different approaches. In the first approach, 3' ends of twelve tiles were extended by 18-nt long overhang sequences to hybridize the dye-modified sequence: (Atto647-TTCATTCTCCTATTACTACC). In the second approach, the 3' ends of same tiles were enzymatically labeled with Atto488-dUTP. (Jena Bioscience, Jena, Germany) For this, Atto488-dUTP (80 µM), CoCl₂ (5 mM), terminal transferase enzyme (16 U/µl, Roche, Penzberg, Germany), and all DNA tiles (400 pmol) were mixed in a 20 µl, 1x TdT reaction buffer and then incubated at 37 °C for 30 min. Then, 2.5 µl of NaOAc (3 M) was added and the solution was filled up to 80 µl with ice-cooled ethanol (99 %). After 1 h incubation at -20°C, samples were centrifuged at 13000 g for 30 min. Then,

samples were washed with 70 % ethanol for 10 min again and the supernatant was discarded. The remaining pellet was dissolved in distilled water.

2.6.3.4. DNA Nanotube Assembly and Purification

For DNA nanotube assembly, 400 nM of dye and folate modified tiles, 800 nM of antisense-ODN and 1.6 μ M of sense-ODN were mixed in a folding buffer (10 mM Tris-HCl, 1 mM EDTA, pH 8.0, 20 mM $MgCl_2$). For the plain nanotube assembly, 1 μ M of unmodified tiles were used. The DNA nanotubes were folded over the course of 16 hrs (5 min at 80°C, cooling down to 65°C at 1 °C/min, cooling down to 25°C at 2.5 °C/h). Purification of the assembled DNA nanotubes were done using 30K Amicon Ultra 0.5 ml centrifuge filters (30000 MWCO, Millipore, Schwalbach, Germany) to remove excess strands that were not folded into the structures. 100 μ l of assembled DNA nanotube solution was mixed with 400 μ l of folding buffer, filled into the centrifuge filter, and centrifuged 3 times at 13000 g for 6 min. After every centrifuge step, the flow-through was removed and the filter was refilled up to 500 μ l with buffer. After final centrifugation, the remaining solution at the bottom of the filter (~ 50 μ l) was pipetted out and the concentration of nanotubes was determined by measuring the optical density at 260 nm.

2.6.3.5. Gel electrophoresis and Transmission Electron Microscopy

DNA nanotubes were analyzed by running samples in an agarose gel. For this, 2% agarose was dissolved in 0.5 x TAE buffer by heating to boiling. $MgCl_2$ (11 mM) and ethidium bromide (0.5 μ g/ml) were added after the cooling and the solution was poured into a gel cask for solidification. Twenty μ l of each filter-purified DNA nanotube sample were mixed with 4 μ l of 6x loading dye before loading into the gel pockets. 6 μ l of 1 kb ladder was also loaded adjacent to the samples. The gel was run for 2 hrs at 70 V in an ice-cold water bath to prevent heat induced denaturation of DNA nanotubes. To visualize DNA nanotubes, a JEM-1011 transmission electron microscope (JEOL) was used. DNA nanotubes were incubated on plasma-exposed (240 kV for 1 min) carbon-coated grids and then negatively stained with 2% uranyl formate for 10s.

2.6.3.6. Stability of DNA Nanotubes

Stability of DNA nanotubes were tested in PBS buffer, DMEM and DMEM containing 10 % FCS separately. 1 μ l of DNA nanotubes (50 ng/ μ l) in 20 μ l of buffer/medium was incubated at 37 °C for different time points. 2 % agarose gel with 11 mM $MgCl_2$ was prepared to analyse samples as mentioned in experimental section 4.6.3.5.

2.6.3.7. Cell culture experiments

HeLa cells were cultured at 37°C, 5% CO₂ and 95% humidity in Dulbecco's modified Eagle's medium (DMEM, Lonza) supplemented with 10% heat-inactivated fetal calf serum (FCS, Invitrogen), 2 mM L-

glutamine, 100 U/ml penicillin and 100 µg/ml streptomycin. Stably GFP-transfected HeLa cell lines were generated by retroviral transduction using an eGFP containing pMP71 vector as described previously [31, 32]. To analyze uptake, DNA nanotubes, oligonucleotides and deoxynucleotide triphosphates were added to HeLa cells at a concentration between 10 and 40 nM for the indicated period of time in DMEM with L-glutamine, penicillin, streptomycin and either supplemented or not with 10 % FCS. For siRNA mediated knockdown experiments, GFP-expressing HeLa cells were seeded in 24-well plates and allowed to adhere overnight. On the next day, cells were either incubated with the indicated nanotubes coupled to GFP-targeting siRNAs or were transfected as a control with siRNA oligonucleotides (75 nM) using Lipofectamine RNAiMAX (Invitrogen). After 48 hrs GFP-knockdown was measured by flow cytometry. The siRNA sequence used to target GFP (siGFP) was 5' GCCACAACGUCUAUAUCAU 3'. As a control (siCTRL) we used the non-targeting RNA sequence 5' GCGCUAUCCAGCUUACGUA 3' described previously [33]. siRNAs were purchased from Eurofins and contained dTdT overhangs.

2.6.3.8. Flow Cytometry and Confocal Fluorescence Microscopy

Flow cytometry was used to determine the uptake of DNA nanotubes, oligonucleotides and deoxynucleotide triphosphates labeled with the fluorescent dyes Atto488 or Atto647 into HeLa cells and to assess the knockdown efficiency of GFP-targeting siRNAs in stably GFP-expressing HeLa cells. For that, after the indicated time points single cell suspensions were prepared and washed several times before analyzing the cells on a FACS Calibur (Becton Dickinson). FlowJo software was used to analyze the data. Confocal fluorescence microscopy was used to determine the subcellular localization of nanotubes and RNAs taken up by HeLa cells. For that, HeLa cells were cultured in CELLview cell culture dishes with a glass bottom (Greiner Bio One). After incubation with Atto488- or Atto647-labeled nanotubes for the indicated time points, cells were washed three times with PBS, and used for live-imaging on a Leica TCS SP5 confocal microscope (Leica Microsystems). Zero-point-two µg/ml Hoechst 33342 and MitoTracker Green (both from Life Technologies) were used according to the manufacturer's protocol to stain nuclei and mitochondria respectively. In order to visualize endosomes, 20 µg/ml dextran labeled with Alexa Fluor 647 or Alexa Fluor 488 (Life Technologies) was added simultaneously with the DNA nanotubes.

2.6.4. Conclusions

In this study, we investigated the cellular delivery of tile-assembled DNA nanotubes carrying siRNAs using GFP-expressing HeLa cells *via* folate targeting. We observed that the nanostructures enter the cells *via* an endosomal pathway but the nanostructures and their siRNA cargo are not capable of reaching the cytoplasm for knockdown and gene silencing. Contingently, no significant decrease in GFP expression levels was detectable and folate modification did not change the uptake kinetics. The stability experiments revealed that unmodified DNA nanotubes are stable at 37 °C up to 8 hrs in the cell media and that they stay intact in PBS buffer containing 2 mM Mg²⁺ or more. However, the extension of the DNA tile strands with sequences that allow the hybridization of siRNA or dye-modified strands drastically decreases the construct's stability, a fact that may have contributed to the unsuccessful folate targeting experiments. Using DNA tiles that were 84-nt long drastically increased the stability in all cell media and buffers with low Mg²⁺ concentrations. Importantly, we observed that DNA strands alone and cleaved

dyes are also uptaken by the cells, which can lead to the misinterpretation of recorded data. Overall, the results presented in this study demonstrate the importance to rigorously test the stability of DNA nanostructures before applications *in vitro* and *in vivo*.

2.6.5. References and Notes of the publication “Cellular Uptake of Tile-Assembled DNA Nanotubes”

1. Bareford, L.M.; Swaan, P.W. Endocytic mechanisms for targeted drug delivery. *Adv Drug Deliv Rev* **2007**, *59*, 748-758.
2. Smith, D.; Schuller, V.; Engst, C.; Radler, J.; Liedl, T. Nucleic acid nanostructures for biomedical applications. *Nanomedicine (Lond)* **2013**, *8*, 105-121.
3. Czech, B.; Hannon, G.J. Small rna sorting: Matchmaking for argonautes. *Nat Rev Genet* **2011**, *12*, 19-31.
4. Kataoka, K.; Harada, A.; Nagasaki, Y. Block copolymer micelles for drug delivery: Design, characterization and biological significance. *Adv. Drug Deliv. Rev.* **2001**, *47*, 113-131.
5. Miller, A.D. Cationic liposomes for gene therapy. *Angew. Chem. Int. Ed.* **1998**, *37*, 1768-1785.
6. Zhou, J.; Rossi, J.J. Therapeutic potential of aptamer-sirna conjugates for treatment of hiv-1. *BioDrugs* **2012**, *26*, 393-400.
7. Lee, H.; Lytton-Jean, A.K.; Chen, Y.; Love, K.T.; Park, A.I.; Karagiannis, E.D.; Sehgal, A.; Querbes, W.; Zurenko, C.S.; Jayaraman, M., et al. Molecularly self-assembled nucleic acid nanoparticles for targeted in vivo sirna delivery. *Nat Nanotechnol* **2012**, *7*, 389-393.
8. Douglas, S.M.; Bachelet, I.; Church, G.M. A logic-gated nanorobot for targeted transport of molecular payloads. *Science* **2012**, *335*, 831-834.
9. Li, J.; Pei, H.; Zhu, B.; Liang, L.; Wei, M.; He, Y.; Chen, N.; Li, D.; Huang, Q.; Fan, C. Self-assembled multivalent DNA nanostructures for noninvasive intracellular delivery of immunostimulatory cpg oligonucleotides. *ACS Nano* **2011**, *5*, 8783-8789.
10. Schuller, V.J.; Heidegger, S.; Sandholzer, N.; Nickels, P.C.; Suhartha, N.A.; Endres, S.; Bourquin, C.; Liedl, T. Cellular immunostimulation by cpg-sequence-coated DNA origami structures. *ACS Nano* **2011**, *5*, 9696-9702.
11. Zhao, Y.-X.; Shaw, A.; Zeng, X.; Benson, E.; Nyström, A.M.; Högberg, B. DNA origami delivery system for cancer therapy with tunable release properties. *ACS Nano* **2012**, *6*, 8684-8691.
12. Jiang, Q.; Song, C.; Nangreave, J.; Liu, X.; Lin, L.; Qiu, D.; Wang, Z.-G.; Zou, G.; Liang, X.; Yan, H., et al. DNA origami as a carrier for circumvention of drug resistance. *J. Am. Chem. Soc.* **2012**, *134*, 13396-13403.
13. Voigt, N.V.; Topping, T.; Rotaru, A.; Jacobsen, M.F.; Ravnsbaek, J.B.; Subramani, R.; Mamdouh, W.; Kjems, J.; Mokhir, A.; Besenbacher, F., et al. Single-molecule chemical reactions on DNA origami. *Nat. Nanotechnol.* **2010**, *5*, 200-203.

14. Rothemund, P.W. Folding DNA to create nanoscale shapes and patterns. *Nature* **2006**, *440*, 297-302.
15. Douglas, S.M.; Dietz, H.; Liedl, T.; Hogberg, B.; Graf, F.; Shih, W.M. Self-assembly of DNA into nanoscale three-dimensional shapes. *Nature* **2009**, *459*, 414-418.
16. Perrault, S.D.; Shih, W.M. Virus-inspired membrane encapsulation of DNA nanostructures to achieve in vivo stability. *ACS Nano* **2014**, *8*, 5132-5140.
17. Mikkilä, J.; Eskelinen, A.-P.; Niemelä, E.H.; Linko, V.; Frilander, M.J.; Törmä, P.; Kostinen, M.A. Virus-encapsulated DNA origami nanostructures for cellular delivery. *Nano Lett.* **2014**, *14*, 2196-2200.
18. Okholm, A.H.; Nielsen, J.S.; Vinther, M.; Sorensen, R.S.; Schaffert, D.; Kjems, J. Quantification of cellular uptake of DNA nanostructures by qPCR. *Methods* **2014**, *67*, 193-197.
19. Ko, S.; Liu, H.; Chen, Y.; Mao, C. DNA nanotubes as combinatorial vehicles for cellular delivery. *Biomacromolecules* **2008**, *9*, 3039-3043.
20. Hong, C.A.; Jang, B.; Jeong, E.H.; Jeong, H.; Lee, H. Self-assembled DNA nanostructures prepared by rolling circle amplification for the delivery of siRNA conjugates. *Chem. Commun.* **2014**, *50*, 13049-13051.
21. Hahn, J.; Wickham, S.F.; Shih, W.M.; Perrault, S.D. Addressing the instability of DNA nanostructures in tissue culture. *ACS Nano* **2014**, *8*, 8765-8775.
22. Seeman, N.C. Construction of three-dimensional stick figures from branched DNA. *DNA Cell Biol.* **1991**, *10*, 475-486.
23. Erben, C.M.; Goodman, R.P.; Turberfield, A.J. Single-molecule protein encapsulation in a rigid DNA cage. *Angew. Chem. Int. Ed. Engl.* **2006**, *45*, 7414-7417.
24. Shih, W.M.; Quispe, J.D.; Joyce, G.F. A 1.7-kilobase single-stranded DNA that folds into a nanoscale octahedron. *Nature* **2004**, *427*, 618-621.
25. Wei, B.; Dai, M.; Yin, P. Complex shapes self-assembled from single-stranded DNA tiles. *Nature* **2012**, *485*, 623-626.
26. Ke, Y.; Ong, L.L.; Shih, W.M.; Yin, P. Three-dimensional structures self-assembled from DNA bricks. *Science* **2012**, *338*, 1177-1183.
27. Yin, P.; Hariadi, R.F.; Sahu, S.; Choi, H.M.; Park, S.H.; Labeau, T.H.; Reif, J.H. Programming DNA tube circumferences. *Science* **2008**, *321*, 824-826.
28. Schiffels, D.; Liedl, T.; Fygenson, D.K. Nanoscale structure and microscale stiffness of DNA nanotubes. *ACS Nano* **2013**, *7*, 6700-6710.
29. Martin, T.G.; Dietz, H. Magnesium-free self-assembly of multi-layer DNA objects. *Nat. Commun.* **2012**, *3*, 1103.
30. Di Michele, L.; Moggetti, B.M.; Yanagishima, T.; Varilly, P.; Ruff, Z.; Frenkel, D.; Eiser, E. Effect of inert tails on the thermodynamics of DNA hybridization. *J. Am. Chem. Soc.* **2014**, *136* (18), 6538-6541.

31. Kobold, S.; Steffen, J.; Chaloupka, M.; Grassmann, S.; Henkel, J.; Castoldi, R.; Zeng, Y.; Chmielewski, M.; Schmollinger, J.C.; Schnurr, M., et al. Selective bispecific t cell recruiting antibody enhances anti-tumor activity of adoptive t cell transfer. *J. Natl. Cancer Inst.* **2014**.
32. Engels, B.; Cam, H.; Schuler, T.; Indraccolo, S.; Gladow, M.; Baum, C.; Blankenstein, T.; Uckert, W. Retroviral vectors for high-level transgene expression in t lymphocytes. *Human gene therapy* **2003**, *14*, 1155-1168.
33. Besch, R.; Poeck, H.; Hohenauer, T.; Senft, D.; Hacker, G.; Berking, C.; Hornung, V.; Endres, S.; Ruzicka, T.; Rothenfusser, S., et al. Proapoptotic signaling induced by rig-i and mda-5 results in type i interferon-independent apoptosis in human melanoma cells. *J. Clin. Invest.* **2009**, *119*, 2399-2411.

2.7. Supporting Information of the publication “Cellular Uptake of Tile-Assembled DNA Nanotubes”

Table 2. 1. The list of oligonucleotide sequences used in the 6-helix tile-tube assembly (oligonucleotides for folate conjugation)

ODN-1	XAAAACGCTAAGCCACCTTTAGATCCAAA
ODN-2	XGGATCTAAAGGACTTCTATCAAAGACGGGACGACTCCGGGAG
ODN-3	XAAACTCCCGGAGTCCGCTGCTGATCAAA
ODN-4	XGATCAGCAGCGCCCGTCTCGACTGCAGAAATAGGACCCCCAG
ODN-5	XAAACTGGGGGTCCTCGAGGCGAAACAAA
ODN-6	XGTTTCGCCTCGTAGCCTTCGCCCCGACGACCTGGCTTAGCGT

X: C8-Alkyne-dUTP

Table 2. 2. The list of oligonucleotide sequences used for fluorescent dye labeling

GGTCGTGCGGACTGTGGAACACCAACGATGCCTGATAGAAGTZ
GCGTGGCAATTGCCATAAATTCATACATAACGGCGCCAGACGZ
TTTCAAGACCGGCACTTGTATGGCGTAGGGCGGGTTTAGCGGZ
CGTTATGTATGCCGCTAAACCTTGCAATGACTGAACTCGAACZ
GTCCCGTCTTTGGATCCGAAAGCCATAATATATCGAGACGGGZ
TCGAAGTCGTGTTTCGAGTTCAAATGTCTATGCGATGCAGCAGZ
GTCATTGCAATAGCTCCCATCATTTAATGTCGTTTACAGTAAZ
GCATAGACATTTTACTGTAAACCTTACGTAACCTACAGCCAZ
ATTTCTGCAGGGAATTCAGCCTATTACATAGGCGAAGGCTAZ
ATGCCAGGAATGGCTGTAAGTTGCATCATGGGGGTCTCAATZ
TACGTAAGGTCAATACTCATCCCTGAGTGATCCATGACCCTTZ
CCCATGATGCAAAGGGTCATGGGTCTGAAAAATTTATGGCAZ

Z: Atto488-dUTP or overhang sequence for Atto647 modified oligonucleotide (GGTAGTAATAGGAGAATG)

Table 2. 3. The list of oligonucleotide sequences used for siRNA labeling.

GGCATCGTTGGCGTCTGGCGCACGACTTCGATTCGGATCCAAGGATGTAGGTGGTAGAG
CGCCCTACGCCAAAAAAGATGGGAGCTAAGGATGTAGGTGGTAGAG
TATATTATGGCCTGCTGCATCTTCCTGGCATGGCTGAATTCCAAGGATGTAGGTGGTAGAG
CGACATTAAATAAAAAAGATGAGTATTGAGGATGTAGGTGGTAGAG
CTATGTGAATAATTGAGGACCATTCACGCTGTTGACAGTAGGATGTAGGTGGTAGAG
GATCACTCAGGAAAAAATACAAGTGCCAGGATGTAGGTGGTAGAG

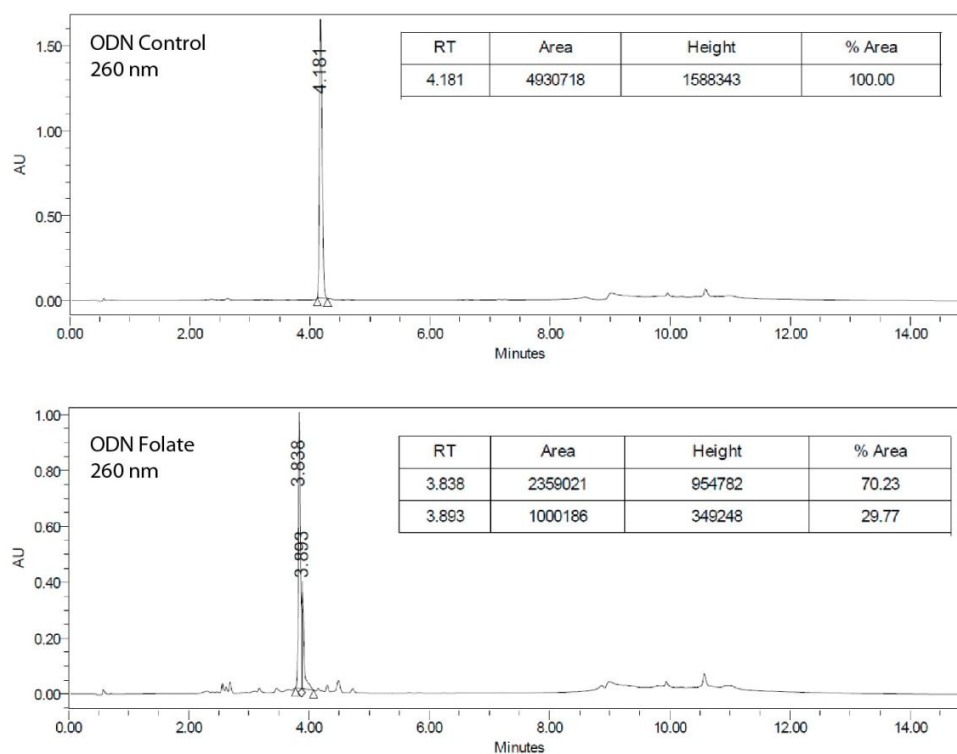


Figure 2. 8. HPLC chromatogram of a single DNA oligonucleotide before and after folate conjugation.

Table 2. 4. Molecular weights of 6 oligonucleotides before and after folate conjugation.

	MW(g/mol)		MW (g/mol) after reaction	
Samples	expected	Experimental	expected	experimental
ODN-1	8913	8920,382	9554,64	9547,765
ODN-2	14355	14602,380	14996,64	14992,571
ODN-3	8937	8931,952	9578,64	9574,670
ODN-4	14197	14195,535	14838,64	14842,370
ODN-5	9075	9071,732	9716,64	9710,265
ODN-6	14119	14142,973	14760,64	14759,459
Folate -PEG3-Azide	641,64			

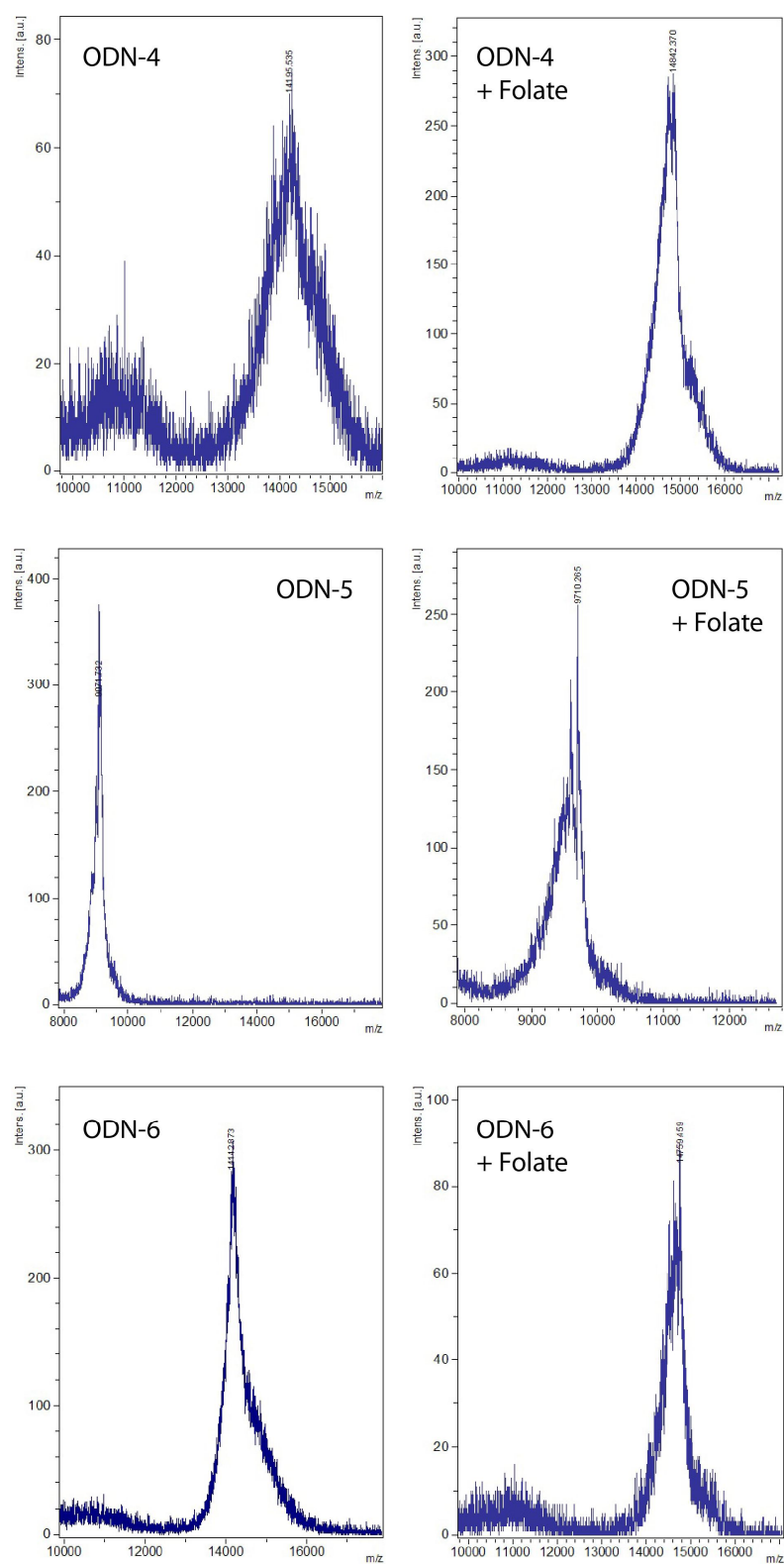


Figure 2. 9. Mass spectrometry analysis of 6 oligonucleotides before and after folate conjugation.

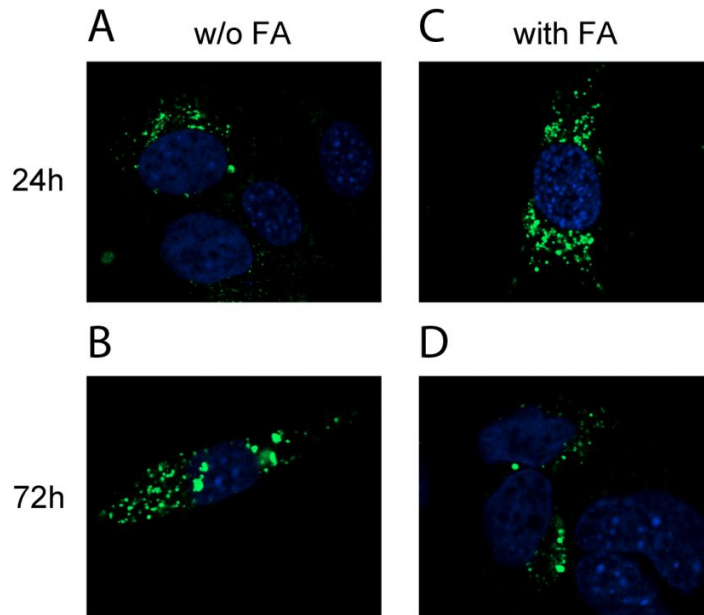


Figure 2. 10. Endosomal uptake of unmodified (a-b) and folate-modified (c-d) DNA nanotubes after 24 hrs and 72 hrs of incubation.

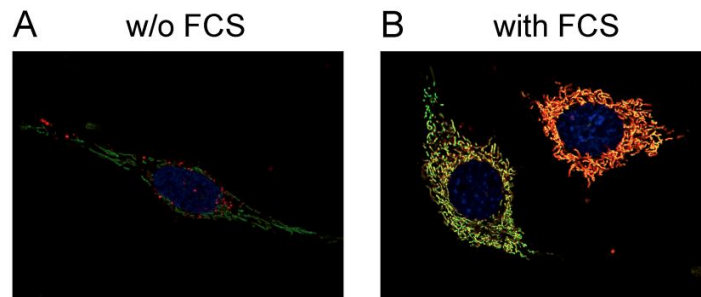


Figure 2. 11. Mitochondrial colocalization of the mitochondrial dye Mito-tracker green (shown in green) and DNA nanotubes (coupled to Atto 647 (shown in Red) after culture medium (a) without FCS and (b) with FCS.

3. One-Step Formation of “Chain-Armor”-Stabilized DNA Nanostructures

3.1. Introduction

Over the last years DNA catenanes gained more interest for future DNA nanotechnology applications as molecular switches or molecular motors. Their topologically interlocked architecture is particularly suited for uses in which tolerance to denaturing conditions is indispensable. Depletion of cations, high temperatures, change of pH or enzymes digestion are indeed critical factors affecting the stability of DNA-based structures. Stability against enzymatic digestion is commonly addressed with the incorporation of artificial bases or backbones.⁹⁷ However, introduction of covalent linkages in DNA strands achieved by enzymatic ligation⁹⁸ or photo crosslinking⁹⁹ is preferred to maintain the structure integrity. Many examples of interlocked DNA and RNA nanostructures such as 2-7 member catenanes,¹⁰⁰ borromean rings,¹⁰¹ trefoil- and other knots¹⁰² from single-stranded and double-stranded nucleic acids have been reported over the last years. Nevertheless, the artificial construction of catenated architectures containing more than 7 rings is limited by the low yield of the products. In the presented work the author disclosed a strategy to overcome DNA catenanes synthesis issues combining the self-assembly features used to fold DNA-nanostructures and the highly efficient click chemistry conjugation method. The use of various DNA-nanostructures, folded using several strand combinations, resulted in a large variety of chain lengths and architectures. The results presented in this work pave the way for a controlled and stoichiometric synthesis of highly membered DNA catenanes with quantitative yields. Additionally, the complete catenation of the structure described herein implies a dramatic increment of the whole DNA-nanostructure stability. This synthetic and stabilization method can be of considerably aid for the preparation of DNA-based drug-delivery shuttles, nano-devices and nano-biosensors still suffering of low stability within complex systems or in absence of appropriate amount of salts.⁸⁷

3.2. DNA Catenane

DNA catenanes (from the Latin word *catena* = chain) are topologically interlocked DNA architectures consisting of two or more cyclic DNA chains that are physically rather than chemically connected to one another like members of a chain. The presence of catenated dimeric DNA rings has been reported in the mitochondria of a human cell line (Fig 3. 1)¹⁰³ and in human leukemic leucocytes.¹⁰⁴

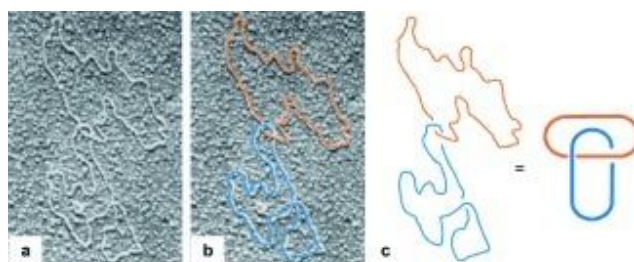


Figure 3. 1. Electron micrographs of circular DNA catenane found in mitochondrial DNA of HeLa cells (a, b) and its graphical representation (c,d). Adapted from “Catenanes: Fifty Years of Molecular Links” G. Gil-Ramírez, D. A. Leigh, A. J. Stephens, 2015, *Angew. Chem. Int. Ed.* **2015**, 54 (21), 6110-6150.

In nature other examples of large DNA catenanes are offered from the mitochondrial DNA, also termed kinetoplast (kDNA), of the protozoa trypanosomatids. The Trypanosomatidae family infects insect, plants and animals and cause human tropical illness such as Chagas disease, sleeping sickness and leishmaniasis. The complicated kDNA of these species is composed of thousands of interlocked mini- and maxi-rings forming an extensive network which can be imaged at Atomic Force Microscope (AFM) (Fig. 3. 2).¹⁰⁵

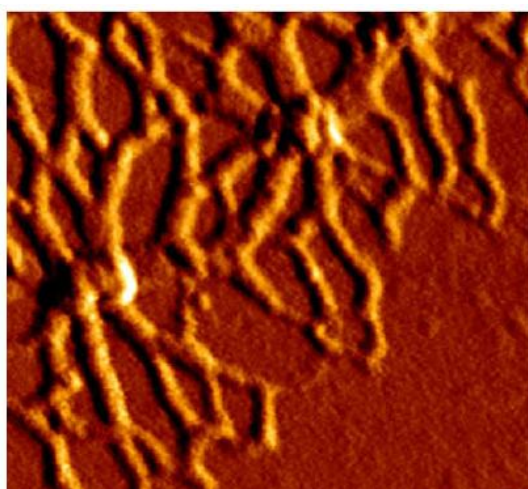


Figure 3. 2. AFM image of isolated kDNA network of the trypanosomatid *C. fasciculata*. Adapted from “The structure of the kinetoplast DNA network of *Crithidia fasciculata* revealed by atomic force microscopy” D. P. Cavalcanti, D. L. Gonçalves, L. T. Costa, W. de Souza, *Micron*, **2011**, 42 (6), 553-559

Mimicking nature to obtain highly membered DNA catenanes is a challenge to which researchers do not have answer yet. In fact, catenated structures composed from two up to seven rings only were obtained

with high synthesis efforts.¹⁰⁰ Several synthesis paths, all based on common hybridization and ligation procedures, are proposed to accomplish catenated architectures. Artificial DNA catenanes are usually synthesized starting from single strands, which have complementary sequences in one region. The double stranded domain formed after hybridization creates the crossing point between the two oligonucleotides. The strands are then enzymatically or chemically ligated. In figure 3. 3 different synthetic routes for the simple two-member DNA catenanes ([2]catenane) are summarized.

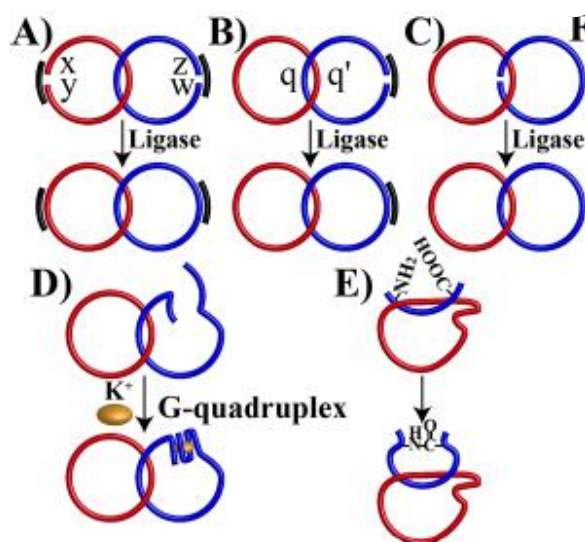


Figure 3. 3. Diverse strategies to obtain [2]catenanes. (A) Enzymatic ligation of two inter-threaded strands. (B) Enzymatic ligation of a single-strand threaded into a circular DNA. (C) Enzymatic ligation of a threaded single strand into a circular DNA, stabilized by base-pairing with the circular DNA at the ligation site. (D) Inter-threading of a single-strand oligonucleotide into a circular DNA and the formation of a K⁺-ion-stabilized G-quadruplex. (E) Covalent linkage (e.g., amide bond) of chemical functionalities associated with the 3'- and 5'-ends of a strand threaded into a circular DNA. Adapted from "Recent Advances in the Synthesis and Functions of Reconfigurable Interlocked DNA Nanostructures" C. H. Lu, A. Cecconello, I. Willner, *J. Am. Chem. Soc.* **2016**, 138 (16), 5172-85.

Larger complexes, such as [3], [5] or [7]catenanes are synthesized following the same strategies illustrated for [2]catenanes. The synthesis of DNA catenanes requires always a purification step where the supramolecular structure is separated from unreacted strands. Synthesis and purification, commonly achieved by HPLC or electrophoretic separation, result in low yields in the range of 10 – 40%.

Interlocked catenanes are ideal structures to be used as molecular devices taking advantage of the mechanical bond connecting their single units. This connection permits the reciprocal movement of the rings only and thereby favors intramolecular rather than intermolecular interaction, as the effective local concentration of the interlocked element is higher than other elements present in solution. The non-covalent interaction can be used to control the movements of the interlocked components such as, for

example, switch between three different station within the catenane.¹⁰⁶ The dynamic transition of the ring position within the catenated structure is obtained by encoding specific binding regions that are alternatively occupied by short strands. The rotary movement through the three stations of the catenane is driven, also in the directionality, by external factors like pH and Hg^{2+} /cysteine administration, which cause displacement/anneal of a C-rich sequence. Externally triggered conformation of [2]catenanes were also exploited as switchable DNAzyme catalytic systems.¹⁰⁷ Deoxyribozymes, or DNAzymes, are DNA molecules that possess catalytic activity mimicking protein enzymes' binding pockets for ligands or catalytic center for chemical reactions. Willner and coworkers designed a two-membered DNA catenane where one ring contained a sequence corresponding to a G-quadruplex region. In the OFF state, G-quadruplex formation is inhibited from its interaction with a portion of the second ring. Through displacement of "fuel" strand with "anti-fuel" strand, reconfiguration of the catenane structure and folding of the G-quadruplex occurs. An hemin molecule complexes with G-quadruplex generating a hemin/G-quadruplex DNAzyme which is able to catalyze H_2O_2 -mediated oxidation reactions. Dynamic mechanical transition was also demonstrated on three-rings system. The [3]catenane was used as scaffold for mechanical switching of gold nanoparticles using specific fuel and blocker strands.¹⁰⁸ Movement of metal nanoparticles on a three ring catenated system was also implemented to control the plasmonic interaction of the nanoparticle with a fluorophore.¹⁰⁸ Indeed, by changing the position of the nanoparticle in respect to the fluorophore enhancement or quenching of the fluorescence was consistent with the theoretical predictions. Synthesis of five¹⁰⁹ or seven¹¹⁰ interlocked rings is accomplished in a stepwise manner. Firstly, smaller elements, composed by two or three catenanes, are synthesized and purified. Afterwards the pure catenanes are associated together by mean of a helper strand, hence generating the large supramolecular structure (Fig 3. 4).

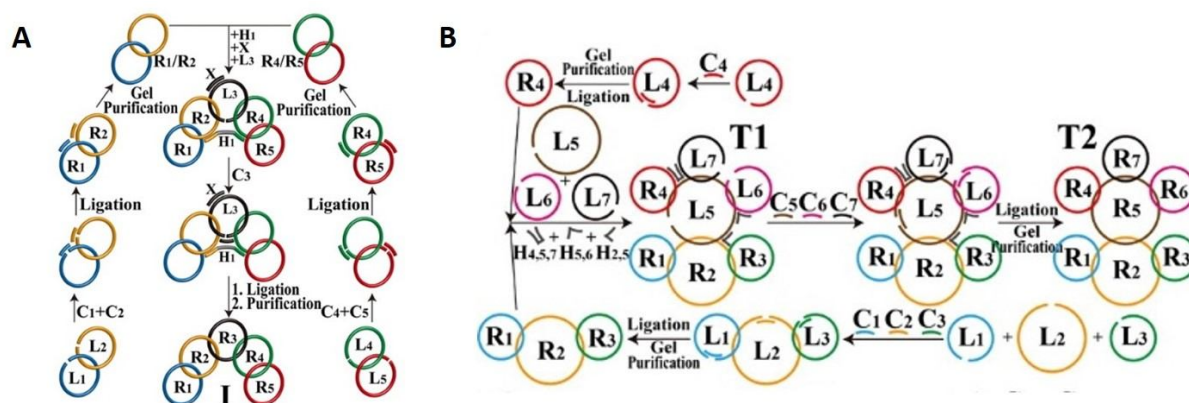


Figure 3. 4. Synthetic strategies for multi-membered DNA catenanes. A) Synthesis of a five-ring interlocked DNA catenane. B) Synthesis of a seven-ring interlocked DNA catenane. Adapted from "Recent Advances in the Synthesis and Functions of Reconfigurable Interlocked DNA Nanostructures" C. H. Lu, A. Cecconello, I. Willner, *J. Am. Chem. Soc.* **2016**, *138* (16), 5172-85.

In the following publication, synthesis of highly-membered DNA catenanes was obtained with high yields in a one-pot stoichiometric reaction. The main advantage of this synthetic strategy lies in the use of a

Single Strand Tile assembled (SST) nanotube to obtain a precise spatial strand pre-organization. The structure selected for this study is a six-helix bundle constituted by 24 oligonucleotides with two different lengths. The longest strands (42mers) contain four domains, each of them is complementary to a region of other four adjacent oligonucleotides. Six shorter strands (22mers) have only two domains and complete the front and the rear part of the structure. In the assembled nanotube the two ends of each strand face each other and once connected form a ring. Thanks to the assembly-driven intertwine, adjacent strands that underwent the same cyclization reaction are catenated and cannot completely denature anymore. The cyclization of the strands is carried out *via* the efficient click chemistry. To this end, alkyne and azide groups are inserted during the solid phase oligonucleotide synthesis at the 3'-end 5'-end of each strand respectively. Once the structure is assembled, the two reactive groups in each oligonucleotide react selectively in presence of Cu(I) resulting in an intramolecular ring closure. This method permits an easy formation of multi-ring DNA catenanes just by designing 6HTs containing different numbers of 5'-azide, 3'-alkyne oligonucleotides (click-tiles). The simultaneous ring closure of all 24 strands results in 24 ring-interlocked catenanes and dramatically increases the stability of the nanostructure even under stringent denaturing conditions.

3.3. Abstract of the publication “One-Step Formation of Chain Armor Stabilized DNA Nanostructures”

DNA-based self-assembled nanostructures are widely used to position organic and inorganic objects with nanoscale precision. A particular promising application of DNA structures is their usage as programmable carrier systems for targeted drug delivery. To provide DNA-based templates that are robust against degradation by elevated temperatures, low ion concentrations, adverse pH conditions, or DNases, we built 6-helix DNA tile tubes consisting of 24 oligonucleotides carrying alkyne groups on their 3'-ends and azides on their 5'-ends. By a mild click reaction, two ends of selected oligonucleotides were covalently connected to form rings and interlocked DNA single-strands, so called DNA catenanes. Strikingly, the structures stayed topologically intact in pure water or even after EtOH precipitation and also if exposed to 95°C if all of the 24 strands were chemically interlocked.

3.4. Author contribution

The author was responsible for the experimental setup, performing the majority of the experiments and analyses.

3.5. Associated Publication:

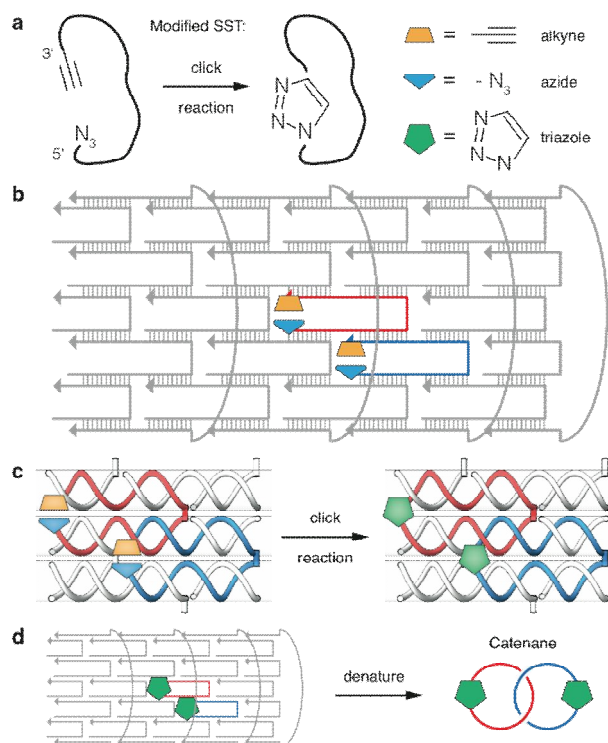
One-Step Formation of Chain Armor Stabilized DNA Nanostructures

Published in:

Cassinelli, V., Oberleitner, B., Sobotta, J., Nickels, P., Grossi, G., Kempter, S., Frischmuth, T., Liedl, T. and Manetto, A., *Angew. Chem. Int. Ed.*, **2015**, 54: 7795–7798.

3.5.1. Introduction

The multi-disciplinary field of DNA nanotechnology, introduced theoretically^[1] and practically^[2] by Nadrian C. Seeman, opened the route to synthesize structures of unprecedented precision at the nanometer scale. Today, DNA-Origami^[3] and the single-stranded tile method (SST)^[4] are routinely used to self-assemble complex nanostructures for various potential applications.^[5] For example, the use of nanosystems for biomedical and diagnostic purposes lead to approaches for cellular immunostimulation,^[6] controlled drug cell delivery to cells,^[7] vaccine design and synthesis,^[8] or membrane channel assembly.^[9] Nevertheless, in most biological applications, DNA nanostructures are exposed to conditions that have adverse effects on Watson-Crick base pairing and can lead to the untimely dissociation of DNA double strands. Cell media, for example, often have concentrations of divalent cations below 2 mM, which is an order of magnitude smaller than Mg^{2+} concentrations used in most assembly protocols for DNA structures. Recent studies showed that low divalent cation concentrations in combination with temperatures of above 35°C are enough to cause the disassembly of a range of DNA objects within 24 hours or less.^[10] A common method to increase the stability of DNA towards nuclease degradation relies on the incorporation of non-natural bases or backbones. However, to maintain topological integrity, covalent linkage of the DNA bases is desirable. Moderate elevated thermal resistance of DNA origami structures by randomly photo-crosslinking the DNA strands with 8-methoxypsoralen^[11] and interlocked DNA and RNA nanostructures such as two to five member catenanes,^[12] borromean rings,^[13] trefoil- and other knots^[14] from single-stranded and double-stranded nucleic acids have been reported over the last years.^[15] However, the artificial assembly of catenated structures containing more than five DNA rings or even more complex systems such as the chain armor-like DNA found in certain single-cell flagellate protozoa (trypanosomatids)^[16] remained challenging.^[17] Nevertheless, such large DNA catenanes are of interest for future DNA nanotechnology applications such as biomedicine in which tolerance to denaturing conditions is indispensable. Here we report the use of SST DNA nanotubes combined with the highly efficient click chemistry method as a platform for the efficient and one-pot stoichiometric assembly of DNA catenanes to an unprecedented complexity of up to 24 DNA rings. Our results demonstrate stoichiometric synthesis of “chain-armor” DNA with almost quantitative yields.



Scheme 3. 1. Graphical exemplification (a) of the click reaction event (b, c) occurring in the DNA nanotube in a pre-organized fashion (d) yielding a DNA catenane.

3.5.2. Results

SST assembly is a modular and reliable method to fold two- and three-dimensional DNA nanoarchitectures from synthetic oligonucleotides.^[18] We here used a 6-helix bundle^[19] hereinafter called 6-helix tube (6HT) consisting of 24 oligonucleotides (Scheme 3. 1). To achieve the formation of DNA catenanes, selected neighboring strands of the 6HT were replaced by (3'-alkyne, 5'-azide)-modified oligonucleotides hereinafter called click-tiles (Scheme 3. 1a) giving rise to modified tubes (MX-tube with X = number of click-tiles included into the structure). The intramolecular cyclization is facilitated by the pre-organization within the folded tube. Moreover, in presence of more than one intertwined click-tile, the simultaneous intramolecular cyclization results in the formation of topologically interlocked ssDNA (Scheme 3. 1b-d). The reaction between alkyne and azide groups catalyzed by copper (I) ions (Copper-catalyzed Azide-Alkyne Cycloaddition, CuAAC)^[20] is here the enabling factor with CuAAC being the most prominent example of click chemistry^[21] due to the high reactivity of its components along with their chemical stability, commercial availability and bio-orthogonality towards e.g. nucleic acids.^[22]

We first introduced two click tiles, each 42mers, within the 6HT structure, namely M2-tube (Scheme 3. 1b). Native agarose gel analysis (2%, 1x TE, 11mM MgCl₂) of the folded M2-tube revealed no detectable shift of the band in respect to the unmodified 6HT tube along with comparable folding yields of up to 90 %. Transmission electron microscopy (TEM) imaging confirmed the correct folding of both

structures. Click reagents (baseclick GmbH, Germany) were then added to both unmodified 6HT and modified M2-tubes and a series of click reaction conditions were tested. In accordance with published data,^[23] the click reagents did not damage the folded structure nor did they influence the electrophoretic properties of both unmodified 6HT and modified M2-tubes even after several hours of reaction at temperatures between 4° and 45°C.

To investigate whether the formation of the two rings within the M2-tube after the click reaction was successful, both unmodified 6HT and modified M2-tubes before and after the click reaction were analyzed by RP-HPLC and LC-MS (supporting information (3.5.6)) and denaturing polyacrylamide gel electrophoresis (PAGE). For the unmodified tubes and M2-tubes before the click reaction, only low molecular weight bands below the 50mer ladder were visible and could be assigned to the individual strands (Figure 3. 5a). As anticipated, only the modified M2-tube after click reaction – marked as M2*-tube - showed a clear band migrating at ~ 100bp. This band was assigned to a newly formed 84mer hetero-dimer (cf. Scheme 3. 1d). Each ring consists of an oligonucleotide covalently connected at its ends via a triazole moiety resulting from the intramolecular CuAAC between the 5'-azide group and the 3'-alkyne group of the oligonucleotide. The pre-organization of these two modified strands within the tube ensures the regio-selectivity of this reaction: the reactive groups of one oligonucleotide are one helix turn (3.4 nm) away from those present in the second modified strand. To support this hypothesis, a free azide was added as competitor to the click reaction mixture along with the M2-tube. The band assigned to the 2-member ring persisted even though the competitor was present in high molar excess (Fig. 3. 21).

To explore whether our approach can be extended to the synthesis of multi-ring DNA catenanes, we designed four more six-helix tubes each containing a different number of click-tiles, which accordingly to our nomenclature were called M7, M11, M20, and M24 tube. Modified tubes treated with the click reaction reagents are additionally marked with an asterisk. The introduction of more than two click-tiles did not influence the correct folding of the tube as confirmed by TEM imaging, nor did it induce a shift in migration speed in agarose gel analysis (Fig 3. 18). Also, the subsequent click reaction carried out on both, unmodified and modified tubes, did not result in structural alterations of the assembled tubes.

The presence of salts – preferably divalent cations such as Mg^{2+} – is necessary for the stability of DNA nanostructures.^[10a] The 6HT used in this study requires 20mM $MgCl_2$ to fold correctly and efficiently. If folded DNA nanotubes were analyzed via agarose gels that miss divalent ions, the nanotubes unfolded and only the individual strands were observed as low molecular weight bands. This principle was used to investigate the assembly and stability of M7*, M11*, M20*, and M24* modified tubes submitted to click reaction. As expected, both unmodified 6HT and tubes before click reaction disassembled completely (Fig. 3. 5b) and tubes after click reaction showed slower migrating bands corresponding to the interlocked catenanes. Remarkably, almost no fast migrating band of individual strands was visible in the lane with the M24* tube, which demonstrates the efficacy of this one-pot stoichiometric multi-cyclization reaction.^[24] This result was further confirmed by an extra set of experiments involving fluorescent labelled click-tiles (3.5.6.16). Strikingly, similar results have been obtained when the catenane-containing nanostructures are heated to 95°C and are then loaded on the gel or after EtOH precipitation of the nanostructures (3.5.6.8 and 3.5.6.9).

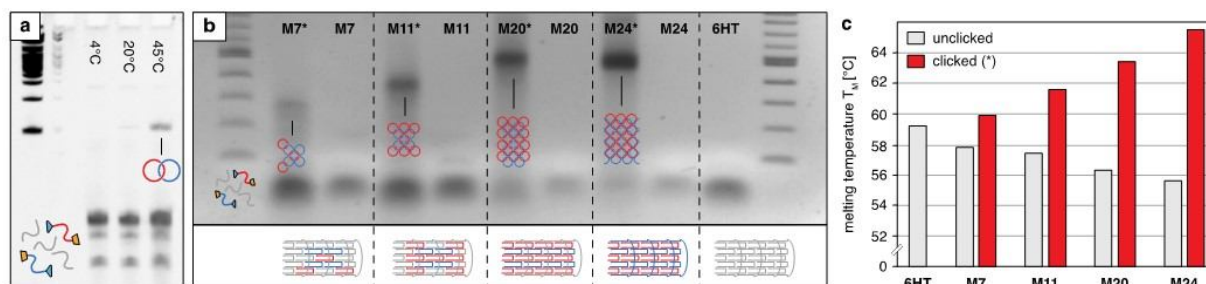


Figure 2. 5. (a) 10% denaturing PAGE analysis of 6HT containing two azide/alkyne modified (M2) strands called M2-tubes after 1.5 hours click reaction at 4°C, 20°C and 45°C (see also figure 2. 15). (b) Native 2% agarose gel electrophoresis missing $MgCl_2$ of tubes containing an increasing amount of *click*-tiles. Modified tubes after click reaction are identified by an asterisk (M7* - M24*) and show the corresponding DNA catenane band. Untreated tubes (M7-M24 and 6HT) unfold during the gel migration and show only lower molecular weight bands of the individual strand. (c) Graphic-bar plot of measured melting temperatures before (grey) and after (red) click reaction.

In a next step, melting transitions of the tubes were measured using a fluorimetric assay with DNA intercalating dyes.^[25] melting temperatures decreased with higher amounts of click-tiles before the reaction while an increasing melting temperature was recorded for tubes with more closed rings (cyclized strands) (Fig. 3. 5c). Compared to the unmodified 6HT, a decrease of 3.6°C was measured when all 24 strands of the tube were substituted with the corresponding click-tiles, which may be due to an energy penalty resulting from the incorporation of the alkyne and azide groups into the DNA structure. If, on the other hand, the click reaction is performed and the catenanes are formed, the melting temperature increases of 6.3°C for the 24-ring structure. This effect could be attributed to the increased local concentration of the partnering DNA sequences in the catenanes. We expected that the M24* tube would remain a monodisperse, covalently locked macromolecule when exposed to stringent denaturing conditions. To corroborate this hypothesis, samples 6HT, M24, and M24* were desalted after regular folding using nitrocellulose membranes. Subsequently, all samples were analyzed in agarose gels. Only the M24* tube survived the desalting process and appeared as a clear band migrating at the correct speed (Fig. 3. 6a).

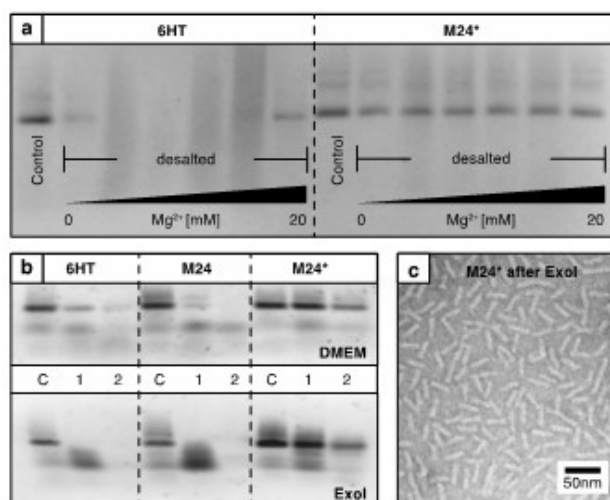


Figure 3. 6. (a) Native agarose gel (2%, 1x TE/MgCl₂) of 6HT (left) and M24* (right) equilibrated *via* micro dialysis with ddH₂O ([Mg²⁺] = 0) or 1x TE buffer containing 0.1, 1, 5, 10 and 20mM MgCl₂. (b) Agarose gels (2%, 1x TE/MgCl₂) of 6HT, M24 and M24*. Top: C = control; 1 = 24hrs at 37°C; 2 = 24hrs at 37°C in DMEM. Bottom: C = control; 1 = 15min at 65°C; 2 = 15min at 65°C, then treated with Exonuclease I for 3hrs at 37°C. (c) TEM micrograph of M24* denatured at 65°C and submitted to 3h Exo I digestion.

Additionally, we also exposed the tubes to Dulbecco's Modified Eagle Medium (DMEM, Merck-Millipore) and incubated them for 24 hours at 37°C. Under these conditions, the M24* tube persisted as a monodisperse nanostructure while the M24 tube and the unmodified 6HT unfolded completely. (Fig. 3. 6b - *top gel*). To further test the stability, the samples were incubated at 65°C for 15 minutes, cooled down in ice-water and submitted to Exonuclease I (Exo I, Thermo Scientific, 10 units) digestion at 37°C for 3 hours. The M24* tubes remained intact after this treatment and appeared as a defined band in the native agarose gel (Fig. 3. 6b – *bottom gel*). TEM imaging of these samples revealed well-defined tubes of the expected size (Fig. 3. 6c).

3.5.3. Conclusion and outlook

The presented cyclization of DNA strands *via* click reaction resulted in efficient formation of interlocked single-stranded rings due to the spatial pre-organization of the reactive groups in a SST assembly. Our method constitutes, to our knowledge, the first example of a one-pot stoichiometry-controlled reaction to form multi-ring DNA catenanes and of chain armor tubes. The resulting increased resistance of such chain armor DNA structures to low cation concentrations, high temperatures, and exonuclease activity could solve stability issues of DNA structures in *in vitro* and *in vivo* applications. The method is not limited to the production of DNA catenanes of varying sizes and chain geometries but could be further applied to assemble oligonucleotides for the synthesis of long single-stranded DNA, thus paving the way to a non-enzymatic gene synthesis approach.

3.5.4. Experimental Section

Oligonucleotides used in this work have two different lengths: 18 x 42mer strands form the centre region and 6 x 28mer strands form the two ends of the tube (Scheme 3. 1b). All tubes were folded by cooling a buffer solution (1x TE, 20mM MgCl₂) containing *n* click-tiles and 24 - *n* unmodified strands (*n* = 0, 2, ..., 24) from 80°C to 65°C in steps of 1°C/min followed by a slower ramp from 65°C to 25°C in steps of 0.5°C every 12min. For the details on click chemistry, HPLC analysis, stability assays consider the Supporting Information (3.5.6).

3.5.5. References and Notes of the publication "One-Step Formation of Chain Armor Stabilized DNA Nanostructures"

- [1] N. C. Seeman, *J. Theor. Biol.* **1982**, *99*, 237-247.
- [2] a) J. Chen, N. C. Seeman, *Nature* **1991**, *350*, 631-633; b) T. J. Fu, N. C. Seeman, *Biochemistry* **1993**, *32*, 3211-3220; c) E. Winfree, F. Liu, L. A. Wenzler, N. C. Seeman, *Nature* **1998**, *394*, 539-544.
- [3] P. W. K. Rothemund, *Nature* **2006**, *440*, 297-302.
- [4] a) Y. Ke, L. L. Ong, W. M. Shih, P. Yin, *Science* **2012**, *338*, 1177-1183; b) B. Wei, M. Dai, P. Yin, *Nature* **2012**, *485*, 623-626.
- [5] a) N. C. Seeman, *Annu. Rev. Biochem.* **2010**, *79*, 65-87; b) D. Smith, V. Schüller, C. Engst, J. Rädler, T. Liedl, *Nanomedicine* **2012**, *8*, 105-121; c) M. Endo, Y. Yang, H. Sugiyama, *Biomater. Science* **2013**, *1*, 347-360.
- [6] a) J. Li, H. Pei, B. Zhu, L. Liang, M. Wei, Y. He, N. Chen, D. Li, Q. Huang, C. Fan, *ACS Nano* **2011**, *5*, 8783-8789; b) V. J. Schüller, S. Heidegger, N. Sandholzer, P. C. Nickels, N. A. Suhartha, S. Endres, C. Bourquin, T. Liedl, *ACS Nano* **2011**, *5*, 9696-9702.
- [7] a) S. M. Douglas, I. Bachelet, G. M. Church, *Science* **2012**, *335*, 831-834; b) Q. Jiang, C. Song, J. Nangreave, X. Liu, L. Lin, D. Qiu, Z.-G. Wang, G. Zou, X. Liang, H. Yan, et al., *J. Amer. Chem. Soc.* **2012**, *134*, 13396-13403; c) H. Lee, A. K. R. Lytton-Jean, Y. Chen, K. T. Love, A. I. Park, E. D. Karagiannis, A. Sehgal, W. Querbes, C. S. Zurenko, M. Jayaraman, et al., *Nat. Nano* **2012**, *7*, 389-393; d) A. S. Walsh, H. Yin, C. M. Erben, M. J. A. Wood, A. J. Turberfield, *ACS Nano* **2011**, *5*, 5427-5432; e) Y.-X. Zhao, A. Shaw, X. Zeng, E. Benson, A. M. Nyström, B. Högberg, *ACS Nano* **2012**, *6*, 8684-8691.
- [8] X. Liu, Y. Xu, T. Yu, C. Clifford, Y. Liu, H. Yan, Y. Chang, *Nano Lett.* **2012**, *12*, 4254-4259.
- [9] M. Langecker, V. Arnaut, T. G. Martin, J. List, S. Renner, M. Mayer, H. Dietz, F. C. Simmel, *Science* **2012**, *338*, 932-936.
- [10] a) J. Hahn, S. F. J. Wickham, W. M. Shih, S. D. Perrault, *ACS Nano* **2014**, *8*, 8765-8775; b) S. D. Perrault, W. M. Shih, *ACS Nano* **2014**, *8*, 5132-5140; c) S. Kocabey, H. Meinl, I. S. MacPherson, V. Cassinelli, A. Manetto, S. Rothenfusser, T. Liedl, F. S. Lichtenegger, *Nanomaterials* **2015**, *5*, 47-60
- [11] A. Rajendran, M. Endo, Y. Katsuda, K. Hidaka, H. Sugiyama, *J. Amer. Chem. Soc.* **2011**, *133*, 14488-14491.

- [12] R. P. Goodman, I. A. T. Schaap, C. F. Tardin, C. M. Erben, R. M. Berry, C. F. Schmidt, A. J. Turberfield, *Science* **2005**, *310*, 1661.
- [13] C. Mao, W. Sun, N. C. Seeman, *Nature* **1997**, *386*, 137-138.
- [14] a) S. M. Du, N. C. Seeman, *Biopolymers* **1994**, *34*, 31-37; b) S. M. Du, B. D. Stollar, N. C. Seeman, *J. Amer. Chem. Soc.* **1995**, *117*, 1194-1200.
- [15] a) S. S. Jester, M. Famulok, *Acc. Chem. Res.* **2014**, *47*, 1700-1709; b) T. Li, F. Lohmann, M. Famulok, *Nat. Commun.* **2014**, *5*, 4940; c) F. Lohmann, J. Valero, M. Famulok, *Chem. Commun.* **2014**, *50*, 6091-6093; d) T. L. Schmidt, A. Heckel, *Nano Lett.* **2011**, *11*, 1739-1742.
- [16] a) J. Chen, C. A. Rauch, J. H. White, P. T. Englund, N. R. Cozzarelli, *Cell* **1995**, *80*, 61-69; b) B. Liu, Y. Liu, S. A. Motyka, E. E. C. Agbo, P. T. Englund, *Trends in Parasitology* **2005**, *21*, 363-369.
- [17] C. H. Lu, X. J. Qi, A. Cecconello, S. S. Jester, M. Famulok, I. Willner, *Angew. Chem. Int. Ed.* **2014**, *53*, 7499-7503; *Angew. Chem.* **2014**, *29*, 7629-7633.
- [18] Y. Ke, L. L. Ong, W. Sun, J. Song, M. Dong, W. M. Shih, P. Yin, *Nat. Chem.* **2014**, *6*, 994-1002.
- [19] F. Mathieu, S. Liao, C. Mao, J. Kopatsch, T. Wang, N.C. Seeman, *Nano Lett.* **2005**, *5*, 661-665
- [20] a) V. V. Rostovtsev, L. G. Green, V. V. Fokin, K. B. Sharpless, *Angew. Chem. Int. Ed.* **2002**, *41*, 2596-2599; *Angew. Chem.* **2002**, *14*, 2708-2711; b) C. W. Tornøe, C. Christensen, M. Meldal, *J. Org. Chem.* **2002**, *67*, 3057-3064.
- [21] H. C. Kolb, M. G. Finn, K. B. Sharpless, *Angew. Chem. Int. Ed.* **2001**, *40*, 2004-2021; *Angew. Chem.* **2001**, *11*, 2056-2075.
- [22] P. M. E. Gramlich, C. T. Wirges, A. Manetto, T. Carell, *Angew. Chem. Int. Ed.* **2008**, *47*, 8350-8358; *Angew. Chem.* **2008**, *44*, 8478-8487.
- [23] N. V. Voigt, T. Topping, A. Rotaru, M. F. Jacobsen, J. B. Ravnsbaek, R. Subramani, W. Mamdouh, J. Kjems, A. Mokhir, F. Besenbacher, K. V. Gothelf, *Nat. Nano* **2010**, *5*, 200-203.
- [24] Inter-strand click reaction cannot be excluded for the three terminal click-tiles (J1S1, J3S1 and J5S1, left side of Figure S3) due to the particular design of this tube. Experimental observations support the formation of small amounts of inter-strand side-products. Anyway, the overall stability of this particular design is not affected by inter-strand reactions.
- [25] T. L. Sobey, S. Renner, F. C. Simmel, *J. Phys.: Condens. Matter* **2009**, *21*, 034112.

3.5.6. Supporting Information of the publication “One-Step Formation of Chain Armor Stabilized DNA Nanostructures”

3.5.6.1. General methods

All buffers were stored at room temperature.

10x TE Buffer pH 8 (Tris 100 mM, EDTA 10 mM): 12.11 g Tris (VWR) and 3.72 g EDTA (VWR) were added to 900 ml ddH₂O. The mixture was stirred at room temperature until the solution was clear and homogenous. The pH was adjusted to pH 8 using a 1M HCl solution. Afterwards the solution was filled up to 1 L with ddH₂O.

2M MgCl₂ Solution: 40.66 g MgCl₂ (hexahydrate, Carl Roth) were added slowly to 100 ml ddH₂O (exothermic reaction). The solution was stirred at room temperature until it became clear

10x TE Buffer, 200mM MgCl₂: 9 ml of 10x TE buffer was transferred into a 15 ml falcon tube and 1ml of 2M MgCl₂ was added. The mixture was thoroughly stirred.

1x TE Buffer with 20mM MgCl₂ (folding buffer): the buffer was prepared using ddH₂O.

10x TBE Buffer pH8 (Tris-HCl 1M, H₃BO₃ 1M, Na-EDTA 20mM): 121.1 g Tris-Cl (Carl Roth), 61.8 g H₃BO₃ (Carl Roth) and 7.44 g Na-EDTA (Carl Roth) were added to 900 ml ddH₂O. The mixture was stirred at room temperature until the solution was clear and homogenous. The pH was adjusted to pH 8 using a 1M HCl solution. Afterwards the solution was filled up to 1 L with ddH₂O.

0.5x TBE Buffer: the buffer was prepared using ddH₂O.

0.5x TBE Buffer containing 11mM MgCl₂: To 100 ml 10x TBE Buffer pH 8, 11 ml 2M MgCl₂ were added. The mixture was filled up to 2 L with ddH₂O.

2% Agarose gel (0.5x TBE Buffer, 11mM MgCl₂): 2.6 g Agarose (Carl Roth) were dissolved in 130 ml of 0.5x TBE buffer and the mixture was heated up to dissolve completely the agarose. A solution of MgCl₂ (715 µl, 2M) was added to the warm mixture and stirred for a while before casting the gel. To obtain better electrophoretic resolutions, thinner gels were casted if required (1 g agarose dissolved in 50 ml 0.5x TBE buffer + 275 µl 2M MgCl₂). Appropriate sample amounts were loaded into the agarose gel using 2 µl 6x Loading Dye (New England Biolab). The running chamber was filled up with 0.5x TBE buffer containing 11mM MgCl₂. A 70 V voltage was applied to the electrophoretic equipment (BioRad) for 2 hours, while the chamber was cooled down. Agarose gels were stained with ethidium bromide (0.25 µmol/l in 0.5x TBE buffer containing 11mM MgCl₂) for 20 minutes and then destained for 10 minutes in 0.5x TBE buffer containing 11mM MgCl₂. Gels were imaged using a UV-transilluminator (biostep) or Gel Doc Ez System (Biorad).

2% Agarose gel missing MgCl₂ (0.5x TBE Buffer): 2.6 g Agarose (Carl Roth) was dissolved in 130 ml of 0.5x TBE buffer and the mixture was heated up to dissolve completely the agarose. To obtain better electrophoretic resolutions, thinner gels were casted if required (1 g agarose dissolved in 50 ml 0.5x TBE buffer). Appropriate sample amounts were loaded into the agarose gel using 2 µl 6x Loading Dye (New England Biolab). The running chamber was filled up with 0.5x TBE buffer. A 70 V voltage was applied to the electrophoretic equipment (BioRad) for 2 hours, while the chamber was cooled down. Agarose gels

were stained with ethidium bromide (0.25 $\mu\text{mol/l}$ in 0.5x TBE buffer) for 20 minutes and then destained for 10 minutes in 0.5x TBE buffer. Gels were imaged using a UV-transilluminator (biostep) or Gel Doc Ez System (Biorad).

10% denaturing polyacrylamide gel electrophoresis (PAGE): A 10% ammonium persulfate (APS, Merck Millipore) solution was prepared in advance dissolving 1 g of APS in 10 ml ddH₂O. Rotiphorese® buffers and gel concentrate (Carl Roth) were used to cast the gel following the supplier instructions. To initiate the polymerization 150 μl 10% APS solution and 10 μl of N,N,N',N''-Tetramethylethylenediamine (TEMED, Sigma Aldrich) were added to the gel mixture, stirred and then the gel was casted. Appropriate sample amounts were loaded into the polyacrylamide gel using 2 μl 6x Loading Dye (New England Biolab). The running chamber was filled up with 0.5x TBE buffer. A 120 V voltage was applied to the electrophoretic equipment (Mini-PROTEAN Tetra Cell system, BioRad) for 1 hour. Gels were stained in 200 ml 0.5x TBE buffer containing 20 μl SYBR Gold Stain (Life Technologies) for 10 minutes and imaged using a UV-transilluminator (biostep) or Gel Doc Ez System (Biorad).

TEM imaging: 2 μl sample was adsorbed for 3 minutes onto glow-discharged, carbon-coated TEM grid (PLANO GmbH). The rest of the drop was discarded. The grid was then rapidly washed with 2% aqueous uranyl formate solution containing 25mM NaOH and afterwards stained for 10 seconds with the same solution. Imaging was performed using a JEM 1011 (Jeol) operated at 80 kV (LMU, Physic Department) or a FEI Tecnai G2 Spirit (Bio)twin operated at 80 kV (Aarhus, iNANO).

RP-HPLC analysis: RP-HPLC analysis were obtained by e2695 separation module (Waters) coupled with a 2998 photodiode array detector (Waters). The samples were separated with a reversed phase XBridge OST C18 column (4.6 mm x 50 mm, Waters) with a particle size of 130 Å and an inner diameter of 2.5 μm . The method used is described in table 3. 1.

Table 3. 1. Analytical HPLC method. Buffer A: 100 ml stock solution (101.19 g Triethylamine, 60.05 ml acetic acid HPLC grade dissolved in 1 L H₂O HPLC grade) + 900 ml H₂O HPLC grade. Buffer B: 100 ml stock solution + 100 ml H₂O HPLC grade + 800 ml Acetonitrile HPLC grade. All HPLC grade solvents were purchased from Fischer Chemicals.

t (min)	T (°C)	Flow (ml/min)	Buffer A (%)	Buffer B (%)
0	23°C	1,5	100	0
7	23°C	1,5	55	45
9	23°C	1,5	15	85
10	23°C	1,5	15	85
14	23°C	1,5	100	0
15	23°C	1,5	100	0

UHPLC-LTQ (Orbitrap): mass analysis were obtained using an UltiMate 1290 Rapid Separation LC (RSLC) (Agilent) coupled to an LTQ-Orbitrap XL (Thermo Scientific). A capillary column (Poroshell 120 EC-C18,

4.6, 250 mm, 2.7 μ m) with an inner diameter of 0.5 μ m was used for the UHPLC-MS analysis and the method applied is described in table 3. 2.

Table 3. 2. UHPLC method. Solvent A: water + 0.1 % (v/v) ammonium carbonate, Solvent B: acetonitrile + 0.1 % (v/v) ammonium carbonate

t (min)	T (°C)	Flow (μ l/min)	Solvent A (%)	Solvent B (%)
0	30°C	40	100	0
10	30°C	40	90	10
20	30°C	40	90	10
22	30°C	40	70	30
30	30°C	40	70	30
32	30°C	40	0	100
42	30°C	40	100	0

Fluorescence gel detection: fluorescence detection was carried out using a TECAN LS 300 Laser scanner (laser 496 nm, Filter 590 Cy3, 200 PMT gain, Large pinhole). Bands intensity quantification was made using the software ImageJ.

3.5.6.2. Oligonucleotides

The oligonucleotides in RP-HPLC grade were purchased by baseclick GmbH (Tutzing, Germany) or Metabion GmbH (Munich, Germany).

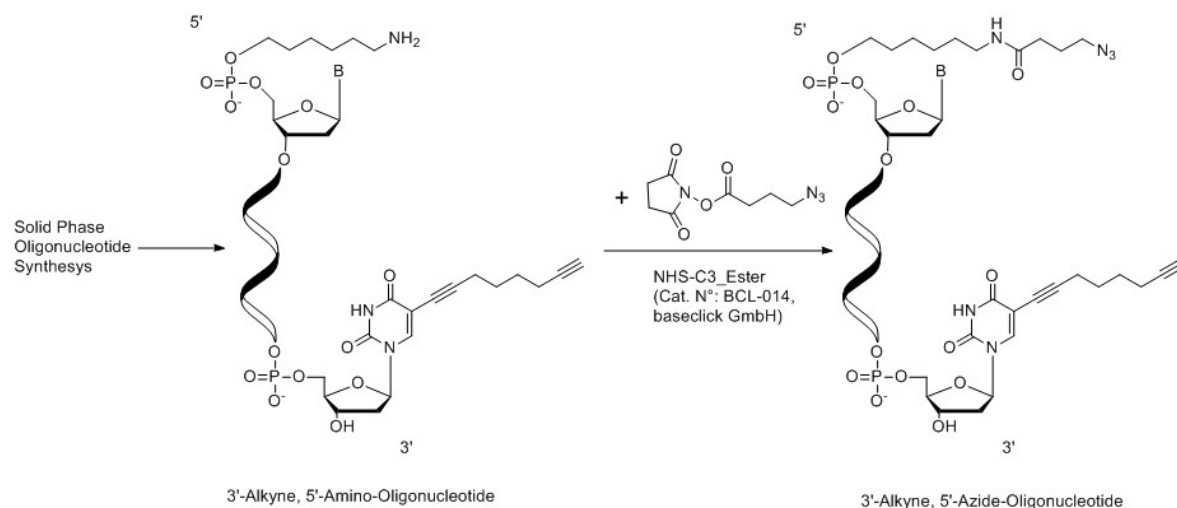
Unmodified strands

Table 3. 3. Sequences of all unmodified strands used in this work.

Oligo code	Sequence 5' -> 3'	Length (bases)
U1R1	AAA ACGCTAAGCCA CCTTTAGATCC AAAT	28
U1R2	GGTCGTGCGG ACTGTCGAACA CCAACGATGCC TGATAGAAGT	42
U1R3	GCGTGGAAT AGCCATAAATT CATACTAACG GCGCCAGACT	42
U1R4	TTTCAAGACC AGCACTTGTAT GCGTAGGGCG GGTTTAGCGT	42
U2R1	GGATCTAAAGG ACTTCTATCA AAGACGGGAC GACTCCGGGAT	42

U2R2	GGCATCGTTGG AGTCTGGCGC ACGACTTCGA TTTCGGATCCT	42
U2R3	CGTTATGTATG ACGCTAAACC TTGCAATGAC TGAACCTGAAT	42
U2R4	CGCCCTACGCC AAA AAA GATGGGAGCTT	28
U3R1	AAA ATCCCGGAGTC CGCTGCTGATC AAAT	28
U3R2	GTCCCGTCTT AGGATCCGAAA GCCATAATATA TCGAGACGGT	42
U3R3	TCGAAGTCGT ATTCGAGTTCA AATGTCTATGC GATGCAGCAT	42
U3R4	GTCATTGCAA AAGCTCCCATC ATTTAATGTCG TTTACAGTAT	42
U4R1	GATCAGCAGCG ACCGTCTCGA CTGCAGAAAT AGGACCCCCAT	42
U4R2	TATATTATGGC ATGCTGCATC TTCCTGGCAT GGCTGAATTCT	42
U4R3	GCATAGACATT ATACTGTAAA ACCTTACGTA ACTTACAGCCT	42
U4R4	CGACATTAAAT AAA AAA GATGAGTATTT	28
U5R1	AAA ATGGGGGTCCT CGAGGCGAAAC AAAT	28
U5R2	ATTTCTGCAG AGAATTCAGCC TATTCACATAG GCGAAGGCTT	42
U5R3	ATGCCAGGAA AGGCTGTAAGT TGCATCATGGG GGTCTCAAT	42
U5R4	TACGTAAGGT AAATACTCATC CCTGAGTGATC CATGACCCTT	42
T6-R11	GTTTCGCCTCG AAGCCTTCGC CCGCACGACC TGGCTTAGCGT	42
T6-R22	CTATGTGAATA ATTGAGGACC ATTGCCACGC TGTTGACAGT	42
T6-R33	CCCATGATGCA AAGGGTCATG GGTCTTGAAA AATTTATGGCT	42
T6-R44	GATCACTCAGG AAA AAA ATACAAGTGCT	28

Modified oligonucleotides (*click*-tiles)



Scheme 3. 2. Synthesis of a generic *click*-tile. The azide group at the 5'-position of the *click*-tile was introduced in a two-step synthesis involving firstly the introduction of a C6-amino linker during the oligonucleotide synthesis followed by the post-synthesis conjugation with the NHS-C3-azide linker. On the other hand, the alkyne group present on the 3'-end of the *click*-tile was directly introduced during the oligonucleotide solid phase synthesis.^[1] Both functionalization protocols proceed smoothly, with high yields and are commercially available.

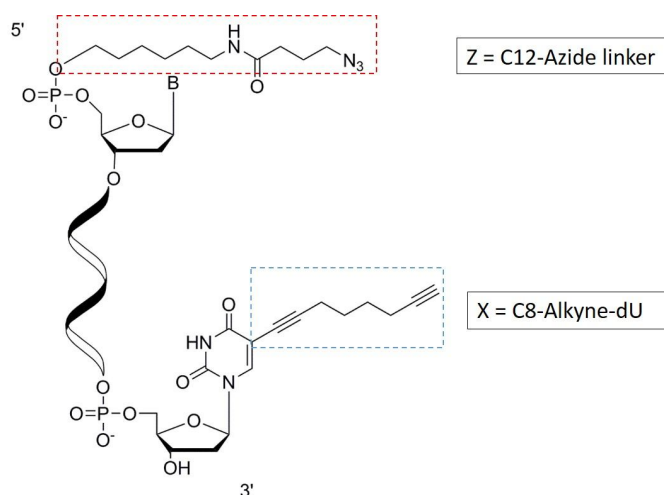


Figure 3. 7. Representation of a generic azide/alkyne modified strand (*click*-tile). In the red box is highlighted the Z modification (C12*-Azide linker conjugated to the 5'-phosphate) and in the blue box the X modification (C8-Alkyne-dU).

* Comparable to a C12 spacer.

Table 3. 4. Sequences of all modified oligonucleotides (*click-tiles*) used in this work. X and Z defined in figure 3. 7.

Oligo code	Sequence	Length (bases)
J1S1	ZAAA ACGCTAAGCCA CCTTAGATCC AAAX	28
J1S2	ZGGTCGTGCGG ACTGTGGAACA CCAACGATGCC TGATAGAAGX	42
J1S3	ZGCGTGGCAAT AGCCATAAATT CATAATAACG GCGCCAGACX	42
J1S4	ZTTTCAAGACC AGCACTTGTAT GCGTAGGGCG GGTTTAGCGX	42
J2S1	ZGGATCTAAAGG ACTTCTATCA AAGACGGGAC GACTCCGGGAX	42
J2S2	ZGGCATCGTTGG AGTCTGGCGC ACGACTTCGA TTTCGGATCCX	42
J2S3	ZCGTTATGTATG ACGCTAAACC TTGCAATGAC TGAAGTCAAX	42
J2S4	ZCGCCCTACGCC AAA AAA GATGGGAGCTX	28
J3S1	ZAAA ATCCCGGAGTC CGCTGCTGATC AAAX	28
J3S2	ZGTCCCGTCTT AGGATCCGAAA GCCATAATATA TCGAGACGGX	42
J3S3	ZTCGAAGTCGT ATTCGAGTTCA AATGTCTATGC GATGCAGCAX	42
J3S4	ZGTCATTGCAA AAGCTCCCATC ATTTAATGTCTG TTTACAGTAX	42
J4S1	ZGATCAGCAGCG ACCGTCTCGA CTGCAGAAAT AGGACCCCCAX	42
J4S2	ZTATATTATGGC ATGCTGCATC TTCCTGGCAT GGCTGAATTCX	42
J4S3	ZGCATAGACATT AACTGTAAA ACCTTACGTA ACTTACAGCCX	42
J4S4	ZCGACATTAAAT AAA AAA GATGAGTATTX	28
J5S1	ZAAA ATGGGGGTCCT CGAGGCGAAAC AAAX	28
J5S2	ZATTTCTGCAG AGAATTCAGCC TATTCACATAG GCGAAGGCTX	42
J5S3	ZATGCCAGGAA AGGCTGTAAGT TGCATCATGGG GGTCTCAAX	42
J5S4	ZTACGTAAGGT AAATACTCATC CCTGAGTGATC CATGACCCTX	42
J6S1	ZGTTTCGCCTCG AAGCCTTCGC CCGCACGACC TGGCTTAGCGX	42

J6S2	ZCTATGTGAATA ATTGAGGACC ATTGCCACGC TGTTGACAGX	42
J6S3	ZCCCATGATGCA AAGGGTCATG GGTCTTGAAA AATTTATGGCX	42
J6S4	ZGATCACTCAGG AAA AAA ATACAAGTG CX	28



Figure 3. 8. Design of the unmodified tile assembled structure (6HT).^[2] The structure has a calculated length of 27 nm and an outer diameter of 8.5 nm. The helices bow slightly outwards due to the electrostatic repulsion between the negatively charged backbones of the DNA.



Figure 3. 9. Design of the completely modified (M24) tile assembled structure. By inserting modification at 3'- and 5'-ends there are no changes in the dimension of the structure.

3.5.6.3. Tubes folding

Table 3. 5. Schematic representation of oligonucleotides composition of the different tubes used in the work. To obtain different catenane patterns, selected unmodified oligonucleotides were replaced in the 6HT design with click-tiles (highlighted by colored boxes).

6HT				M2				M7			
U5R1	U5R2	U5R3	U5R4	U5R1	U5R2	J5S3	U5R4	U5R1	J5S2	U5R3	U5R4
U4R1	U4R2	U4R3	U4R4	U4R1	U4R2	J4S3	U4R4	U4R1	J4S2	U4R3	U4R4
U3R1	U3R2	U3R3	U3R4	U3R1	U3R2	U3R3	U3R4	U3R1	U3R2	J3S3	U3R4
U2R1	U2R2	U2R3	U2R4	U2R1	U2R2	U2R3	U2R4	U2R1	U2R2	J2S3	U2R4
U1R1	U1R2	U1R3	U1R4	U1R1	U1R2	U1R3	U1R4	U1R1	U1R2	U1R3	J1S4
T6-R11	T6-R22	T6-R33	T6-R44	T6-R11	T6-R22	T6-R33	T6-R44	T6-R11	T6-R22	T6-R33	J6S4
M11				M20				M24			
U5R1	J5S2	U5R3	J5S4	J5S1	J5S2	J5S3	J5S4	J5S1	J5S2	J5S3	J5S4
U4R1	J4S2	J4S3	U4R4	J4S1	J4S2	J4S3	J4S4	J4S1	J4S2	J4S3	J4S4
U3R1	U3R2	J3S3	U3R4	J3S1	J3S2	J3S3	J3S4	J3S1	J3S2	J3S3	J3S4
U2R1	J2S2	J2S3	U2R4	J2S1	J2S2	J2S3	J2S4	J2S1	J2S2	J2S3	J2S4
U1R1	J1S2	U1R3	J1S4	J1S1	J1S2	J1S3	J1S4	J1S1	J1S2	J1S3	J1S4
J6S1	T6-R22	T6-R33	J6S4	T6-R11	T6-R22	T6-R33	T6-R44	J6S1	J6S2	J6S3	J6S4

3.5.6.4. Folding mixture

Accordingly to table 3. 5 each strand (1μl, 0.05 nmol) was added to 10 μl 10x TE Buffer containing 200mM MgCl₂ and completed with ddH₂O up to 100 μl. This premix was briefly mixed and folded using a thermocycler (MJ Mini, BioRad). The final concentration of the tube was 0.5μM.

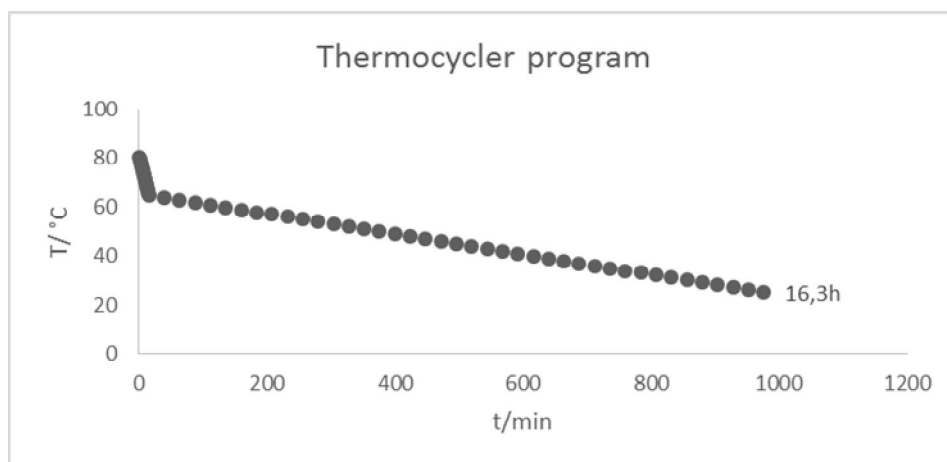


Figure 3. 10. Graphical diagram of the folding program used in this work. The folding program consist of a cooling ramp from 80°C to 65°C, with a decrement of 1° per minute and then from 64°C to 25°C with a decrement of 0.5°C each 12 minutes.

Agarose gel of 6HT and M2 tubes

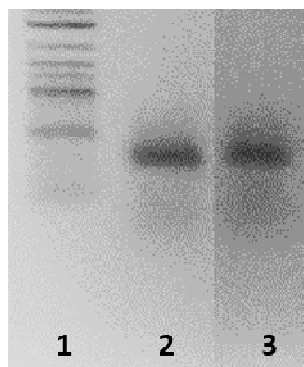


Figure 3. 11. 2% Agarose gel (0.5x TBE Buffer, 11 mM mgCl_2) of 6HT and M2-tube after folding (*lane 1. 2-Log DNA ladder, lane 2. 6HT, lane 3. M2-tube*). The insertion of two *click*-tiles does not affect the folding process since no shift of the bands was detectable in the agarose gel electrophoresis analysis.

For agarose gel electrophoresis analysis of M7, M11, M20 and M24 see Figure 3. 18.

3.5.6.5. Click reaction

Tubes treated with click reaction reagents are additionally marked with an asterisk (e.g. M2-tube becomes M2 tube after click reaction).*

For a preliminary click optimization, different parameters (Cu(I) sources, temperatures and times) were tested on M2-tube. 6HT was used as negative control. Click reactions were carried out using two

different copper (I) sources: CuBr (baseclick) and a heterogeneous catalyst included in a labeling kit (OligoClickM-Reload, baseclick), which is stable even in oxygenated aqueous solutions.

CuBr catalyst: 0.1M solution of the Cu(I)-ligand, tris[(1-hydroxypropyl-1H-1,2,3-triazol-4-yl)methyl]amine (THPTA) was prepared using 10 mg THPTA (baseclick) dissolved in 230 μ l *Click Solution* (baseclick). CuBr (5 mg, baseclick) was dissolved in 350 μ l of *Click Solution* and promptly added to 2 volumes of THPTA 0.1M. The CuBr/THPTA mixture was always freshly prepared and immediately added to the samples (0.5 μ M) in a volume ratio of 0.5:1. The reaction mixture was stirred (maximum 200 rpm) in a thermomixer for different time ranges (from 0.5 hour to 5 hours) and at different temperatures (from 4° to 45°C).

OligoClickM-Reload catalyst: Following the supplier instructions, 40 μ l of the solution containing the folded nanostructure (0.5 μ M) were added to the heterogeneous catalyst pre-impregnated with 15 μ l of the water-soluble *Activator* included into the kit. The reaction mixture was gently mixed at defined reaction temperatures and times. The mixture was then transferred in a fresh vial and the heterogeneous catalyst discharged. The sample was analyzed without any further purification step.

The click reaction does not have negative effect on the folding of the structures, as proved by agarose gel electrophoresis (Fig 3. 12) and TEM (Fig 3. 13)

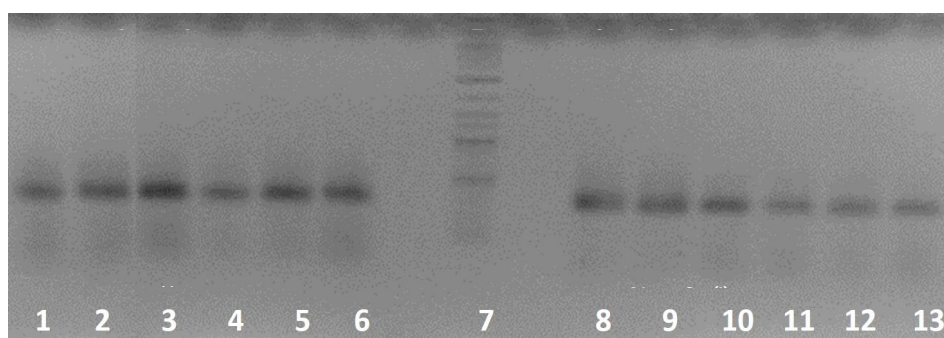


Figure 3. 12. 6HT and M2* tubes after click reaction with baseclick catalyst for 1.5 hours (2% Agarose gel 0.5x TBE buffer, 11mM MgCl₂). From lane 1 to lane 3: 6HT submitted to click reaction at 4°C (lane 1), 20°C (lane 2) and 45°C (lane 3). From lane 4 to lane 6: M2-tube submitted to click reaction at 4°C (lane 4), 20°C (lane 5) and 45°C (lane 6). Lane 7: 2-Log DNA ladder (New England Biolabs). From lane 8 to lane 10: 6HT negative controls (in absence of catalyst) at 4°C (lane 8), 20°C (lane 9) and 45°C (lane 10). From lane 11 to lane 13: M2 negative controls (in absence of catalyst) at 4°C (lane 11), 20°C (lane 12) and 45°C (lane 13).

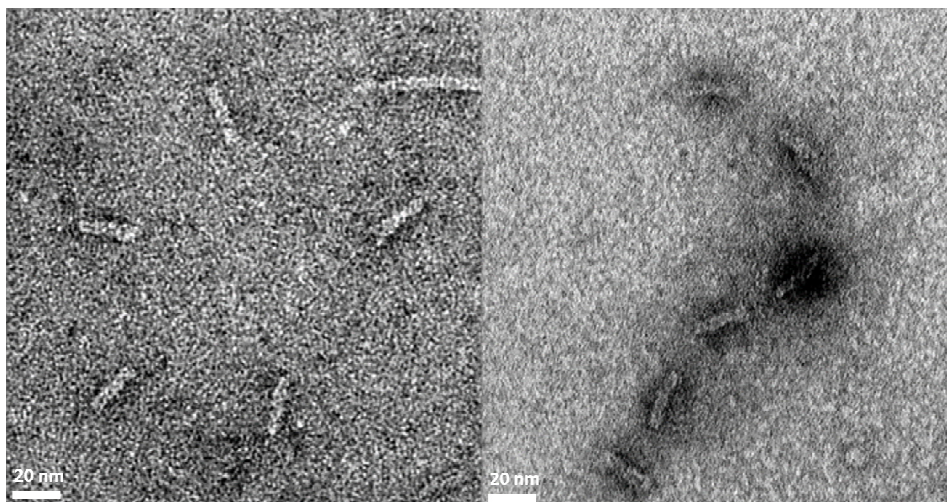


Figure 3. 13. TEM micrographs of M2* tubes. After click reaction (OligoClickM-Reload catalyst, 3 hours, 32°C), the tubes do not look damaged.

TEM micrographs of modified nanotubes after click reaction

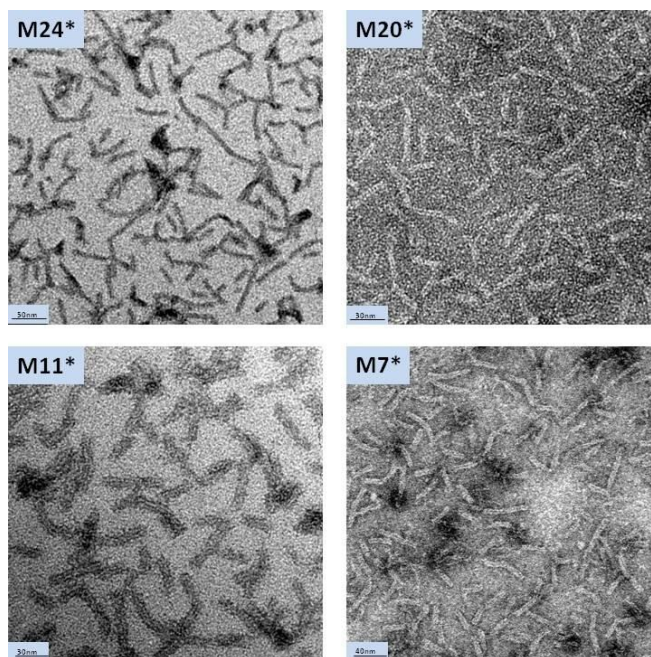


Figure 3. 14. TEM imaging of nanotubes after click reaction. Upper left: M24* tubes, upper right: M20* tubes, bottom left: M11* tubes, bottom right: M7* tubes. All tubes showed no detectable damage in the structure after click reaction (OligoClickM-Reload catalyst, 3 hours, 32°C).

Denaturing PAGE of M2 tubes before and after click reaction

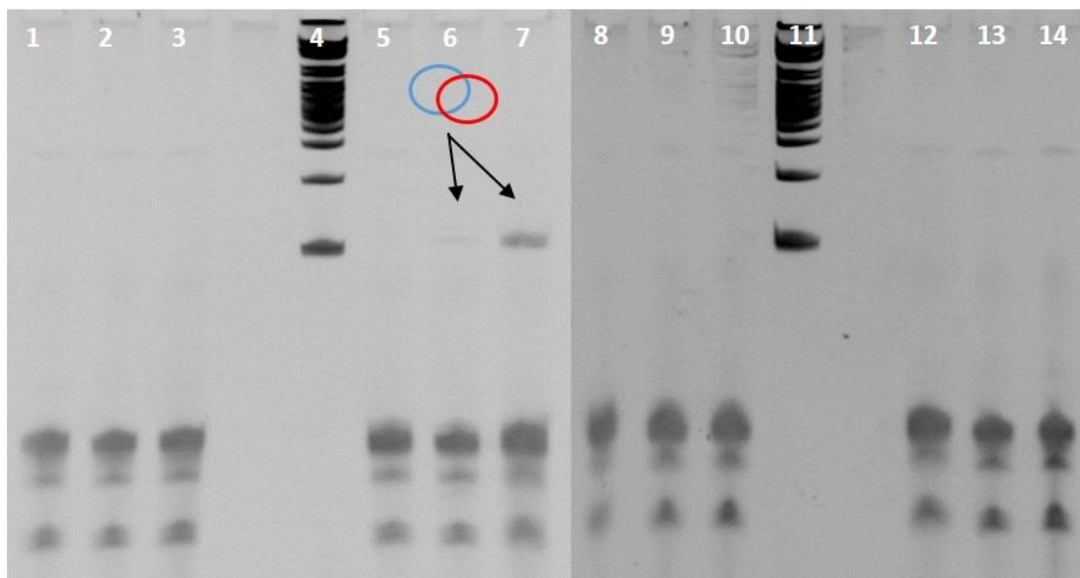


Figure 3. 15. 10% denaturing PAGE analysis of 6HT and M2* tubes after click reaction using the OligoClickM-Reload kit (1.5 hours, different temperatures). From lane 1 to lane 3: 6HT reacted at 4°C (lane 1), 20°C (lane 2) and 45°C (lane 3). Lane 4 and lane 11: 2-Log DNA ladder (New England Biolabs). From lane 5 to lane 7: M2-tubes reacted at 4°C (lane 4), 20°C (lane 5) and 45°C (lane 6). From lane 8 to lane 10: 6HT negative controls (in absence of catalyst) at 4°C (lane 8), 20°C (lane 9) and 45°C (lane 10). From Lane 12 to lane 14: M2-tubes negative controls (in absence of catalyst) at 4°C (lane 12), 20°C (lane 13) and 45°C (lane 14). Under these conditions (1.5 hours), click reaction occurs only at 20°C (low yield, weak band, lane 6) and at 45°C (high yield, stronger band, lane 7).

3.5.6.6. Click reaction optimization

Other tests were performed to find out the best click reaction condition for this system. CuBr and the heterogeneous catalyst of OligoClickM-Reload kit were compared in a narrower range of temperature (23°C to 32°C) and over different time interval (2.5 hours, 3.5 hours and 5 hours).

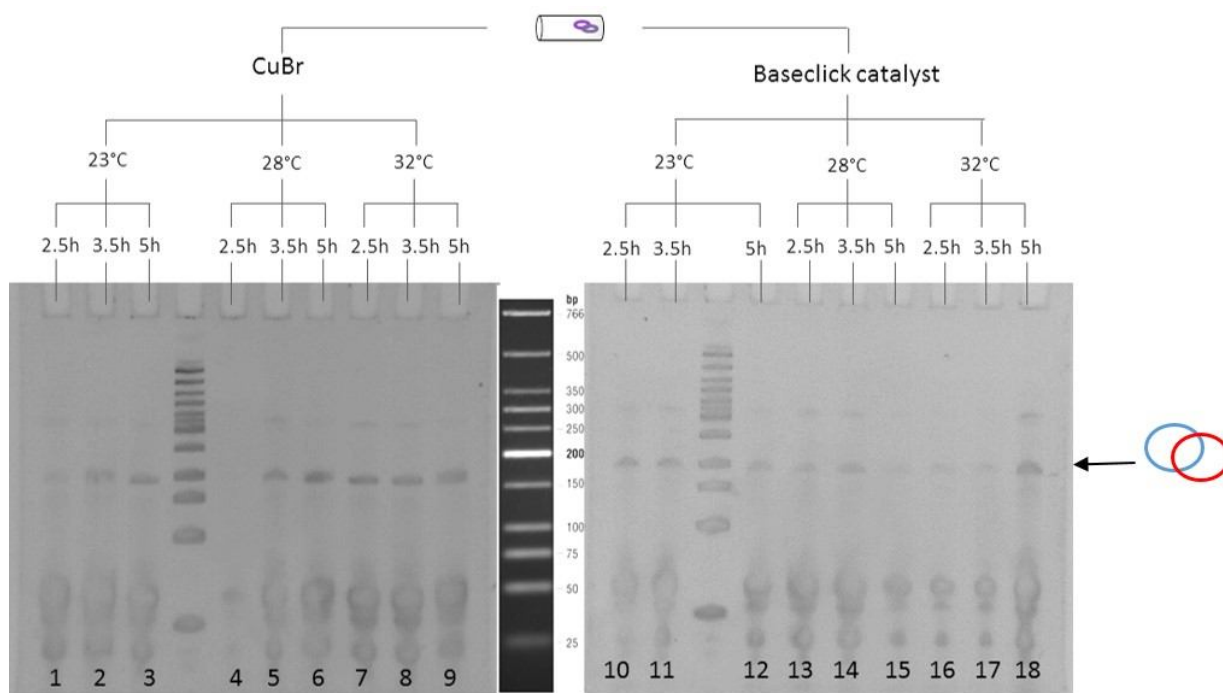


Figure 3. 16. Optimization of the click reaction (10% denaturing PAGE). Low molecular ladder (New England Biolabs) was used for this PAGE. The yields of the click reaction (formation of the 2-member ring) were comparable between all the different assays when using CuBr, while the heterogeneous catalyst performed better at 32°C for 5 hours reaction.

Click reaction at 4°C

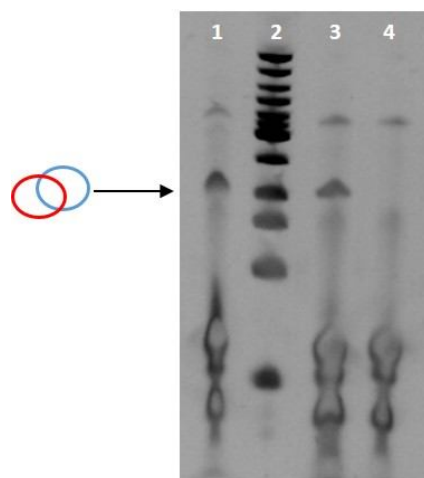


Figure 3. 17. 10% denaturing PAGE of M2-tubes reacted at 4°C using two different Cu(I) sources: Click reaction using CuBr at 4°C (*lane 1*); Low molecular ladder (New England Biolabs, *lane 2*); click reaction using the heterogeneous catalyst at 40°C (*lane 3*) and at 4°C (*lane 4*). At 4°C CuBr catalyst performed better than the heterogeneous catalyst. The latter yielded the 2-member ring at 40°C.

3.5.6.7. Stability of catenane

Reacted and unreacted nanotubes showed similar electrophoretic mobility when loaded onto a 2% agarose gel containing divalent cations (Mg^{2+}) as visible in figure 3. 18.

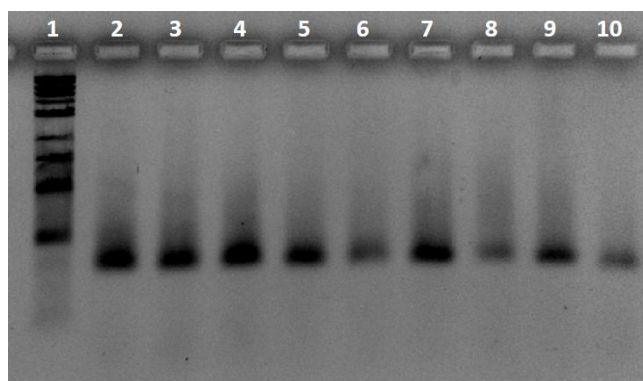


Figure 3. 18. 2% agarose (0.5x TBE Buffer containing 11 mM MgCl_2) control gel to test the correct folding of the tubes before and after click reaction. *Lane 1*: 2-Log DNA ladder; *lane 2*: M7* tubes; *lane 3*: M7-tubes; *lane 4*: M11* tubes; *lane 5*: M11-tubes; *lane 6*: M20* tubes; *lane 7*: M20-tubes; *lane 8*: M24* tubes; *lane 9*: M24-tubes; *lane 10*: 6HT.

To prove that DNA catenanes obtained after the click reaction were topologically interlocked, samples were loaded into agarose gel missing MgCl_2 . Namely, the reacted nanotubes (10 μl , 900 μM in *folding buffer*) were loaded into a 2% agarose gel (0.5x TBE buffer) without MgCl_2 . The corresponding structures before click reaction (M7, M11, M20 and M24) and 6HT were loaded in the same gel as references (Fig. 2. 19).

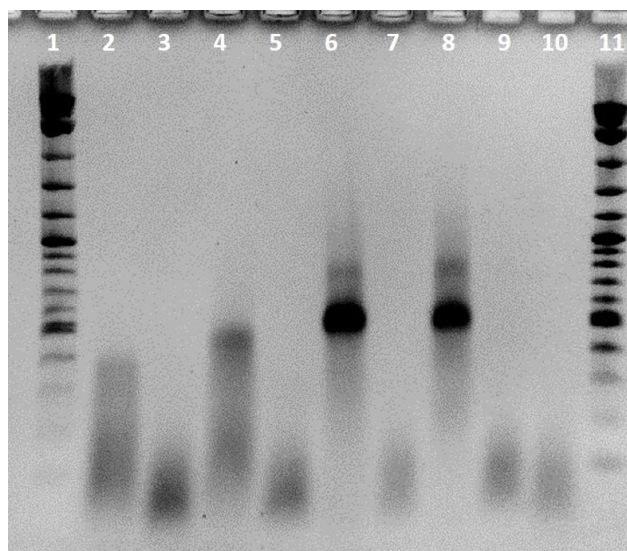


Figure 3. 19. 2% agarose gel (0.5x TBE buffer) missing MgCl_2 to test visualize the DNA catenanes formed after click reaction. *Lane 1:* 2-Log DNA ladder; *lane 2:* M7* tubes \rightarrow 7-member catenanes; *lane 3:* M7-tubes; *lane 4:* M11* tubes \rightarrow 11-member catenanes; *lane 5:* M11-tubes; *lane 6:* M20* tubes \rightarrow 20-member catenanes; *lane 7:* M20-tubes; *lane 8:* M24* tubes \rightarrow 24-member catenanes; *lane 9:* M24-tubes; *lane 10:* 6HT; *lane 11:* 2-Log DNA ladder.

In agarose gel without MgCl_2 the tubes not submitted to click reaction revealed only a broad band at low molecular weight corresponding to the unfolded strands, while the samples treated with click reagents showed higher molecular weight bands assigned to DNA catenanes.

3.5.6.8. Resistance to heating (95°C) of DNA catenanes after click reaction

To further test the presence of DNA catenane after the click reaction under denaturing conditions, the reacted and the unreacted samples were heated for 2 minutes at 95°C before loading them into a 2% agarose gel (0.5x TBE buffer) without MgCl_2 .

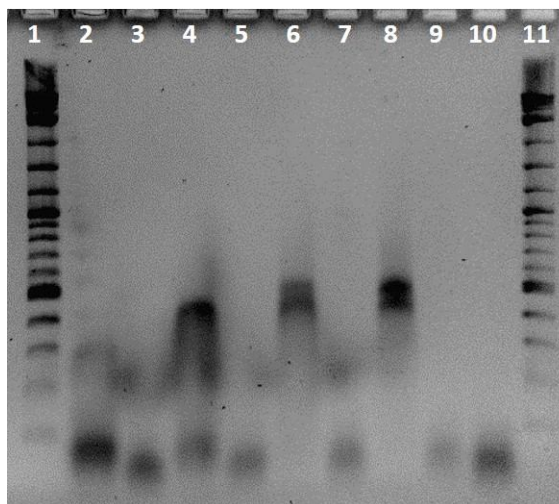


Figure 3. 20. 2% agarose gel (0.5x TBE buffer) missing MgCl_2 of treated and untreated samples after thermal denaturation (2 minutes at 95°C). *Lane 1:* 2-Log DNA ladder; *lane 2:* M7* tubes \rightarrow 7-member catenanes; *lane 3:* M7-tubes; *lane 4:* M11* tubes \rightarrow 11-member catenanes; *lane 5:* M11-tubes; *lane 6:* M20* tubes \rightarrow 20-member catenanes; *lane 7:* M20-tubes; *lane 8:* M24* tubes \rightarrow 24-member catenanes; *lane 9:* M24-tubes; *lane 10:* 6HT; *lane 11:* 2-Log DNA ladder.

The DNA catenane bands were present for reacted samples confirming the presence of larger entities assigned to DNA catenanes. Unreacted samples unfolded due to the denaturing treatment and the absence of divalent cation in the gel. The DNA catenane bands are not well defined due probably to the negative effect of MgCl_2 at high temperature.^[3]

3.5.6.9. Resistance of DNA catenanes to ethanol precipitation

We tested the resistance of the DNA catenanes (present in M7*, M11*, M20* and M24* tubes) to desalting procedure and subsequent ethanol precipitation. The same procedure was carried out on M7, M11, M20, M24 tubes and 6HT as control. Desalting procedure was performed on nitrocellulose membrane (Millipore). Petri dish was filled up with 40 ml ddH_2O , the membrane was placed on the liquid surface and a drop of sample (10 μL) was pipette on it. After 20 minutes, the drop was recollected into a vial containing 10 μL sodium acetate (3M) and mixed thoroughly. Finally 1 ml 100% cold ethanol was added to the mixture and stored at -20°C overnight. The EtOH phases were discharged after centrifugation (20 minutes, 15300 rpm, 4°C) and the pellets were washed once with cold ethanol 70%. At the end of the precipitation procedure, the samples were re-suspended in 30 μL H_2O HPLC grade and analyzed by 2% agarose gel (0.5x TBE buffer) missing MgCl_2 . The gel (Fig. 3. 5b) showed sharp DNA catenanes bands, meaning that the nanostructure submitted to click reaction and thus the DNA catenanes formed within were resistant to this stress procedure, while unreacted samples and 6HT showed only a low molecular band due to the unfolded oligonucleotides.

3.5.6.10. Competitive click reaction

The small fluorescent dye 6-FAM Azide (baseclick) was added to a solution of M2-tubes (10 μ l, 5 pmol, 0.5 μ M) containing two alkynes (10 pmol alkynes). In a first setup a 2.5 times (2.5 μ l, 25 pmol) molar excess on respect of total amount of alkynes was used. Alternatively, a 20 times (20 μ l, 200 pmol) molar excess was applied. The positive control consisted of a mono-alkyne modified oligonucleotide (5 μ l, 5 nmol, 1mM) mixed and reacted with a FAM-azide solution (2.5 μ l, 25 nmol, 10mM). The negative control consisted of the M2-tubes (10 μ l, 5 pmol, 0.5 μ M) mixed with the click reaction reagents in absence of any competitive azide. All four samples were submitted to click reaction at 45°C for 1.5 hours using OligoClickM-Reload kit. The reaction mixtures were analyzed afterwards using 10% denaturing PAGE analysis. The efficient formation of 2-member ring catenane is highlighted in figure 3. 21.

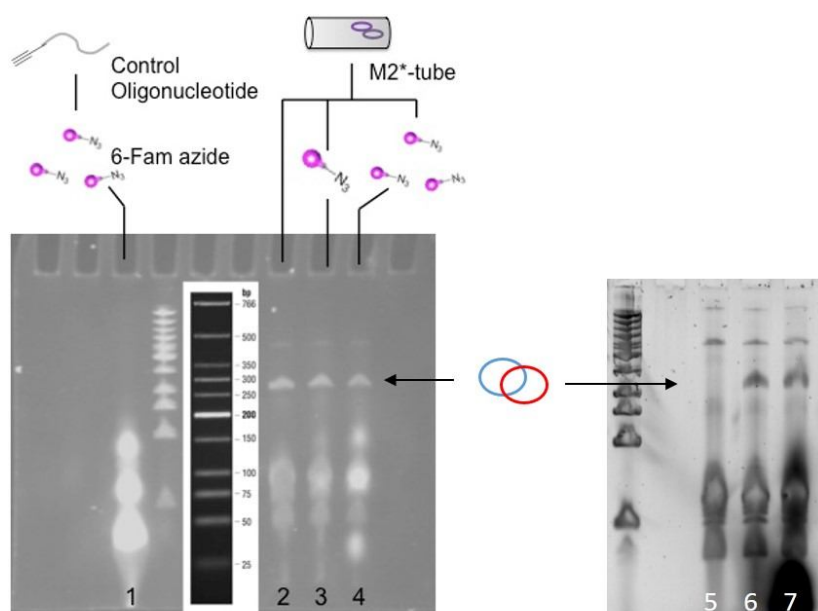


Figure 3. 21. 10% denaturing PAGE of competitive click reaction. *Lane 1:* positive control with mono-alkyne modified oligonucleotides; *Lane 2 and 6:* negative control samples (M2-tubes reacted without 6-FAM azide); *Lane 3:* click reaction on M2-tube in presence of 2.5 equivalents of 6-FAM azide; *Lane 4:* click reaction on M2-tube in presence of 20 equivalents of 6-FAM azide; *Lane 5:* M2-tubes reacted without 6-FAM azide and without copper catalyst; *Lane 7:* click reaction on M2-tube in presence of 1000 equivalents of 6-FAM azide. The ladder used in this gel is Low molecular ladder (New England Biolabs).

Although the presence of a large excess of competitor (up to 1000 fold excess) the click reaction between the two *click*-tiles inside the M2-tube was preferred, as proved by the persistence of the band assigned to the 2-member ring catenane.

3.5.6.11. RP-HPLC and MS

Starting from the observation that unmodified oligonucleotides have a different retention time in RP-HPLC from the respective *click*-tiles, we used RP-HPLC as analytical method to get more insight on ring formation efficacy. *Click*-tiles (42mer) introduced in the M2 design and corresponding unmodified oligonucleotides were independently analyzed by RP-HPLC, generating the appropriate references (Fig. 3. 22 – 3. 25).

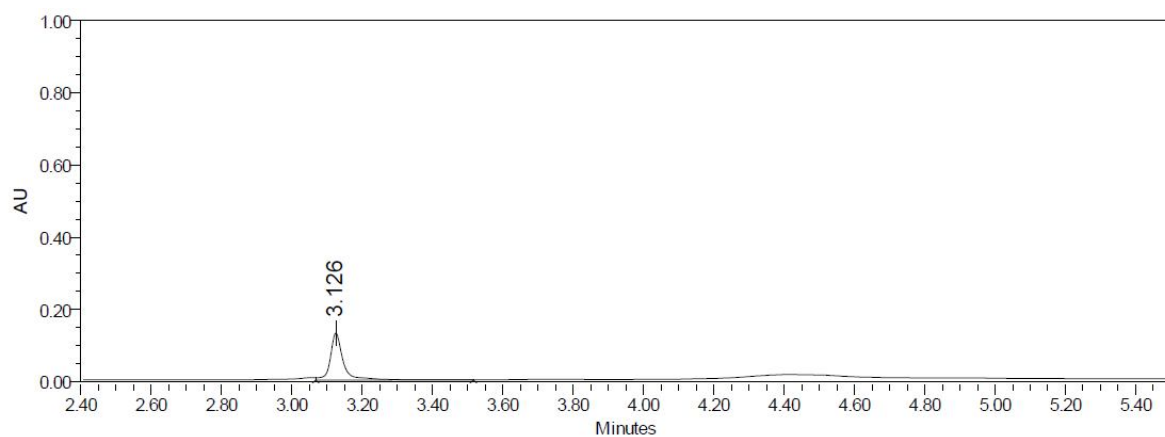


Figure 3. 22. HPLC chromatogram of U4R3 unmodified strand. U4R3 (4 μ L, 50 μ M) was diluted with 16 μ L H₂O HPLC grade (Final concentration 10 μ M – Injection Volume 18 μ L). The unmodified strand U4R3 showed a retention time of 3.12 min.

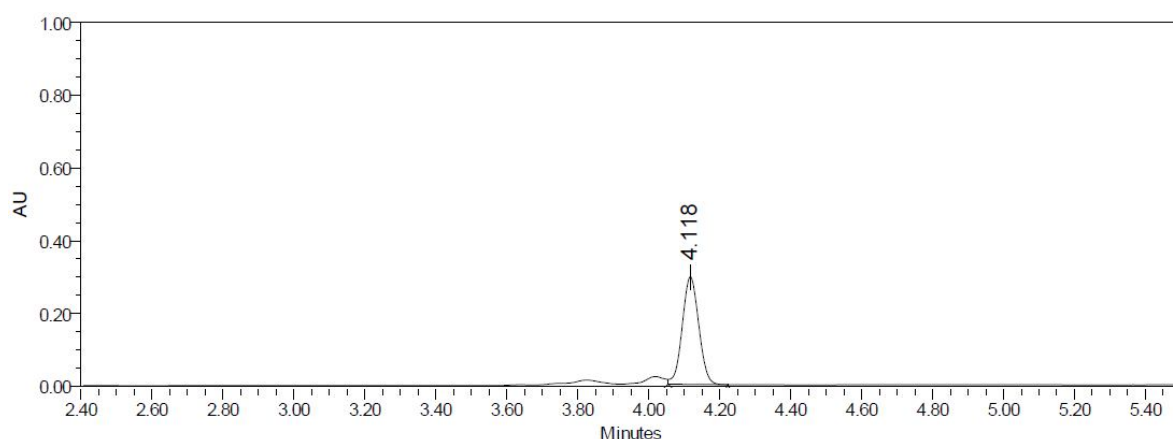


Figure 3. 23. HPLC chromatogram of *click*-tile J4S3. J4S3 (4 μ L, 50 μ M) was diluted with 16 μ L H₂O HPLC grade (Final concentration 10 μ M – Injection Volume 18 μ L). The *click*-tile J4S3 showed a retention time of 4.11 min, 1 minute later than the corresponding unmodified strand U4R3.

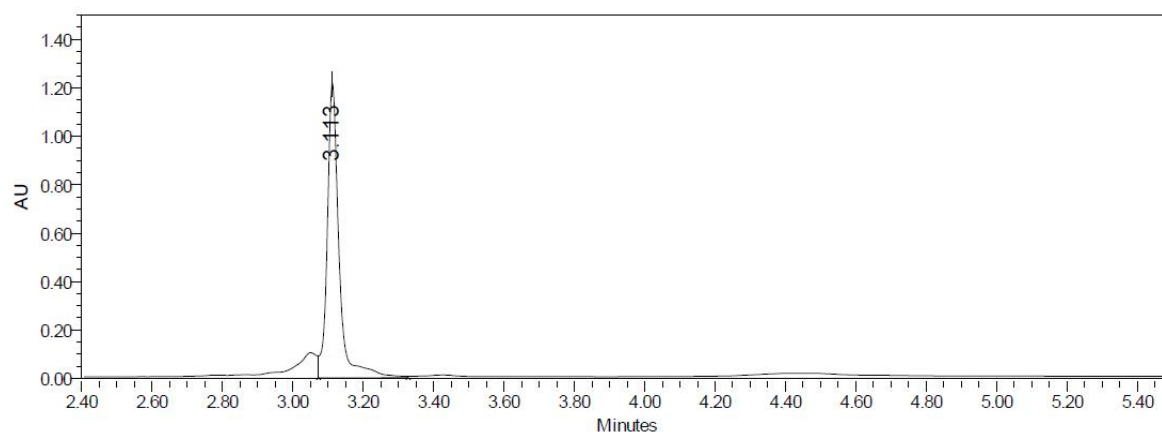


Figure 3. 24. HPLC chromatogram of U5R3 unmodified strand. U5R3 (4 μ L, 50 μ M) was diluted with 16 μ L H₂O HPLC grade (Final concentration 10 μ M – Injection Volume 18 μ L). The unmodified strand U5R3 showed a retention time of 3.11 min.

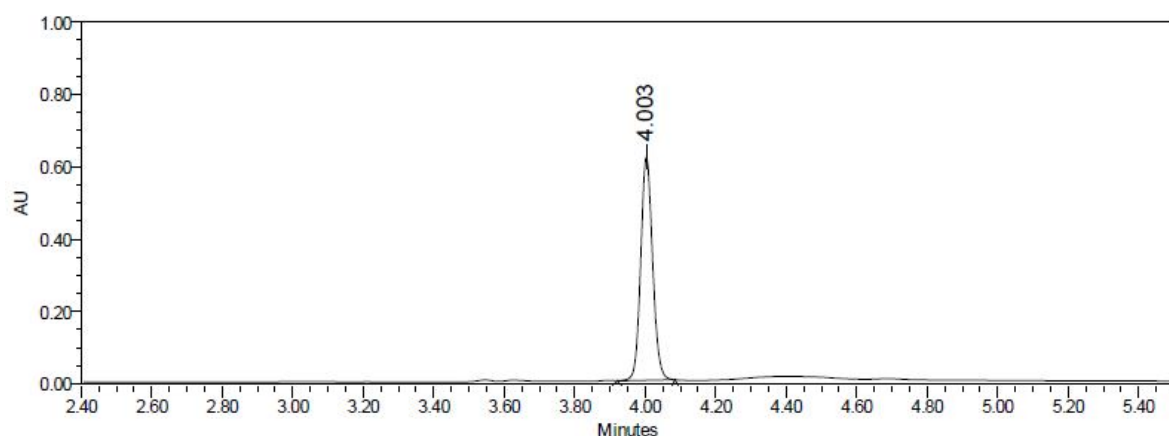


Figure 3. 25. HPLC chromatogram of *click*-tile J5S3. J5S3 (4 μ L, 50 μ M) was diluted with 16 μ L H₂O HPLC grade (Final concentration 10 μ M – Injection Volume 18 μ L). The *click*-tile J5S3 showed a retention time of 4.00 min, 1 minute later than the corresponding unmodified strand U5R3.

The folded structures 6HT, M2-tubes and M2* tubes (each consisting of 24 oligonucleotides) were separately analyzed by RP-HPLC as well (Fig. 2. 26 – 2. 28).

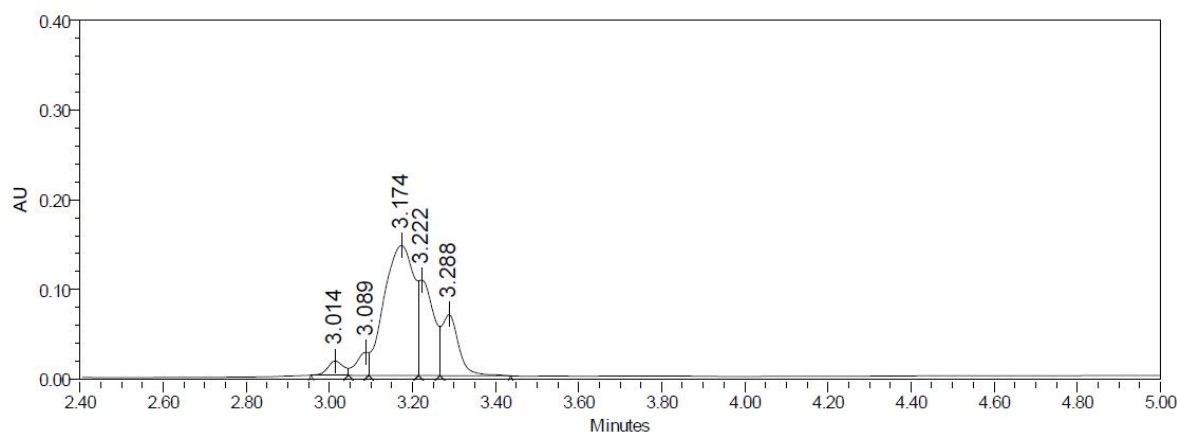


Figure 3. 26. HPLC chromatogram of 6HT. 6HT (20 μ L in *folding buffer*) was diluted to 500 μ L with *folding buffer* and filtrated using Amicon Centrifugal filters (Millipore) following the supplier instructions. Just before the injection, the recovered sample (30 μ L) containing the folded tube was submitted to mechanical stress (1 minute vortex and 1 minute ultrasound) to promote denaturation of the nanostructure and eventually a better HPLC resolution (28 μ L injection volume). The analysis of the complete strand mixture (6HT) by RP-HPLC lead to a large chromatogram peak in the range between 2.9 and 3.3 minutes.

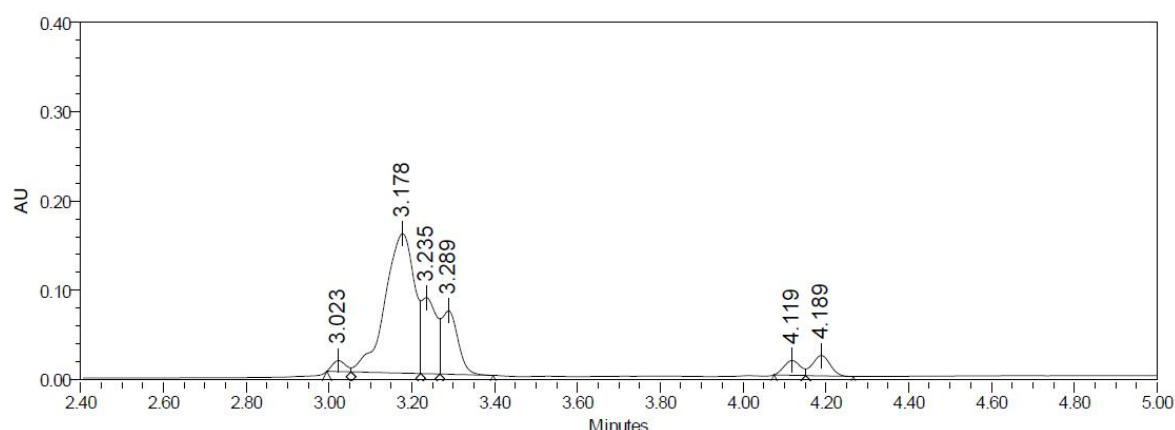


Figure 3. 27. HPLC chromatogram of M2-tubes. M2-tubes (20 μ l in *folding buffer*) was diluted to 500 μ l with *folding buffer* and filtrated using Amicon Centrifugal filters (Millipore). Just before the injection, the recovered sample (30 μ L) containing the folded tube was submitted to mechanical stress (1 minute vortex and 1 minute ultrasound) to promote denaturation of the nanostructure and eventually a better HPLC resolution (28 μ l injection volume). The *click*-tiles were well separated from the rest of unmodified oligonucleotides, thus being easily detectable as double peak at 4.1 minutes.

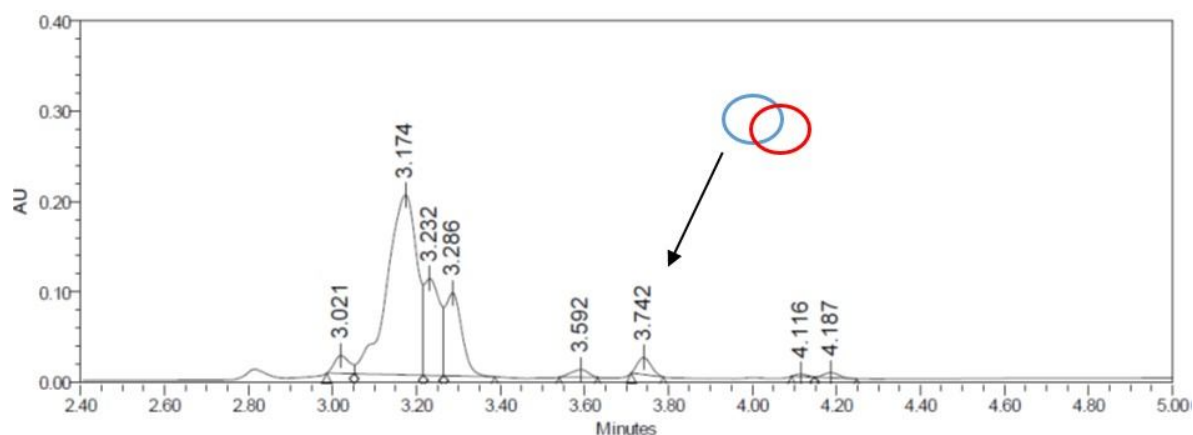


Figure 3. 28. HPLC chromatogram of M2* tubes. M2* tubes (40 μ l in *folding buffer*) was diluted to 500 μ l with *folding buffer* and filtrated using Amicon Centrifugal filters (Millipore). Just before the injection, the recovered sample (30 μ L) containing the folded tube was submitted to mechanical stress (1 minute vortex and 1 minute ultrasound) to promote denaturation of the nanostructure and eventually a better HPLC resolution (28 μ l injection volume). After carrying the *click* reaction on the M2-tube, the HPLC chromatogram showed the formation of a new peak at 3.7 min, which was assigned to the newly formed 2-members ring catenane. The two *click*-tiles (double peak at 4.1 minutes) were clearly consumed during the reaction.

The fraction at 3.7 min containing the isolated two-member ring catenane, collected from analytical HPLC, was concentrated by evaporation in a SpeedVac (Christ AVC 2-25 CD coupled with cooling trap Christ CT 04-50 SR). The dried sample was re-suspended in 50 μ l H₂O HPLC grade and analyzed by LC-MS (UHPLC – LTO, Orbitrap, Thermo Scientific) as showed in figures 3. 29 – 3. 32.

Table 3. 6. Calculated value of dimer-ions.

-	M (g/mol)	[M-8] ⁸⁻	[M-9] ⁹⁻	[M-10] ¹⁰⁻
Two-member catenane	26665.36	3332.16	2961.80	2665.52

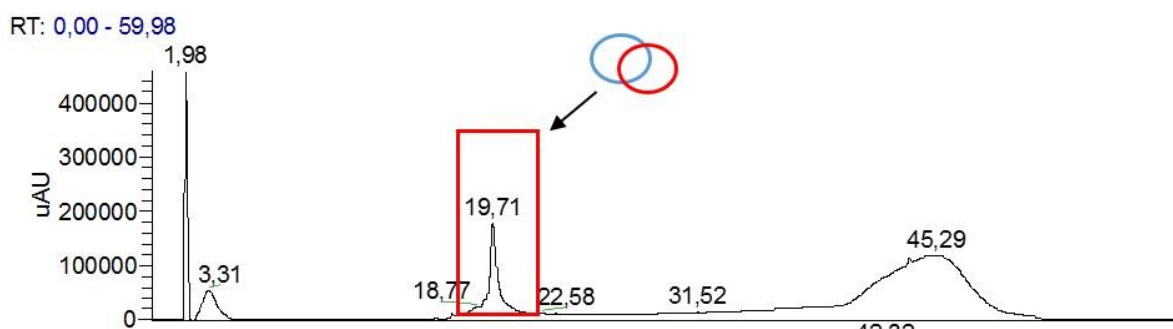


Figure 3. 29. UHPLC chromatogram analysis of isolated 3.7 min HPLC peak. The UHPLC chromatogram showed the peak of the isolated two-member ring catenane (red box) at 19.71 minutes. This peak was further analyzed in the coupled mass spectrometer.

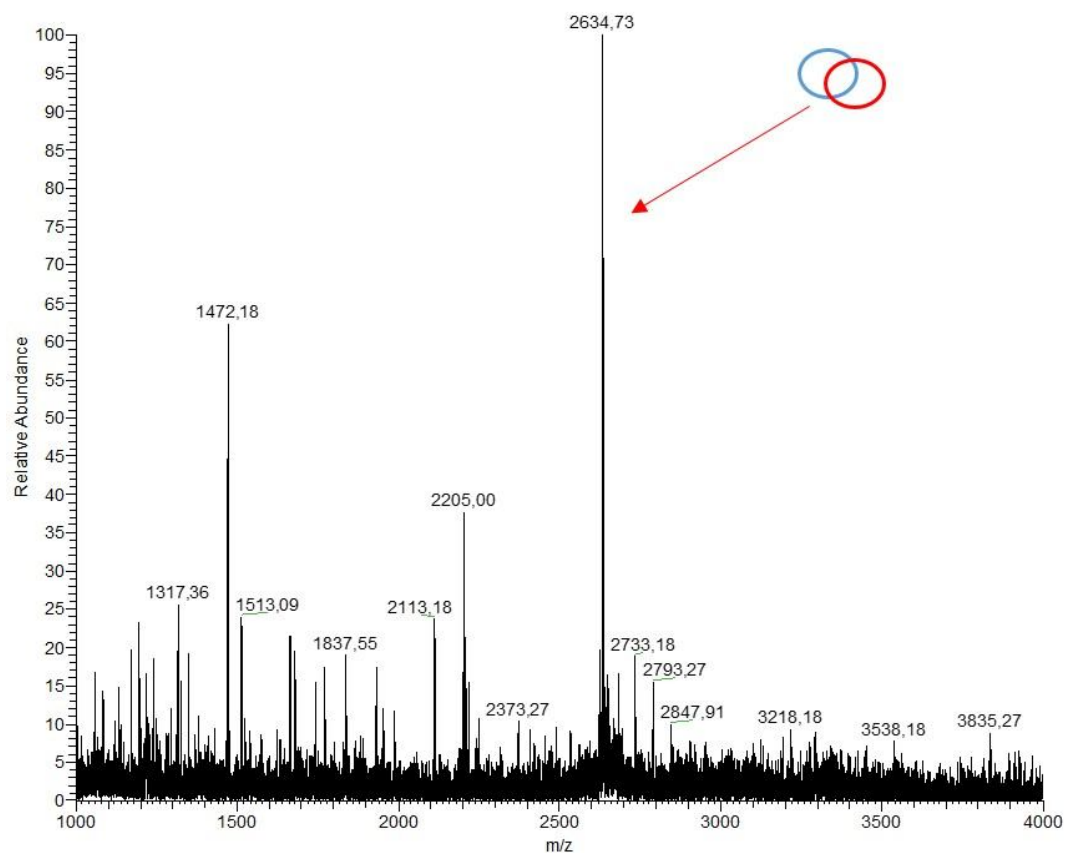


Figure 3.30. ITMS - pESI full ms spectrum of UHPLC 19.71 min peak. The red arrow indicates the mass of $m/z = [M-10]^{10-}$. Calcd. 2665.52 m/z. Found: 2634.73 m/z.

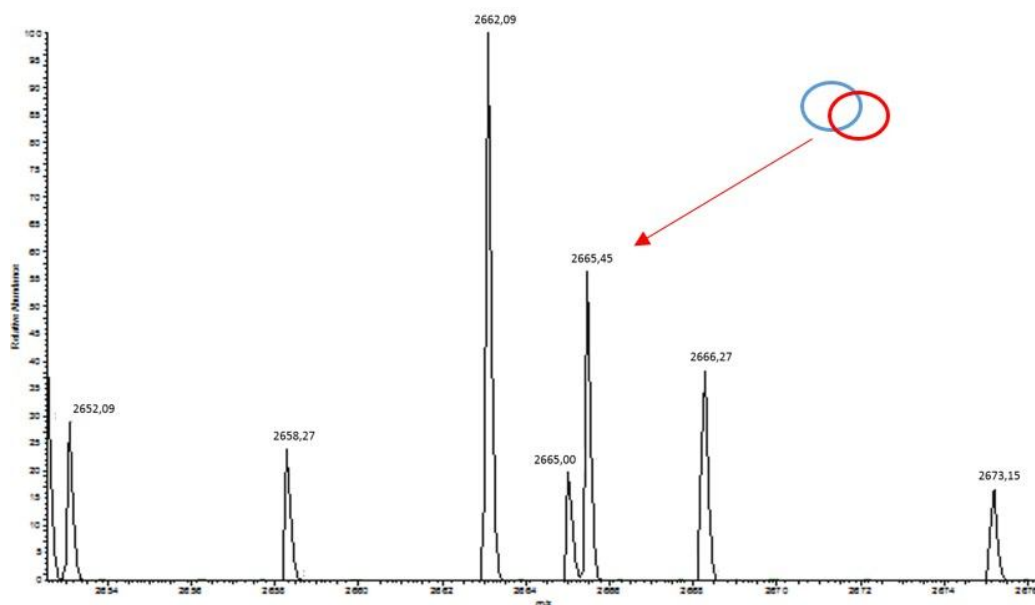


Figure 3. 31. Zoom of spectrum in figure S24 in the region of the mass peak 2634.73. The exact mass of $m/z = [M-10]^{10-}$ is indicated from the red arrow ($[M-10]^{10-}$ Calcd. 2665.52 m/z. Found: 2665.45 m/z).

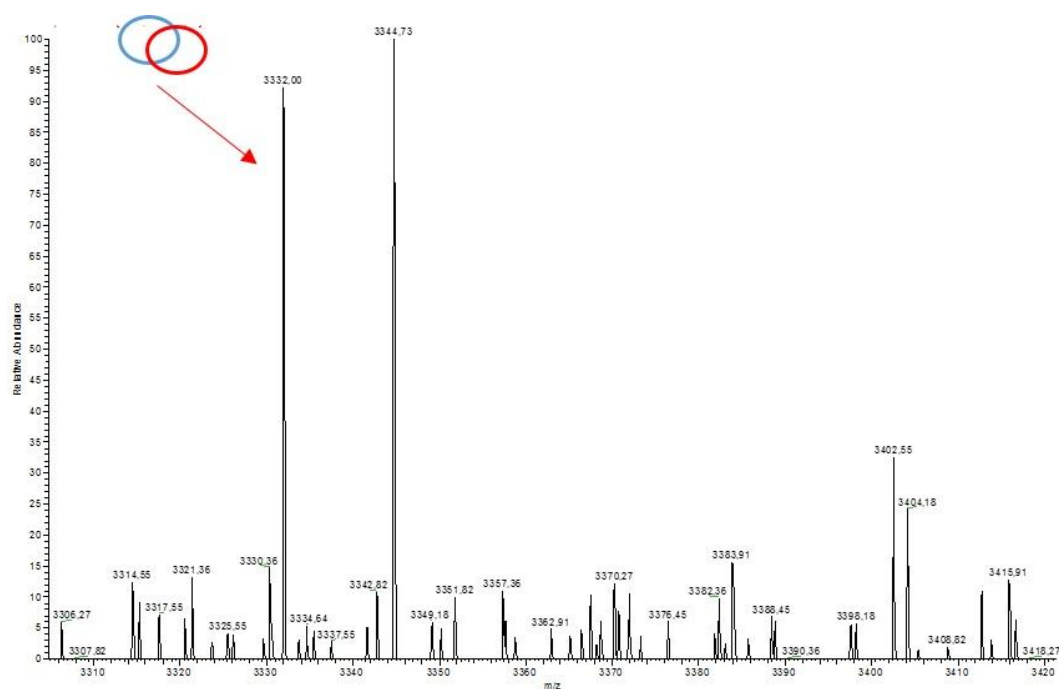


Figure 3. 32. ITMS - pESI full ms spectrum of UHPLC 19.71 min peak. The red arrow indicates the mass of $m/z = [M-8]^{8-}$. Calcd. 3332.00 m/z. Found: 3332.00 m/z).

The results showed the expected masses assigned to the new formed two-member ring catenane. Depurination during electron spray ionization (ESI) mass analysis^[4] could explain some discrepancies in the overall peak analysis.

3.5.6.12. Desalting experiments

Petri dishes were filled up with 40 ml H₂O HPLC grade. Nitrocellulose membranes (Millipore) were individually placed on the water surface of different petri dishes and sample drops (typically 10 μ l) were carefully pipetted on them. After 20 minutes desalted samples (estimated [Mg⁺⁺] = 0) were analyzed by 2% agarose gel electrophoresis and TEM imaging (e.g. Fig. 3. 34). Alternatively each membrane was transferred to dishes containing buffers with different concentrations of Mg⁺⁺ and dialyzed for further 20 minutes. The samples were re-collected and analyzed by 2% agarose gel electrophoresis (Fig. 3. 6a).

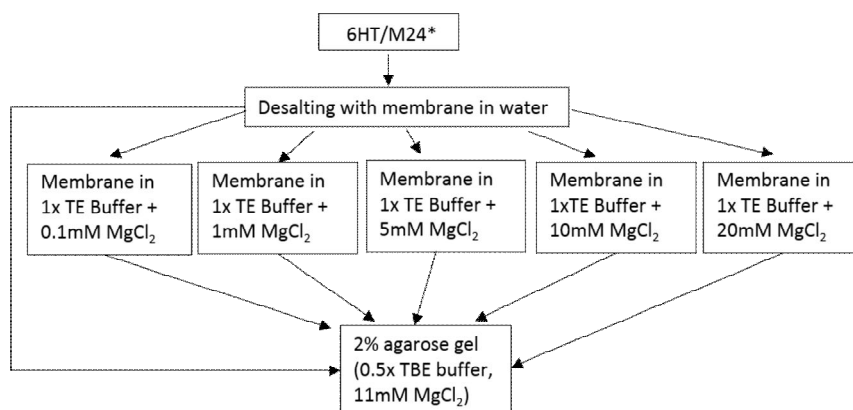


Figure 3. 33. Scheme of the desalting experiments. Nanotubes were subsequently measured in pure water or in buffers containing 0.1, 1, 5, 10 and 20mM MgCl₂ respectively.

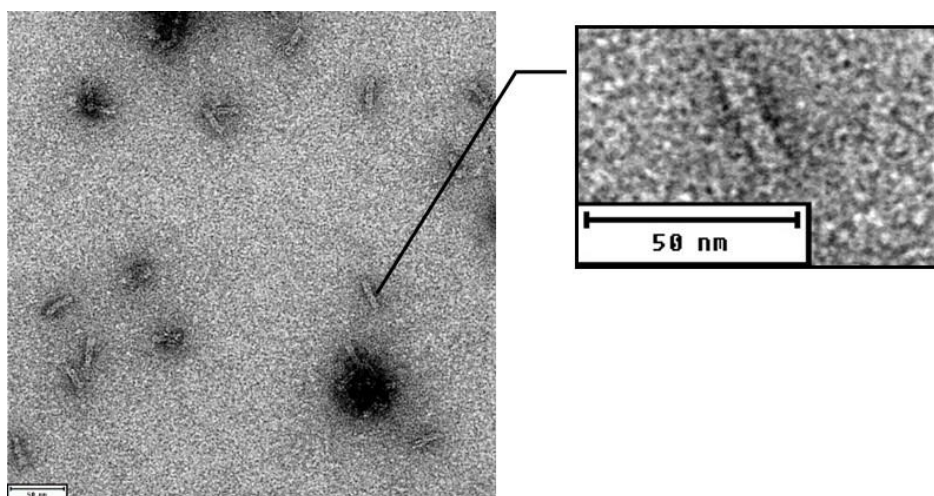


Figure 3. 34. TEM micrograph – and enlargement - of M24* tubes after desalting procedure. M24* tubes are still correctly folded when dissolved in pure water (Calculated nanotube length = 27 nm).

3.5.6.13. Melting profiles^[5]

To better investigate the melting behavior of the tile assembly structures, melting profiles were obtained using a real time PCR machine (LightCycler 480 System, Roche). The tested objects were diluted to a concentration of ca. 20nM in *folding buffer* (20 μ l final volume). As control, a duplex DNA (23mer, 2.4 μ M) was submitted to the same heating ramp. A solution of a DNA intercalating dye (SYBRGold 1x, Invitrogen) was added to each sample. The fluorescence was recorded over a heating ramp (25°C – 90°C, 0.06 °C/sec, 10 acquisitions per °C). Data were analyzed using the Light Cycler 480 Software (Roche).

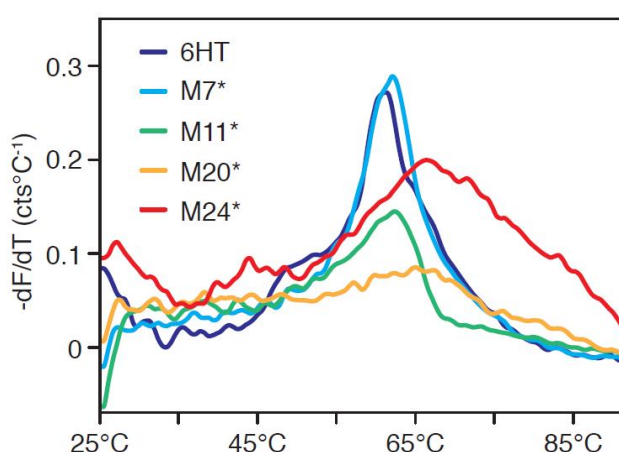


Figure 3. 35. Melting profile diagram of 6HT, M7*, M11*, M20* and M24* tubes.

3.5.6.14. Thermal denaturing and subsequent Exo I digestion

This experiment was designed to mimic the denaturing conditions encountered in cells and other living systems, mainly due to low salt concentrations, in presence of an enzyme with nuclease activity. To this end, 6HT, M24 and M24* (1 pmol) were submitted to a heating step at 65°C for 15 minutes and then quickly cooled down in ice-water for 5 minutes. Afterwards the structures were submitted to Exo I digestion (10 U, 3 hours, 37°C) and then placed at -20°C to stop the enzymes activity. The samples were analyzed by 2% agarose gel containing 11mM MgCl₂ and TEM imaging (Fig. 3. 6b bottom, and 3. 6c).

3.5.6.15. Incubation in Dulbecco's modified Eagle Medium (DMEM)

This experiment was designed to prove the stability of M24* tubes in a typical cell culture medium. To this end, 6HT, M24 and M24* (500 fmol) were diluted in DMEM (Merck Millipore) up to 12.5 µl. A negative control was made diluting 500 fmol of each structure in their folding buffer (1x TE Buffer, 20mM MgCl₂) up to 12.5 µl. Both the assay and the negative control were incubated 24 hours at 37°C in thermocycler. The samples were analyzed using a 2% agarose gel (0.5x TBE Buffer containing 11mM MgCl₂) (Fig. 3. 6b, top).

3.5.6.16. Rate of strand incorporation in the structure and DNA-catenane formation yields

Strand incorporation rate and overall DNA-catenane formation yields were estimated to be almost quantitative by interpretation of various gels as shown in main text and in these pages. Anyway, agarose gel is surely not the preferred method to quantify the strand incorporation rate within the structure. It can be very challenging to verify if all 24 strands are incorporated into the structure and thus a 24-member DNA-catenane is formed after the click reaction merely by gel interpretation. The radioactive assay used by Ding et al.^[6] proved to be a reliable method to quantify strand incorporation rate, hence a fluorescent modified version of this assay was used in this work. Four *click*-tiles were selected among the 24 possible strands to be representative of a general behavior. Each of those *click*-tiles was fluorescent labelled with TAMRA and called hereinafter fluo-*click*-tiles. Four distinct tubes, each including one fluo-*click*-tiles were separately folded. These tubes were loaded into agarose gels with or without MgCl₂ before and after click reaction and analyzed using a gel laser scanner. This experimental setup allows a better quantification of unfolded strands within the folded structure into the mixture. A schematic representation of this setup for one single tube is depicted in figures 3. 36 and 3. 37.

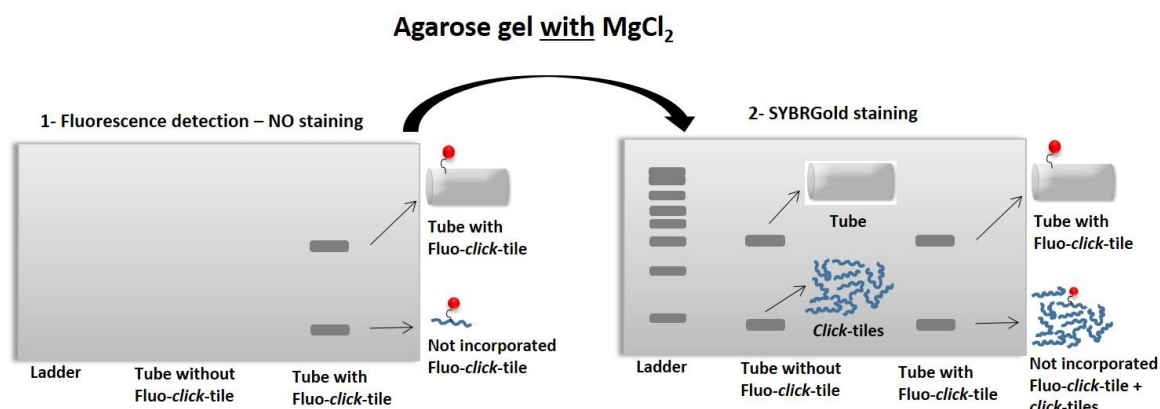


Figure 3. 36. Schematic representation of the experimental setup for the strands incorporation rate test. Folded tubes containing one fluo-*click*-tile, along with other 23 *click*-tiles, are loaded into agarose gel containing $MgCl_2$. Gel is then imaged at gel laser scanner and only the samples containing fluo-*click*-tiles are detected (left gel picture). The same gel is afterwards stained with SYBRGold and hence even the structures without fluorescent labelling are visible (right gel picture).

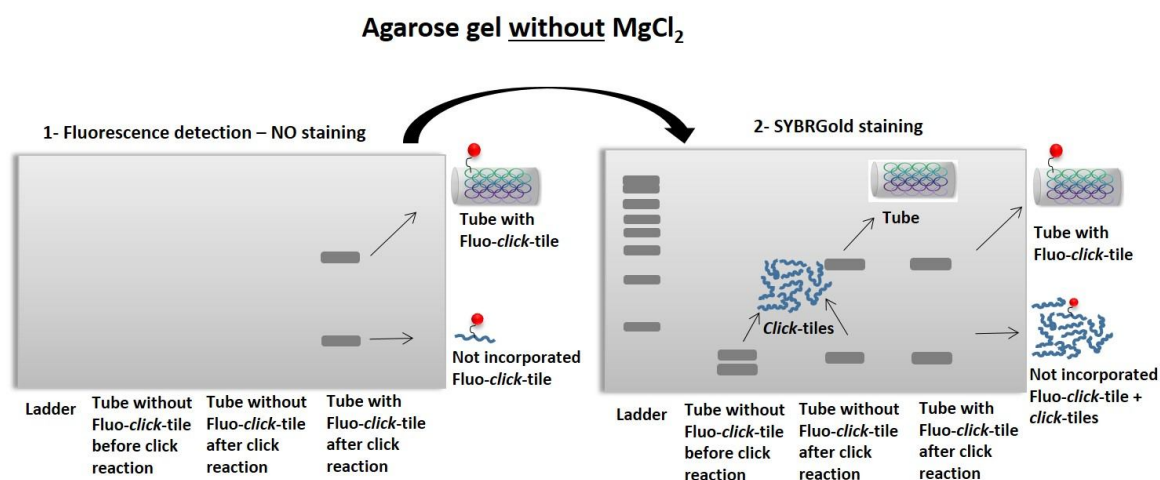


Figure 3. 37. Schematic representation of the experimental setup for the rate of strands incorporation test. Tubes containing one fluo-*click*-tile, along with other 23 *click*-tiles, are loaded on agarose gel without $MgCl_2$. Gel is then imaged at gel laser scanner and only the samples containing fluo-*click*-tiles are detected. A low molecular weight band is to be expected only in case of incomplete click reaction (left gel picture). The same gel is afterwards stained with SYBRGold and hence even the structures without fluorescent labelling are visible. Only the structures submitted to click reaction will show the tube bands. Structures before click reaction will result in a band at low molecular weight (right gel picture).

Table 3. 7. Sequences of the four TAMRA labelled *click*-tiles (fluo-*click*-tiles) used in this work. X and Z are the alkyne and the azide groups respectively as defined in figure S1. **Y** is dT-TAMRA.

Oligo code	Sequence	Length (bases)
V1C1	ZAAA ACGCTAAGCCA CCTT Y AGATCC AAAX	28
V4C3	ZGCATAGACATT ATAC Y GTAAA ACCTTACGTA ACTTACAGCCX	42
V5C2	ZATTT Y GCAG AGAATTCAGCC TATTCACATAG GCGAAGGCTX	42
V6C3	ZCCCATGATGCA AAGGGTCATG GGTCTTGAAA AATTTA Y GGCX	42



Figure 3. 38. Design of the completely modified tile assembled structure (all 24 strands are azide/alkyne modified) containing the fluo-*click*-tile V1C1 (M24-A). The red dot corresponds to the fluorescent labelled position.

M24-B

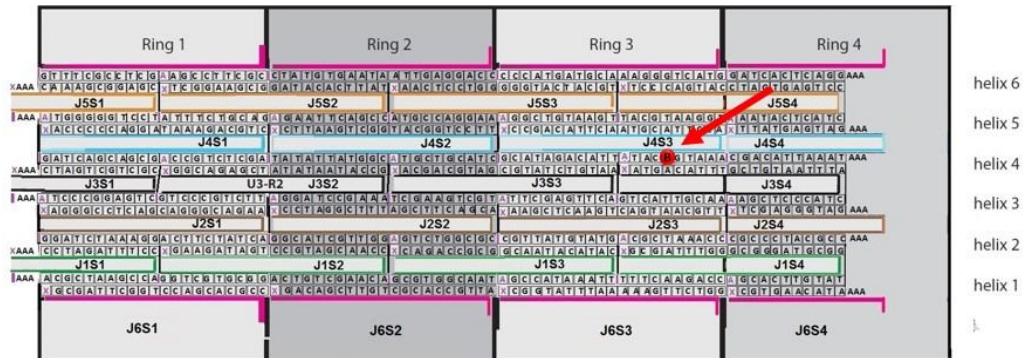


Figure 3. 39. Design of the completely modified tile assembled structure (all 24 strands are azide/alkyne modified) containing the fluo-click-tile V4C3 (M24-B). The red dot corresponds to the fluorescent labelled position.

M24-C



Figure 3. 40. Design of the completely modified tile assembled structure (all 24 strands are azide/alkyne modified) containing the fluo-click-tile V5C2 (M24-C). The red dot corresponds to the fluorescent labelled position.

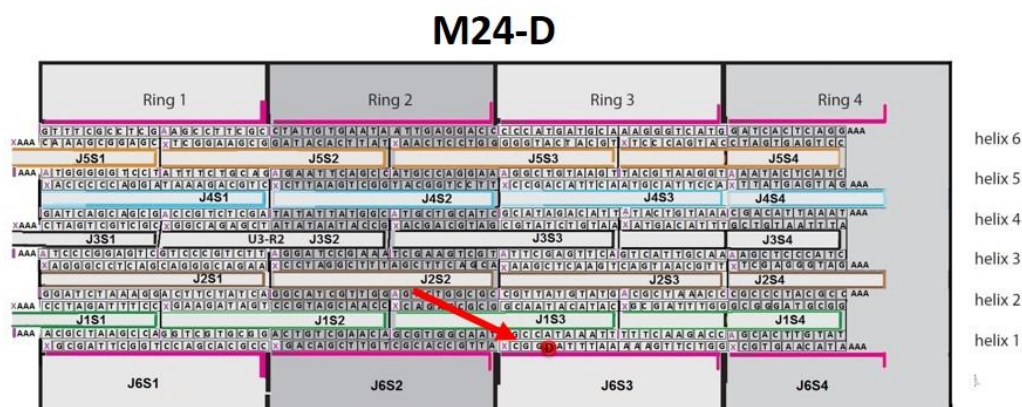


Figure 3. 41. Design of the completely modified tile assembled structure (all 24 strands are azide/alkyne modified) containing the fluo-*click*-tile V6C3 (M24-D). The red dot corresponds to the fluorescent labelled position.

Tubes folding

Table 3. 8. Schematic representation of strands composition of the different labelled tubes (M24A-D) used in the work. Each labelled strand (fluo-*click*-tile, highlighted by colored boxes) is added together with other 23 *click*-tiles.

M24-A				M24-B			
J5S1	J5S2	J5S3	J5S4	J5S1	J5S2	J5S3	J5S4
J4S1	J4S2	J4S3	J4S4	J4S1	J4S2	V4C3	J4S4
J3S1	J3S2	J3S3	J3S4	J3S1	J3S2	J3S3	J3S4
J2S1	J2S2	J2S3	J2S4	J2S1	J2S2	J2S3	J2S4
V1C1	J1S2	J1S3	J1S4	J1S1	J1S2	J1S3	J1S4
J6S1	J6S2	J6S3	J6S4	J6S1	J6S2	J6S3	J6S4
M24-C				M24-D			
J5S1	V5C2	J5S3	J5S4	J5S1	J5S2	J5S3	J5S4
J4S1	J4S2	J4S3	J4S4	J4S1	J4S2	J4S3	J4S4
J3S1	J3S2	J3S3	J3S4	J3S1	J3S2	J3S3	J3S4
J2S1	J2S2	J2S3	J2S4	J2S1	J2S2	J2S3	J2S4
J1S1	J1S2	J1S3	J1S4	J1S1	J1S2	J1S3	J1S4
J6S1	J6S2	J6S3	J6S4	J6S1	J6S2	V6C3	J6S4

Tubes are folded following the procedure and the folding program previously described (3.5.6.4). After folding, tubes were reacted at 32°C for 5 hours with click reagents as described previously (3.5.6.5).

Agarose gel containing MgCl_2 of folded fluorescent labelled tubes

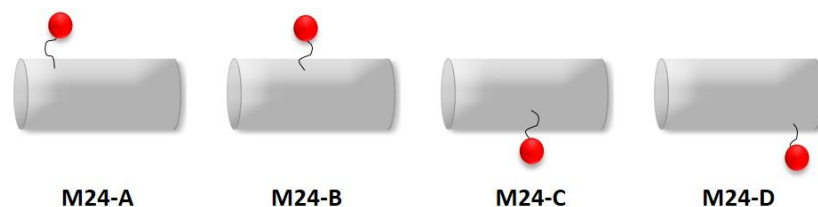


Figure 3. 42. Schematic representation of M24-A, M24-B, M24-C and M24-D tubes (before click reaction).

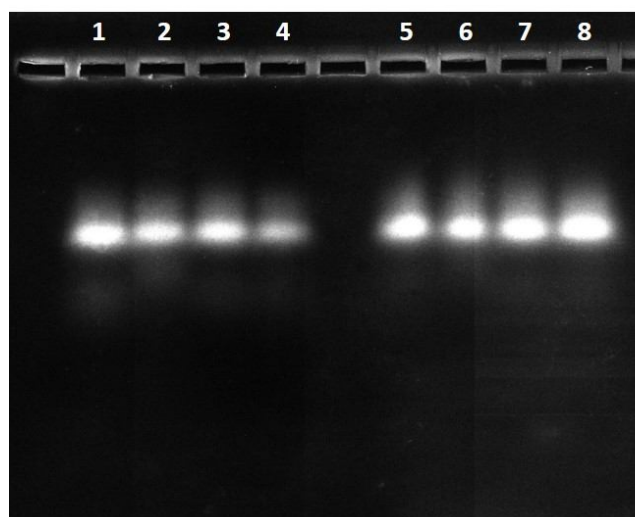


Figure 3. 43. 2% agarose (0.5x TBE Buffer containing 11 mM MgCl_2), NO gel staining, only fluorescence detection. The fluorescence is due to TAMRA labelled strand incorporated into the structure. *Lane 1:* M24-A tube, no treatment; *lane 2:* M24-B tube, no treatment; *lane 3:* M24-C tube, no treatment; *lane 4:* M24-D tube, no treatment; *lane 5:* M24-A tube after Amicon purification; *lane 6:* M24-B tube after Amicon purification; *lane 7:* M24-C tube after Amicon purification; *lane 8:* M24-D tube after Amicon purification. The Amicon purification described in page S19 ensure removal of not incorporated strands from the mixture containing the tube.

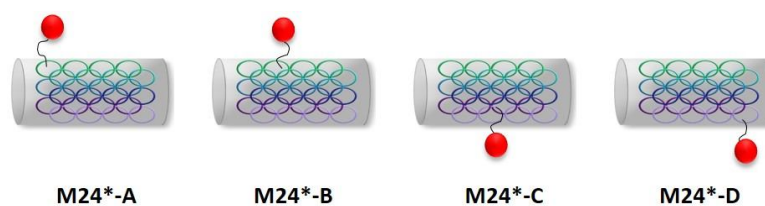


Figure 3. 44. Schematic representation of M24*-A, M24*-B, M24*-C and M24*-D tubes (after click reaction).

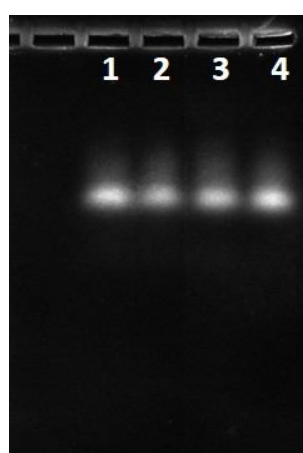


Figure 3. 45. 2% agarose (0.5x TBE Buffer containing 11 mM MgCl_2), NO gel staining, only fluorescence detection. The fluorescence is due to TAMRA labelled strand incorporated into the structure. *Lane 1:* M24*-A tube; *lane 2:* M24*-B tube; *lane 3:* M24*-C tube; *lane 4:* M24*-D tube. Tubes have been submitted to click reaction after the Amicon purification step.

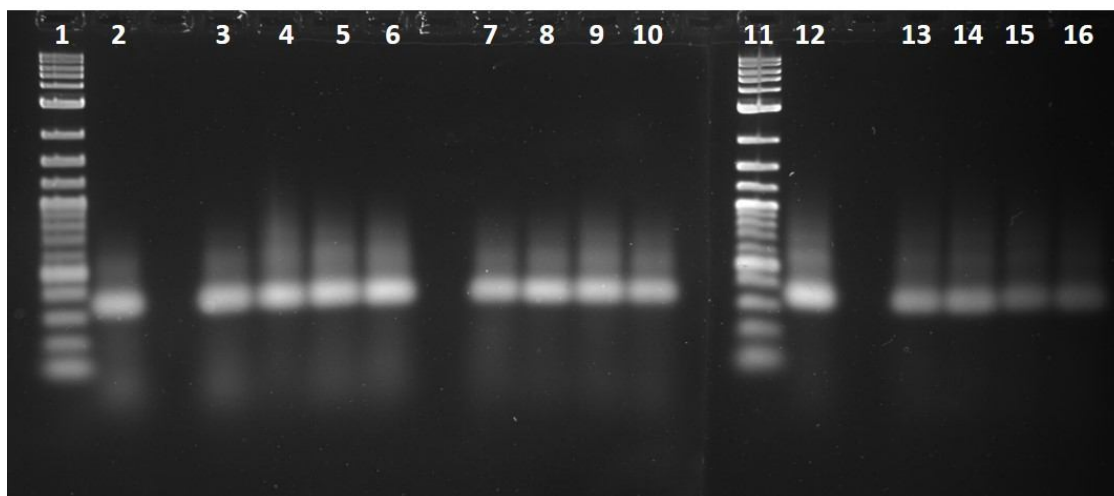


Figure 3. 46. 2% agarose (0.5x TBE Buffer containing 11 mM MgCl_2), SYBRGold staining. *Lane 1:* 2-Log DNA ladder (New England Biolabs); *lane 2:* M24-tube, no treatment; *lane 3:* M24-A tube, no treatment; *lane 4:* M24-B tube, no treatment; *lane 5:* M24-C tube, no treatment; *lane 6:* M24-D tube, no treatment; *lane 7:* M24-A tube after Amicon purification; *lane 8:* M24-B tube after Amicon purification; *lane 9:* M24-C tube after Amicon purification; *lane 10:* M24-D tube after Amicon purification. *Lane 11:* 2-Log DNA ladder (New England Biolabs); *Lane 12:* M24* tube; *lane 13:* M24*-A tube; *lane 14:* M24*-B tube; *lane 15:* M24*-C tube; *lane 16:* M24*-D tube. The asterisk indicates that the tube was submitted to click reaction.

Agarose gel without MgCl_2 of fluorescent labelled tubes

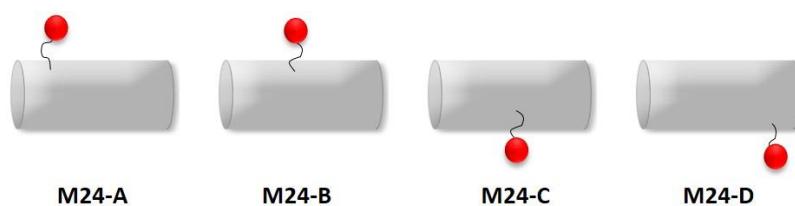


Figure 3. 47. Schematic representation of M24-A, M24-B, M24-C and M24-D tubes (before click reaction).

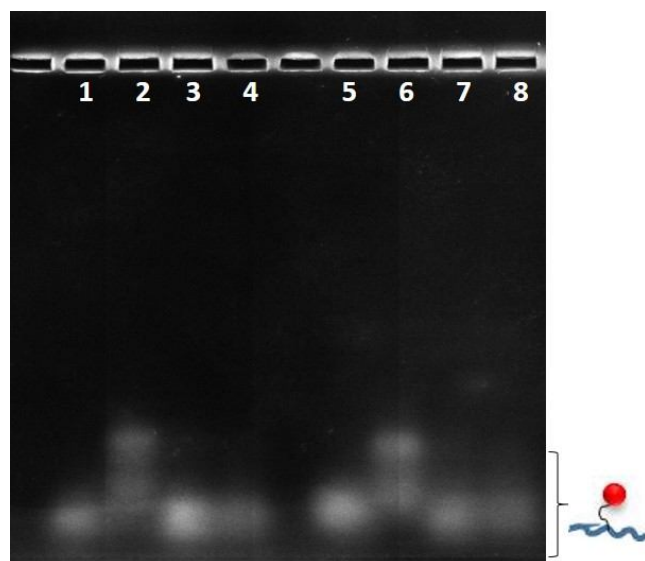


Figure 3. 48. 2% agarose (0.5x TBE Buffer without MgCl_2), NO gel staining, only fluorescence detection. The fluorescence is due to TAMRA labelled strand. *lane 1*: M24-A tube, no treatment; *lane 2*: M24-B tube, no treatment; *lane 3*: M24-C tube, no treatment; *lane 4*: M24-D tube, no treatment; *lane 5*: M24-A tube after Amicon purification; *lane 6*: M24-B tube after Amicon purification; *lane 7*: M24-C tube after Amicon purification; *lane 8*: M24-D tube after Amicon purification. Only the low molecular band of the TAMRA labelled strand is visible since the tube unfold during the run in the gel without MgCl_2 .

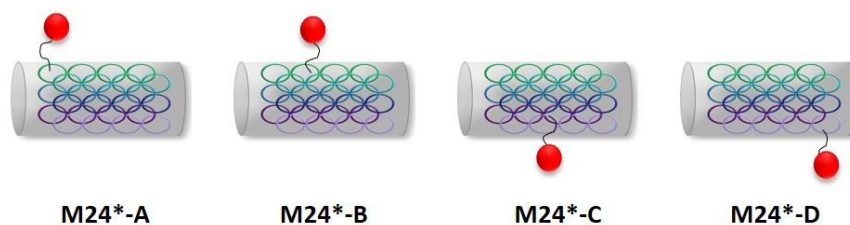


Figure 3. 49. Schematic representation of M24*-A, M24*-B, M24*-C and M24*-D tubes (after click reaction).

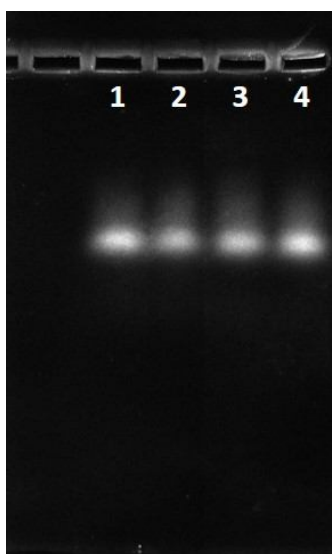


Figure 3. 50. 2% agarose (0.5x TBE Buffer without MgCl_2), NO gel staining, only fluorescence detection. The fluorescence is due to TAMRA labelled strand incorporated into the structure. *Lane 1:* M24*-A tube; *lane 2:* M24*-B tube; *lane 3:* M24*-C tube; *lane 4:* M24*-D tube. Tubes have been submitted to click reaction after the Amicon purification step and remain folded also if loaded into gel without MgCl_2 .

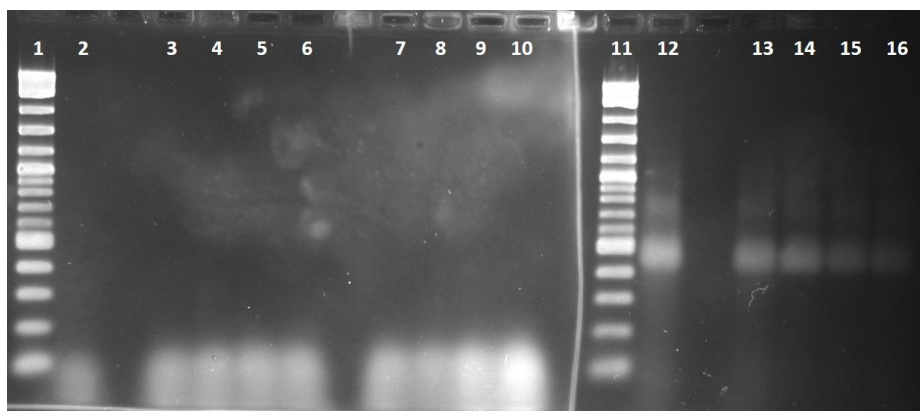


Figure 3. 51. 2% agarose (0.5x TBE Buffer without MgCl_2), SYBRGold staining. *Lane 1:* 2-Log DNA ladder (New England Biolabs); *lane 2:* M24-tube, no treatment; *lane 3:* M24-A tube, no treatment; *lane 4:* M24-B tube, no treatment; *lane 5:* M24-C tube, no treatment; *lane 6:* M24-D tube, no treatment; *lane 7:* M24-A tube after Amicon purification; *lane 8:* M24-B tube after Amicon purification; *lane 9:* M24-C tube after Amicon purification; *lane 10:* M24-D tube after Amicon purification. *Lane 11:* 2-Log DNA ladder (New England Biolabs); *Lane 12:* M24* tube; *lane 13:* M24*-A tube; *lane 14:* M24*-B tube; *lane 15:* M24*-C tube; *lane 16:* M24*-D tube. The asterisk indicates that the tube was submitted to click reaction.

Fluorescence plots from agarose gel containing MgCl_2 .

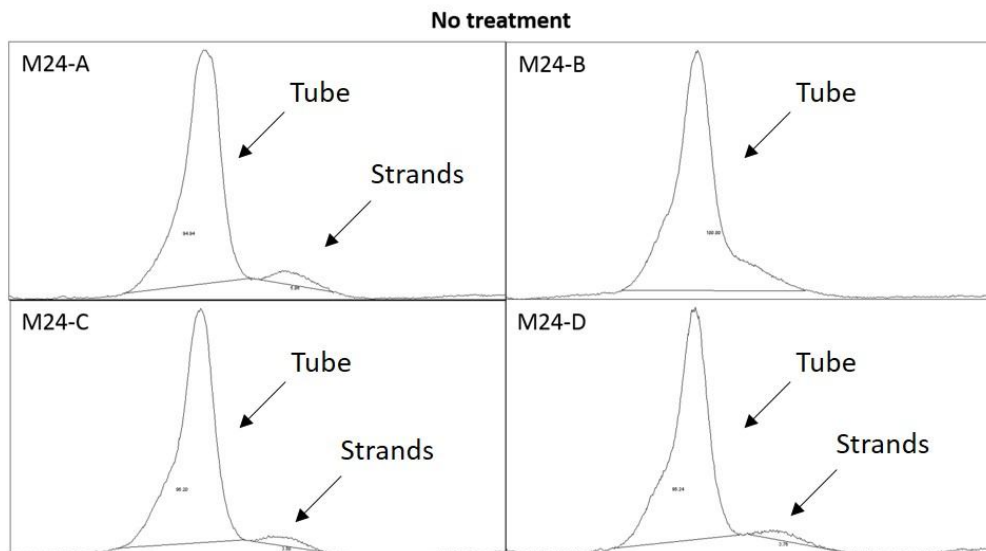


Figure 3. 52. Fluorescence plots obtained from 2% agarose gel containing 11mM MgCl_2 (Figure 3. 43 - M24-A tube = Lane 1; M24-B tube = Lane 2; M24-C tube = Lane 3; M24-D tube = Lane 4). Fluorescence detect for samples without treatment (after the folding). Percentages of fluorescence are reported in Table 3. 9.

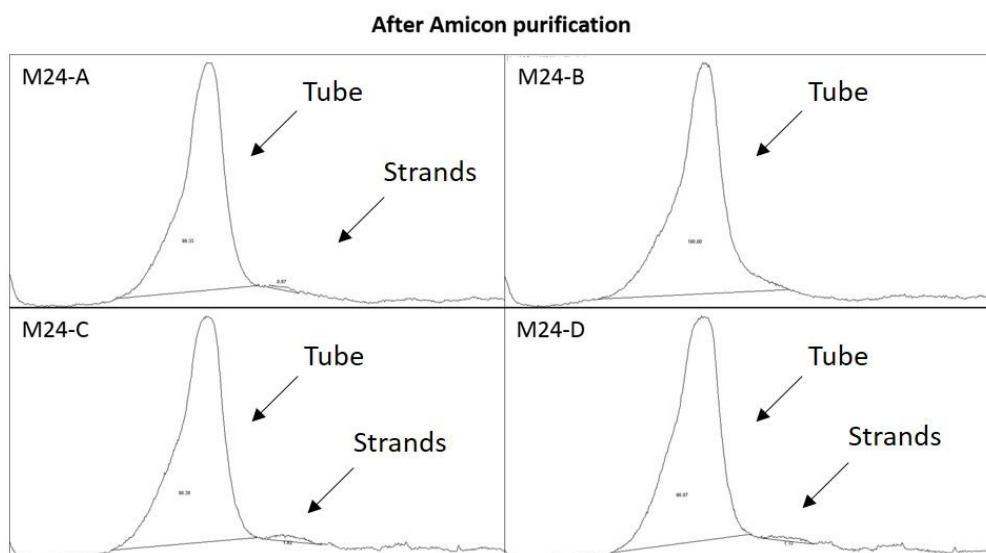


Figure 3. 53. Fluorescence plots obtained from 2% agarose gel containing 11mM MgCl_2 (Figure 3. 43 - M24-A tube = Lane 5; M24-B tube = Lane 6; M24-C tube = Lane 7; M24-D tube = Lane 8). Fluorescence detect for samples after Amicon purification. Percentages of fluorescence are reported in Table 3. 9.

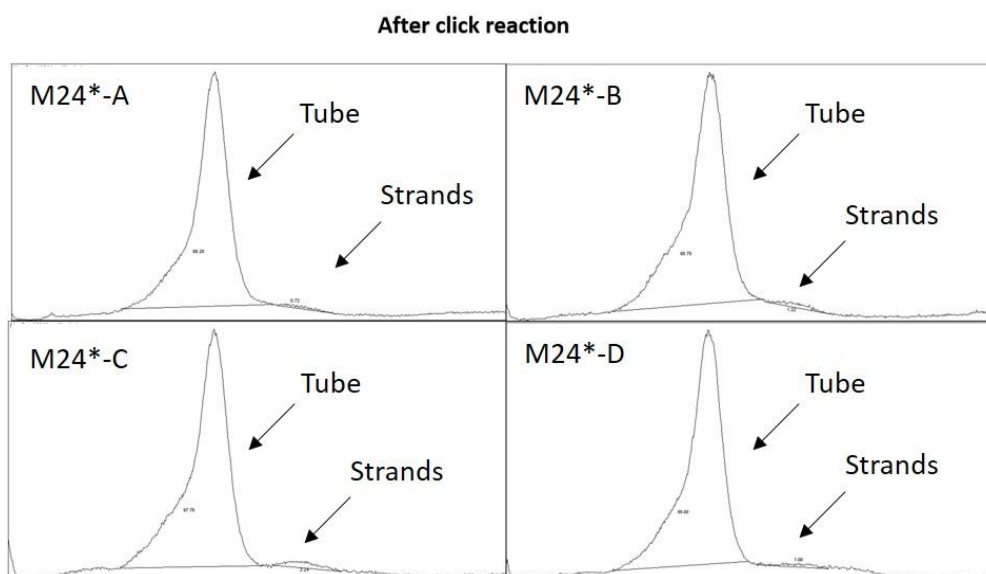


Figure 3. 54. Fluorescence plots obtained from 2% agarose gel containing 11mM $MgCl_2$ (Figure 3. 45 - M24-A tube = Lane 1; M24-B tube = Lane 2; M24-C tube = Lane 3; M24-D tube = Lane 4). Fluorescence detect for samples after click reaction. Percentages of fluorescence are reported in Table 3. 9.

Table 3. 9. Fluorescent bands quantification.

M24 A	% tube	% strands	M24 B	% tube	% strands
No treatment	94.9	5.1	No treatment	100.0	0.0
After Amicon	99.3	0.7	After Amicon	100.0	0.0
After click	99.3	0.7	After click	98.8	1.2
M24 C	% tube	% strands	M24 D	% tube	% strands
No treatment	96.2	3.8	No treatment	96.2	3.8
After Amicon	98.4	1.6	After Amicon	98.9	1.1
After click	97.8	2.2	After click	99.0	1.0

Fluorescence plots from agarose gel without MgCl₂.

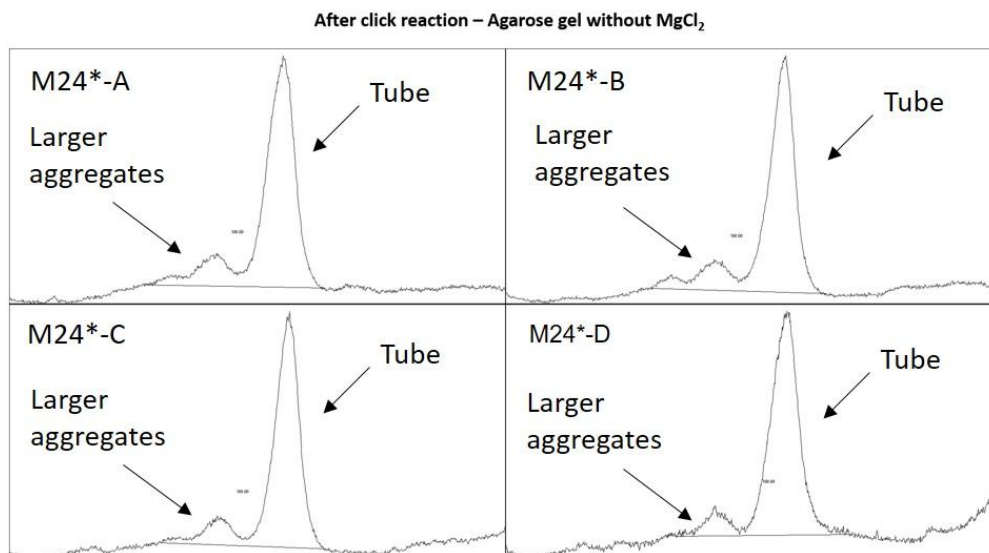


Figure 3.55. Fluorescence plots obtained from 2% agarose gel without MgCl₂ (Figure 2. 50 - M24*-A tube = Lane 1; M24*-B tube = Lane 2; M24*-C tube = Lane 3; M24*-D tube = Lane 4). Fluorescence detection for samples after click reaction. No fluorescence was detected at low molecular weight, meaning that the click reaction has a quantitative yield.

In conclusion, the detection of the fluorescent ratio between the folded tube and the low molecular weight band of the unfolded fluo-*click*-tiles showed a high efficient folding yield exceeding 95%. Moreover, using the same setup it was possible to quantify the efficacy of the click reaction, which showed quantitative yields for all four fluorescent tubes. This conclusion can be reasonably extended to all the other strands in the structure.

3.5.6.17. Catenation between terminal 28mers

The three short strands on one end of the structure (J1S1, J3S1 and J5S1, left side of Figure 3.9) have an extension of poly-dA (AAA) in both 3' and 5' ends, both functionalized with click reactive groups.

In this case the alkyne and azide groups are not pre-assembled in that region and possible inter-strand reaction cannot be excluded.

In order to clarify this point a tube using 21 un-modified strands and those three short terminal *click*-tiles was folded. Additionally, a tube containing only one of those short terminal *click*-tiles was folded as control. The tubes were submitted to click reaction and then analyzed *via* denaturing PAGE. If inter-strand coupling occurs, then dimers or trimers of those *click*-tiles will be formed and thus detected in

PAGE as higher molecular weight bands. If only intra-strand cyclization occurs, then only low molecular bands should be visible in the PAGE similarly to that generated by the control tube (see scheme in figure 3. 56).

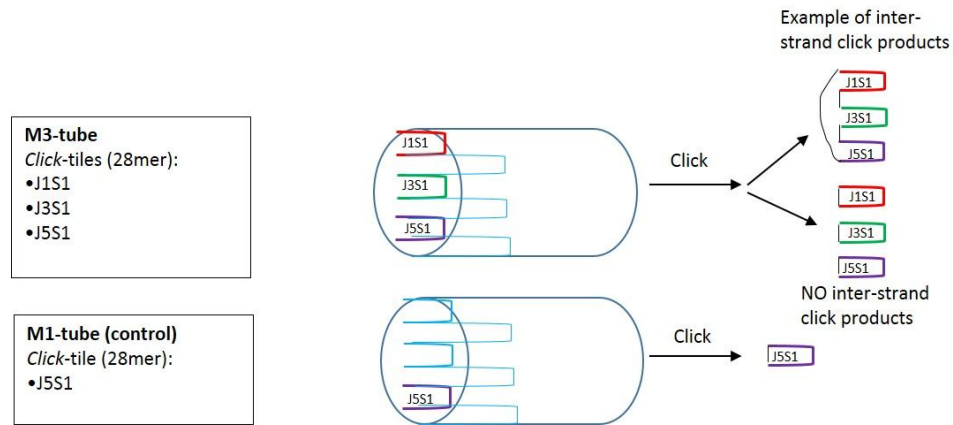


Figure 3. 56. Scheme of the experimental setup to test possible inter-strand reactions among the terminal 28mer *click*-tiles.

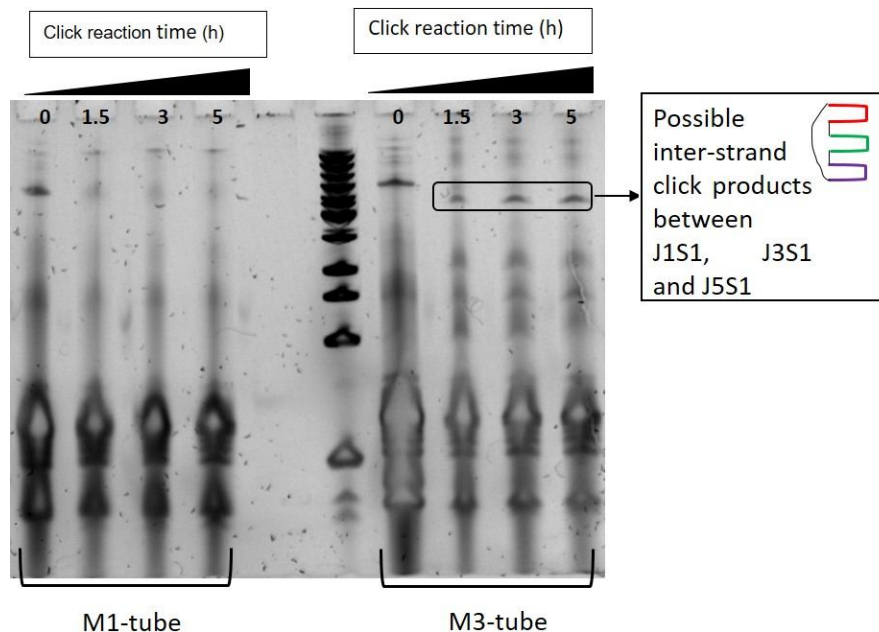


Figure 3. 57. 10% denaturing PAGE of M1-tube and M3-tube, SYBRGold staining. From left to right: M1-tube before click reaction (lane1), M1* tube submitted to click reaction for 1.5 hours (lane 2), for 3 hours (lane 3), for 5 hours (lane 4), Low molecular DNA ladder (New England Biolabs, lane 6), M3-tube before click reaction (lane7), M3* tube submitted to click reaction for 1.5 hours (lane 8), for 3 hours (lane 9), for 5 hours (lane 10).

New bands are formed after click reaction of the M3-tube suggesting the formation of inter-strand structures. The bands increase in intensity with a longer reaction time. This “side-reaction” is due to the particular architecture of the tube containing poly-A ends and can be easily overcome with a proper design. The overall stability of this particular design is not affected by inter-strand reactions.

3.5.6.18. References for the supporting information of the publication “One-Step Formation of Chain-Armor-Stabilized DNA Nanostructures”

- [1] J. Gierlich, G. A. Burley, P. M. E. Gramlich, D. M. Hammond, T. Carell, *Org. Lett.* **2006**, *8*, 3639-3642.
- [2] P. Yin, *Science* **2008**, *321*, 824-826.
- [3] a) B. Hogberg, T. Liedl, W. M. Shih, *J. Am. Chem. Soc.* **2009**, *131*, 9154-9155; b) W. Yang, J. Y. Lee, M. Nowotny, *Molecular Cell*, *22*, 5-13; c) V. A. Bloomfield, D. M. Crothers, I. Tinoco, *Nucleic Acids: Structures, Properties, and Functions*, University Science Books, **2000**.
- [4] I. D. T. IDT, **2011**.
- [5] T. L. Sobey, S. Renner, F. C. Simmel, *J. Phys: Condensed Matter* **2009**, *21*, 034112.
- [6] B. Ding, N.C. Seeman, *Science* **2006**, *31*, 1583.

4. Ultra-stable DNA nanostructures and their applications in life science

This section contains unpublished results.

4.1. Introduction

The following section describes the further development for *in vitro* applications of the chain armor approach⁸⁹ described in Chapter 3.5. The increased stability of SST nanotubes achieved by click chemistry enables the nanostructures to withstand harsh conditions such as high temperatures, ethanol precipitation, complete depletion of cations and exonuclease digestion. These improved features are matching the need of DNA nanostructures in order to be applied in biological environments. The use of DNA nanostructures as carrier for drug delivery is strongly encouraged by characteristics such as nanometer spatial control, inherent biocompatibility of nucleic acids and possibility of functionalization with a high variety of (bio)chemical molecules. Furthermore, the development of complex and dynamic structures able to carry and precisely release therapeutics have been previously reported.⁷⁹ Nevertheless, DNA-based nanostructures suffer of instability in biological environments such as cell culture medium. A destabilizing factor within this environment is the depletion of positive ions; for instance, in a standard HeLa cell culture medium the concentration of magnesium is around 0.4 mM.⁸⁷ This value is more than an order of magnitude below the concentration generally used for folding and store intact DNA nanostructures. Lower cation concentrations induce the disassembly of the nano-architecture in its single components, thus losing structural information essential for the desired application. In order to solve this issue few stabilization approaches have been previously reported and summarized in the general introduction of this thesis (Chapter 1. 14). Those published methods significantly differ from the covalent structural stabilization approach presented in Chapter 3. 5. Here the increased stability of chain armor structures in Dulbecco's Modified Eagle Medium (DMEM) was successfully demonstrated. Another stability issue in biological application is the presence of nucleases which degrade exogenous DNA. In this case catenation revealed to be a useful tool to avoid exonucleases digestion as well. Indeed, in the catenated structure the strands are circularized and exonuclease is not able to bind any 3'-end to start DNA digestion. These promising improvements pave the way to the efficient application of DNA nano-constructs within complex environments such as cell culture medium.

4.2. Targeted delivery

Targeted cell delivery is one of the most sought-after objectives regarding administration of therapeutics since it would enable a more focused and effective treatment reducing off-target effects. A commonly used strategy to perform cell transfection[†] of DNA nanostructures is the attachment of targeting molecules such as cell-penetrating peptides,¹¹¹ aptamers¹¹² or folate moieties⁸⁰ among others.

[†] The term transfection commonly refers to the introduction of naked or purified nucleic acids by non-viral methods into eukaryotic cells. In the presented work this terminology is more generally used to define the delivery of DNA nanostructures into cells, thus not implying transmission of genetic information.

Specifically, folic acid – conjugate base folate - is the vitamin B essential for *de novo* synthesis of nucleotides and its uptake is essential for cells in the proliferating state.⁹⁴ The uptake of folate molecules follows a receptor-mediated endocytosis pathway through cell membrane receptors. These are often overexpressed in malignant cell lines and therefore folate and its derivatives are often used as efficient targeting agent for anti-cancer drug delivery.¹¹³

In cell delivery studies, nanostructures may further require a cell tracking dye in addition to a targeting agent. A functionalization strategy widely used in DNA nanotechnology is based on the hybridization of DNA sequences protruding from the structure with complementary sequences bearing the functional molecule. For example, conjugation of gold nanoparticles to DNA structures is typically carried out by hybridization of protruding sequences to complementary strands that are bonded to gold nanoparticles through thiol-terminated groups.⁶⁹ Although this strategy is straightforward, the resulting conjugation is based only on non-covalent forces, thus being susceptible to denaturation causing dissociation of the functional molecule. Covalent bond formation between the DNA nanostructure and functional moieties is a secure method to avoid detachment of the conjugated molecule. Thiol and amino modified oligonucleotides can form stable conjugation products reacting with maleimide or N-hydroxysuccinimide-ester (NHS) labels respectively.¹¹⁴ Copper(I)-catalyzed alkyne-azide cycloaddition (CuAAC) - also commonly termed click reaction - is a valuable alternative to the above mentioned conjugation strategies.

4.3. Design

In this section, the efficient CuAAC is applied as a tool on a SST nanotube to achieve simultaneously stabilization and selective functionalization with two different moieties. The resulting enhanced stability and covalent conjugation of functional molecules envision the use of DNA structures created with this strategy for applications in demanding complex environments.

The starting design of the ultra-stable chain armor DNA nanostructure described by Cassinelli et al.⁸⁹ was further developed by the addition of “click-reactive” functionalization sites in two regions of the structure, the head and the body (Fig. 4. 1). This was practically achieved through the introduction of new oligonucleotides listed in Table 4. 1.

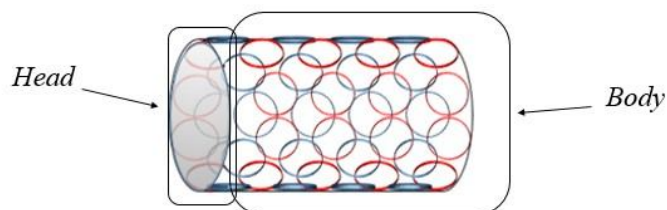


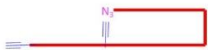
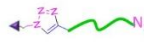



Figure 4. 1. Graphical representation of the two regions of the nanotube where functionalization sites have been introduced.

Table 4. 1. Nomenclature and graphical representation of the different modified oligonucleotide sets used in this work.

Code	Name	Graphical Representation	Location
ct-ODNXX	click-tiles		Body + Head
bct-ODNXX	"body-functional" click-tiles		Body
hct-ODNXX	"head-functional" click-tiles		Head
rc-ODN	reporter oligonucleotide		External/Head
con-ODNXX	Connector oligonucleotides		External

Where XX is the sequential number identifying the oligonucleotide.

Five click-tiles (ct-ODNs) are replaced with five "body-functional" click-tiles (bct-ODNs) in the body region. Each bct-ODN has the same sequence as the replaced ct-ODN, but includes an alkyne modified base (C8-alkyne-dU) within the sequence. The position of the modified base is selected in order to have the alkyne residue pointing outwards from the structure, thus enhancing the reactivity towards external azide tags. In the head region three click-tiles (ct-ODN1, ct-ODN9 and ct-ODN17) were replaced with three elongated strands ("head-functional" click-tiles: hct-ODN1, hct-ODN2, hct-ODN3) carrying an azide at the 5'-end and two alkyne groups, one within the sequence and the second at the 3'-end. The latter points out of the structure for the conjugation of a "reporter click oligonucleotide (rc-ODN), while the first alkyne is located within the structure facing the 5'-end azide for the ring closure stabilization-click. The rc-ODN contains a second functional moiety at the 3'-end and an azide group at the 5'-end. A splint oligonucleotide - hereinafter called connector oligonucleotide (con-ODN) - hybridizes half of its sequence with the elongated sequence of hct-ODNs and the other half with the rc-ODN allowing a selective incorporation of rc-ODNs in the structure. In this architecture the alkyne group of the hct-ODNs and the azide of the rc-ODN are in close proximity resulting in efficient conjugation. These modifications, combined with precise spatial organization typical of DNA architectures, enable the one-pot synthesis of a stable and multi-functionalized DNA nanostructure *via* click chemistry.

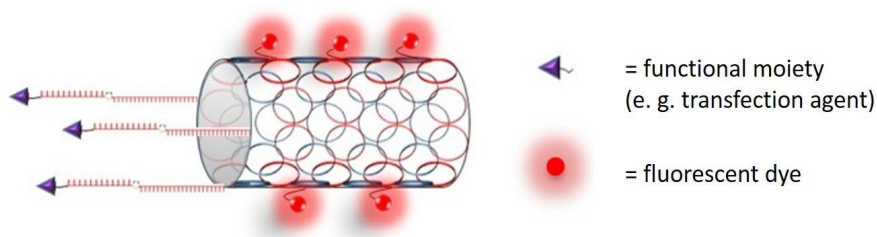


Figure 4. 2. Graphical representation of a ultra-stable multi-functionalized DNA nanotube.

A complete list of the strands used in the study can be found in the Appendix 4.17.

4.4. Results

4.4.1. Gel detection limit

The selectivity and efficacy of bio-conjugation *via* click chemistry is a key point of this study and therefore was thoroughly investigated. The functionalization concept is initially proven by the conjugation of a fluorescent azide - namely TAMRA-azide - to the structure containing additional alkyne residues as described above. The fluorophore absorbs in the UV region emitting in a wavelength range detected by the CCD camera of the gel UV-imager used during this work. In this way, imaging of unstained gels results in visualization of bands only belonging to TAMRA-conjugated species. Although the sensitivity of this detection method is not comparable with a gel imager equipped with a fluorescent detector, this approach ensured a qualitative analysis of the conjugates. An agarose gel electrophoretic analysis of a mono-TAMRA labeled tube was used to set the lower fluorophore signal detectable with the imager in use. To this end, one strand is synthesized including in the sequence a TAMRA labeled nucleotide. With this experimental setup, mono-TAMRA labeled structures can be detected in agarose gel till a concentration of 42nM (Fig. 4. 3). The lowest dilution (Lane 8, 42nM) contains 8% of the initial amount of material loaded in Lane 2 (no dilution, 500nM). This value is considered as reference for further TAMRA signal evaluation on agarose gel.

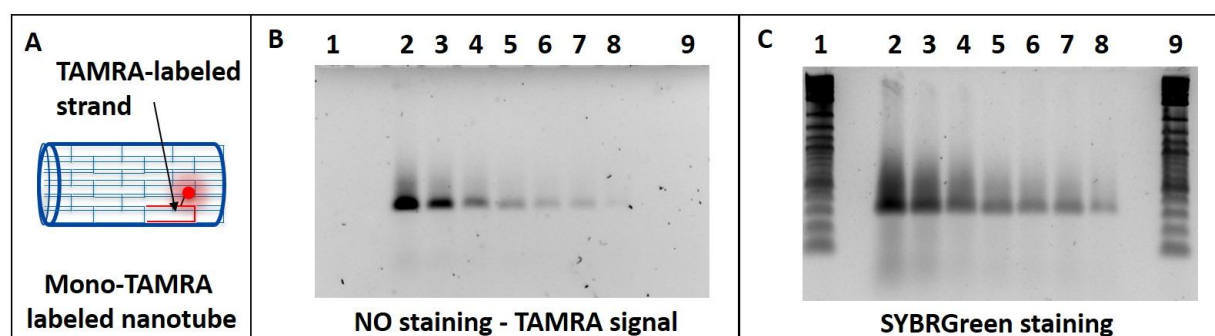


Figure 4. 3. Agarose gel 2%, 0,5x TBE containing 11mM MgCl_2 . Dilution scale of mono-TAMRA labeled nanotube. A) Schematic representation of the mono-TAMRA labeled nanotube used in this assay. B) Unstained agarose gel. C) SYBRGreen stained agarose gel. Lane 1 and 9: 2 Log DNA Ladder containing SYBRGold staining; Lane 2: 1500 fmol (500 nM); Lane 3: 750 fmol (250 nM); Lane 4: 375 fmol (125 nM); Lane 5: 250 fmol (83 nM); Lane 6: 187 fmol (62 nM) ; Lane 7: 150 fmol (50 nM) ; Lane 8: 125 fmol (42 nM).

4.4.2. Local alkyne/azide concentration

Before performing functionalization of the structure, the local concentration of click reactive groups in each click-tile within the folded nanostructure was investigated. As described above, alkyne and azide groups are facing each other thanks to the spatial *pre*-organization given from the nanotube assembly. This disposition strengthens the efficacy of triazole formation catalyzed by Cu(I). An external azide present in the system can react with the alkyne of a click-tile within the nanostructure, thus hindering the cyclization of the oligonucleotide. This kind of competitive reaction is useful to determine at which competitor concentration the intramolecular reaction of ring closure is not favored anymore. This assay allows setting a concentration upper limit of an external azide for selective body functionalization of the nanotube without affecting the formation of the chain armor architecture. A single ct-ODN (ct-ODN23, Fig. 4. 4A) within a folded 6HT architecture undergoes Cu(I)-mediated intramolecular cyclization in presence of increasing amount of a TAMRA azide. In agarose gel without staining the TAMRA signal corresponding to the labeled tube was visible for reactions with a competitor concentration starting from 133 μM , namely a fluorophore concentration 500 times higher than the nominal ct-ODN23 alkyne concentration (Fig. 4. 4B, Lane 7).

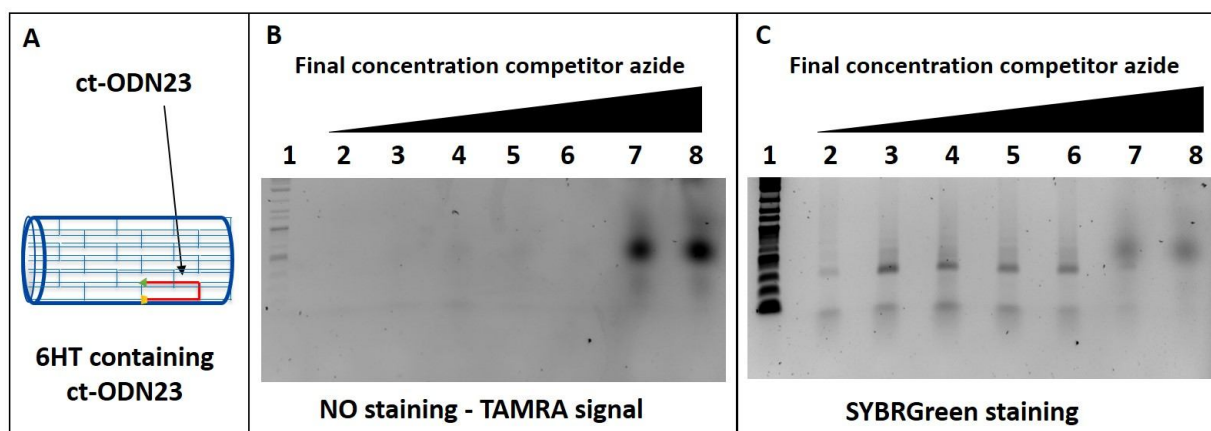


Figure 4. A) Schematic representation of the 6HT containing ct-ODN23 used in this assay. B) and C) Agarose gel 2% 0,5x TBE buffer containing 11mM $MgCl_2$ imaged without staining (B) and after SYBRGreen staining (C). Lane 1: 2-Log DNA ladder containing SYBRGold staining; Lane 2: Tube reacted with 50 molar excess of TAMRA azide (13 μM); Lane 3: Tube reacted with 100 molar excess of TAMRA azide (26 μM); Lane 4: Tube reacted with 200 molar excess of TAMRA azide (52 μM); Lane 5: Tube reacted with 300 molar excess of TAMRA azide (78 μM); Lane 6: Tube reacted with 400 molar excess of TAMRA azide (104 μM); Lane 7: Tube reacted with 500 molar excess of TAMRA azide (133 μM); Lane 8: Tube reacted with 1000 molar excess of TAMRA azide (266 μM).

Click-tiles reactivity against external azides can be different in relation to the strand location within the structure. Indeed, strands having 3' and 5' reacting groups exposed to the solution and not hindered from other strands are in principle more likely to suffer from intermolecular side-reaction. Investigation of this aspect is accomplished using a 6HT containing a click-tile in the head region (ct-ODN17, Fig. 4. 5A) and the same experimental setup as described before. In this special case, fainting TAMRA signals are observed in the range of fluorophore concentration between 52 μM and 104 μM (Lane 4 – 6, Fig. 4. 5B). Similarly to the structure containing ct-ODN23, a significant TAMRA labeled tube band is detected at a competitor concentration of 133 μM . (Fig. 4. 5B, Lane 7). Hence, the position of the ct-ODN within the structure influences only slightly the reactivity behavior of the click groups.

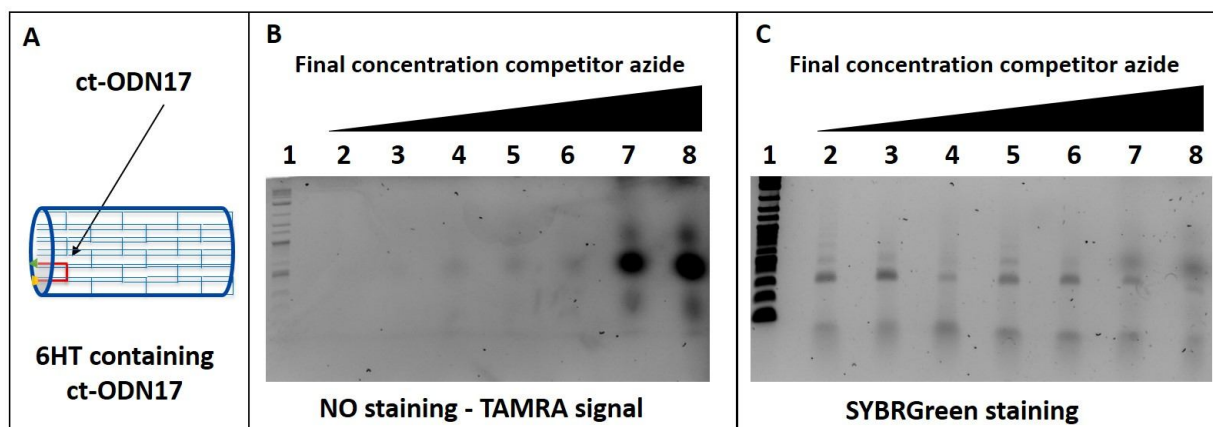


Figure 4. 5. A) Schematic representation of the 6HT containing ct-ODN17 used in this assay. B) and C) Agarose gel 2% 0.5x TBE buffer containing 11mM MgCl₂ imaged without staining (B) and after SYBRGreen staining (C). Lane 1: 2-Log DNA ladder containing SYBRGold staining; Lane 2: Tube reacted with 50 molar excess of TAMRA azide (13 μ M); Lane 3: Tube reacted with 100 molar excess of TAMRA azide (26 μ M); Lane 4: Tube reacted with 200 molar excess of TAMRA azide (52 μ M); Lane 5: Tube reacted with 300 molar excess of TAMRA azide (78 μ M); Lane 6: Tube reacted with 400 molar excess of TAMRA azide (104 μ M); Lane 7: Tube reacted with 500 molar excess of TAMRA azide (133 μ M); Lane 8: Tube reacted with 1000 molar excess of TAMRA azide (266 μ M).

These results demonstrate that the rigid spatial organization achieved in the assembled structure causes an increase of the effective concentration of the two reactive groups in respect of the nominal concentration of the single oligonucleotides. Indeed, the translational and rotational entropy of two independent molecules that interact in solution – intermolecular reaction - decrease at the moment of their interaction, while two groups on the same molecule – intramolecular reaction - have already lost several degrees of entropy.¹¹⁵ In the ideal case where two groups are immobilized in specific positions, optimal for their interaction, there is a minimal loss of entropy and a very effective reaction is observed. This particular situation resembles the one occurring in the system used, where alkyne and azide groups are constrained in close proximity within the nanotube. At a TAMRA concentration of 133 μ M the alkyne residue of the oligonucleotide starts to react with the competitor azide instead of undergoing intramolecular cyclization with the azide on the same strand, meaning that starting from this concentration the competitor azide can be considered in excess in respect to the effective molarity of the alkyne group of the click-tile. This observation can lead to a quantification of the local alkyne concentration, which results to be 200 fold higher ($\approx 100 \mu$ M) than the nominal one (500 nM). This study is necessary to understand the amount of external azide that can be used to efficiently label the alkyne free positions for the “body” functionalization avoiding undesired reactions with the click-tiles which can destabilize the entire structure.

4.4.3. Body-labeling

An important feature of this elaborated structure is the simultaneous accomplishment of its stabilization by chain armor formation and conjugation of external azides on alkyne groups pointing out of the nanotube body. Investigation of this aspect is carried out by means of either a one-pot or a stepwise approach. The analyses were performed taking advantage of TAMRA azide readout as easy detection method on agarose gel with or without MgCl_2 . In M24 tubes (6HT composed of 24 click-tiles) one to five click-tiles are replaced by the analogous bct-ODNs (Fig 4. 6A). In the one-pot approach, chain armor formation and body labeling are accomplished through a single click reaction (Fig 4. 6C) whereas in the stepwise strategy these two reactions are performed using two subsequent CuAAC assays (Fig. 4. 6B-C).

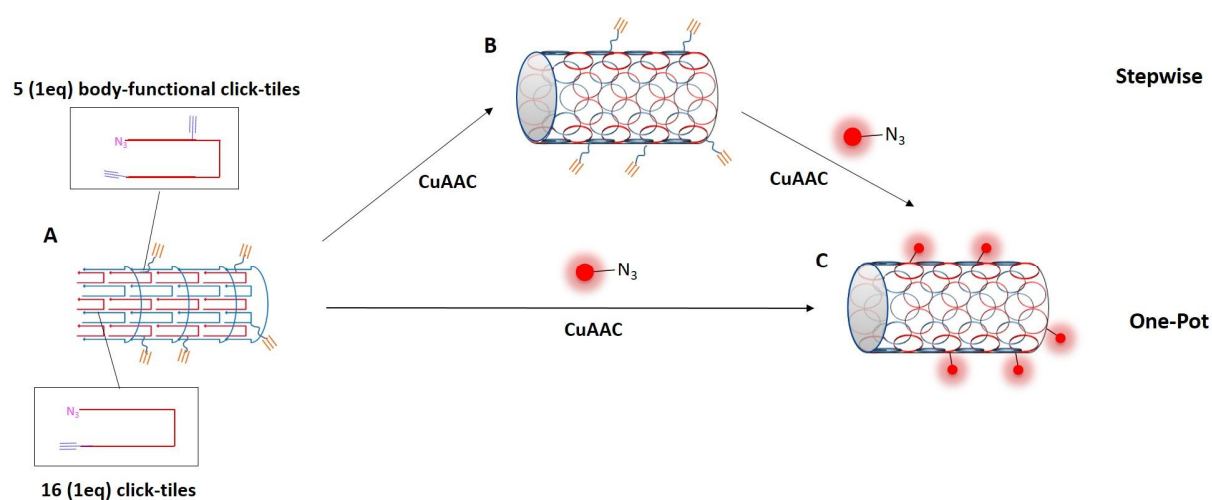


Figure 4. 6. Graphical representation of stepwise and one-pot experimental setup.

Both reaction mixtures, along with appropriate references, are firstly analyzed on agarose gel containing MgCl_2 . The analysis of the unstained gel displays only bands corresponding to TAMRA-labeled nanostructures (Fig. 4. 7A). The subsequent ethidium bromide staining confirmed the correct folding of the structure after click reaction in presence of an external azide (Fig. 4. 7B). The position of the fluorophore within the nanotube is then analyzed using a gel without MgCl_2 .

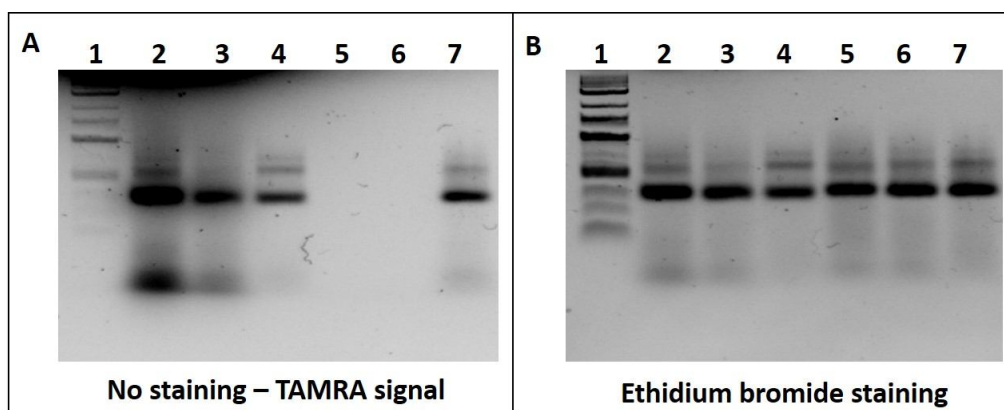


Figure 4. 7. Agarose gel 2% 0,5x TBE buffer containing 11mM MgCl_2 imaged without staining (A) and after ethidium bromide staining. One-pot and stepwise click reaction yielding stabilization and labeling of DNA nanotube containing 3 bct-ODNs. Lane 1: 2-Log DNA ladder containing SYBRGold staining; Lane 2: tube containing 3 bct-ODNs submitted to one-pot click reaction. Lane 3: tube containing 3 bct-ODNs submitted to stepwise click reaction; Lane 4: Reference M24*-tube containing 3 TAMRA labeled click-tiles submitted to click reaction. Lane 5: tube containing 3 bct-ODNs before one-pot click reaction; Lane 6: tube containing 3 bct-ODNs before stepwise click reaction; Lane 7: Reference M24*-tube containing 3 TAMRA labeled click-tiles before click reaction.

Analysis on agarose gel missing MgCl_2 is a useful method to elucidate the success of both kinds of click reactions.⁸⁹ The depletion of magnesium cations in gel, indeed, is a denaturing factor for self-assembled structures. Contrarily, structures stabilized by click chemistry do not unfold during the electrophoretic run and show a defined band at the expected tube weight (Lane 2-4, Fig. 4. 8A-B). Additionally, these bands are detectable in absence of staining, demonstrating the effective fluorophore labeling. Merging these two observations demonstrates that the click reaction successfully induces covalent stabilization and conjugation of an external molecule with high efficiency and selectivity even in a one-pot manner.

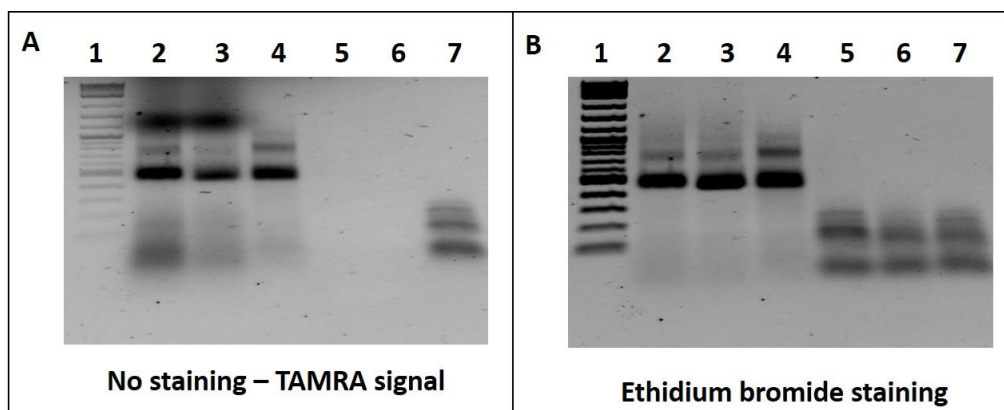

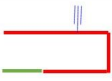

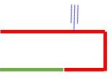
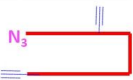
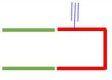



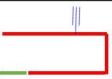


Figure 4. 8. Agarose gel 2% 0.5x TBE buffer missing $MgCl_2$ imaged without staining (A) and after ethidium bromide staining (B). One-pot and stepwise click reaction yielding stabilization and labeling of DNA nanotube containing 3 bct-ODNs. Lane 1: 2-Log DNA ladder containing SYBRGold staining; Lane 2: tube containing 3 bct-ODNs submitted to one-pot click reaction. Lane 3: tube containing 3 bct-ODNs submitted to stepwise click reaction; Lane 4: Reference M24*-tube containing 3 TAMRA labeled click-tiles submitted to click reaction. Lane 5: tube containing 3 bct-ODNs before one-pot click reaction; Lane 6: tube containing 3 bct-ODNs before stepwise click reaction; Lane 7: Reference M24*-tube containing 3 TAMRA labeled click-tiles before click reaction.

Nevertheless, these conclusions have been corroborated using alternative analytical methods such as Reverse Phase High Pressure Liquid Chromatography (RP-HPLC) and polyacrylamide gel electrophoresis (PAGE). HPLC is not a commonly used method for characterization of such complex DNA nanostructures due to the large number of oligonucleotides within the system. Nevertheless, a small structure like the nanotube used for this study was already analyzed by the author with this method allowing the detection of the formation of a two membered DNA catenanes as described above.⁸⁹ Here, this analytic method is further applied to observe the body labeling rate on the tube. Body-functional oligonucleotides have all the same length (42 bases), thus the chromatographic separation can be challenging. Therefore, for this study five analogs of bct-ODNs have been designed (Tab. 4. 2). These strands have different sizes and lack the alkyne and azide groups at the two termini. This set of strands – hereinafter called bat-ODNs - replaces corresponding bct-ODNs within the six-helix tube structure. Short sequences fill the gap originated from these bat-ODN truncated strands in order to maintain the rigidity of the nanotube given by complete double strand formation.

Table 4. 2. List and graphical representation of body-functional click-tiles (bct-ODNs) and alkyne-functional tiles (bat-ODNs) used in the study. The green sequences reported aside of bat-ODNs depict unmodified sequences used to fill the gaps originated from the shortened strands.

Original bct-ODNs			Truncated bat-ODNs		
body-functional click-tiles (bct-ODNs)			body-functional alkyne-tiles (bat-ODNs)		
Name	Graphical representation	#bases	Name	Graphical representation	#bases
bct-ODN1		42	bat-ODN1		31
bct-ODN2		42	bat-ODN2		27
bct-ODN3		42	bat-ODN3		20
bct-ODN4		42	bat-ODN4		42
bct-ODN5		42	bat-ODN5		37

Truncated bat-ODN oligonucleotides present a clear shift in the chromatogram before and after click reaction when analyzed alone and all five together. However, HPLC analysis of the entire tube containing all 24 strands turned out to be an inaccurate method to determine labeling rate on bat-ODNs. The proportion between the peaks areas and the real oligonucleotides ratio within the tube is not fully respected in the chromatogram. Therefore, tube labeling yield calculation based on peaks areas could be misleading.

Alternatively, the body-labelling efficiency is analyzed by PAGE using the same structural concept described above. Polyacrylamide gel analysis is sensitive enough to distinguish difference of one nucleotide or small molecules conjugation within an oligonucleotide. For this assay, a shortened strand (20mers instead of a 42mer, bat-ODN3) replaces the unmodified oligonucleotide u-ODN15 in the folding of a 6HT. bat-ODN3 has the same sequence of the central 20 bases of u-ODN15. Short sequences (11mer each) fill the gaps left from bat-ODN3. Due to the truncated size, bat-ODN3 migrates during PAGE analysis faster than all other oligonucleotides composing the nanotube (Lane 4, Fig. 4. 9B). After click reaction, the conjugation of the oligonucleotide with TAMRA is noticeable as a band shifted to higher molecular weight and visible in the unstained gel (Lane 3 and 5, Fig. 4. 9A). TAMRA labeling on nanotube occurs quantitatively since no rest of unreacted bat-ODN3 can be observed in PAGE.

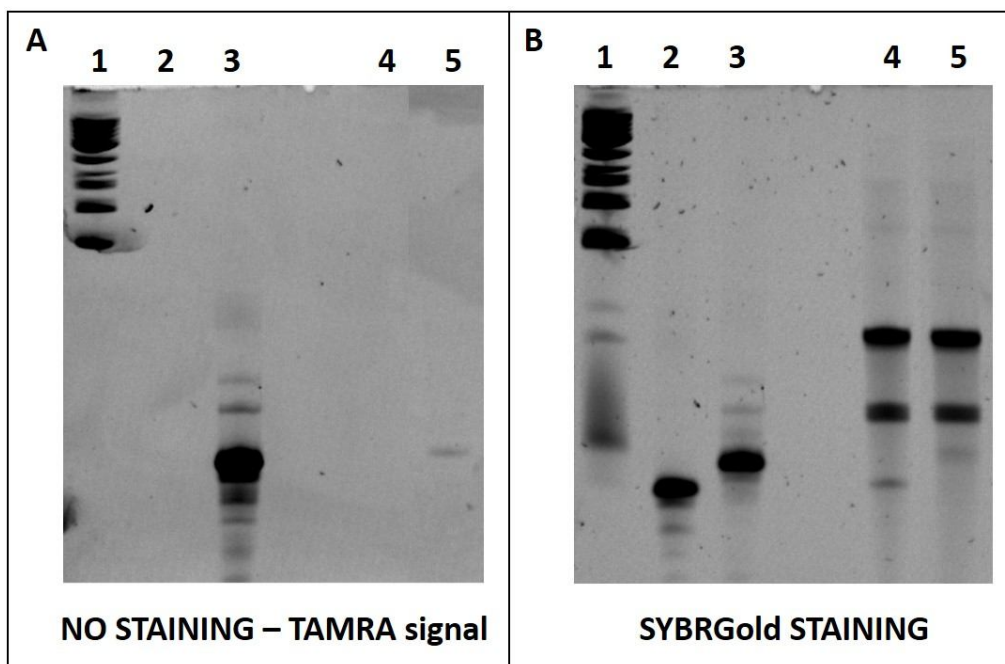
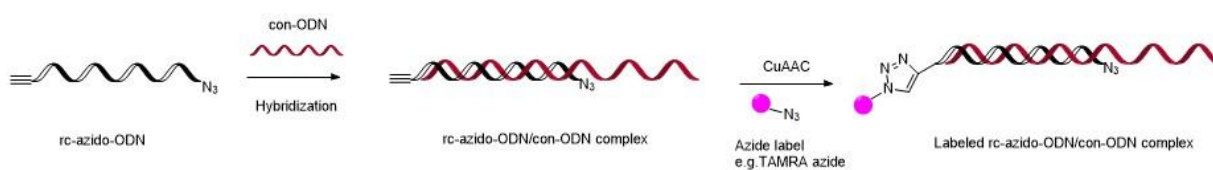


Figure 4. 9. Denaturing PAGE 20% (8M urea) imaged without staining (A) and after SYBRGold staining (B). Labeling efficiency on body alkyne positions. Lane 1: Low molecular DNA ladder containing SYBRGold staining; Lane 2: bat-ODN3; Lane 3: TAMRA labeled bat-ODN3; Lane 4: 6HT containing bat-ODN3 before click reaction; Lane 5: 6HT containing bat-ODN3 after click reaction with 50 equivalents of TAMRA azide.

Summarizing, the tested click reaction conditions (50 equivalents external azide, 5 hours reaction, 32°C) cooperate to accomplish an efficient catenation of the entire structure and a simultaneous quantitative labeling of the alkyne residues on the body of the tube.

4.4.4. Head-labeling

The head functionality is inserted by the help of a reporter-click oligonucleotide (rc-ODN), as conceived in the above described design. In a first attempt, a strand bearing an alkyne residue at the 3'-end and an azide group at the 5'-end was used as rc-ODN, hereinafter called rc-azido-ODN. The coexistence of alkyne and azide group in the same strand can lead to undesired intramolecular cyclization or uncontrolled polymerization during the click reaction. Therefore, a preliminary hybridization step between the rc-azido-ODN and an extended complementary sequence (con-ODN) is necessary in order to minimize unwanted side products. In this way, the newly formed double strand confers enough rigidity to favor the reaction of the 3'-alkyne with an external azide (Scheme 4. 1). The conversion of the click ligation is complete. However, the RP-HPLC analysis shows two main chromatogram peaks: the desired TAMRA labeled rc-azido-ODN at 5.3 minutes and the putative intramolecular ligated product at 3.7 minutes (Fig. 4. 10B).



Scheme 4. 1. Preparation of labeled-azide rc-ODN starting from alkyne-azide rc-ODN.

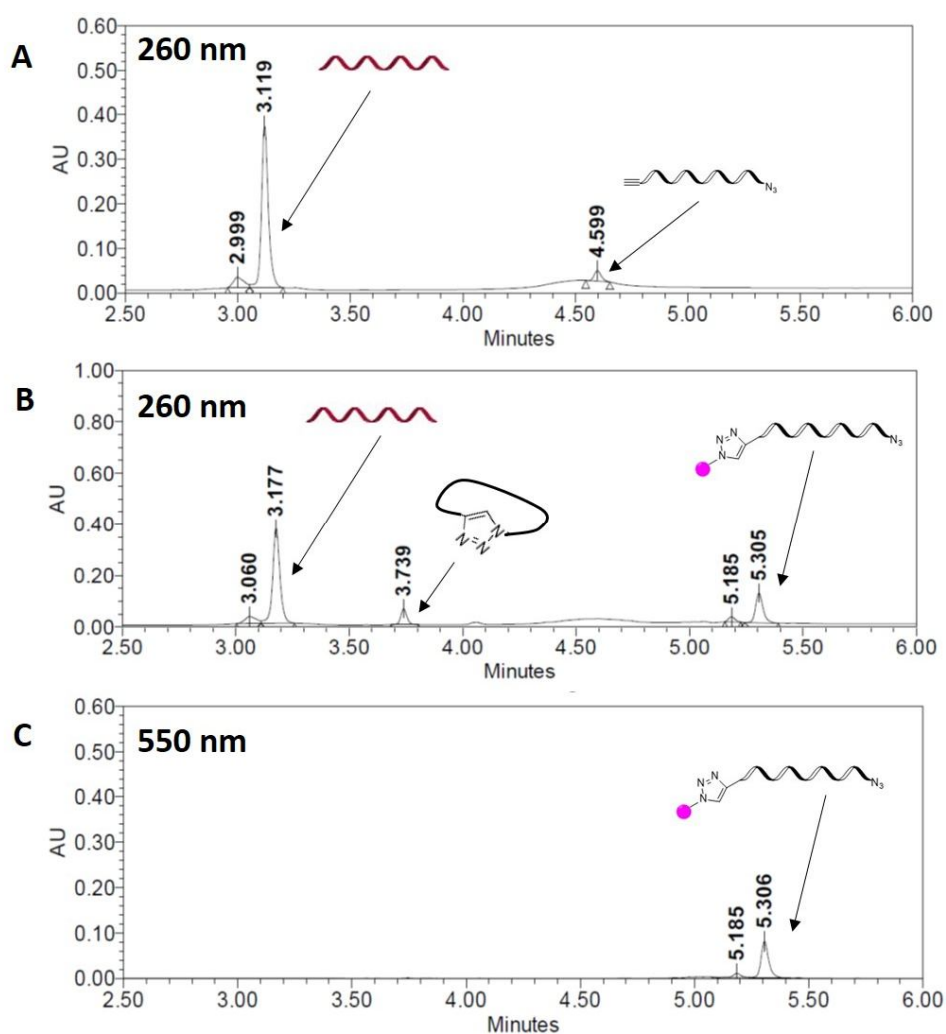


Figure 4. 10. HPLC analysis of each step involved in the preparation of TAMRA labeled-azide rc-ODN starting from rc-azido-ODN. A) HPLC chromatogram at 260 nm of alkyne-azide rc-ODN/con-ODN complex after hybridization; B) HPLC chromatogram at 260 nm of TAMRA labeled rc-azido-ODN/con-ODN complex; C: HPLC chromatogram at 550 nm of TAMRA labeled rc-azido-ODN/con-ODN complex.

The complex TAMRA-labeled rc-azido-ODN/con-ODN is then added to the folding mixture used to fold the nanotube. Gel electrophoresis analysis shows the incorporation of the labeled reporter oligonucleotide in conjunction with a considerable presence of unincorporated labeled strand (Fig. 4. 11A). TAMRA signals at the tube height on agarose gel missing MgCl_2 , demonstrate that the complex TAMRA-azide rc-ODN/con-ODN is effectively incorporated in the nanotube and joined with the rest of the structure *via* click chemistry (Fig. 4. 11B, Lane 2 and 3).

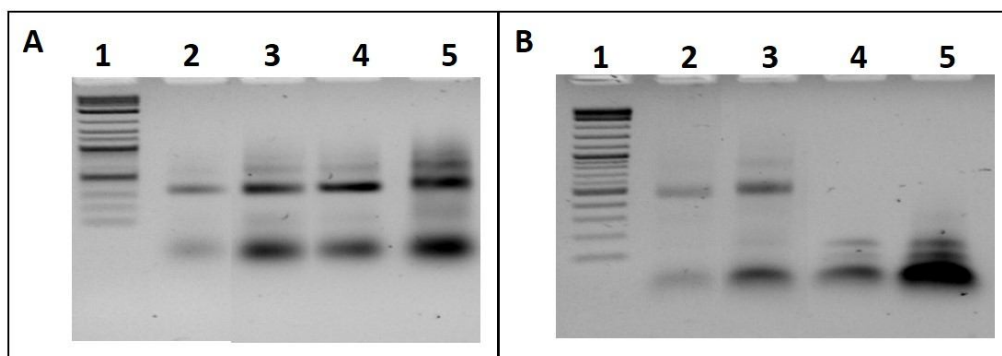
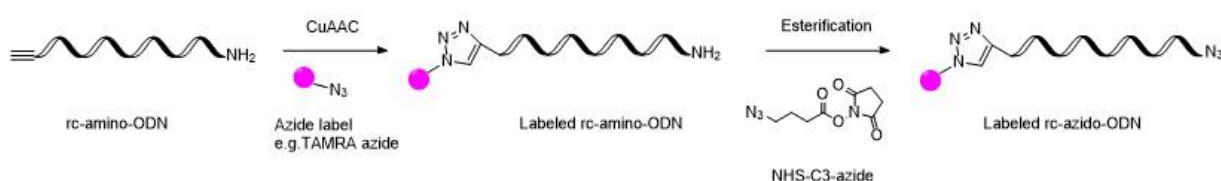


Figure 4. 11. 2% agarose gel 0,5x TBE buffer with 11mM MgCl_2 (A) and without MgCl_2 imaged without staining (only TAMRA signal detection). Lane 1: 2-Log DNA ladder containing SYBRGold; Lane 2: M24-tube containing one TAMRA labeled rc-azido-ODN/con-ODN after click reaction; Lane 3: M24-tube containing three TAMRA labeled rc-azido-ODN/con-ODN after click reaction; Lane 4: M24-tube containing one TAMRA labeled rc-azido-ODN/con-ODN before click reaction; Lane 5: M24-tube containing three TAMRA labeled rc-azido-ODN/con-ODN before click reaction.

A more effective labeling of the reporter oligonucleotide can be achieved replacing the azide residue at the 5'-end with an amino group (rc-amino-ODN), whose reaction is not catalyzed by Cu(I) . In this approach the functionalized rc-ODN is obtained from a two-step procedure, involving a first conjugation *via* click chemistry with the selected functional moiety and a subsequent introduction of the azide group *via* esterification of the 5'-amino group with a NHS-azide linker (Scheme 4. 2). The production of TAMRA labeled rc-azido-ODN occurs in quantitative yield, as confirmed by RP-HPLC and MALDI-Tof mass analysis (Fig. 4. 12A-H).



Scheme 4. 2. Two steps procedure for preparation of labeled-azide rc-ODN.

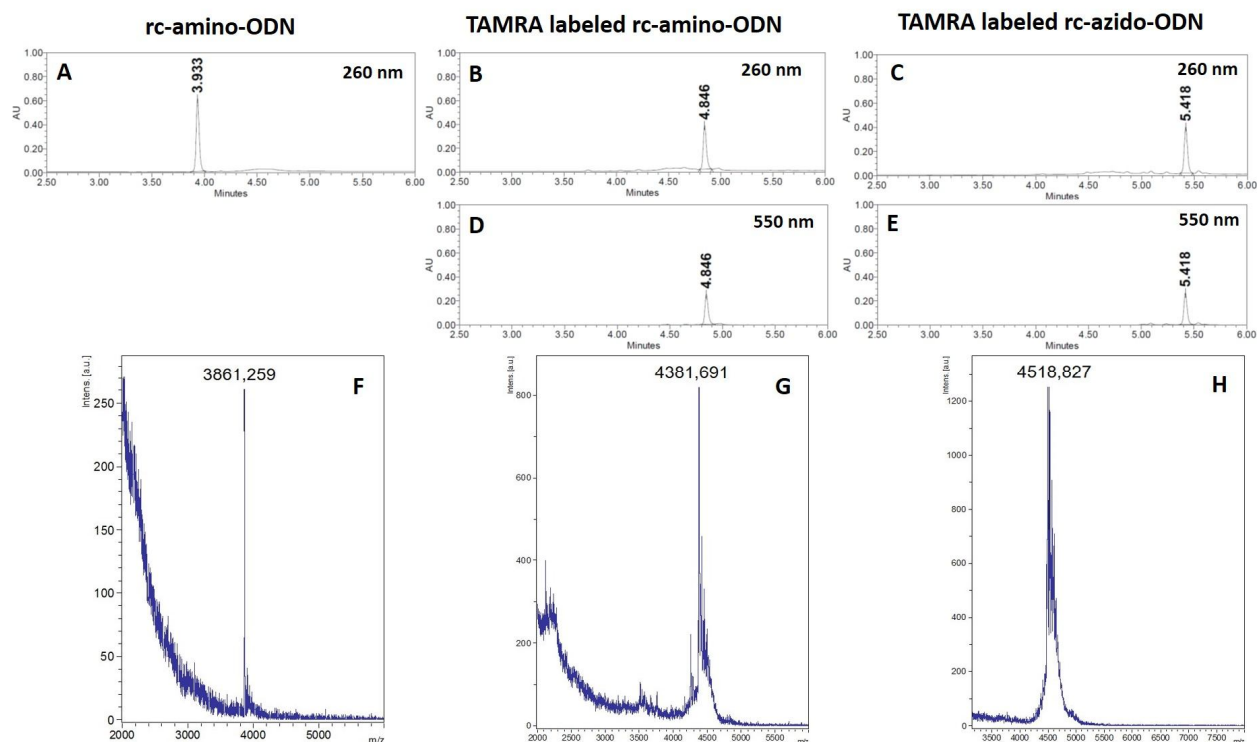


Figure 4. 12. HPLC and MALDI analysis of each step involved in the labeled-azido rc-ODN preparation. A) HPLC chromatogram at 260 nm of rc-amino-ODN; B) HPLC chromatogram at 260 nm of TAMRA labeled rc-amino-ODN; C) HPLC chromatogram at 260 nm of TAMRA labeled rc-azido-ODN; D) HPLC chromatogram at 550 nm of TAMRA labeled rc-amino-ODN; E) HPLC chromatogram at 550 nm of TAMRA labeled rc-azido-ODN; F) MALDI-TOF spectrum of rc-amino-ODN (calculated mass: 3873 g/mol; Experimental mass: 3861,259 g/mol); G) MALDI-TOF spectrum of TAMRA labeled rc-amino-ODN (calculated mass: 4385,56 g/mol; Experimental mass: 4381,691 g/mol); H) MALDI-TOF spectrum of TAMRA labeled rc-azido-ODN (calculated mass: 4516,46 g/mol; Experimental mass: 4518,827 g/mol).

The incorporation of the TAMRA labeled rc-azido-ODN in the nanotube occurs within the folding procedure using a connector strand (con-ODN). The newly formed double strand forces the azide group of the labeled rc-azido-ODN to face the alkyne on the hct-ODN. In this way their selective reactivity is maximized. Four connector strands - including 0 to 3 spacers at the click ligation site - were synthesized and screened to evaluate the best click strand ligation efficiency. The various length of the spacer (from 0.34 nm to 1.36 nm) do not have a detectable influence on the click reaction, which occurs very efficiently with each of the four con-ODNs.

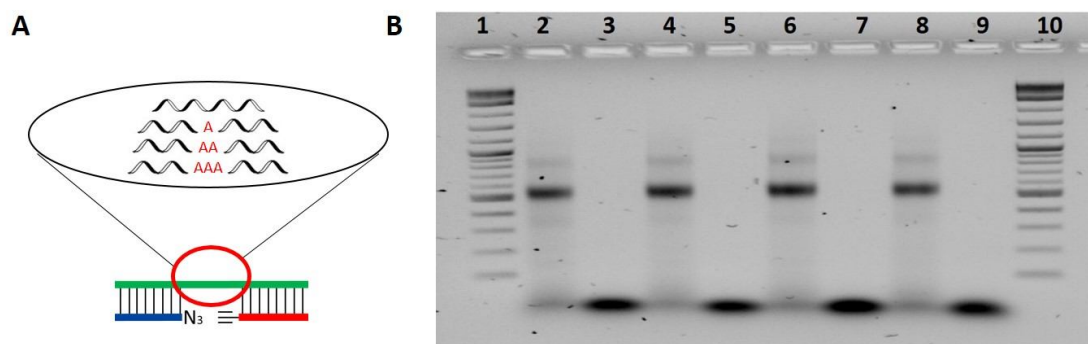


Figure 4. 13. A) Graphical representation of the spacers used during the click strand ligation. B) Agarose gel 2%, 0.5x TBE buffer missing $MgCl_2$ imaged without staining (only TAMRA signal detection). Lane 1 and 10: 2-Log DNA ladder containing SYBRGold; Lane 2: M24-tube containing 3 TAMRA-azide rc-ODNs and 3 con-ODN with no spacer after click reaction; Lane 3: M24-tube containing 3 TAMRA-azide rc-ODNs and 3 con-ODN with no spacer before click reaction; Lane 4: M24-tube containing 3 TAMRA-azide rc-ODNs and 3 con-ODN with one A as spacer after click reaction; Lane 5: M24-tube containing 3 TAMRA-azide rc-ODNs and 3 con-ODN with one A as spacer before click reaction; Lane 6: M24-tube containing 3 TAMRA-azide rc-ODNs and 3 con-ODN with two A as spacer after click reaction; Lane 7: M24-tube containing 3 TAMRA-azide rc-ODNs and 3 con-ODN with two A as spacer before click reaction; Lane 8: M24-tube containing 3 TAMRA-azide rc-ODNs and 3 con-ODN with three A as spacer after click reaction; Lane 9: M24-tube containing 3 TAMRA-azide rc-ODNs and 3 con-ODN with three A as spacer before click reaction.

The preparation of labeled rc-azido-ODN starting from rc-amino-ODN is a straightforward procedure that deliver quantitative yield and its product is efficiently incorporated in the nanotube. Therefore this strategy is selected for the subsequent modular synthesis of multi-labeled nanostructures.

4.4.5. One-pot reaction

Once the effective functionalization of both head and body regions was independently demonstrated, all different modified ct-ODNs were combined together with the residual 16 ct-ODNs for the folding of the tube nanostructure. Namely, five bct-ODNs (1 eq. each), three hct-ODNs (1 eq. each), one labeled rc-azido-ODNs (3 eq.) and one con-ODNs (3 eq.) were mixed with 16 ct-ODNs (1 eq. each) as shown in figure 4. 14. The self-assembly of the nanotube results in the organization of all strands with nanometric precision enabling the simultaneous formation of 32 triazoles within the nanostructure after the addition of Cu(I) catalyst and an external azide. Thus, through a single one-pot CuAAC three different kinds of click reactions are simultaneously accomplished. Specifically, 24 strands undergo catenation, five positions are labeled with an external azide and three "head" alkyne residues are conjugated with a strand carrying an additional functionality. This combination of highly pre-organized 3D nanostructures and outstanding efficacy of the CuAAC leads to an unprecedented covalent multi-functionalization of ultra-stable DNA architectures.

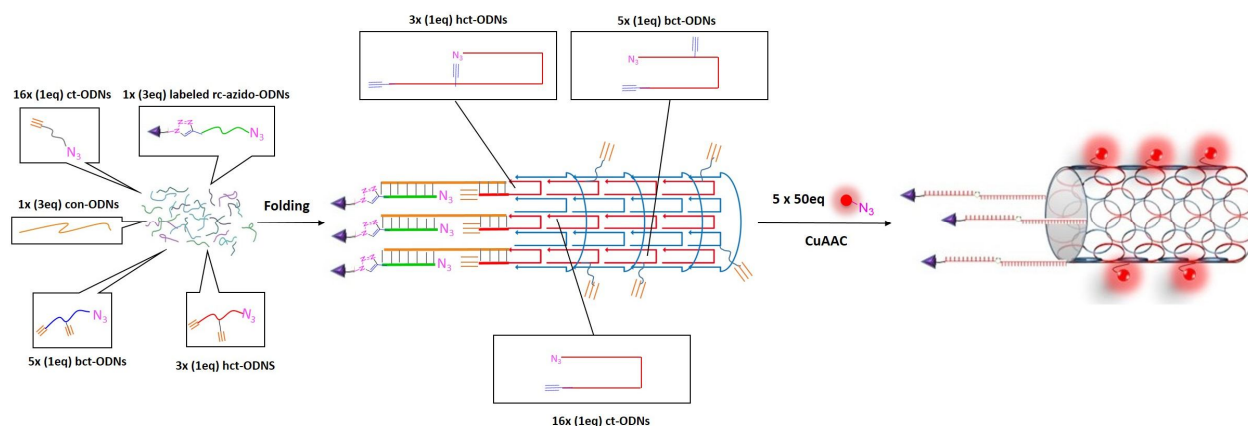


Figure 4. 14. Graphical representation of the components of the nanotube participating to the folding procedure and the subsequent one-pot click reaction on the structure.

Accordingly to this strategy, a nanotube structure bearing three folate-labeled rc-azido-ODNs was efficiently assembled. The following one-pot click reaction in presence of TAMRA azide yielded a chain armor DNA covalently connected to three folate moieties in the head region and five fluorophores in the body region. The stable bi-functionalized tube shows a persistent and fluorescent band in unstained agarose gel missing MgCl_2 confirming the successful accomplishment of stabilization and multi-labeling of the structure (Fig. 4. 15A1).

The validation of this double functionalization strategy is achieved by using a nanostructure covalently conjugated with three fluorescein dyes (FAM) in the head region and five cyanine-5 analogue dyes (Eterneon-Red) in the body region. Agarose gel analyzed with a fluorescent detector shows co-localization of the two fluorescent bands, confirming the successful one-pot double functionalization of the nanostructure (Fig. 4. 15B – D).

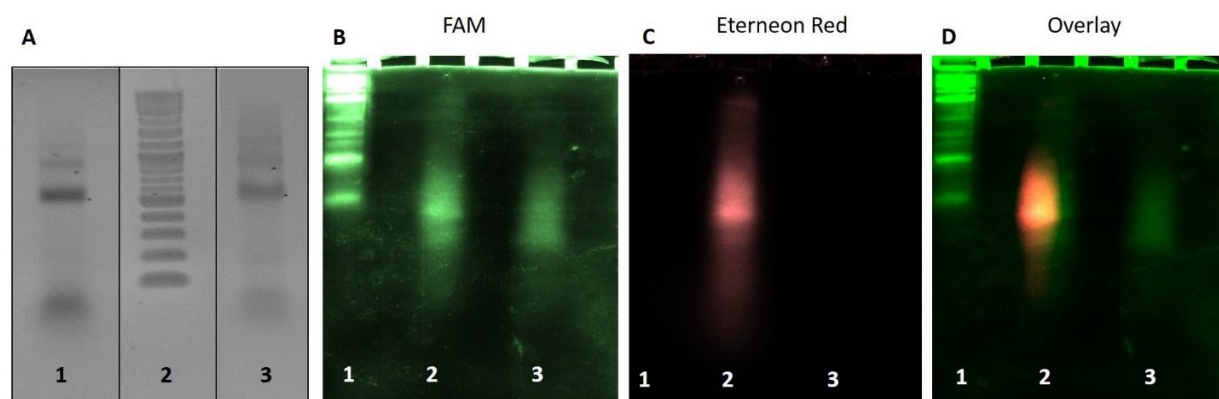


Figure 4. 15. A) 2% agarose gel 0,5x TBE buffer missing $MgCl_2$. 1) TAMRA signal (no staining) of 3Folate-, 5TAMRA- labeled M24*-tube. 2) 2-Log DNA ladder containing SYBRGold. 3) Ethidium bromide staining of 3Folate-, 5TAMRA- labeled M24*-tube. B) 2% agarose gel, 0,5x TBE buffer containing 11 mM $MgCl_2$, unstained. Lane 1: 2-Log DNA ladder containing SYBRGold; Lane 2: FAM signal (no staining) of 3FAM-, 5Eterneon Red labeled M24*-tube; Lane 3: FAM signal (no staining) of 3FAM-labeled M24-tube. C) 2% agarose gel, 0,5x TBE buffer containing 11 mM $MgCl_2$, unstained. Lane 1: 2-Log DNA ladder containing SYBRGold; Lane 2: Eterneon Red signal (no staining) of 3FAM-, 5Eterneon Red labeled M24*-tube; Lane 3: Eterneon Red signal (no staining) of 3FAM-labeled M24-tube. D) 2% agarose gel, 0,5x TBE buffer containing 11 mM $MgCl_2$, unstained. Lane 1: 2-Log DNA ladder containing SYBRGold; Lane 2: overlaid FAM-Eterneon Red signal (no staining) of 3FAM-, 5Eterneon Red labeled M24*-tube; Lane 3: overlaid FAM-Eterneon Red signal (no staining) of 3FAM-labeled M24-tube.

This strategy enables the assembly of stable nanostructures with a high degree of modularity. Therefore, two different functional tags can be selectively and covalently ligated to the system in a one-pot fashion maintaining the original design. This aspect was exploited by creating various sorts of functional nanotubes conjugated with different fluorescent dyes and other classes of molecules, such as folate, sugars, peptides and cholesterol. The CuAAC reaction does not affect the structural integrity of the nanotube as observed during Transmission Electron Microscopy (TEM) imaging (Fig 4. 16). Micrographs show structures respecting the calculated dimensions (around 30 nm length and 8 nm width).

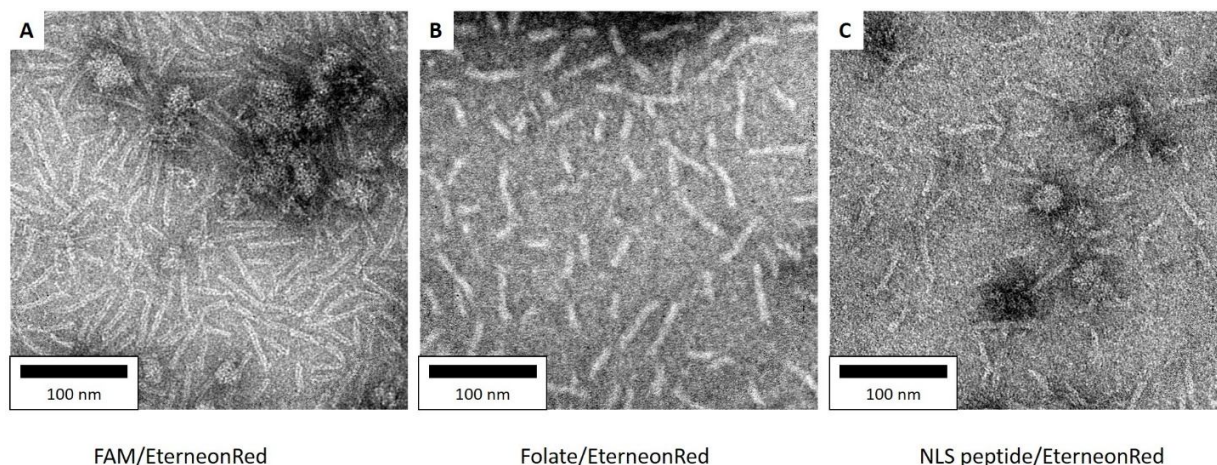


Figure 4. 16. TEM images of ultra-stable multifunctionalized DNA nanotubes. A) 3FAM-, 5Eterneon Red-labeled nanotubes; B) 3Folate-, 5Eterneon Red-labeled nanotubes; C) 3NLS peptide-, 5Eterneon Red-labeled nanotube.

4.4.6. Cell delivery applications

One appealing application of these functionalized ultra-stable nanotubes is the targeted cell delivery of diagnostic or therapeutic molecules. As proof-of-concept, the ultra-stable DNA nanotube is decorated with three folate-labeled rc-azido-ODNs as targeting ligand and five Eterneon Red as cell-tracking dye. The preparation of folate-labeled rc-azido-ODN was achieved accordingly to the procedure explained above (4.4.4, Scheme 4. 2) resulting in high yields (Fig. 4. 17).

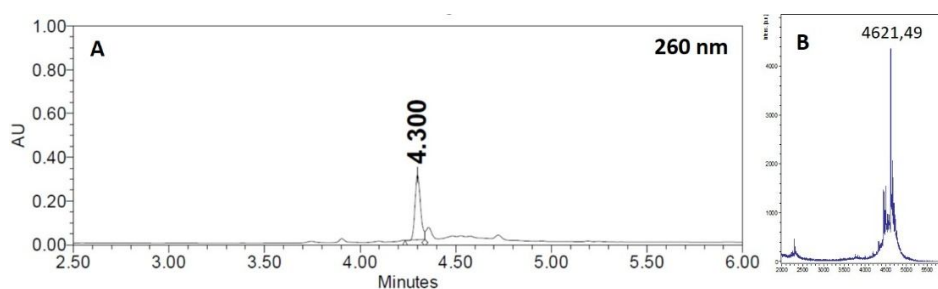


Figure 4. 17. HPLC and MALDI-TOF analysis of folate-azide rc-ODN. A) HPLC chromatogram at 260 nm of folate-azide rc-ODN; B) MALDI-TOF spectrum of folate-azide rc-ODN (Calculated mass: 4645,64 g/mol, experimental mass: 4621,49).

This folate/Eterneon Red nanotube was tested for targeted cell delivery on HeLa cells known to overexpress folate receptors. Cellular uptake of folate-functionalized nano-objects is reported to be favored than delivery of naked structures⁸⁰. Simultaneously EdU cell proliferation assay is performed in order to monitor the effect of the DNA nanostructure on the cell cycle. Cell uptake of folate-conjugated nanotube occurs significantly even in proliferating cells demonstrating that this ultra-stable carrier does not interfere with the cell cycle (Fig. 4. 18A and 4. 18B). The labeled structure is effectively internalized in cells as confirmed by confocal microscopy analysis (Fig. 4. 19A-C). A chain armor nanotube without folate was prepared and used as negative control. Surprisingly, the internalization of this control structure was also observed in a few HeLa cells (Fig. 4. 18C and 4. 18D). In conclusion, an increased targeted delivery driven by the folate was not fully discernible in this preliminary study and further investigations are required.

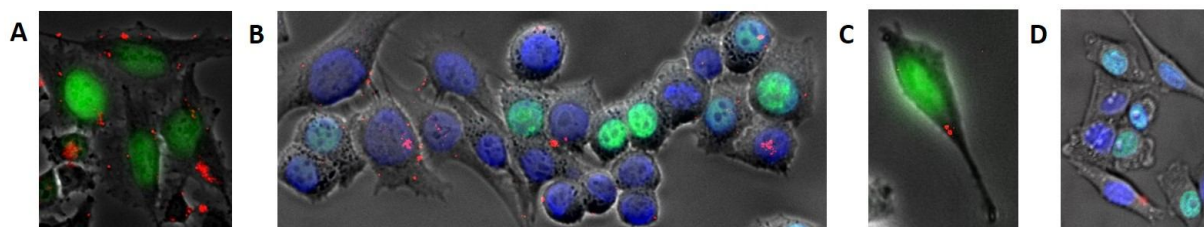


Figure 4. 18. Fluorescence microscopy imaging of HeLa cells transfected with DNA nanostructures. Nuclei containing new synthesized DNA, are labeled with FAM azide (green) using a cell proliferation kit. Nuclei are stained with Hoechst (blue). As “tracking dye” on the nanostructures Eterneon Red (red) was chosen. A and B) HeLa cells incubated 2 hours with 3 Folate-, 5 Eterneon Red residue-labeled nanotubes and simultaneous EdU proliferation assay C and D) HeLa cells incubated 2 hours with 5 Eterneon Red-label-bearing nanotubes and simultaneous EdU proliferation assay.

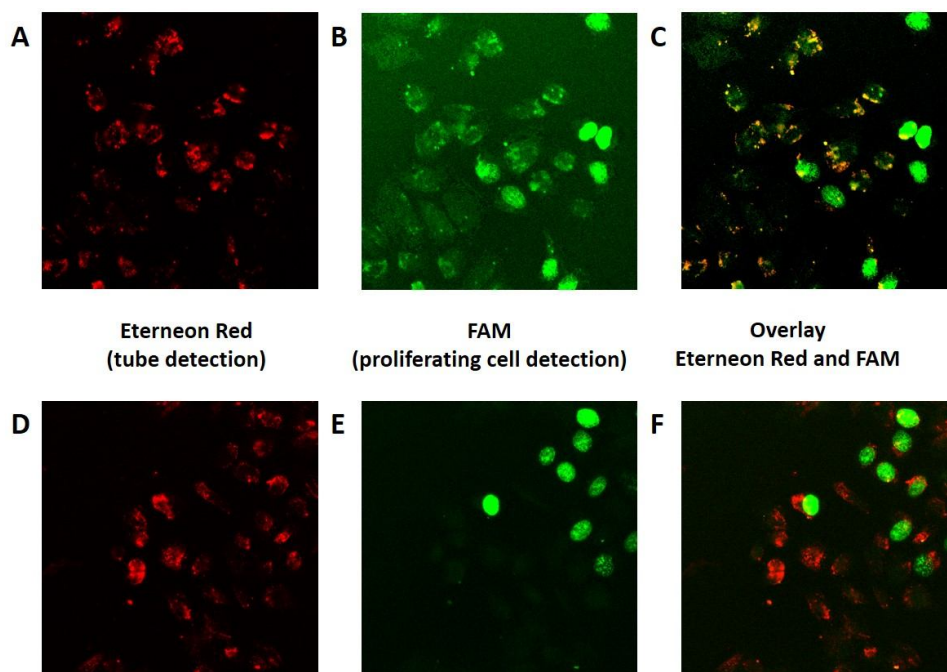


Figure 4. 19. Confocal microscopy imaging of HeLa cells transfected with DNA nanostructures. Nuclei containing newly synthesized DNA are labeled with FAM azide (green) using a cell proliferation kit. As “tracking dye” on the nanostructures Eterneon Red (red) was chosen. A-C) HeLa cells incubated 2 hours with 3 Folate-, 5 Eterneon Red residue-labeled nanotubes and simultaneous EdU proliferation assay. A) Detection at Eterneon Red wavelength (red). B) Detection at FAM wavelength (green). C) Overlay of the two channels. D-F) HeLa cells incubated 2 hours with 5 Eterneon Red residue-labeled nanotubes and simultaneous EdU proliferation assay. D) Detection at Eterneon Red wavelength (red). E) Detection at FAM wavelength (green). F) Overlay of the two channels.

Structures bearing different kinds of targeting ligand molecules in the two regions of the nanotube – head and body – have been assembled in order to confirm the high modularity of this system (Fig. 4. 20A). Cell uptake is observed in all cases supporting the hypothesis that the uptake of the nanotube in HeLa cells, like other architectures, is principally attributable to its compact structure and to a minor extent to the targeting agent used (Fig. 4. 20B-E).¹¹⁶

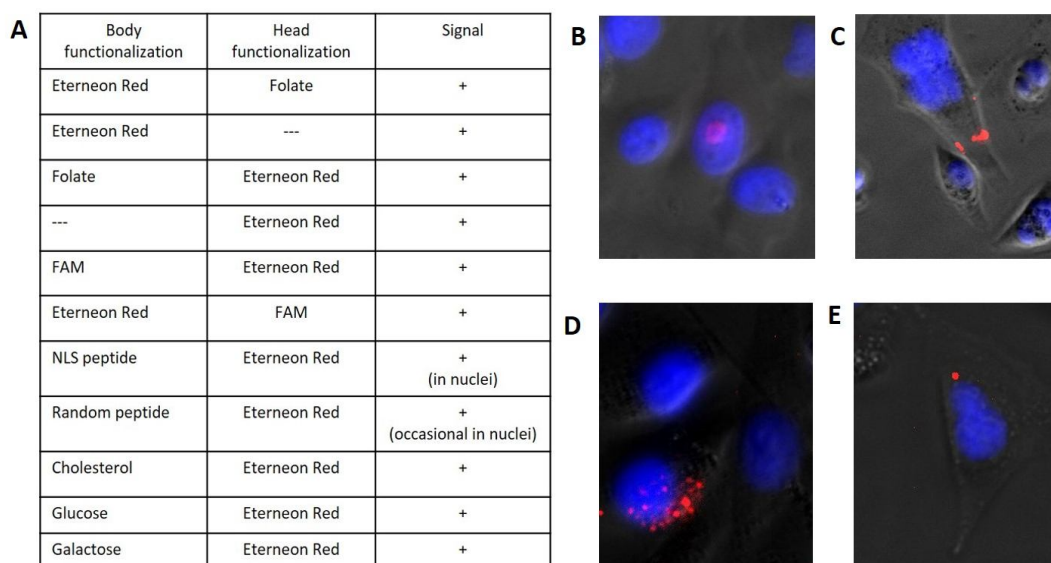


Figure 4. 20. Functionalization modularity of the ultra-stable nanotube. A) Table listing the combination of functional molecules attached to the nanotube and results obtained for cell uptake; B) Fluorescence microscopy imaging of HeLa cells transfected with 3 Eterneon Red-, 5 NLS peptide residue-labeled nanotubes; C) Fluorescence microscopy imaging of HeLa cells transfected with 3 Eterneon Red-, 5 Cholesterol residue-labeled nanotubes; D) Fluorescence microscopy imaging of HeLa cells transfected with 3 Eterneon Red-, 5 Galactose residue-labeled nanotubes; E) Fluorescence microscopy imaging of HeLa cells transfected with 3 Eterneon Red-, 5 Glucose residue-labeled nanotubes.

4.5. Conclusion and outlook

Summarizing, in this study an efficient method for the one-pot synthesis of an ultra-stable and multifunctional DNA nanostructure is described. The stable chain armor based structure is implemented for the connection of functionalities in a covalent manner *via* click chemistry. The step-by-step approach showed that CuAAC occurs quantitatively on both the head and the body region of the structure. Subsequently, the covalent multi-labeling of the nanotube and the simultaneous chain armor formation are efficiently achieved with a one-pot click reaction. The formation of 32 triazoles within the structure further ensures the coexistence of two functionalities even under denaturing conditions. The results achieved in this study suggest this method as a solid labeling alternative to the “environment-sensitive” sticky-ends approach. Stabilization via chain armor and covalent conjugation of transfection, therapeutic or diagnostic agents propose a concrete new strategy for developing of a new class of stable and multifunctional DNA nano-object for *in-vitro* and *in-vivo* applications.

The design used in this study was chosen for the simplicity and low number of strands implied. These structural characteristics are ideal for preliminary studies in the frame of the establishment of a new strategy. Nevertheless, adopting small modifications on the actual design the modularity and the density of the functionalities can be easily increased. Furthermore, a challenging development is to adapt this

strategy to larger and more complex structures, such as DNA origami, where the herein studied features can create a benefit for biological applications.

4.6. Materials and methods

4.6.1. Buffer used in this work

10x TE Buffer pH 8 (Tris 100 mM, EDTA 10 mM): 12.11 g Tris (VWR) and 3.72 g EDTA (VWR) were added to 900 ml ddH₂O. The mixture was stirred at room temperature until the solution was clear and homogenous. The pH was adjusted to pH 8 using a 1M HCl solution. Afterwards the solution was filled up to 1 L with ddH₂O.

2M MgCl₂ Solution: 40.66 g MgCl₂ (hexahydrate, Carl Roth) were added slowly to 100 ml ddH₂O (exothermic reaction). The solution was stirred at room temperature until it became clear

10x TE Buffer, 200mM MgCl₂: 9 ml of 10x TE buffer was transferred into a 15 ml falcon tube and 1ml of 2M MgCl₂ was added. The mixture was thoroughly stirred.

1x TE Buffer with 20mM MgCl₂ (folding buffer): the buffer was prepared using ddH₂O.

10x TBE Buffer pH8 (Tris-Cl 1M, H₃BO₃ 1M, Na-EDTA 20mM): 121.1 g Tris-Cl (Carl Roth), 61.8 g H₃BO₃ (Carl Roth) and 7.44 g Na-EDTA (Carl Roth) were added to 900 ml ddH₂O. The mixture was stirred at room temperature until the solution was clear and homogenous. The pH was adjusted to pH 8 using a 1M HCl solution. Afterwards the solution was filled up to 1 L with ddH₂O.

0.5x TBE Buffer: the buffer was prepared using ddH₂O.

0.5x TBE Buffer containing 11mM MgCl₂: To 100 ml 10x TBE Buffer pH 8, 11 ml 2M MgCl₂ were added. The mixture was filled up to 2 L with ddH₂O.

4.6.2. Gel electrophoresis

2% Agarose gel (0.5x TBE Buffer, 11mM MgCl₂): 1 g Agarose (Carl Roth) were dissolved in 50 ml of 0.5x TBE buffer and the mixture was heated up to dissolve completely the agarose. A solution of MgCl₂ (275 µl, 2M) was added to the warm mixture and stirred for a while before casting the gel. Appropriate sample amounts were loaded into the agarose gel using 2 µl 6x Loading Dye (New England Biolabs). The running chamber was filled up with 0.5x TBE buffer containing 11mM MgCl₂. A 70 V voltage was applied to the electrophoretic equipment (BioRad) for 2 hours, while the chamber was cooled down. Agarose gels were stained with ethidium bromide (0.25 µmol/l in 0.5x TBE buffer containing 11mM MgCl₂) for 20 minutes and then destained for 10 minutes in 0.5x TBE buffer containing 11mM MgCl₂. Alternatively gels were stained with SYBRGreen (Thermo Fisher Scientific) following supplier protocol. Gels were imaged using the imager Gel Doc Ez System (Biorad).

2% Agarose gel missing MgCl₂ (0.5x TBE Buffer): 1 g Agarose (Carl Roth) was dissolved in 50 ml of 0.5x TBE buffer and the mixture was heated up to dissolve completely the agarose. Appropriate sample amounts were loaded into the agarose gel using 2 µl 6x Loading Dye (New England Biolabs). The running chamber was filled up with 0.5x TBE buffer. A 70 V voltage was applied to the electrophoretic equipment (BioRad) for 2 hours, while the chamber was cooled down. Agarose gels were stained with ethidium bromide (0.25 µmol/l in 0.5x TBE buffer) for 20 minutes and then destained for 10 minutes in 0.5x TBE

buffer. Alternatively gels were stained with SYBRGreen (Thermo Fisher Scientific) following supplier protocol. Gels were imaged using the imager Gel Doc Ez System (Biorad).

20% denaturing polyacrylamide gel electrophoresis (PAGE) (8M Urea): A 10% ammonium persulfate (APS, Merck Millipore) solution was prepared in advance dissolving 1 g of APS in 10 ml ddH₂O. 4.8 g urea (Sigma Aldrich) were added to 6.6 mL 30% Acrylamide/Bis-acrylamide (19:1 ratio) solution and 1 mL 10x TE buffer. After dissolving of urea, ddH₂O is added till the achievement of a final volume of 20 mL. To initiate the polymerization 150 µl 10% APS solution and 10 µl of N,N,N'',N''-Tetramethylethylenediamine (TEMED, Sigma Aldrich) were added to the gel mixture, stirred and then the gel was casted. Appropriate sample amounts were loaded into the polyacrylamide gel using 2 µl 6x Loading Dye (New England Biolab). The running chamber was filled up with 0.5x TBE buffer. A 120 V voltage was applied to the electrophoretic equipment (Mini-PROTEAN Tetra Cell system, BioRad) for 1 hour. Gels were stained in 200 ml 0.5x TBE buffer containing 20 µl SYBR Gold Stain (Life Technologies) for 10 minutes and imaged using the imager Gel Doc Ez System (Biorad).

4.6.3. TEM imaging

2 µL sample was adsorbed for 3 minutes onto glow-discharged, carbon-coated TEM grid (PLANO GmbH). The rest of the drop was discarded. The grid was then rapidly washed with 2% aqueous uranyl formate solution containing 25mM NaOH and afterwards stained for 10 seconds with the same solution. Imaging was performed using a JEM 1011 (Jeol) operated at 80 kV (LMU, Physic Department).

4.6.4. RP-HPLC analysis

RP-HPLC analyses were obtained by e2695 separation module (Waters) coupled with a 2998 photodiode array detector (Waters). The samples were separated with a reversed phase XBridge OST C18 column (4.6 mm x 50 mm, Waters) with a particle size of 130 Å and an inner diameter of 2.5 µm. The method used is described in table 4. 3.

Table 4. 3. Analytical HPLC method. Buffer A: 100 ml stock solution (101.19 g Triethylamine, 60.05 ml acetic acid HPLC grade dissolved in 1 L H₂O HPLC grade) + 900 ml H₂O HPLC grade. Buffer B: 100 ml stock solution + 100 ml H₂O HPLC grade + 800 ml Acetonitrile HPLC grade. All HPLC grade solvents were purchased from Fischer Chemicals.

t (min)	T (°C)	Flow (ml/min)	Buffer A (%)	Buffer B (%)
0	23°C	1,5	100	0
7	23°C	1,5	55	45
9	23°C	1,5	15	85
10	23°C	1,5	15	85
14	23°C	1,5	100	0
15	23°C	1,5	100	0

4.6.5. Folding procedure

Depending on the assay, different kinds of nanotubes were folded during this work. A schematic representation of the oligonucleotides composing the nanotubes is reported before each experiment description. Strands were mixed stoichiometrically and were subsequently added to 10 µl 10x TE buffer containing 200mM MgCl₂. Finally the folding mixture is completed with ddH₂O up to 100 µl. This premix was briefly mixed and folded using a thermocycler (MJ Mini, BioRad) with the cooling ramp showed in Figure 4. 21. The final concentration of the tube was 0.5µM.

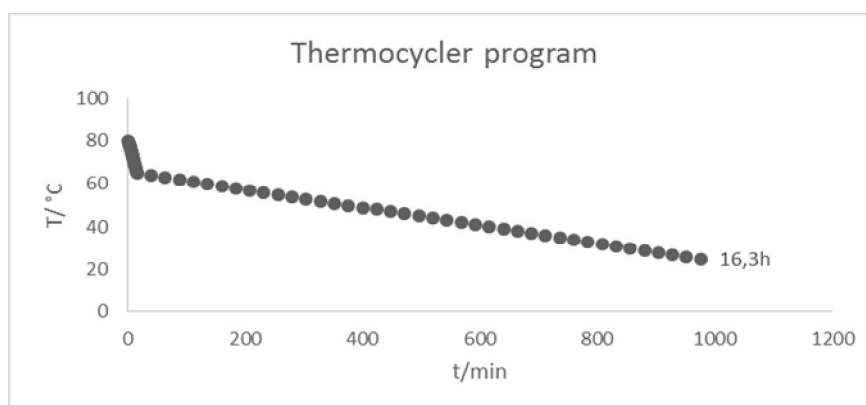


Figure 4. 21. Graphical diagram of the folding program used in this work. The folding program consist of a cooling ramp from 80°C to 65°C, with a decrement of 1° per minute and then from 64°C to 25°C with a decrement of 0.5°C each 12 minutes.

4.6.6. Gel detection limit

Table 4. 4. Schematic representation of the oligonucleotides composing nanotube used to determine the lower detection limit of TAMRA-labeled tube on agarose gel.

u-ODN1	u-ODN2	u-ODN3	u-ODN4
u-ODN5	u-ODN6	u-ODN7	u-ODN8
u-ODN9	u-ODN10	u-ODN11	u-ODN12
u-ODN13	u-ODN14	V4C3	u-ODN16
u-ODN17	u-ODN18	u-ODN19	u-ODN20
u-ODN21	u-ODN22	u-ODN23	u-ODN24

V4C3: ZGCATAGACATTTTAC^PGTAAAACCTTACGTAACCTACAGCCX

Where: Z = azide; X = C8-alkyne-dU; ^P = TAMRA labeled dT

4.6.7. Click Reaction

Chainmail formation: Following the supplier instructions, 40 μ l of the solution containing the folded nanostructure (0.5 μ M) were added to the heterogeneous catalyst pre-impregnated with 15 μ l of the water-soluble *Activator* included in the baseclick oligo labeling kit. The reaction mixture was gently mixed 32°C for 5 hours. The mixture was then transferred in a fresh vial and the heterogeneous catalyst discharged.

Body labeling: Following the suppliers instructions, 40 μ l of the solution containing the folded nanostructure (0.5 μ M) were added to the heterogeneous catalyst pre-impregnated with 15 μ l of the water-soluble *Activator* included into the kit. 1 μ l of 1 mM azide is added to the reaction mixture and gently mixed at 32°C for 5 hours. The mixture was then transferred in a fresh vial and the heterogeneous catalyst discharged.

Head labeling (click reaction on rc-ODN): The conditions of click reaction are valid for both rc-azido-ODN and rc-amino-ODN. Following the supplier instructions, 3 μ l of rc-ODN (0.5 μ M, 1.5 nmol) were added to the heterogeneous catalyst pre-impregnated with 10 μ l of the water-soluble *Activator* included into the kit. 7.5 μ l (75 pmol, 50 eq.) of 10 mM azide is added to the reaction mixture and gently mixed at 32°C for 3 hours. The mixture was then transferred in a fresh vial and the heterogeneous catalyst discharged. The mixture is purified from excess of unreacted azide via ethanol precipitation. Finally the concentration was set to 0.5 mM. The labeled-azido-rc-ODN was used as such for folding procedure. The labeled-amino-rc-ODN is reacted with an NHS-C3-azide linker in order to add an azide group to the oligonucleotide. Therefore 2 μ L (1nmol) labeled-rc-amino-ODN undergo esterification with 1000eq NHS-C3-azide in DMSO (5 μ L, 1000nmol). The reaction was carried out at room temperature mixing for 3 hours. The subsequent ethanol precipitation removed the unreacted linker. Finally the oligonucleotide concentration was set to 0.05mM and the resulting labeled-azido-rc-ODN used as such for folding of a nanotube.

One-pot click reaction: Following baseclick's instructions for the oligo labeling kit, 40 μ l of the solution containing the folded nanostructure (0.5 μ M) were added to the heterogeneous catalyst pre-

impregnated with 15 μl of the water-soluble *Activator* included into the kit. 1 μl (1 nmol, 50 eq.) of a 1 mM azide solution is added to the reaction mixture and gently mixed at 32°C for 5 hours. The mixture was then transferred in a fresh vial and the heterogeneous catalyst discharged.

4.6.8. Local alkyne/azide concentration

Table 4. 5. Schematic representation of the oligonucleotides composing the two kind of nanotubes used to determine the local concentration of alkyne within the click-tile.

A	u-ODN1	u-ODN2	u-ODN3	u-ODN4
	u-ODN5	u-ODN6	u-ODN7	u-ODN8
	u-ODN9	u-ODN10	u-ODN11	u-ODN12
	u-ODN13	u-ODN14	u-ODN15	u-ODN16
	u-ODN17	u-ODN18	u-ODN19	u-ODN20
	u-ODN21	u-ODN22	ct-ODN23	u-ODN24

B	u-ODN1	u-ODN2	u-ODN3	u-ODN4
	u-ODN5	u-ODN6	u-ODN7	u-ODN8
	u-ODN9	u-ODN10	u-ODN11	u-ODN12
	u-ODN13	u-ODN14	u-ODN15	u-ODN16
	ct-ODN17	u-ODN18	u-ODN19	u-ODN20
	u-ODN21	u-ODN22	u-ODN23	u-ODN24

20 μl of the solution containing the folded nanostructure (0.5 μM) were added to the heterogeneous catalyst pre-impregnated with 7.5 μl of the water-soluble *Activator* included into the kit. Increasing amount of TAMRA azide were added to the reaction mixture as listed in table 4. 6.

Table 4. 6. Amounts used in the assays for the determination of local alkyne/azide concentration of a click-tile.

Test	V nanotube	nmol tube	Eq TAMRA azide	V TAMRA azide	nmol TAMRA azide
1	20 μl	0,01 nmol	50 eq	0,5 μl (1mM)	0.5 nmol
2	20 μl	0,01 nmol	100 eq	1 μl (1mM)	1 nmol
3	20 μl	0,01 nmol	200 eq	2 μl (1mM)	2 nmol
4	20 μl	0,01 nmol	300 eq	3 μl (1mM)	3 nmol
5	20 μl	0,01 nmol	400 eq	4 μl (1mM)	4 nmol
6	20 μl	0,01 nmol	500 eq	0.5 μl (10mM)	5 nmol
7	20 μl	0,01 nmol	1000 eq	1 μl (10mM)	10 nmol

The reaction mixtures were gently mixed at 32°C for 5 hours. The mixture was then transferred in a fresh vial and the heterogeneous catalyst discharged.

4.6.9. Head labeling (incorporation of labeled rc-azido-ODN within the nanostructure)

Table 4. 7. Schematic representation of the oligonucleotides composing the nanotubes used to determine the incorporation of the labeled rc-azido-ODN.

3 eq labeled rc- azido-ODN + 3 eq con- ODN	hct-ODN1	ct-ODN2	ct-ODN3	ct-ODN4
	ct-ODN5	ct-ODN6	ct-ODN7	ct-ODN8
	hct-ODN2	ct-ODN10	ct-ODN11	ct-ODN12
	ct-ODN13	ct-ODN14	ct-ODN15	ct-ODN16
	hct-ODN3	ct-ODN18	ct-ODN19	ct-ODN20
	ct-ODN21	ct-ODN22	ct-ODN23	ct-ODN24

4.6.10. One-pot click reaction

Table 4. 8. Schematic representation of the oligonucleotides composing the nanotubes used for the one pot click reaction.

3 eq labeled rc- azido-ODN + 3 eq con- ODN	hct-ODN1	ct-ODN2	ct-ODN3	ct-ODN4
	ct-ODN5	ct-ODN6	bct-ODN1	ct-ODN8
	hct-ODN2	bct-ODN2	ct-ODN11	ct-ODN12
	ct-ODN13	ct-ODN14	bct-ODN3	ct-ODN16
	hct-ODN3	bct-ODN4	ct-ODN19	ct-ODN20
	ct-ODN21	ct-ODN22	bct-ODN5	ct-ODN24

4.6.11. Cell culture

In vitro experiments were performed thanks to baseclick's collaboration at the LMU physics department facilities of Prof. Tim Liedl and at the LMU chemistry department in the laboratories of Prof. Thomas Carell. Briefly, HeLa cells were cultured at 37°C, 5% CO₂ and 95% humidity in Dulbecco's modified Eagle's medium (DMEM) supplemented with 10% heat-inactivated fetal bovine serum (FBS), 2 mM L-glutamine, 100 U/ml penicillin and 100 µg/ml streptomycin. The cells were seeded on 24-well plates (Sarsted) or 8-wells plates (ibidi) and allowed to adhere overnight. After incubation with DNA nanostructures cell were stained with Hoechst in order to identify nuclei.

4.6.12. Nanostructure incubation

The incubation of the nanotubes was done at 37°C by diluting the starting solution of the nanostructures to a final concentration of 50 nM DNA nanostructure in cell culture medium. Different incubation times were tested. After the treatment, medium containing the nanotube was removed and the cells were washed with PBS. Imaging was carried out using a fluorescence microscope (Nikon) and confocal microscope (Zeiss). The images were optimized and merged using the software ImageJ.

4.6.13. Cell proliferation assay

The EdU proliferation assay (baseclick) was carried out following the supplier's user manual. EdU stock solution (2x) was diluted (1x) with the incubation medium, namely cell culture medium already containing the labeled DNA nanotubes. After 2 hours, the incubation medium was removed and cells were washed with PBS. Fixation, permeabilization and click reaction were executed in accordance to the provided user manual. The click reaction was performed using either FAM azide (Abs: 496 nm; Em: 516 nm) or Eterneon-Red azide (Abs: 643 nm; Em: 662 nm). Detection of proliferated cells was carried out using a fluorescence microscope (Nikon) and confocal microscope (Zeiss). The images shown above were optimized and merged using the software ImageJ.

4.7. Appendix

Oligo sequences and their nomenclature used in the text:

Table 4. 9. Unmodified oligonucleotides (u-ODNs) used in this work

unmodified oligonucleotide (u-ODNXX)	Sequence
u-ODN1	AAA ACGCTAAGCCA CCTTTAGATCC AAAT
u-ODN2	GGTCGTGCGG ACTGTGGAACA CCAACGATGCC TGATAGAAGT
u-ODN3	GCGTGGCAAT AGCCATAAATT CATAATAACG GCGCCAGACT
u-ODN4	TTTCAAGACC AGCACTTGTAT GGCCTAGGGCG GGTTTAGCGT
u-ODN5	GGATCTAAAGG ACTTCTATCA AAGACGGGAC GACTCCGGGAT
u-ODN6	GGCATCGTTGG AGTCTGGCGC ACGACTTCGA TTTCGGATCCT
u-ODN7	CGTTATGTATG ACGCTAAACC TTGCAATGAC TGAAGTCAAT
u-ODN8	CGCCCTACGCC AAA AAA GATGGGAGCTT
u-ODN9	AAA ATCCCGGAGTC CGCTGCTGATC AAAT
u-ODN10	GTCCCGTCTT AGGATCCGAAA GCCATAATATA TCGAGACGGT
u-ODN11	TCGAAGTCGT ATTCGAGTTCA AATGTCTATGC GATGCAGCAT
u-ODN12	GTCATTGCAA AAGCTCCATC ATTTAATGTGC TTTACAGTAT
u-ODN13	GATCAGCAGCG ACCGTCTCGA CTGCAGAAAT AGGACCCCAT
u-ODN14	TATATTATGGC ATGCTGCATC TTCCTGGCAT GGCTGAATTCT
u-ODN15	GCATAGACATT ATACTGTAAA ACCTTACGTA ACTTACAGCCT
u-ODN16	CGACATTAAAT AAA AAA GATGAGTATTT
u-ODN17	AAA ATGGGGTCTT CGAGGCGAAAC AAAT
u-ODN18	ATTTCTGCAG AGAATTCAGCC TATTCACATAG GCGAAGGCTT
u-ODN19	ATGCCAGGAA AGGCTGTAAGT TGCATCATGGG GGTCCTCAAT
u-ODN20	TACGTAAGGT AAATACTCATC CCTGAGTGATC CATGACCCTT
u-ODN21	GTTTCGCCTCG AAGCCTTCGC CCGCACGACC TGGCTTAGCGT
u-ODN22	CTATGTGAATA ATTGAGGACC ATTGCCACGC TGTTGACAGT
u-ODN23	CCCATGATGCA AAGGGTCATG GGTCTTGAAA AATTTATGGCT
u-ODN24	GATCACTCAGG AAA AAA ATACAAGTGCT

Table 4. 10. Click-tiles (ct-ODNs) used in this work

click tile (ct-ODNXX)	Sequence
ct-ODN1	ZAAA ACGCTAAGCCA CCTTTAGATCC AAAX
ct-ODN2	ZGGTCGTGCGG ACTGTGGAACA CCAACGATGCC TGATAGAAGX
ct-ODN3	ZGCGTGGCAAT AGCCATAAATT CATAATAACG GCGCCAGACX
ct-ODN4	ZTTTCAAGACC AGCACTTGTAT GGCCTAGGGCG GGTTTAGCGX
ct-ODN5	ZGGATCTAAAGG ACTTCTATCA AAGACGGGAC GACTCCGGGAX
ct-ODN6	ZGGCATCGTTGG AGTCTGGCGC ACGACTTCGA TTTCGGATCCX
ct-ODN7	ZCGTTATGTATG ACGCTAAACC TTGCAATGAC TGAAGTCAAX
ct-ODN8	ZCGCCCTACGCC AAA AAA GATGGGAGCTX
ct-ODN9	ZAAA ATCCCGGAGTC CGCTGCTGATC AAAX
ct-ODN10	ZGTCCCGTCTT AGGATCCGAAA GCCATAATATA TCGAGACGGX

ct-ODN11	ZTCGAAGTCGT ATTCGAGTTCA AATGTCTATGC GATGCAGCAX
ct-ODN12	ZGTCATTGCAA AAGCTCCCATC ATTTAATGTCG TTTACAGTAX
ct-ODN13	ZGATCAGCAGCG ACCGTCTCGA CTGCAGAAAT AGGACCCCCAX
ct-ODN14	ZTATATTATGGC ATGCTGCATC TTCCTGGCAT GGCTGAATTCX
ct-ODN15	ZGCATAGACATT ATACTGTAAA ACCTTACGTA ACTTACAGCCX
ct-ODN16	ZCGACATTAAAT AAA AAA GATGAGTATTX
ct-ODN17	ZAAA ATGGGGGTCCT CGAGGCCGAAAC AAAX
ct-ODN18	ZATTTCTGCAG AGAATTCAGCC TATTCACATAG GCGAAGGCTX
ct-ODN19	ZATGCCAGGAA AGGCTGTAAGT TGCATCATGGG GGTCTCAAX
ct-ODN20	ZTACGTAAGGT AAATACTCATC CCTGAGTGATC CATGACCCTX
ct-ODN21	ZGTTTCGCCTCG AAGCCTTCGC CCGCACGACC TGGCTTAGCGX
ct-ODN22	ZCTATGTGAATA ATTGAGGACC ATTGCCACGC TGTTGACAGX
ct-ODN23	ZCCCATGATGCA AAGGGTCATG GGTCTTGAAA AATTTATGGCX
ct-ODN24	ZGATCACTCAGG AAA AAA ATACAAGTGCX

Where X is C8-Alkyne dU; Z is C11-Azide linker

Table 4. 11. Body functional click tiles (bct-ODNs) used in this work

body (functional) click tile (bct-ODNXX)	Sequence
bct-ODN1	ZCG TTA XGT ATG ACG CTA AAC CTT GCA ATG ACT GAA CTC GAA X
bct-ODN2	ZGT CCC GTC TTA GGA TCC GAA AGC CAX AAT ATA TCG AGA CGG X
bct-ODN3	ZGC ATA GAC ATT ATA CXG TAA AAC CTT ACG TAA CTT ACA GCC X
bct-ODN4	ZAT TTC XGC AGA GAA TTC AGC CTA TTC ACA TAG GCG AAG GCT X
bct-ODN5	ZCC CAT GAT GCA AAG GGT CAT GGG TCT TGA AAA ATT TAX GGC X

Where X is C8-Alkyne dU; Z is C11-Azide linker

Table 4. 12. Head functional click tiles (hct-ODNs) used in this work

head (functional) click tile (hct-ODNXX)	Sequence
hct-ODN1	ZAA AAC GCT AAG CCA CCT TXA GAT CCA AXC AGA TAC TCG GX
hct-ODN2	ZAA AAT CCC GGA GTC CGC TGC TGA TCA AXC AGA TAC TCG GX
hct-ODN3	ZAA AAT GGG GGT CCT CGA GGC GAA ACA AXC AGA TAC TCG GX

Where X is C8-Alkyne dU; Z is C11-Azide linker

Table 4. 13. Reporter oligonucleotides (rc-ODN) used in this work

Reporter click oligonucleotide (rc-ODN)	Sequence
rc-amino-ODN	LTA TGC GCT CTT X
rc-azido-ODN	ZTA TGC GCT CTT X

Where X is C8-Alkyne dU; L is C6-Amino Linker; Z is C11-Azide linker

Table 4. 14. Connection oligonucleotides (con-ODNs) used in this work.

Connector (con-ODN)	Sequence
con-ODN1	AAA GAG CGC ATA ACC GAG TAT CTG
con-ODN2	AAA GAG CGC ATA AAC CGA GTA TCT G
con-ODN3	AAA GAG CGC ATA AAA CCG AGT ATC TG
con-ODN4	AAA GAG CGC ATA AAA ACC GAG TAT CTG

Table 4. 15. Body functional alkyne tiles (bat-ODNs) used in this work.

body (functional) Alkyne tile (bat-ODN)	Sequence
bat-ODN1	CGT TAX GTA TGC CGC TAA ACC TTG CAA
bat-ODN2	GTC CCG TCT TTG GAT CCG AAA GCC AXA ATA TAT CGA GAC GGG
bat-ODN3	ATA CXG TAA AAC CTT ACG TA
bat-ODN4	ATT TCX GCA GGG AAT TCA GCC TAT TCA CAT AGG CGA A
bat-ODN5	AAG GGT CAT GGG TCT TGA AAA ATT TAX GGC A

Where X is C8-Alkyne dU;

Table 4. 16. Unmodified sequences filling the gaps left from shortened oligonucleotides (ubat-ODNs) used in this work.

unmodified sequences filling for body (functional) Alkyne tile (ubat-ODNXX)	Sequence
ubat-ODN1	TGA CTG AAC TCG AAC
ubat-ODN3a	GCA TAG ACA TT
ubat-ODN3b	ACT TAC AGC CA
ubat-ODN4	GGC TA
ubat-ODN5	ACG TAG TAC CC

5. Fluorescent labelling of *in situ* hybridisation probes through the copper-catalysed azide-alkyne cycloaddition reaction

5.1. Introduction

Chromosomal abnormalities responsible of diseases and tumors are efficiently investigated by fluorescence *in situ* hybridization (FISH) techniques. Fluorescent labeling of probes can be achieved by several approaches, among which Nick Translation is one of the most used. However, this approach is not suited for labeling of short and single-stranded probes required in particular FISH applications.¹¹⁷ In the presented work copper(I)-catalyzed azide-alkyne cycloaddition (CuAAC), also defined as click chemistry, is presented as an alternative oligo labeling method for preparation of FISH probes. Click chemistry yielded successful labeled short single-stranded oligonucleotides as well as long double-stranded PCR fragments which were tested in FISH experiment on plant chromosomes and nuclei. Moreover, this labeling strategy was demonstrated to be compatible with other cytological techniques such as immunohistochemistry (IHC) and 5-ethynyl-deoxyuridine-based cell proliferation assays.

5.2. Fluorescence *in situ* Hybridization (FISH)

Fluorescence *in situ* hybridization is a cytogenetic analytic technique allowing the detection and eventually determine the position of specific DNA sequences on chromosomes. Probes, which have complementary sequences to specific genomic regions, are used to find homologous sequences and form a double strand (hybridization). In general, *in situ* hybridization techniques are used in medical diagnostic field, where those methodologies are applied for detection of genetic abnormalities such as gene fusion, aneuploidy, loss of a chromosomal region or of the entire chromosome and for identification of oncogenes.

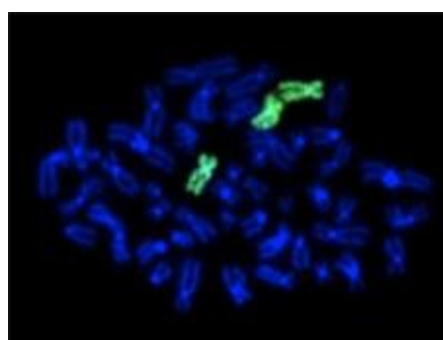


Figure 5. 1. Fluorescence *in situ* hybridization (FISH) analysis on chromosomes from a patient affected by trisomy 10. The green chromosomes are the three copies of chromosome 10. Source: <http://www.swissperinatalinstitute.com>

Earlier, identification of abnormalities in chromosomes, such as deletions, depletion, duplications or translocations was achieved by banding techniques.¹²⁰ Whereas the resolution of this method is in the range of 5×10^6 base pairs, some chromosomal aberrations are too small or complex to be detected with this technique. Therefore the more sensitive and refined *in situ* hybridization (ISH) method was developed. In 1969 two independent research groups published their results about *in situ* hybridization.¹¹⁸ In their works radioactively labeled probes were used and hybridization was visualized after autoradiographic exposure. Rapidly, radioactive labels were replaced by safer fluorescent probes developing Fluorescent *in situ* Hybridization (FISH) method.¹¹⁹ Through the years, the sensitivity of this technique was increased by simultaneous development of the optical systems and use of more effective detection methods such as antibodies, fluorochromes and colloidal gold nanoparticles¹²⁰ among others. Higher resolution in the detection of chromosomal regions was recently demonstrated using Oligo-PAINT probes.⁶⁷ The authors reported the visualization of single copy genes was achieved using single-molecule super-resolution methodologies, lowering the resolution limit to 5 kilobases (kb), an order of magnitude than the one achieved with standard FISH protocols.

Conceptually, FISH is a very straightforward technique that is based on probes hybridization to their complementary sequences on chromosomes previously fixed on a microscope slide. If the probe contains already fluorescent tags, the hybridization sites can be directly detected via fluorescence microscope analysis. In the case where the probes contains haptens, a subsequent fluorescent labeling step is required before microscope imaging.

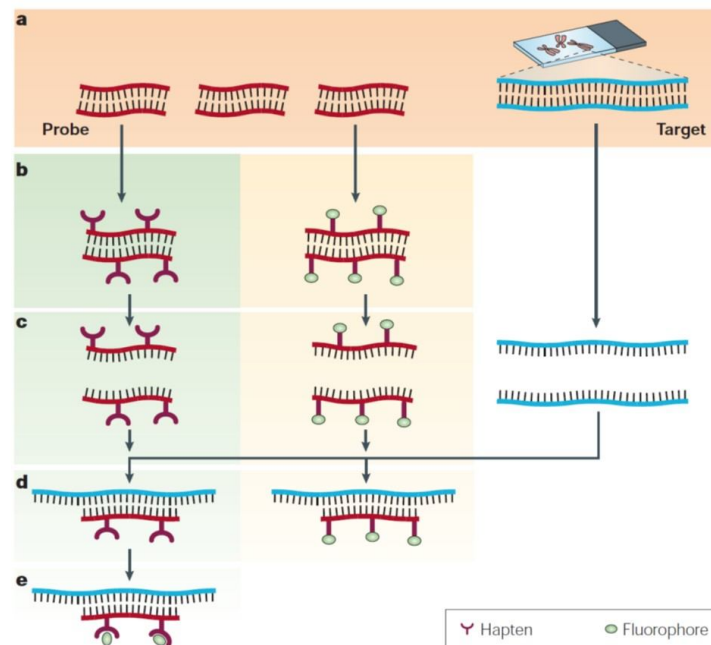


Figure 5. 2. Graphical representation of fluorescence in situ hybridization (FISH) procedure. A) DNA probe (red) and target DNA (blue) are the basic elements needed for FISH. B) Labeling of the probes. Left: indirect labeling. Right: direct labeling. C) Probes and Target DNA denaturation D) Hybridization E) Labeling of hybridized probes bearing haptens. Adapted from “The new cytogenetics: blurring the boundaries with molecular biology” M. R. Speicher, N. P. Carter, *Nat Rev Genet*, **2005**, 6 (10), 782-792.

The targets of FISH probes are mRNA and nuclear DNA of either interphase or metaphase chromosomes. FISH analysis on DNA can be performed on chromosomes fixed on a glass slide but also directly on bone marrow, blood smears or fixed and sectioned tissues.

As stated in the methodology name, FISH concerns the use of fluorescently labeled probes for identification of specific sequences within a target. Fluorophores can be incorporated in probes by conjugation with the nucleic acid¹¹⁹, or by connection of the nucleic acid with non-fluorescent molecules – haptens or biotin – that bind fluorescent moieties after hybridization.¹²¹ The former method is defined as “direct labeling”, while the latter is named “indirect labeling”. After hybridization of the target with non-fluorescent probes, the sample is treated with fluorophore-labeled antibody or avidin enabling the probes to become fluorescent. The indirect labeling procedure, compared to the direct labeling, is more time-consuming as it consists of a step more and the introduction of fluorescent antibodies can give background signal. On the other hand, in the indirect labeling multiple fluorophore association on the same molecule is possible enabling a more intense signal. Furthermore, increase of the intensity of fluorophores can be achieved also by “sandwiching”, namely additional round of fluorescent antibodies labeling. Alternatively the fluorescence can be increased using enzymes conjugates of avidin or antibodies.¹²² These enzymes catalyze reactions which result in fluorescent products remaining localized near the hybridization site.

The type of probe need to be chosen in relation to the target and the application of the FISH assay. “Chromosome-painting” is a technique that implies the use of fluorescently labeled probes, which are chromosome-specific. Hybridization of these probes allows detection of individual chromosomes in metaphase or interphase and eventual identification of numeric or structural aberrations. The “painting” of a whole chromosome is achieved with complex DNA probes derived from single chromosomes, amplified and labeled. Repetitive sequences are another type of FISH probes specifically hybridizing to chromosomal regions containing short sequences repeated many times. Those chromosomal portions are present in the center (centromeres) or at each end (telomers) of the chromosomes and are important marker for disease detection. For example, FISH centromeric probes specific for chromosome 8 are used for detection of trisomy in patients affected by myelodysplastic syndrome or acute myeloid leukemia¹²³. Human telomers, instead, are six-nucleotide G-rich sequences (TTAGGG) repeated about 2500 times and have the fundamental function to protect the chromosome from deterioration or fusion with neighboring chromosomes.¹²⁴ They gained increasing interest as many studies proved telomers involvement in tumorigenesis and aging processes. A third type of FISH probes are locus-specific probes, which are particularly useful for identification of translocation, inversion or deletions in specific chromosomal regions.¹²⁵ Their size can vary from 1 kb to 1 Mb depending from the nature of their cloning vector.

Labeling of DNA FISH probes can be achieved by different approaches such as Nick translation, random priming, PCR or end labeling. Nick translation is a method that allows the incorporation of labeled nucleotides within a DNA fragment by the activity of two enzymes, namely deoxyribonuclease I (DNase I) and DNA polymerase I.¹²⁶ DNase I creates nicks in the DNA originating a free 3' hydroxyl groups where DNA polymerase I adds fluorescent nucleotides. The resulting labeled product is a pool of dsDNA strands, therefore denaturation is required before hybridization with the target. Random priming is a labeling technique based on the use of small random oligonucleotides (hexamers, octamers or nonamers) as primers for the synthesis of labeled DNA fragments. These primers anneal to a denature DNA fragment and by means of the Klenow enzyme labeled nucleotides are incorporated in the new strands.

Polymerase chain reaction (PCR) is mostly used for generation of labeled versions of entire chromosomal DNA. In particular, degenerated oligonucleotides-primer PCR (DOP-PCR) enable efficient amplification of the DNA of interest using as template flow-sorted, microdissected or isolated yeast artificial (YAC) chromosomes. End labeling or tailing is a procedure allowing selective functionalization of 5' or 3' termini of the probe. At the 5' end the enzyme T4 Polynucleotide Kinase (T4 PNK) adds a phosphate group which can be conjugated with aliphatic linkers for further functionalization with fluorescent labels or haptens¹²⁷. Labeling of 3' end occurs using Terminal Deoxynucleotidyl Transferase (TdT), enzyme which catalyzes addition of labeled triphosphates.¹²⁸ When dideoxynucleotide triphosphates are used for labeling only a single nucleotide is added to the 3' terminus since the nucleotide has no OH groups on the 3' position of the sugar residue and therefore a further nucleotide cannot be attached. Conversely the use of deoxynucleotides triphosphates enables the addition of multiple nucleotides at the 3' end.

Nowadays the great number of available *in situ* hybridization procedures enables a deep understanding of chromosomal organization and modifications. Continuous improvement in the field of fluorescence microscopy, digital imaging and bioinformatics contributes to the constantly development of new FISH protocols for diversify applications. Furthermore, probes labeling is a crucial aspect to consider and to further improve in order to obtain an increased assays sensitivity. Click chemistry is a reliable method for conjugation of fluorescent tags on nucleic acids and therefore can be adopted as an efficient method for FISH probes preparation.

5.3. Abstract of the publication “Fluorescent labelling of *in situ* hybridisation probes through the copper-catalysed azide-alkyne cycloaddition reaction”

In situ hybridisation is a powerful tool to investigate the genome and chromosome architecture. Nick translation (NT) is widely used to label DNA probes for fluorescence *in situ* hybridisation (FISH). However, NT is limited to the use of long double-stranded DNA and does not allow the labelling of single-stranded and short DNA, e.g. oligonucleotides. An alternative technique is the copper (I)-catalysed azide-alkyne cycloaddition (CuAAC), at which azide and alkyne functional groups react in a multistep process catalysed by copper (I) ions to give 1,4-distributed 1, 2, 3-triazoles at a high yield. We successfully applied this technique to label short single stranded DNA probes as well as long PCR-derived double stranded probes and tested them by FISH on plant chromosomes and nuclei. The hybridisation efficiency of differently labelled probes was compared to those obtained by conventional labelling techniques. We show that copper (I)-catalysed azide-alkyne cycloaddition-labelled probes are reliable tools to detect different types of repetitive sequences on chromosomes opening new promising routes for the detection of single copy gene. Moreover, a combination of FISH using such probes with other techniques, e.g. immunohistochemistry (IHC) and cell proliferation assays using 5-Ethynyl-deoxyuridine is herein shown to be easily feasible.

5.4. Author's contribution

The author contributes for *pre-click* probes labeling *via* click chemistry and probes characterization by HPLC and MALDI-TOF spectrometry.

5.5. Associate Publication

Fluorescent labelling of in situ hybridisation probes through the copper-catalysed azide-alkyne cycloaddition reaction

Published in: Hesse S., Manetto A., Cassinelli V., Fuchs J., Ma L., Raddaoui N., Houben A., *Chromosome Research* **2016**, 1-9.

5.5.1. Introduction

In situ hybridisation using fluorescence-based detection is a powerful tool to physically map high- and single-copy sequences. Initially, the detection of hybridised sequences was possible only by using radioisotopic labels and autoradiography. Nowadays, two approaches, i.e. direct and indirect labelling, are widely used for fluorescent labelling of specific target sequences. The direct labelling is carried out by the use of DNA probes possessing fluorochrome-conjugated dNTPs for hybridisation (Wiegant, Ried et al. 1991). Indirect labelling implies the use of non-fluorescent modified nucleotides, which are detected fluorescent later, e.g., by fluorochrome conjugated antibodies (Kelly, Kornis et al. 1970, Pinkel, Gray et al. 1986, Pinkel, Straume et al. 1986).

For labelling of DNA probes for fluorescence *in situ* hybridisation (FISH) Nick translation, random-primed labelling and PCR can be used. The most feasible approach is the widely used nick translation (Rigby, Dieckmann et al. 1977). However, nick translation requires double-stranded template DNA and therefore does not allow labelling of single-stranded and/or short probes like oligonucleotides (Kelly, Cozzarelli et al. 1970). Moreover, the efficiency of nick translation labelling strongly depends on DNase I activity and the type of modified deoxynucleotides (Rigby, Dieckmann et al. 1977).

Here, we tested an alternative technique to label double and single stranded DNA probes by use of the Cu(I)-catalysed azide-alkyne cycloaddition (CuAAC) for its suitability for FISH. CuAAC, which is based on a classical Huisgen 1,3-dipolar cycloaddition, probably represents the best example of so called click-chemistry reactions (Kolb, Finn et al. 2001). In presence of copper(I) azide and alkyne functional groups react 107 to 108 time faster compared to the uncatalysed 1,3-dipolar cycloaddition leading only to 1,4-distributed 1,2,3-triazoles at a high yield (Fig. 5. 3A) (Rostovtsev, Green et al. 2002, Tornøe, Christensen et al. 2002). This technique benefits from a simple setup of the reaction conditions and neither interacts with nor interferes with a biological system (high bioorthogonality (Sletten and Bertozzi 2011)). Thereby – among several other applications - the bioconjugation (formation of complexes by covalently linking functional molecules to molecules of biological origin) of complex biomolecules such as nucleic acids is enabled (Rozkiewicz, Gierlich et al. 2007, Gramlich, Wirges et al. 2008, Salic and Mitchison 2008). For FISH probe preparation, alkyne-bearing deoxynucleotides are first incorporated into the DNA strand either enzymatically (e.g. PCR) or via oligonucleotide solid phase synthesis. In a second step, fluorochrome-coupled azides are used to label alkyne-bearing DNA probes either before hybridisation for direct labelling, or after hybridisation for indirect labelling via a CuAAC reaction (Fig. 5. 3B). Here, we show that CuAAC-labeled probes are a reliable tool to detect different types of repetitive sequences on plant chromosomes. Moreover, we found that this technique is combinable with immunohistochemistry and cell proliferation assays using labelling of replication via 5-Ethynyl-deoxyuridine (EdU).

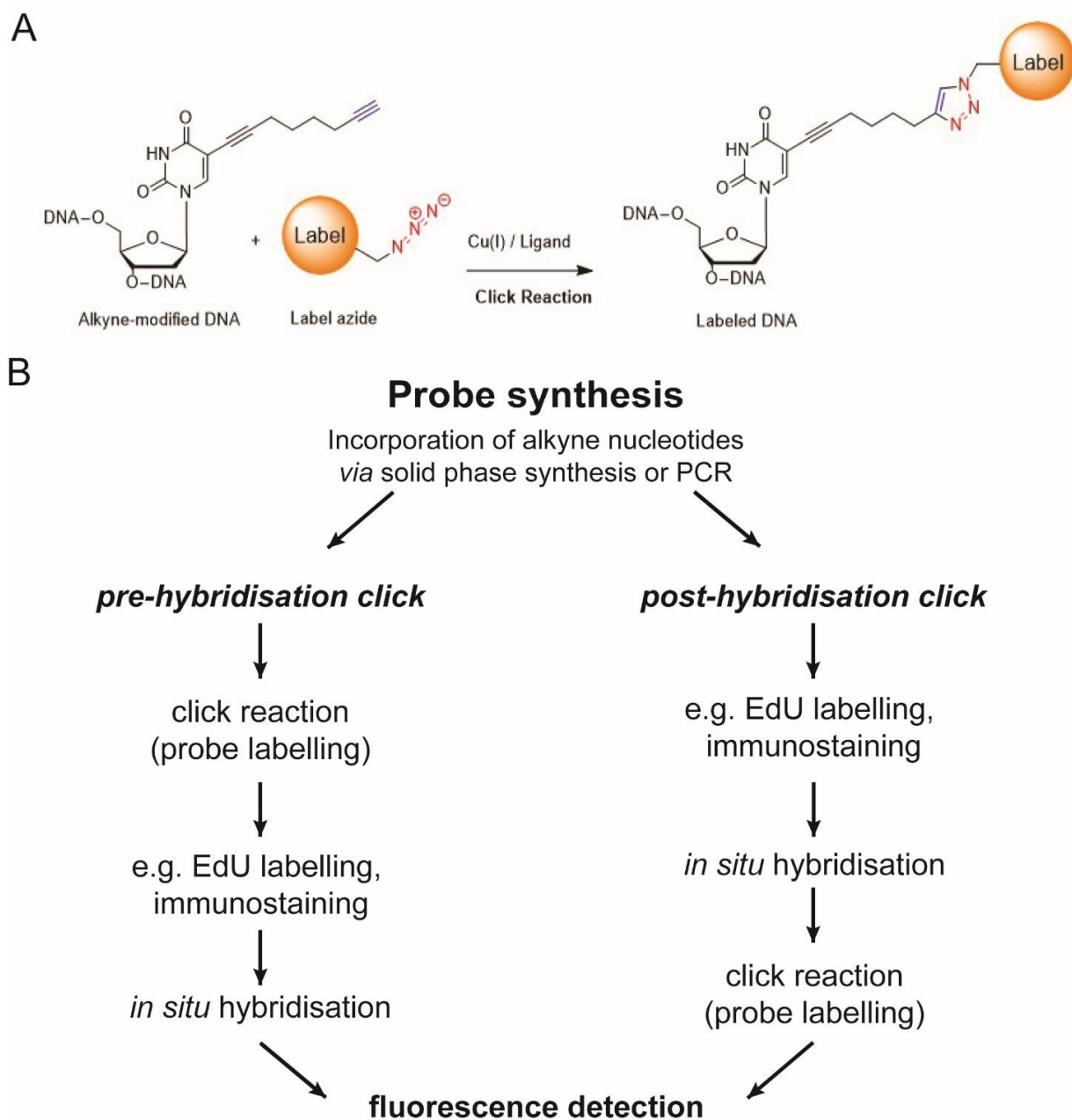


Figure 5. 3. The CuAAC reaction can be used to functionalise alkyne-modified DNA nucleobases. (A) The CuAAC is a Huisgen 1,3-dipolar cycloaddition where alkyne-labelled DNA (blue) and azide-coupled dyes (red) react to provide labelled DNA fluorescence *in situ* hybridisation (FISH) probes. This reaction is catalysed by Copper (I) ions, which are stabilised by polytriazole ligands. (B) Possible applications of click chemistry for FISH by pre- or post-hybridisation click reaction labelling in combination with immunostaining or EdU labelling.

5.5.2. Material and methods

5.5.2.1. Plants materials

Rye (*Secale cereale* L. cv. Petkuser Sommerroggen), barley (*Hordeum vulgare* L. cv. Morex and Emir), and hexaploid wheat (*Triticum aestivum* L. cv. Kanzler) were grown at green house conditions (16h light, 22°C day/16°C night). *Arabidopsis thaliana* ecotypes Pro-0 (Proaza, Asturias) : (ID no. 8213, (Fulcher, Teubenbacher et al. 2015)), and Hov1-10: 1065 bp ((ID no. 6035) (ID no. 6035)) were grown until rosette stage at short day (8h light, 21°C) afterwards at long day conditions (16h light, 21°C) at green houses.

5.5.2.2. Preparation of mitotic chromosomes for FISH

Rye, wheat and barley seeds were etiolated for 2-3 days. Root tips were cut, synchronised overnight in ice-cold water, fixed in 3:1 ethanol/glacial acid (Carl Roth, cat. no. 9165, Merck, cat. no. 100066, respectively) and kept at -20°C until use. For mitotic chromosome preparation, root tips were washed in ice-cold water and digested (50-60 min, 37°C) in an enzyme cocktail (1% cellulose (Calbichem, cat. no. 219466), 1% pectolyase Y-23 (Sigma-Aldrich, cat. no. P3026), 1% cytohelicase (Sigma-Aldrich, cat. no. C8274) in citrate buffer (0.01 M tri-Sodium citrate dihydrate (Carl Roth, cat. no. 4088) and 0.01 M citric acid (Carl Roth, cat. no. 6490); pH 4.5-4.8)). Afterwards, root tips were washed in 0.01 M citrate buffer and ice-cold ethanol consecutively. For preparation of mitotic chromosome spreads, the root tips were transferred to glacial acid/ethanol 3:1 (200 µl/25 root tips) and were disrupted with a dissection needle. 8 µl of this mitotic cell suspension was dropped on glass slides placed on ice, air-dried and stored in 100% ethanol at 4°C (Aliyeva-Schnorr, Ma et al. 2015). *A. thaliana* slide preparation was performed according to Armstrong et al. (1998) with minor modifications (Armstrong, Fransz et al. 1998). Flower buds were fixed in ethanol/glacial acid (3:1), washed and digested in an enzyme cocktail (0.07% cellulase, 0.1% pectolyase, 0.1% cytohelicase in 0.01 M citric buffer). After washing, flower buds were disrupted on a slide in 10 µl of 60% acetic acid and placed on a hot plate (43°C, 1min). The cell suspension was covered with fixative and air-dried. For FISH, *A. thaliana* slides were treated with pepsin (2 min, 38°C; 0.05 mg/ml; Sigma-Aldrich, cat. no. 10108057001), washed and fixed (10 min, RT, 4% formaldehyde (Carl Roth, cat. no. 4979)). After washing and dehydration in ethanol, the slides were used for FISH.

5.5.2.3. Preparation and sorting of isolated nuclei

Isolation of nuclei was performed according to Doležel, Binarova et al. (1989) with slight modifications (Doležel, Binarova et al. 1989). ~0.1 g leave material was fixed in 4% formaldehyde in Tris buffer (10 mM Tris (Carl Roth, cat. no. 5429); 10 mM Na₂EDTA (Carl Roth, cat. no. 8043); 100 mM NaCl (Carl Roth, cat. no. 9265); 0.1% Triton X-100 (AppliChem, cat. no. A 1388); pH 7.5) on ice for 20 minutes in a centrifugal vacuum concentrator (Eppendorf, model 5301). After two times washes in Tris buffer on ice, the leaves were chopped in 1 ml isolation buffer (15 mM Tris; 2 mM Na₂EDTA; 0.5 mM Spermine tetrahydrochloride (Serva); 80 mM KCl (Carl Roth, cat. no. 6781); 20 mM NaCl; 15 mM β -mercaptoethanol (Carl Roth, cat. no. 4227); 0.1% Triton X-100; pH 7.5). The resulting suspension was

filtered in a 5 ml polystyrene round-bottom tube with 35 µm cell strainer snap cap (Falcon, product # 352235). Nuclei were stained with 1.5 µg/ml 4',6-diamidino-2-phenylindole (DAPI; Thermo Fischer, cat. no. 1306) and flow-sorted into Eppendorf tubes using a BD FACS Aria II (BD Biosciences). For barley 2C nuclei and for *A. thaliana* ecotype Pro-0 and Hov1-10 endopolyploid 4C nuclei were collected. Equal amounts of sucrose solution (40% sucrose (Carl Roth, cat. no. 4621) in Tris buffer; pH 7.5) and flow-sorted nuclei (approx. 450 nuclei/µl) were pipetted on glass slides, gently mixed, air-dried overnight and kept at -20°C.

5.5.2.4. FISH probe preparation

Arabidopsis-type telomeric and microsatellite alkyne-bearing oligonucleotides (Table 5. 1) were synthesised using an ABI 394 DNA/RNA Synthesiser (Applied Biosystems) and C8-Alkyne-dU phosphoramidites at baseclick GmbH (Neuried, Germany). The subsequent click reaction was performed using the OligoClick labelling Kit (cat. no. BCK-FISH, baseclick GmbH) according to provided manual. Alkyne-bearing oligonucleotides and fluorescent labelled oligonucleotides were analysed using RP-HPLC (Waters) equipped with a photodiode array detector (Waters) and a reversed phase column (XBridge OST C18, 4.6 mm x 50 mm, Waters) using a gradient method (from 45% to 85% acetonitrile buffer). Correct masses were measured with an Auto-Flex II MALDI-TOF (Brucker Daltonics).

Probes for detection of the rye centromeric retrotransposon Bilby (Francki 2001) were generated by PCR from pSC-A vector containing a 583 bp fragment of Bilby using the PCR Labelling Kit (cat. no. PCR-Click 555, baseclick GmbH) according to the manual. Sequences TTTGCGACAATGACTCAAGC and TGTAGCTCATCGTGGAGTCG were used as forward and reverse primers, respectively. Annealing temperature was 58°C. In the triphosphate solution (dATP, dCTP, dGTP, dTTP), dTTP was substituted to 100% by C8-Alkyne-dUTP (baseclick GmbH). PCR products were purified using QIAQuick PCR purification Kit (Qiagen). The 5'-labelled *Arabidopsis*-type telomere probe (CCCTAAA)₄ was produced by Eurofins Genomics (Ebersberg, Germany). Nick translation labelled telomere probes were produced via PCR according to Ijdo et al. (Ijdo, Wells et al. 1991) with minor changes. PCR was accomplished using primers (CCCTAA)₃ and (TTAGGG)₃ without template (Eurofins Genomics) and Taq DNA polymerase (Qiagen, cat. no. 201207). Annealing temperature was 60°C. Nick translation was performed using a NT Labelling Kit (Jena Bioscience GmbH, Jena Germany) according to the manual with the following triphosphates 0.5 mM dATP, 0.5 mM dCTP, 0.5 mM dGTP, 0.25 mM dTTP and 0.25 mM Aminoallyl-dUTP-5/6-TAMRA (Jena Bioscience GmbH).

Table 5. 1. Synthesised alkyne-modified FISH probes

Name	Sequence (label position underlined)
4PTel4	CCC <u>I</u> AA ACC C <u>I</u> AAAC CC <u>I</u> AAA CCC <u>I</u> AA A
4PTel2	CCC <u>I</u> AA ACC CTAAAC CC <u>I</u> AAA CCC TAA A
3PTel3	CCC <u>I</u> AA ACC C <u>I</u> AAAC CC <u>I</u> AAA
3PTel2	CCC <u>I</u> AA ACC CTAAAC CC <u>I</u> AAA
CTT	CTT C <u>I</u> T CTT CTT C <u>I</u> T CTT CTT C<u>I</u>T CTT CTT

Underlined letters stand for the alkyne-modified bases (C8-Alkyne-dU)

5.5.2.5. Fluorescence *in situ* hybridisation using pre- or post-hybridisation click probes

Selected preparations of mitotic chromosomes were post-fixed (4% formaldehyde in 2x SSC (300 mM NaCl; 30 mM tri-sodium citrate dehydrate, pH 7.0); 10 min/RT) and washed in 2x SSC. After dehydration (70%, 90%, 100% ethanol) slides were air-dried. Denaturation was performed on a heating plate (80°C/2 min). Hybridisation was done in a moisture chamber (37°C/overnight). Alkyne-labelled or fluorochrome-labelled probes in DS 20 (20% dextran sulfate (Sigma-Aldrich, cat. no. D 8906), 50% deionised formamide (Sigma-Aldrich, cat. No. 4767), 300 mM NaCl, 30 mM tri-sodium citrate dehydrate, 50 mM phosphate buffer, pH 7.0) were used for post- and pre- hybridisation, respectively. Washed slides were mounted in Vectashield (Vector Laboratories, cat. no. H1000) containing DAPI (10 ng/μl; Thermo Fischer, cat. no. D1306).

5.5.2.6. Combined EdU-based DNA replication analysis and FISH using pre-clicked probes

Germinated seeds were grown for 2h in darkness on filter paper (Macherey Nagel, cat. no. MN616) soaked with 15 μM 5-Ethynyl-deoxyuridine (BCK-EdU555, baseclick GmbH, Neuried) and afterwards placed for 2.5h on deionised water only. Root tips were cut and mitotic metaphases were accumulated by treatment with ice-cold water overnight. Mitotic slides were prepared as described above. To detect 5-ethynyl-deoxyuridine, the CuAAC reaction using 5-TAMRA-Azide was performed according to manufacturer's protocol (BCK-EdU555, baseclick GmbH). After washing, slides were dehydrated in ethanol and used for FISH with pre-hybridisation CuAAC probes as described above.

5.5.2.7. Combined immunohistochemistry and hybridisation of pre-hybridisation CuAAC labelled FISH probes

Root tips were fixed (4% paraformaldehyde in 1x PBS (137 mM NaCl, 2.7 mM KCl; 10 mM Na₂HPO₄ (Carl Roth, cat. no. 4984); 1.8 mM KH₂PO₄ (Carl Roth, cat. no. 3904; pH 7.4)), washed in ice-cold 1x PBS and digested in an enzyme cocktail (see above). After washing in ice-cold 1x PBS, single root tips were transferred to glass slides and squashed in 1x PBS+ 0.001% Tween-20 using cover slips (Th. Geyer, cat. no. 7695024). After removal of the cover slip by liquid nitrogen, slides were stored in 1x PBS. Incubation with primary (90 min/37°C rabbit anti-grass CENH3 (Sanei, Pickering et al. 2011)) and secondary antibodies (donkey anti-rabbit coupled to Alexa 647 (60 min/37°C; Dianova, cat. no. 711-606-152)) was performed. Slides were washed, dehydrated (70%, 90% and 100% ethanol), air-dried and fixed in ethanol/glacial acid (3:1; 24-48 h/ in dark). Subsequently, the slides were air-dried and incubated with DS20 (12 h/37°C). After short washing (2x SSC containing 0.1% Triton X100) slides were dehydrated and air-dried. For denaturation, slides were incubated in 0.2 N NaOH (in 70% ethanol/10 min/RT), dehydrated and air-dried. Alkyne-modified probes were heated up (5 min/95°C) in DS 20 before application on slides. FISH was performed at 37°C overnight using pre-hybridisation-labelled CTT and 4PTel4 probes. Slides were washed and afterwards mounted in Vectashield containing DAPI (10 ng/μl).

5.5.2.8. Quantification of telomeric FISH signals

Acquisition of FISH signal was carried out using an Olympus BX61 microscope equipped with an Orca ER CCD camera (Hamamatsu). For quantification of telomeric FISH signals, flow-sorted endopolyploid nuclei (4C) of *Arabidopsis thaliana* were used. For each FISH probe 300 nuclei were analysed. Statistical analysis was done using Kruskal-Wallis ANOVA followed by median test (STATISTICA data analysis software system, Statsoft, USA). Factorial effects and differences between groups were considered as significant at $P < 0.05$.

5.5.3. Results and discussion

To examine whether the Cu(I)-catalysed azide-alkyne cycloaddition (CuAAC) is suitable for the synthesis of FISH probes, we designed oligonucleotides recognizing the *Arabidopsis*-type telomeric sequence (TTTAGGG)_n. The solid phase-synthesised alkyne-modified oligonucleotides were labelled before hybridisation with TAMRA fluorochrome at defined positions using the CuAAC technique (Tab. 5. 1). FISH of mitotic barley and *A. thaliana* chromosomes resulted in telomere repeat-typical signals at distal parts of the chromosomes, demonstrating that CuAAC labelled probes are suitable for the *in situ* detection of telomeric sequences by FISH (Fig. 5. 4A).

To investigate whether the length of probes and the quantity of fluorochromes conjugated to the probe influences the performance of CuAAC labelled FISH probes, oligonucleotides consisting of either 3 or 4 5'-CCCTAAA-3' repeats each labelled with 2 to 4 fluorochromes were synthesised and compared to conventional nick translation and 5' labelled probes. Regardless of oligonucleotide length and fluorochrome number, the telomere signals were detected by all probes on flow-sorted barley interphase nuclei (Fig. 5. 4B). Quantification of fluorescence signal intensities of telomere probes after

FISH was not feasible due to the telomere length variations of individual chromosomes as been shown by Wang (1991). For a precise signal quantification identical sized telomeres are a prerequisite. Unfortunately a discrimination of telomeres of individual chromosomes was not feasible. Next, we evaluated whether the CuAAC-labeled telomere probes show differences in their detection properties by quantification of telomeric FISH signals detected on flow-sorted endopolyploid nuclei (4C) of *Arabidopsis* ecotypes having either short or long telomeres. *A. thaliana* ecotype Pro-0 is characterised by rather long telomeres (~9.3 kb) while Hov 1-10 is possessing ~1 kb long telomeres only. (Fulcher, Teubenbacher et al. 2015). Comparison of the mean number of detected telomere signals revealed that the performance of all probes was best in the ecotype having long telomeres (Fig. 5. 4C). Significantly lower number of detected FISH signals in the Hov ecotype possibly reflects a different clustering of telomeres in interphase. Furthermore, the short telomere length of the Hov ecotype could potentially be below the detection limit of the telomeric probes. The lower performance of the nick translated-labelled probes in both ecotypes was most likely due to better hybridisation abilities of the oligonucleotide probes (Bradley, Zamechek et al. 2009). Moreover the efficiency of DNA polymerase I – used in the NT assay - to incorporate fluorescently labelled deoxynucleotides is low reaching around 2-4% (Yu, Chao et al. 1994). Possessing 2 to 4 fluorochromes CuAAC-labeled telomere probes have a higher labelling rate than nick translated-labelled probes, which could also account for a better probe performance.

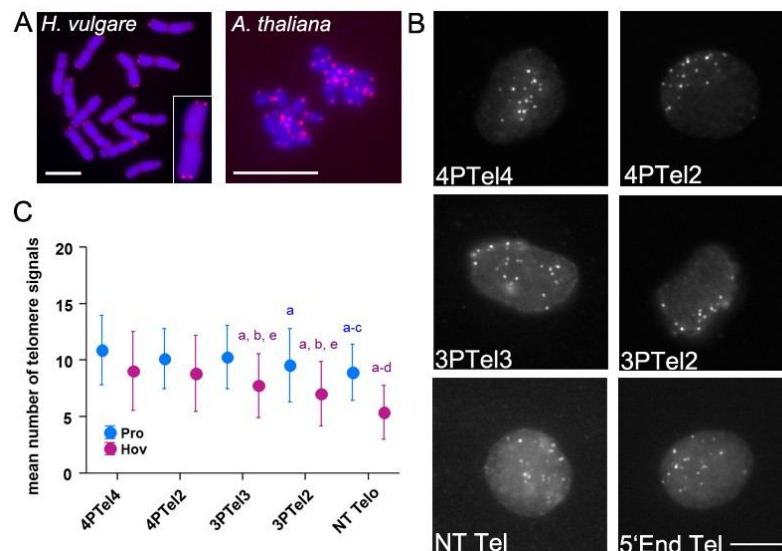


Figure 5. 4. CuAAC-labelled DNA probes are suitable for FISH. (A) Representative images of CuAAC labelled *Arabidopsis*-type telomere ((TTTAGG)_n) probes (in red) hybridised on mitotic chromosomes of barley and *A. thaliana*. Inset shows a further enlarged chromosome. Exemplary images (B) of CuAAC labelled probes (4PTel2, 4PTel2, 3PTel3, 3PTel2, nick translation labelled telomere probe and 5' end labelled probe) hybridised on sorted 2C barley nuclei. All scale bars represent 10 μ m (A; B). (C) Quantification of detected telomeric FISH signals on sorted 4C nuclei of *Arabidopsis* ecotypes possessing long (Pro ~9.3 kb) and short (Hov ~1 kb) telomers by CuAAC labelled telomere probes and nick translation labelled telomere probe. Statistical analysis revealed that performance of all probes was markedly better in the Pro ecotype, as compared with the Hov ecotype. Significant differences ($P < 0.05$;

protected two-way ANOVA followed by Bonferroni post hoc test) are labelled with letters a-e at which (a) means significant different to 4PTel4, (b) to 4PTel2, (c) to 3PTel3, (d) 3PTel2, (e) to nick translated telomere probes.

Further, we addressed the question whether the CuAAC reaction can also be performed after probe hybridisation, similarly to indirect labelling approaches. This would be advantageous because alkyne-labelled probes can be labelled after *in situ* hybridisation with various fluorochromes depending on specific needs or experimental settings. To investigate this, the same set of alkyne-modified telomeric probes (Tab. 5. 1) were hybridised to mitotic wheat chromosomes, followed by an on-slide CuAAC reaction (post-hybridisation click). For comparison, a conventional nick translation-labelled telomere probe was co-hybridised. Figure 5. 5A shows that post-hybridisation labelling of CuAAC probes indeed resulted in clearly detectable telomeric signals similar to the signals of the nick translation labelled control probes.

To validate whether pre- and post-hybridisation click labelled probes target the same chromosomal sites, we hybridised the pre-hybridisation fluorescently labelled microsatellite (CTT)10 probes simultaneously with a (CTT)10 probes that were modified with alkyne only. Subsequently, the latter probe was labelled on-slide by a CuAAC reaction. We found that both types of probes resulted in comparable hybridisation patterns (Fig. 5. 5B). The same applies for rye centromere-specific probe (Bilby) synthesised by PCR (Fig. 5. 5C).

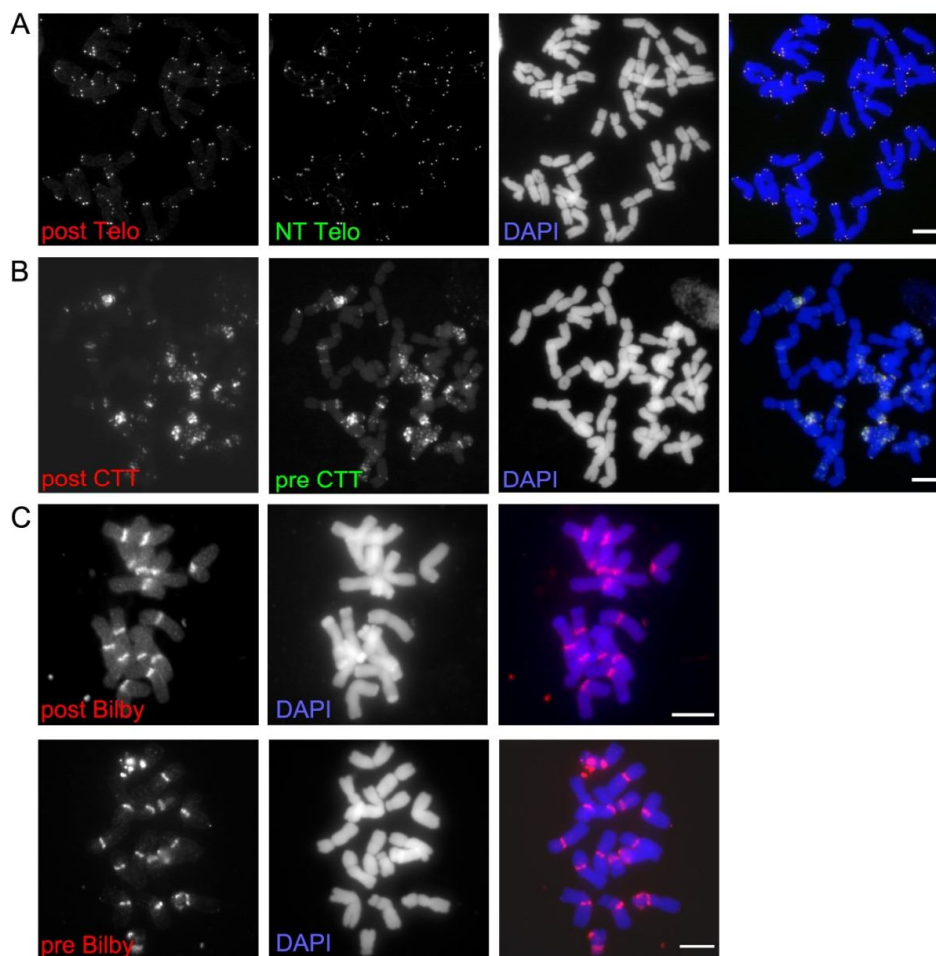


Figure 5. 5. Combination of pre- and post-hybridisation click-labelled probes on (A, B) wheat and (C) rye metaphase chromosomes. Alkyne conjugated oligonucleotides probes were hybridised to the specimen and on-slide labelled via CuAAC. (A) Detection of post-hybridisation labelled 4PTel2 and nick translation labelled Arabidopsis-type telomere probes showing co-localised hybridisation signals. (B) Pre- and post-hybridisation click-labelled microsatellite (CTT)10 probes showed a comparable distribution of hybridisation signals. (C) Pre- and post- hybridisation click labelling of rye centromere-specific probe (Bilby) synthesised via the CuAAC-based PCR assay (PCR-Click555 Kit). All scale bars represent 10 µm.

To explore a range of potential applications of click chemistry-based probes, we combined FISH with two standard cytological techniques, i.e. immunohistochemistry and labelling of DNA replication via 5-Ethynyl-deoxyuridine (EdU) uptake. After performance of immunohistochemistry detecting the centromeric variant of histone H3 (CENH3) and click chemistry- based cell proliferation assay, pre-hybridisation click-labelled telomere and microsatellite probes (4PTel4; (CTT)10) were successfully hybridised on barley metaphase chromosomes (Fig. 5. 6A, B). Note that post-hybridisation labelling of both probes via CuAAC reaction resulted in additional labelling of unreacted alkynes groups of EdU.

Moreover, the CuAAC reaction was insufficient on specimens previously fixed by paraformaldehyde most likely due to penetration problems.

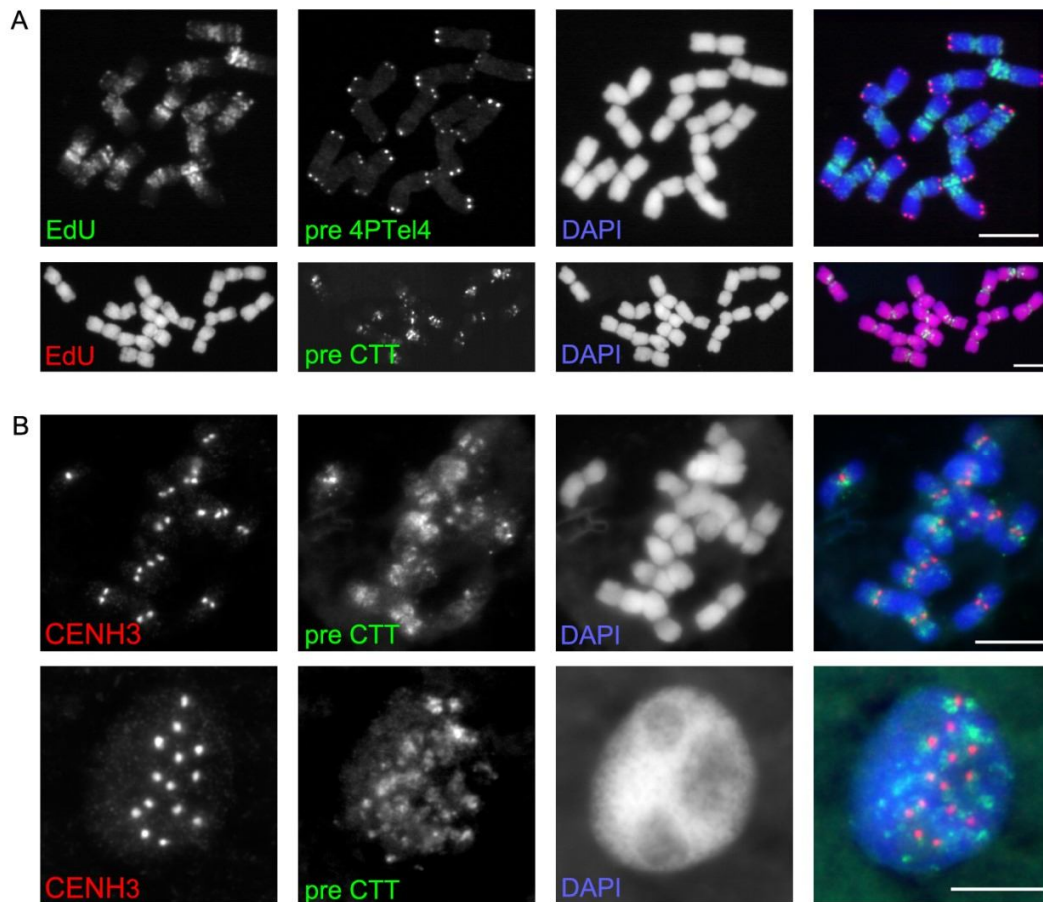


Figure 5. 6. Combination of CuAAC-labelled microsatellite probes with immunohistochemistry and labelling of replication via 5-Ethynyl-deoxyuridine (EdU). (A) FISH of barley using pre-hybridisation click-labelled microsatellite (CTT)10 and telomeric probes combined with labelling of early and late replication via EdU. (B) Immunolabelling of CENH3 was successfully combined with FISH using pre-hybridisation click-labelled microsatellite probes ((CTT)10) on metaphase chromosomes and interphase nucleus of barley. All scale bars represent 10 μm.

Thus, we showed that CuAAC-labeled probes represent a reliable tool to detect different types of repetitive sequences on chromosomes and nuclei. Importantly, we demonstrated that CuAAC reaction-based labelling technique can be combined with immunohistochemistry and cell proliferation assays via 5-Ethynyl-deoxyuridine (EdU) without loss of sensitivity. This renders CuAAC reaction-based labelling technique as a valid and flexible tool in cytogenetics and cell biology with possible applications in the detection of single copy genes by CuAAC probes. In addition, this method allows for labelling of any type

of FISH probe e.g, long or short, single or double stranded DNA probes. Moreover CuAAC labelling works in a modular manner. Depending on the experimental needs one and the same alkyne-labelled probe can be detected with different kinds of label to suit the single experiments. Comparison between different labelling techniques revealed a comparable sensitivity of CuAAC probes to that of conventionally labelled probes.

5.5.4. References for the publication “Fluorescent labelling of *in situ* hybridisation probes through the copper-catalysed azide-alkyne cycloaddition reaction”

- Aliyeva-Schnorr, L., L. Ma and A. Houben (2015). A Fast Air-dry Dropping Chromosome Preparation Method Suitable for FISH in Plants. *J Vis Exp*, **2015**, (106).
- Armstrong, S. J., P. Fransz, D. F. Marshall and G. H. Jones (1998). Physical mapping of DNA repetitive sequences to mitotic and meiotic chromosomes of *Brassica oleracea* var. *alboglabra* by fluorescence *in situ* hybridization. *Heredity*, **1998**, 81: 666-673.
- Bradley, S., L. Zamechek and J. Aurich-Costa (2009). Oligonucleotide FISH Probes. Fluorescence *In Situ* Hybridisation (FISH)- *Application Guide*, **2009**, 1: 67-73.
- Dolezel, J., P. Binarova and S. Lucretti (1989). Analysis of Nuclear-DNA Content in Plant-Cells by Flow-Cytometry. *Biologia Plantarum* **1989**, 31(2): 113-120.
- Francki, M. G. (2001). Identification of Bilby, a diverged centromeric Ty1-copia retrotransposon family from cereal rye (*Secale cereale* L.). *Genome* **2001**, 44(2): 266-274.
- Fulcher, N., A. Teubenbacher, E. Kerdaffrec, A. Farlow, M. Nordborg and K. Riha (2015). Genetic architecture of natural variation of telomere length in *Arabidopsis thaliana*. *Genetics* **2015**, 199(2): 625-635.
- Gramlich, P. M., C. T. Wirges, A. Manetto and T. Carell (2008). Postsynthetic DNA modification through the copper-catalyzed azide-alkyne cycloaddition reaction. *Angew. Chem. Int. Ed. Engl.* **2008**, 47(44): 8350-8358.
- Ijdo, J. W., R. A. Wells, A. Baldini and S. T. Reeders (1991). Improved telomere detection using a telomere repeat probe (TTAGGG)_n generated by PCR. *Nucleic Acids Res.* **1991**, 19(17): 4780.

- Kelly, R. B., N. R. Cozzarelli, M. P. Deutscher, I. R. Lehman and A. Kornberg (1970). Enzymatic synthesis of deoxyribonucleic acid. XXXII. Replication of duplex deoxyribonucleic acid by polymerase at a single strand break. *J Biol. Chem.* **1970**, 245(1): 39-45.

- Kelly, S., R. Korn and J. Burns (1970). Sex ratio in phenylketonuria. *Lancet* **1970**, 2(7667): 314-315.

- Kolb, H. C., M. G. Finn and K. B. Sharpless (2001). Click Chemistry: Diverse Chemical Function from a Few Good Reactions. *Angew. Chem. Int. Ed. Engl.* **2001**, 40(11): 2004-2021.

- Pinkel, D., J. W. Gray, B. Trask, G. van den Engh, J. Fuscoe and H. van Dekken (1986). Cytogenetic analysis by in situ hybridization with fluorescently labeled nucleic acid probes. *Cold Spring Harb Symp Quant Biol* **1986**, 51 Pt 1: 151-157.

- Pinkel, D., T. Straume and J. W. Gray (1986). Cytogenetic analysis using quantitative, high-sensitivity, fluorescence hybridization. *Proc. Natl. Acad. Sci. USA* **1986**, 83(9): 2934-2938.

- Rigby, P. W., M. Dieckmann, C. Rhodes and P. Berg (1977). Labeling deoxyribonucleic acid to high specific activity *in vitro* by nick translation with DNA polymerase I. *J. Mol. Biol.* **1977**, 113(1): 237-251.

- Rostovtsev, V. V., L. G. Green, V. V. Fokin and K. B. Sharpless (2002). A stepwise Huisgen cycloaddition process: copper(I)-catalyzed regioselective "ligation" of azides and terminal alkynes. *Angew. Chem. Int. Ed. Engl.* **2002**, 41(14): 2596-2599.

- Rozkiewicz, D. I., J. Gierlich, G. A. Burley, K. Gutschiedl, T. Carell, B. J. Ravoo and D. N. Reinholdt (2007). Transfer printing of DNA by "click" chemistry. *ChemBiochem* **2007**, 8(16): 1997-2002.

- Salic, A. and T. J. Mitchison (2008). A chemical method for fast and sensitive detection of DNA synthesis *in vivo*. *Proc. Natl. Acad. Sci. USA* **2008**, 105(7): 2415-2420.

- Sanei, M., R. Pickering, K. Kumke, S. Nasuda and A. Houben (2011). Loss of centromeric histone H3 (CENH3) from centromeres precedes uniparental chromosome elimination in interspecific barley hybrids. *Proc. Natl. Acad. Sci. USA* **2011**, 108(33): E498-505.

- Sletten, E. M. and C. R. Bertozzi (2011). From mechanism to mouse: a tale of two biorthogonal reactions." *Acc. Chem. Res.* **2011**, 44(9): 666-676. Tornøe, C. W., C. Christensen and M. Meldal (2002). Peptidotriazoles on solid phase: [1,2,3]-triazoles by regiospecific copper(i)-catalyzed 1,3-dipolar cycloadditions of terminal alkynes to azides. *J Org Chem* **2002**, 67(9): 3057-3064.

- Wang, S., ; Lapitan, N.L.V.; Tsuchiya, T. (1991). Characterization of telomeres in Horde vulgar chromosomes by *in situ* hybridization I. Normal diploid barley. *Jpn. J. Genet.* **1991**, 66(3): 313-316.

- Wiegant, J., T. Ried, P. M. Nederlof, M. van der Ploeg, H. J. Tanke and A. K. Raap (1991). *In situ* hybridization with fluoresceinated DNA. *Nucleic Acids Res* **1991**, 19(12): 3237-3241.

- Yu, H., J. Chao, D. Patek, R. Mujumdar, S. Mujumdar and A. S. Waggoner (1994). Cyanine dye dUTP analogs for enzymatic labeling of DNA probes. *Nucleic Acids Res* **1994**, 22(15): 3226-3232.

6. List of abbreviations

2D	Two dimensional
3D	Three dimensional
6HT	Six Helix Tube
A	Adenine (Adenosine)
Å	Angstrom
AFM	Atomic Force Microscopy
APS	Ammonium Persulfate
bp	base pair
BrdU	5-bromo-2'-deoxyuridine
C	Cytosine (Cytidine)
CuAAC	Cu(I)-catalysed azide-alkyne cycloaddition
dd	double distilled
DMEM	Dulbecco's modified Eagle Medium
DMT	4,4'-dimethoxytrityl
DNA	Deoxyribonucleic acid
dNTP	Deoxynucleoside triphosphates
ds	Double Strand
EDTA	Ethylenediaminetetraacetic acid
EdU	5-Ethynyl-deoxyuridine
EScoDNA	European School of DNA Nanotechnology
EtOH	Ethanol
FISH	Fluorescence <i>in situ</i> hybridisation
FRET	Förster resonance energy transfer
G	Guanine (Guanosine)
GFP	Green Fluorescent Protein
h	hour(s)
HPA	3-Hydroxypicolinic acid

HPSF	High Purity Salt Free
IHC	Immunohistochemistry
kb	kilobase (1000 bases)
kDNA	kinetoplast DNA
L	Liter
LC-MS	Liquid chromatography–mass spectrometry
M	molar
m/z	mass/charge
MALDI-ToF	Matrix-assisted laser desorption ionization time of flight
min	minutes
MX	Modified tube (where X is the number of click-tiles within the structure)
NT	Nick translation
nt	nucleotide
PAGE	Polyacrylamide gel electrophoresis
PBS	Phosphate Buffer Saline
PCR	Polymerase chain reaction
RP-HPLC	Reverse Phase High Pressure Liquid Chromatography
siRNA	small interfering ribonucleic acid
ss	Single Strand
SST	Single Strand Tile
T	Thymine (Thymidine)
TBE	Tris-Borate-EDTA (Buffer)
TBTA	Tris[(1-benzyl-1H-1,2,3-triazol-4-yl)methyl]amine
TE	Tris-EDTA (Buffer)
TEM	Transmission Electron Microscopy
TEMED	N,N,N',N'-Tetramethylethane-1,2-diamine
THPTA	Tris(3-hydroxypropyltriazolylmethyl)amine
T _m	Melting Temperature

U	unit
V	Volt

7. Bibliography

1. Watson, J. D.; Crick, F. H. C., Molecular Structure of Nucleic Acids: A Structure for Deoxyribose Nucleic Acid. *Nature* **1953**, 171 (4356), 737-738.
2. Liedl, T.; Simmel, F. C., Determination of DNA Melting Temperatures in Diffusion-Generated Chemical Gradients. *Ana./Chem.* **2007**, 79 (14), 5212-5216.
3. Wallace, R. B.; Shaffer, J.; Murphy, R. F.; Bonner, J.; Hirose, T.; Itakura, K., Hybridization of synthetic oligodeoxyribonucleotides to Φ X 174 DNA: the effect of single base pair mismatch. *Nucleic Acids Res.* **1979**, 6 (11), 3543-3558.
4. John SantaLucia, J.; Hicks, D., The Thermodynamics of DNA Structural Motifs. *Annu. Rev. Biophys. Bio.* **2004**, 33 (1), 415-440.
5. Müller, S., Nucleic acids from a to Z - A concise Encyclopedia. *Wiley-VCH, Ed. Wiley-VCH Verlag GmbH & Co. KGaA*: **2008**; pp I-XIV.
6. (a) Meselson, M.; Stahl, F. W., THE REPLICATION OF DNA IN ESCHERICHIA COLI. *Proc.Natl. Acad. Sci. USA* **1958**, 44 (7), 671-682; (b) Bessman, M. J.; Lehman, I. R.; Simms, E. S.; Kornberg, A., Enzymatic Synthesis of Deoxyribonucleic Acid: II. GENERAL PROPERTIES OF THE REACTION. *J. Biol. Chem.* **1958**, 233 (1), 171-177.
7. Khorana, H. G., Nucleic acid synthesis. *Pure Appl. Chem.* **1968**, 17 (3-4), 349-382.
8. Itakura, K.; Bahl, C.; Katagiri, N.; Michniewicz, J.; Wightman, R.; Narang, S., A modified triester method for the synthesis of deoxyribopolynucleotides. *Canadian J. Chem.* **1973**, 51 (21), 3649-3651.
9. Froehler, B. C.; Ng, P. G.; Matteucci, M. D., Synthesis of DNA via deoxynucleoside H-phosphonate Intermediates. *Nucleic Acids Res.* **1986**, 14 (13), 5399-5407.
10. Caruthers, M. H.; Barone, A. D.; Beaucage, S. L.; Dodds, D. R.; Fisher, E. F.; McBride, L. J.; Matteucci, M.; Stabinsky, Z.; Tang, J. Y., Chemical synthesis of deoxyoligonucleotides by the phosphoramidite method. *Method Enzymol.* **1987**, 154, 287-313.
11. Goullain, T.; Sidorov, A.; Mignet, N.; Thorpe, S. J.; Lee, S. E.; Grasby, J. A.; Williams, D. M., Enhancing the catalytic repertoire of nucleic acids. II. Simultaneous incorporation of amino and imidazolyl functionalities by two modified triphosphates during PCR. *Nucleic Acids Res.* **2001**, 29 (9), 1898-1905.
12. Tasara, T.; Angerer, B.; Damond, M.; Winter, H.; Dörhöfer, S.; Hübscher, U.; Amacker, M., Incorporation of reporter molecule-labeled nucleotides by DNA polymerases. II. High-density labeling of natural DNA. *Nucleic Acids Res.* **2003**, 31 (10), 2636-2646.
13. Gierlich, J.; Gutsmedl, K.; Gramlich, P. M. E.; Schmidt, A.; Burley, G. A.; Carell, T., Synthesis of Highly Modified DNA by a Combination of PCR with Alkyne-Bearing Triphosphates and Click Chemistry. *Chem. – Eur. J.* **2007**, 13 (34), 9486-9494.

14. Jawalekar, A. M.; Meeuwenoord, N.; Cremers, J. G. O.; Overkleeft, H. S.; van der Marel, G. A.; Rutjes, F. P. J. T.; van Delft, F. L., Conjugation of Nucleosides and Oligonucleotides by [3+2] Cycloaddition. *J. Org. Chem.* **2008**, *73* (1), 287-290.
15. Alvira, M.; Eritja, R., Synthesis of Oligonucleotides Carrying 5'-5' Linkages Using Copper-Catalyzed Cycloaddition Reactions. *Chem. Biodiversity* **2007**, *4* (12), 2798-2809.
16. Seo, T. S.; Li, Z.; Ruparel, H.; Ju, J., Click Chemistry to Construct Fluorescent Oligonucleotides for DNA Sequencing. *J. Org. Chem.* **2003**, *68* (2), 609-612.
17. Kolb, H. C.; Finn, M. G.; Sharpless, K. B., Click Chemistry: Diverse Chemical Function from a Few Good Reactions. *Angew. Chem. Int. Ed.* **2001**, *40* (11), 2004-2021.
18. Padwa, A.; Pearson, W. H., *Synthetic Applications of 1,3-Dipolar Cycloaddition Chemistry Toward Heterocycles and Natural Products*. Wiley **2003**.
19. Rostovtsev, V. V.; Green, L. G.; Fokin, V. V.; Sharpless, K. B., A Stepwise Huisgen Cycloaddition Process: Copper(I)-Catalyzed Regioselective "Ligation" of Azides and Terminal Alkynes. *Angew. Chem. Int. Ed.* **2002**, *41* (14), 2596-2599.
20. Tornøe, C. W.; Christensen, C.; Meldal, M., Peptidotriazoles on Solid Phase: [1,2,3]-Triazoles by Regiospecific Copper(I)-Catalyzed 1,3-Dipolar Cycloadditions of Terminal Alkynes to Azides. *J. Org. Chem.* **2002**, *67* (9), 3057-3064.
21. (a) Díaz, D. D.; Punna, S.; Holzer, P.; McPherson, A. K.; Sharpless, K. B.; Fokin, V. V.; Finn, M. G., Click chemistry in materials synthesis. 1. Adhesive polymers from copper-catalyzed azide-alkyne cycloaddition. *J. Pol. Sci. A1* **2004**, *42* (17), 4392-4403; (b) Himo, F.; Lovell, T.; Hilgraf, R.; Rostovtsev, V. V.; Noodleman, L.; Sharpless, K. B.; Fokin, V. V., Copper(I)-Catalyzed Synthesis of Azoles. DFT Study Predicts Unprecedented Reactivity and Intermediates. *J. Am. Chem. Soc.* **2005**, *127* (1), 210-216.
22. (a) Jin, L.; Tolentino, D. R.; Melaimi, M.; Bertrand, G., Isolation of bis(copper) key intermediates in Cu-catalyzed azide-alkyne "click reaction". *Sci. Adv.* **2015**, *1* (5); (b) Worrell, B. T.; Malik, J. A.; Fokin, V. V., Direct evidence of a dinuclear copper intermediate in Cu(I)-catalyzed azide-alkyne cycloadditions. *Science* **2013**, *340* (6131), 457-60.
23. Seela, F.; Sirivolu, V. R., DNA Containing Side Chains with Terminal Triple Bonds: Base-Pair Stability and Functionalization of Alkynylated Pyrimidines and 7-Deazapurines. *Chem. Biodiversity* **2006**, *3* (5), 509-514.
24. Gierlich, J.; Burley, G. A.; Gramlich, P. M. E.; Hammond, D. M.; Carell, T., Click Chemistry as a Reliable Method for the High-Density Postsynthetic Functionalization of Alkyne-Modified DNA. *Org. Lett.* **2006**, *8* (17), 3639-3642.
25. Burley, G. A.; Gierlich, J.; Mofid, M. R.; Nir, H.; Tal, S.; Eichen, Y.; Carell, T., Directed DNA Metallization. *J. Am. Chem. Soc.* **2006**, *128* (5), 1398-1399.

26. Fischler, M.; Simon, U.; Nir, H.; Eichen, Y.; Burley, G. A.; Gierlich, J.; Gramlich, P. M. E.; Carell, T., Formation of Bimetallic Ag–Au Nanowires by Metallization of Artificial DNA Duplexes. *Small* **2007**, 3 (6), 1049-1055.
27. Gramlich, P. M. E.; Warncke, S.; Gierlich, J.; Carell, T., Click–Click–Click: Single to Triple Modification of DNA. *Angew. Chem. Int. Ed.* **2008**, 47 (18), 3442-3444.
28. (a) Salic, A.; Mitchison, T. J., A chemical method for fast and sensitive detection of DNA synthesis in vivo. *Proc. Natl. Acad. Sci. USA* **2008**, 105 (7), 2415-2420; (b) Oberleitner, B.; Manetto, A.; Frischmuth, T., EdU statt BrdU: eine Alternative zur Detektion der Zellproliferation. *BIOspektrum* **2014**, 20 (2), 188-190.
29. Feynman, R. P., There's Plenty of Room at the Bottom. *Engineering and Science* **1960**, 23 (5), 22-36.
30. Norio, T., On the Basic Concept of 'Nano-Technology'. *Proc. Intl. Conf. Prod. Eng. Tokyo, Japan Society of Precision Engineering* **1974**.
31. Mansoori, G.; Fauzi Soelaiman, T., Nanotechnology - An Introduction for the Standards Community. *J. ASTM Int.* **2005**, 2 (6), 1-22.
32. Faraji, A. H.; Wipf, P., Nanoparticles in cellular drug delivery. *Bioorgan. Med. Chem.* **2009**, 17 (8), 2950-2962.
33. Angell, C.; Xie, S.; Zhang, L.; Chen, Y., DNA Nanotechnology for Precise Control over Drug Delivery and Gene Therapy. *Small* **2016**, 12 (9), 1117-1132.
34. Bloomfield, V. A.; Crothers, D. M.; Tinoco, I., Nucleic Acids: Structures, Properties, and Functions. *University Science Books* **2000**.
35. Carlson, R., The changing economics of DNA synthesis. *Nat. Biotech* **2009**, 27 (12), 1091-1094.
36. Peng, Z.; Liu, H., Bottom-up Nanofabrication Using DNA Nanostructures. *Chem. Mater.* **2016**, 28 (4), 1012-1021.
37. Seeman, N. C., Nucleic acid junctions and lattices. *J. Theor. Biol.* **1982**, 99 (2), 237-247.
38. Chen, J.; Seeman, N. C., Synthesis from DNA of a molecule with the connectivity of a cube. *Nature* **1991**, 350 (6319), 631-633.
39. Jones, M. R.; Seeman, N. C.; Mirkin, C. A., Programmable materials and the nature of the DNA bond. *Science* **2015**, 347 (6224).
40. Li, X.; Yang, X.; Qi, J.; Seeman, N. C., *J. Am. Chem. Soc.* **1996**, 118, 6131.
41. Seeman, N. C., Nanomaterials Based on DNA. *Annu. Rev. Biochem.* **2010**, 79 (1), 65-87.

42. Winfree, E.; Liu, F.; Wenzler, L. A.; Seeman, N. C., Design and self-assembly of two-dimensional DNA crystals. *Nature* **1998**, *394* (6693), 539-544.
43. Rothemund, P. W. K., Folding DNA to create nanoscale shapes and patterns. *Nature* **2006**, *440* (7082), 297-302.
44. Högberg, B.; Liedl, T.; Shih, W. M., Folding DNA Origami from a Double-Stranded Source of Scaffold. *J. Am. Chem. Soc.* **2009**, *131* (26), 9154-9155.
45. Zhang, H.; Chao, J.; Pan, D.; Liu, H.; Huang, Q.; Fan, C., Folding super-sized DNA origami with scaffold strands from long-range PCR. *Chem. Commun.* **2012**, *48* (51), 6405-6407.
46. Douglas, S. M.; Dietz, H.; Liedl, T.; Hogberg, B.; Graf, F.; Shih, W. M., Self-assembly of DNA into nanoscale three-dimensional shapes. *Nature* **2009**, *459* (7245), 414-418.
47. Ke, Y.; Douglas, S. M.; Liu, M.; Sharma, J.; Cheng, A.; Leung, A.; Liu, Y.; Shih, W. M.; Yan, H., Multilayer DNA Origami Packed on a Square Lattice. *J. Am. Chem. Soc.* **2009**, *131* (43), 15903-15908.
48. Andersen, E. S.; Dong, M.; Nielsen, M. M.; Jahn, K.; Subramani, R.; Mamdouh, W.; Golas, M. M.; Sander, B.; Stark, H.; Oliveira, C. L. P.; Pedersen, J. S.; Birkedal, V.; Besenbacher, F.; Gothelf, K. V.; Kjems, J., Self-assembly of a nanoscale DNA box with a controllable lid. *Nature* **2009**, *459* (7243), 73-76.
49. Han, D.; Pal, S.; Nangreave, J.; Deng, Z.; Liu, Y.; Yan, H., DNA Origami with Complex Curvatures in Three-Dimensional Space. *Science* **2011**, *332* (6027), 342-346.
50. Wei, B.; Dai, M.; Yin, P., Complex shapes self-assembled from single-stranded DNA tiles. *Nature* **2012**, *485* (7400), 623-626.
51. Ke, Y.; Ong, L. L.; Shih, W. M.; Yin, P., Three-Dimensional Structures Self-Assembled from DNA Bricks. *Science* **2012**, *338* (6111), 1177-1183.
52. Benson, E.; Mohammed, A.; Gardell, J.; Masich, S.; Czeizler, E.; Orponen, P.; Hogberg, B., DNA rendering of polyhedral meshes at the nanoscale. *Nature* **2015**, *523* (7561), 441-444.
53. Andersen, E. S.; Dong, M.; Nielsen, M. M.; Jahn, K.; Lind-Thomsen, A.; Mamdouh, W.; Gothelf, K. V.; Besenbacher, F.; Kjems, J., DNA Origami Design of Dolphin-Shaped Structures with Flexible Tails. *ACS Nano* **2008**, *2* (6), 1213-1218.
54. Douglas, S. M.; Marblestone, A. H.; Teerapittayanon, S.; Vazquez, A.; Church, G. M.; Shih, W. M., Rapid prototyping of 3D DNA-origami shapes with caDNANO. *Nucleic Acids Res.* **2009**, *37* (15), 5001-6.
55. Martin, T. G.; Dietz, H., Magnesium-free self-assembly of multi-layer DNA objects. *Nat. Commun.* **2012**, *3*, 1103.
56. Sobczak, J.-P. J.; Martin, T. G.; Gerling, T.; Dietz, H., Rapid Folding of DNA into Nanoscale Shapes at Constant Temperature. *Science* **2012**, *338* (6113), 1458-1461.

57. Jungmann, R.; Liedl, T.; Sobey, T. L.; Shih, W.; Simmel, F. C., Isothermal Assembly of DNA Origami Structures Using Denaturing Agents. *J. Am. Chem. Soc.* **2008**, *130* (31), 10062-10063.
58. Bellot, G.; McClintock, M. A.; Lin, C.; Shih, W. M., Recovery of intact DNA nanostructures after agarose gel-based separation. *Nat. Meth.* **2011**, *8* (3), 192-194.
59. Lin, C.; Perrault, S. D.; Kwak, M.; Graf, F.; Shih, W. M., Purification of DNA-origami nanostructures by rate-zonal centrifugation. *Nucleic Acids Res.* **2012**.
60. Stahl, E.; Martin, T. G.; Praetorius, F.; Dietz, H., Facile and Scalable Preparation of Pure and Dense DNA Origami Solutions. *Angew. Chem. Int. Ed.* **2014**, *53* (47), 12735-12740.
61. Douglas, S. M.; Chou, J. J.; Shih, W. M., DNA-nanotube-induced alignment of membrane proteins for NMR structure determination. *Proc. Natl. Acad. Sci. USA* **2007**, *104* (16), 6644-6648.
62. Fu, J.; Liu, M.; Liu, Y.; Woodbury, N. W.; Yan, H., Interenzyme Substrate Diffusion for an Enzyme Cascade Organized on Spatially Addressable DNA Nanostructures. *J. Am. Chem. Soc.* **2012**, *134* (12), 5516-5519.
63. Stein, I. H.; Schüller, V.; Böhm, P.; Tinnefeld, P.; Liedl, T., Single-Molecule FRET Ruler Based on Rigid DNA Origami Blocks. *ChemPhysChem* **2011**, *12* (3), 689-695.
64. Schmied, J. J.; Gietl, A.; Holzmeister, P.; Forthmann, C.; Steinhauer, C.; Dammeyer, T.; Tinnefeld, P., Fluorescence and super-resolution standards based on DNA origami. *Nat. Meth.* **2012**, *9* (12), 1133-1134.
65. Steinhauer, C.; Jungmann, R.; Sobey, T. L.; Simmel, F. C.; Tinnefeld, P., DNA Origami as a Nanoscopic Ruler for Super-Resolution Microscopy. *Angew. Chem. Int. Ed.* **2009**, *48* (47), 8870-8873.
66. Jungmann, R.; Steinhauer, C.; Scheible, M.; Kuzyk, A.; Tinnefeld, P.; Simmel, F. C., Single-molecule kinetics and super-resolution microscopy by fluorescence imaging of transient binding on DNA origami. *Nano Lett.* **2010**, *10* (11), 4756-61.
67. Beliveau, B. J.; Boettiger, A. N.; Avendano, M. S.; Jungmann, R.; McCole, R. B.; Joyce, E. F.; Kim-Kiselak, C.; Bantignies, F.; Fonseka, C. Y.; Erceg, J.; Hannan, M. A.; Hoang, H. G.; Colognori, D.; Lee, J. T.; Shih, W. M.; Yin, P.; Zhuang, X.; Wu, C.-t., Single-molecule super-resolution imaging of chromosomes and in situ haplotype visualization using Oligopaint FISH probes. *Nat. Commun.* **2015**, *6*.
68. Johnson-Buck, A.; Su, X.; Giraldez, M. D.; Zhao, M.; Tewari, M.; Walter, N. G., Kinetic fingerprinting to identify and count single nucleic acids. *Nat. Biotech.* **2015**, *33* (7), 730-732.
69. Kuzyk, A.; Schreiber, R.; Fan, Z.; Pardatscher, G.; Roller, E.-M.; Hoge, A.; Simmel, F. C.; Govorov, A. O.; Liedl, T., DNA-based self-assembly of chiral plasmonic nanostructures with tailored optical response. *Nature* **2012**, *483* (7389), 311-314.
70. Acuna, G. P.; Moller, F. M.; Holzmeister, P.; Beater, S.; Lalkens, B.; Tinnefeld, P., Fluorescence enhancement at docking sites of DNA-directed self-assembled nanoantennas. *Science* **2012**, *338* (6106), 506-10.

71. Schreiber, R.; Kempter, S.; Holler, S.; Schüller, V.; Schiffels, D.; Simmel, S. S.; Nickels, P. C.; Liedl, T., DNA Origami-Templated Growth of Arbitrarily Shaped Metal Nanoparticles. *Small* **2011**, 7 (13), 1795-1799.
72. Liu, J.; Geng, Y.; Pound, E.; Gyawali, S.; Ashton, J. R.; Hickey, J.; Woolley, A. T.; Harb, J. N., Metallization of Branched DNA Origami for Nanoelectronic Circuit Fabrication. *ACS Nano* **2011**, 5 (3), 2240-2247.
73. Voigt, N. V.; Topping, T.; Rotaru, A.; Jacobsen, M. F.; Ravnsbaek, J. B.; Subramani, R.; Mamdouh, W.; Kjems, J.; Mokhir, A.; Besenbacher, F.; Gothelf, K. V., Single-molecule chemical reactions on DNA origami. *Nat. Nano* **2010**, 5 (3), 200-203.
74. Kocabey, S.; Kempter, S.; List, J.; Xing, Y.; Bae, W.; Schiffels, D.; Shih, W. M.; Simmel, F. C.; Liedl, T., Membrane-Assisted Growth of DNA Origami Nanostructure Arrays. *ACS Nano* **2015**, 9 (4), 3530-3539.
75. Langecker, M.; Arnaut, V.; Martin, T. G.; List, J.; Renner, S.; Mayer, M.; Dietz, H.; Simmel, F. C., Synthetic Lipid Membrane Channels Formed by Designed DNA Nanostructures. *Science* **2012**, 338 (6109), 932-936.
76. Burns, J. R.; Al-Juffali, N.; Janes, S. M.; Howorka, S., Membrane-Spanning DNA Nanopores with Cytotoxic Effect. *Angew. Chem. Int. Ed.* **2014**, 53 (46), 12466-12470.
77. Walsh, A. S.; Yin, H.; Erben, C. M.; Wood, M. J. A.; Turberfield, A. J., DNA Cage Delivery to Mammalian Cells. *ACS Nano* **2011**, 5 (7), 5427-5432.
78. (a) Jiang, Q.; Song, C.; Nangreave, J.; Liu, X.; Lin, L.; Qiu, D.; Wang, Z.-G.; Zou, G.; Liang, X.; Yan, H.; Ding, B., DNA Origami as a Carrier for Circumvention of Drug Resistance. *J. Am. Chem. Soc.* **2012**, 134 (32), 13396-13403; (b) Zhang, Q.; Jiang, Q.; Li, N.; Dai, L.; Liu, Q.; Song, L.; Wang, J.; Li, Y.; Tian, J.; Ding, B.; Du, Y., DNA Origami as an In Vivo Drug Delivery Vehicle for Cancer Therapy. *ACS Nano* **2014**, 8 (7), 6633-6643; (c) Zhao, Y.-X.; Shaw, A.; Zeng, X.; Benson, E.; Nyström, A. M.; Högberg, B., DNA Origami Delivery System for Cancer Therapy with Tunable Release Properties. *ACS Nano* **2012**, 6 (10), 8684-8691.
79. Douglas, S. M.; Bachelet, I.; Church, G. M., A Logic-Gated Nanorobot for Targeted Transport of Molecular Payloads. *Science* **2012**, 335 (6070), 831-834.
80. Lee, H.; Lytton-Jean, A. K. R.; Chen, Y.; Love, K. T.; Park, A. I.; Karagiannis, E. D.; Sehgal, A.; Querbes, W.; Zurenko, C. S.; Jayaraman, M.; Peng, C. G.; Charisse, K.; Borodovsky, A.; Manoharan, M.; Donahoe, J. S.; Truelove, J.; Nahrendorf, M.; Langer, R.; Anderson, D. G., Molecularly self-assembled nucleic acid nanoparticles for targeted in vivo siRNA delivery. *Nat. Nano* **2012**, 7 (6), 389-393.
81. Li, J.; Pei, H.; Zhu, B.; Liang, L.; Wei, M.; He, Y.; Chen, N.; Li, D.; Huang, Q.; Fan, C., Self-Assembled Multivalent DNA Nanostructures for Noninvasive Intracellular Delivery of Immunostimulatory CpG Oligonucleotides. *ACS Nano* **2011**, 5 (11), 8783-8789.
82. Schüller, V. J.; Heidegger, S.; Sandholzer, N.; Nickels, P. C.; Suhartha, N. A.; Endres, S.; Bourquin, C.; Liedl, T., Cellular Immunostimulation by CpG-Sequence-Coated DNA Origami Structures. *ACS Nano* **2011**, 5 (12), 9696-9702.

83. Sellner, S.; Kocabey, S.; Nekolla, K.; Krombach, F.; Liedl, T.; Rehberg, M., DNA nanotubes as intracellular delivery vehicles in vivo. *Biomaterials* **2015**, *53*, 453-463.
84. Mikkilä, J.; Eskelinen, A.-P.; Niemelä, E. H.; Linko, V.; Frilander, M. J.; Törmä, P.; Kostainen, M. A., Virus-Encapsulated DNA Origami Nanostructures for Cellular Delivery. *Nano Lett.* **2014**, *14* (4), 2196-2200.
85. Lee, D. S.; Qian, H.; Tay, C. Y.; Leong, D. T., Cellular processing and destinies of artificial DNA nanostructures. *Chem. Soc. Rev.* **2016**, *45* (15), 4199-225.
86. Keum, J. W.; Bermudez, H., Enhanced resistance of DNA nanostructures to enzymatic digestion. *Chem. Commun. (Camb)* **2009**, (45), 7036-8.
87. Hahn, J.; Wickham, S. F. J.; Shih, W. M.; Perrault, S. D., Addressing the Instability of DNA Nanostructures in Tissue Culture. *ACS Nano* **2014**, *8* (9), 8765-8775.
88. Conway, J. W.; McLaughlin, C. K.; Castor, K. J.; Sleiman, H., DNA nanostructure serum stability: greater than the sum of its parts. *Chem. Commun.* **2013**, *49* (12), 1172-1174.
89. Cassinelli, V.; Oberleitner, B.; Sobotta, J.; Nickels, P.; Grossi, G.; Kempter, S.; Frischmuth, T.; Liedl, T.; Manetto, A., One-Step Formation of "Chain-Armor"-Stabilized DNA Nanostructures. *Angew. Chem. Int. Ed.* **2015**, *54* (27), 7795-7798.
90. Ko, S.; Liu, H.; Chen, Y.; Mao, C., DNA Nanotubes as Combinatorial Vehicles for Cellular Delivery. *Biomacromolecules* **2008**, *9* (11), 3039-3043.
91. Kanasty, R.; Dorkin, J. R.; Vegas, A.; Anderson, D., Delivery materials for siRNA therapeutics. *Nat. Mater.* **2013**, *12* (11), 967-977.
92. Alabi, C.; Vegas, A.; Anderson, D., Attacking the genome: emerging siRNA nanocarriers from concept to clinic. *Cur. Opin. Pharmacol.* **2012**, *12* (4), 427-433.
93. Giljohann, D. A.; Seferos, D. S.; Prigodich, A. E.; Patel, P. C.; Mirkin, C. A., Gene Regulation with Polyvalent siRNA-Nanoparticle Conjugates. *J. Am. Chem. Soc.* **2009**, *131* (6), 2072-2073.
94. Lee, R. J.; Low, P. S., Folate as a Targeting Device for Proteins Utilizing Folate Receptor-Mediated Endocytosis. In *Drug Targeting: Strategies, Principles, and Applications*, Francis, G. E.; Delgado, C., Eds. Humana Press: Totowa, NJ, **2000**, 69-76.
95. Zhao, X.; Li, H.; Lee, R. J., Targeted drug delivery via folate receptors. *Expert Opin. Drug Del.* **2008**, *5* (3), 309-319.
96. Smith, D. M.; Sch; #252; Iler, V.; Forthmann, C.; Schreiber, R.; Tinnefeld, P.; Liedl, T., A Structurally Variable Hinged Tetrahedron Framework from DNA Origami. *Journal of Nucleic Acids* **2011**, *2011*, 9.

97. El-Sagheer, A. H.; Brown, T., Synthesis and Polymerase Chain Reaction Amplification of DNA Strands Containing an Unnatural Triazole Linkage. *J. Am. Chem. Soc.* **2009**, *131* (11), 3958-3964.
98. O'Neill, P.; Rothmund, P. W. K.; Kumar, A.; Fygenson, D. K., Sturdier DNA Nanotubes via Ligation. *Nano Lett.* **2006**, *6* (7), 1379-1383.
99. Rajendran, A.; Endo, M.; Katsuda, Y.; Hidaka, K.; Sugiyama, H., Photo-Cross-Linking-Assisted Thermal Stability of DNA Origami Structures and Its Application for Higher-Temperature Self-Assembly. *J. Am. Chem. Soc.* **2011**, *133* (37), 14488-14491.
100. Lu, C.-H.; Cecconello, A.; Willner, I., Recent Advances in the Synthesis and Functions of Reconfigurable Interlocked DNA Nanostructures. *J. Am. Chem. Soc.* **2016**, *138* (16), 5172-5185.
101. Mao, C.; Sun, W.; Seeman, N. C., Assembly of Borromean rings from DNA. *Nature* **1997**, *386* (6621), 137-138.
102. Du, S. M.; Seeman, N. C., The construction of a trefoil knot from a DNA branched junction motif. *Biopolymers* **1994**, *34* (1), 31-37.
103. Hudson, B.; Vinograd, J., Catenated Circular DNA Molecules in HeLa Cell Mitochondria. *Nature* **1967**, *216* (5116), 647-652.
104. Clayton, D. A.; Vinograd, J., Circular Dimer and Catenate Forms of Mitochondrial DNA in Human Leukaemic Leucocytes. *Nature* **1967**, *216* (5116), 652-657.
105. Cavalcanti, D. P.; Gonçalves, D. L.; Costa, L. T.; de Souza, W., The structure of the kinetoplast DNA network of *Crithidia fasciculata* revealed by atomic force microscopy. *Micron* **2011**, *42* (6), 553-559.
106. Lu, C.-H.; Cecconello, A.; Elbaz, J.; Credi, A.; Willner, I., A Three-Station DNA Catenane Rotary Motor with Controlled Directionality. *Nano Lett.* **2013**, *13* (5), 2303-2308.
107. Hu, L.; Lu, C. H.; Willner, I., Switchable catalytic DNA catenanes. *Nano Lett.* **2015**, *15* (3), 2099-103.
108. Elbaz, J.; Cecconello, A.; Fan, Z.; Govorov, A. O.; Willner, I., Powering the programmed nanostructure and function of gold nanoparticles with catenated DNA machines. *Nat. Commun.* **2013**, *4*, 2000.
109. Lu, C. H.; Qi, X. J.; Cecconello, A.; Jester, S. S.; Famulok, M.; Willner, I., Switchable reconfiguration of an interlocked DNA olympiadane nanostructure. *Angew. Chem. Int. Ed. Engl.* **2014**, *53* (29), 7499-503.
110. Lu, C. H.; Cecconello, A.; Qi, X. J.; Wu, N.; Jester, S. S.; Famulok, M.; Matthies, M.; Schmidt, T. L.; Willner, I., Switchable Reconfiguration of a Seven-Ring Interlocked DNA Catenane Nanostructure. *Nano Lett.* **2015**, *15* (10), 7133-7.
111. Holm, T.; Johansson, H.; Lundberg, P.; Pooga, M.; Lindgren, M.; Langel, U., Studying the uptake of cell-penetrating peptides. *Nat. Protocols* **2006**, *1* (2), 1001-1005.

112. Levy-Nissenbaum, E.; Radovic-Moreno, A. F.; Wang, A. Z.; Langer, R.; Farokhzad, O. C., Nanotechnology and aptamers: applications in drug delivery. *Trends Biotechnol.* **2008**, 26 (8), 442-449.
113. Robert J. Lee, P. S. L., Folate as a Targeting Device for Proteins Utilizing Folate Receptor-Mediated Endocytosis. *Meth. Mol. Med.* **2000**, 25.
114. Dong, Y.; Liu, D.; Yang, Z., A brief review of methods for terminal functionalization of DNA. *Methods* **2014**, 67 (2), 116-122.
115. Krishnamurthy, V. M.; Semetey, V.; Bracher, P. J.; Shen, N.; Whitesides, G. M., Dependence of Effective Molarity on Linker Length for an Intramolecular Protein-Ligand System. *J. Am. Chem. Soc.* **2007**, 129 (5), 1312-1320.
116. Graf, F., DNA Origami Nanoparticles for Cell Delivery: The Effect of Shape and Surface Functionalization on Cell Internalization. *Doctoral dissertation, Harvard University.* **2012**.
117. Morrison, L. E.; Ramakrishnan, R.; Ruffalo, T. M.; Wilber, K. A., Labeling Fluorescence In Situ Hybridization Probes for Genomic Targets. In *Molecular Cytogenetics: Protocols and Applications*, Fan, Y.-S., Ed. *Humana Press*: Totowa, NJ, **2003**, 21-40.
118. (a) Gall, J. G.; Pardue, M. L., Formation and Detection of RNA-DNA Hybrid Molecules in Cytological Preparations. *Proc. Natl. Acad. Sci. USA* **1969**, 63 (2), 378-383; (b) John, H. A.; Birnstiel, M. L.; Jones, K. W., RNA-DNA hybrids at the cytological level. *Nature* **1969**, 223 (5206), 582-7.
119. Rudkin, G. T.; Stollar, B. D., High resolution detection of DNA-RNA hybrids in situ by indirect immunofluorescence. *Nature* **1977**, 265 (5593), 472-473.
120. Csaki, A.; Garwe, F.; Steinbrück, A.; Maubach, G.; Festag, G.; Weise, A.; Riemann, I.; König, K.; Fritzsche, W., A Parallel Approach for Subwavelength Molecular Surgery Using Gene-Specific Positioned Metal Nanoparticles as Laser Light Antennas. *Nano Lett.* **2007**, 7 (2), 247-253.
121. Langer, P. R.; Waldrop, A. A.; Ward, D. C., Enzymatic synthesis of biotin-labeled polynucleotides: novel nucleic acid affinity probes. *Proc. Natl. Acad. Sci. USA* **1981**, 78 (11), 6633-6637.
122. Diwu, Z.; Klaubert, D. H.; Haugland, R. P. Spectral properties and biological applications of ELF enzyme substrates that yield fluorescent precipitates at the enzymatic activity sites, **1999**; 265-274.
123. Gozzetti, A.; Le Beau, M. M., Fluorescence in situ hybridization: uses and limitations. *Semin. hematol.* **2000**, 37 (4), 320-33.
124. Baerlocher, G. M.; Mak, J.; Tien, T.; Lansdorp, P. M., Telomere length measurement by fluorescence in situ hybridization and flow cytometry: Tips and pitfalls. *Cytometry* **2002**, 47 (2), 89-99.
125. Bishop, R., Applications of fluorescence in situ hybridization (FISH) in detecting genetic aberrations of medical significance. *Bioscience Horizons* **2010**, 3 (1), 85-95.
126. Rigby, P. W. J.; Dieckmann, M.; Rhodes, C.; Berg, P., Labeling deoxyribonucleic acid to high specific activity in vitro by nick translation with DNA polymerase I. *J. Mol. Bio.* **1977**, 113 (1), 237-251.

127. Grant, G. P. G.; Qin, P. Z., A facile method for attaching nitroxide spin labels at the 5' terminus of nucleic acids. *Nucleic Acids Res.* **2007**, 35 (10), e77-e77.
128. Schmitz, G. G.; Walter, T.; Seibl, R.; Kessler, C., Nonradioactive labeling of oligonucleotides in vitro with the hapten digoxigenin by tailing with terminal transferase. *Anal. Biochem.* **1991**, 192 (1), 222-31.